School of Medicine
Ysgol Meddygaeth

CHARACTERISING THE ROLE OF EXTRACELLULAR VESICLES IN TUBEROUS SCLEROSIS COMPLEX

DOCTOR OF PHILOSOPHY

2022

MUIREANN NÍ BHAOIGHILL

SUMMARY

Tuberous Sclerosis Complex (TSC) is a rare autosomal-dominant genetic disease, caused by loss-of-function mutations in *TSC1* or *TSC2* tumour suppressor genes. *TSC1/TSC2* mutations cause hyperactivation of mammalian Target Of Rapamycin Complex 1 (mTORC1), a master regulator of cell growth and survival, causing development of hamartomas (benign growths) in vital organs, including the kidneys, brain, heart, and lungs. While intracellular signalling is well elucidated in TSC, little is currently known about how TSC tumour cells signal intercellularly to propagate optimal tumour growth and survival. A key mechanism of intercellular signalling is the secretion of small extracellular vesicles (sEVs) that transfer bioactive material from their parental cells to recipient cells in the tumour microenvironment and at distant sites. Thus, the aim of this research was to characterise the role of sEVs in TSC tumour biology. Additionally, sEVs from TSC patient plasma were examined for candidate biomarkers. This research showed that TSC kidney tumour angiomyolipoma (AML) cells secrete sEVs with classical biophysical and molecular characteristics. These AML sEVs were found to have a distinct RNA cargo, enriched in networks associated with various tumour-supporting processes, including extracellular matrix remodeling, growth factor and receptor binding, and angiogenesis. AML sEVs also had a distinct protein cargo (compared to control sEVs) with potential to promote pro-tumoral signalling. Standard-of-care mTORC1 inhibitor rapamycin treatment did not alter characteristics of secreted sEVs, but sEVs from rapamycin-treated AML cells had altered protein cargo and subsequent reduced signalling activation capacity compared to sEVs from untreated AML cells. Lastly, three proteins were found to have elevated expression in TSC patient plasma sEVs compared to healthy donor control sEVs, suggesting their potential as the first biofluid-based biomarkers for TSC. This study reveals important new knowledge about the contribution of sEVs to TSC tumour growth, and their potential application as disease biomarkers.

WORD COUNT 50,888

CONTENTS

FIGURES

TABLES

ABBREVIATIONS

A	
AACR	American Association for Cancer Research
ADAMs	A distintegrin and metalloproteinases
ADP	Adenosine diphosphate
AGO2	Argonuate 2
ALIX	ALG-2-interacting protein X
AML	Angiomyolipoma
AMPK	AMP-activated protein kinase
AP-1	Activator protein 1
ARF6	ADP ribosylation factor 6
ASMase	Acid sphingomyelinase
ATG12	Autophagy-related 12
ATM	Ataxia-telangiectasia mutated
ATP	Adenosine triphosphate
B	
BC	Breast cancer
BCA	Bicinchoninic acid
BMP	Bone morphogenic protein
bp	Base pair
BSA	Bovine serum albumin
C	
CAF	Cancer-associated fibroblast
Cas9	CRISPR-associated protein 9
CC	Coiled coil
CCL2	C-C motif chemokine 2
CCL20	C-C motif chemokine 20
CD	Cluster of differentiation
cDNA	Complementary DNA
COSMIC	Catalogue of Somatic Mutations in Cancer
CO_2	Carbon dioxide
CRC	Colorectal cancer
CRISPR	Clustered regularly interspaced short palindromic repeats
Cryo-EM	Cryogenic electron microscopy
CT	Computerised tomography
CTLA4	Cytotoxic T-lymphocyte associated protein 4
D	
DAPI	4′,6-diamidino-2-phenylindole
DEGs	Differentially expressed genes
DEPTOR	DEP domain-containing mTOR interacting protein
DMEM	Dulbecco’s modified eagle’s media
DMSO	Dimethyl sulfoxide
DNA	Deoxyribonucleic acid
DOI	Digital Object Identifier
dNTPs	Deoxynucleoside triphosphate
DTT	Dithiothreitol
dUTP	Deoxyuridine triphosphate

	D20	Deuterium oxide
E		
	EDTA	Ethylenediaminetetraacetic acid
	ECM	Extracellular matrix
	EEA1	Early endosome antigen 1
	eEF2K	Eukaryotic elongation factor 2 kinase
	eIF4E	Eukaryotic initiation factor 4E
	eIF4F	Eukaryotic initiation factor 4F
	eIF4G	Eukaryotic initiation factor 4G
	EGFR	Epidermal growth factor receptor
	ELISA	Enzyme-linked immunosortbant assay
	EMT	Epithelial-to-mesenchymal transition
	ENO1	Enolase α/1
	ENO2	Enolase γ/2
	ER	Endoplasmic reticulum
	ERK	Extracellular signal-regulated kinases
	ESCRT	Endosomal-sorting complexes required for transport
	EV	Extracellular vesicle
	EV-dep	EV-depleted
	EVs	Extracellular vesicles
F		
	FATS	Fast adipose tracking system
	FBS	Fetal bovine serum
	FDA	Food and Drug Administration
	FDR	False discovery rate
	FGF	Fibroblast growth factor
	FKBP12	FK binding protein 12
G		
	GAPDH	Glyceraldehyde-3-Phosphate Dehydrogenase
	GC	Guanine cytosine
	GF	Growth factor
	GFR	Glomerular filtration rate
	GO	Gene ontology
	GRP94	Glucose-regulated protein 94
	GSEA	Gene set enrichment analysis
	GTP	Guanosine triphosphate
H		
	H	Hydrogen
	HBSS	Hank's balanced salt solution
	HCC	Hepatocellular carcinoma
	HD	Healthy donor
	Hep B	Hepatitis B
	HGF	Hepatocyte growth factor
	HIF-1 α	Hypoxia inducible factor-1α
	hnRNPA2B1	Heterogeneous nuclear ribonucleoprotein A2B1
	HPF-c	Human pulmonary fibroblast-c
	HPV	Human papilloma virus
	Hsp90	Heat shock protein 90
	H_2O	Water

I	
IF	Immunofluorescence microscopy
IgG	Immunoglobulin
ILVs	Intraluminal vesicles
IL-6	Interleukin-6
IL-10	Interleukin-10
Indel	Insertion/deletion
IRS	Insulin receptor substrate
ISEV	International Society of Extracellular Vesicles
J	
JAK	Januskinases
K	
K	Potassium
kb	Kilobase
kDa	Kilodalton
KIFC1	Kinesin family member C1
L	
LAM	Lymphangioleiomyomatosis
LAMP	Lysosome-associated membrane protein
LDS	Lithium dodecyl sulfate
lncRNA	Long non-coding RNA
M	
MAP	Mitogen activated protein
MAPK	Mitogen activated protein kinase
MEF	Mouse embryonic fibroblast
MF	Molecular function
MHC	Major histocompatibility complex
miEAA	miRNA Enrichment and Annotation
mIMCD3	Mouse inner medullary collecting duct D3
miRDB	MicroRNA Target Prediction Database
miRNA	Micro RNA
MISEV	Minimal information for studies of extracellular vesicles
mLST8	Mammalian lethal with SEC13 protein 8
MM	Multiple myeloma
MMP	Matrix metalloproteinase
MRI	Magnetic resonance imaging
mRNA	Messenger RNA
MS	Mass spectrometry
mTOR	Mammalian/mechanistic target of rapamycin
mTORC1	Mammalian/mechanistic target of rapamycin complex 1
mTORC2	Mammalian/mechanistic target of rapamycin complex 2
MVs	Microvesicles
MVBs	Multivesicular bodies
N	
Na	Sodium
NADH	Nicotinamide adenine dinucleotide + hydrogen
NaCl	Sodium chloride
NaF	Sodium fluoride
NCBI	National Center for Biotechnology Information

	NF1	Neurofibromatosis type 1
	NK-κB	Nuclear factor kappa B
	NMI	No mutation identified
	ns	Non-statistically significant
	NSCLC	Non-small cell lung cancer
	NSMase	Neutral sphingomyelinase
	NTA	Nanoparticle tracking analysis
O		
	OMIM	Online Mendelian Inheritance In Man
	ORA	Over-representation analysis
	ORF	Open reading frame
	OS	Overall survival
	O_2	Oxygen
P		
	p adj.	Adjusted *p* value
	PBS	Phosphate buffered saline
	PCA	Principal Component Analysis
	PDCD4	Programmed cell death 4
	PD1	Programmed cell death protein 1
	PEG	Poly-ethylene glycol precipitation
	Pen strep	Penicillin streptomycin
	PIC	Protease inhibitor cocktail
	PI3K	Phosphatidylinositol-3-kinase
	PKCalpha	Protein kinase C alpha
	PKD	Polycystic kidney disease
	PLD2	Protein phospholipase D2
	PMSF	Phenylmethylsulfonyl fluoride
	PNET	Pancreatic neuroendocrine tumours
	Poly-A	Polyadenylated
	PPAR	Peroxisome proliferator-activated receptor
	PP2A	Protein phosphate 2A
	PRAS40	Proline rich Akt substrate 40
	Protor-1	Protein observed with RICTOR
	PSA	Prostate specific antigen
	PTC	Premature termination codon
	PTEN	Phosphatase and tensin homolog
	PVDF	Polyvinylidene difluoride
	p53	Tumor protein 53
	p90RSK	p90 ribosomal S6 kinase
Q		
	qPCR	Quantitative polymerase chain reaction
R		
	Rab	RAS-related protein
	Rac1	Rac Family Small GTPase 1
	RAPTOR	Regulatory-associated protein of mammalian target of rapamycin
	RCC	Renal cell carcinoma
	REDD1	Regulated in development and DNA damage responses 1
	Rheb	Ras homolog enriched in brain
	RICTOR	Rapamycin-insensitive companion of mammalian target of rapamycin

	RIN	RNA integrity number
	RIPA	Radioimmunoprecipitation assay
	RISC	RNA-induced silencing complex
	RNA	Ribonucleic acid
	RNA-Seq	RNA sequencing
	RNPs	Ribonucleoproteins
	rpS6	Ribosomal protein 6
	rRNA	Ribosomal RNA
	RTK	Receptor tyrosine kinase
S		
	SD	Standard deviation
	SDS-PAGE	Sodium dodecyl-sulfate polyacrylamide gel electrophoresis
	SEC	Size-exclusion chromatography
	SEGA	Subependymal giant cell astrocytoma
	sEV	Small extracellular vesicle
	sEVs	Small extracellular vesicles
	SGK1	Serum/glucocorticoid regulated kinase 1
	SIN1	Stress-activated kinase-interacting protein
	SIRT4	Sirtuin 4
	SKAR	S6K1 aly/REF-like target
	SMAD	Suppressor of Mothers against Decapentaplegic
	SM-proteins	Sec1/Munc-18 related proteins
	SNAP	Soluble Nethylmaleimide sensitive fusion attachment protein
	SNARE	Soluble N-ethylmaleimide-sensitive fusion attachment protein receptor
	SREBP-1	Sterol regulatory element binding protein 1
	STAM	Signal-transducing adaptor molecule
	STAT3	Signal transducer and activator of transcription 3
	SUMO	Small ubiquitin-like modifier
	SYK	Spleen tyrosine kinase
	SYNCRIP	Synaptotagmin Binding Cytoplasmic RNA Interacting Protein
	S1P	Sphingosine 1-phosphate
	S6	Ribosomal protein S6
	S6K1	Ribosomal S6 kinase 1
T		
	TBC1D7	Tre2-Bub2-Cdc16 1 domain family member 7
	TBS	Tris-buffered saline
	TBST	Tris-buffered saline-Tween 20
	TCGA	The Cancer Genome Atlas
	TGF-β	Transforming growth factor beta
	TIF-IA	Transcription initiation factor IA
	TME	Tumour microenvironment
	TNBC	Triple-negative breast cancer
	TNFα	Tumor necrosis factor alpha
	TRAIL	TNF-related apoptosis-inducing ligand
	tRNA	Transfer RNA
	TRF	Time-resolved fluorescence
	TSC	Tuberous sclerosis complex
	TSC+mTORi	TSC patient receiving mTOR inhibitor treatment
	TSC1	Tuberous sclerosis complex 1; hamartin

	TSC2	Tuberous sclerosis complex 2; tuberin
	TSG101	Tumor susceptibility gene 101 protein
U		
	ULK1	Unc-51 Like Autophagy Activating Kinase 1
	USA	United States of America
V		
	VAMP7	Vesicle-associated membrane protein 7
	VE-cadherin	Vascular endothelial-cadherin
	VEGF	Vascular endothelial growth factor
	VEGFA	Vascular endothelial growth factor A
	VEGFD	Vascular endothelial growth factor D
	VEGFR	Vascular endothelial growth factor receptor
	VEGFR2	Vascular endothelial growth factor receptor 2
	Vps34	vacuolar protein sorting 34
	Vsp4	Voltage-sensing phosphatase 4
W		
	Wnt	Wingless/integrated
Y		
	YBX1	Y-Box binding protein 1
	YY1	Yin Yang 1
2		
	2D	Two-dimensional
3		
	3D	Three-dimensional
	3'UTR	3' untranslated region
4		
	4EBP1	Eukaryotic initiation factor 4E-binding protein 1

Units of measurement used throughout are those set out by the International System of Units (SI).

Amino acids and their corresponding three-letter and one-letter codes are listed in **Appendix A**.

Proteins and corresponding encoding genes related to the Proteome Profiler Human XL Oncology array (**Chapter 5**) are listed in **Table 2.4**.

ACKNOWLEDGEMENTS

Firstly, I would like to express my sincerest thanks to the Tuberous Sclerosis Association for funding this project. This work would not have been possible without you. I am also very grateful for the opportunity you have given to me, both on a professional and personal level. I would like to thank the TSC research community for being so supportive and encouraging to early-career researchers, and for advocating for patients. TSC patients and their families deserve a particularly special mention: your strength and perseverance will always stay with me. You are an inspiration.

I owe a huge thanks to my supervisors, Dr Elaine Dunlop and Dr Jason Webber. Elaine and Jason, thank you for all your guidance, encouragement, support, and kindness during my time working with you. You have helped me grow and learn so much, and I wouldn't be the scientist I am today without you both. Thank you for everything.

I would also like to thank Prof Aled Clayton and Prof Jeremy Cheadle for their support and appraisal of this project over the past four years. My thanks also to Prof Andrew Tee and Prof Rachel Errington for their advice through the course of this work. I would like to thank Dr Helen Pearson and Dr Ryan Pink for examining this Thesis, and thank you to Prof Simon Reed for chairing my *viva voce* examination.

Thank you to Dr Karen Reed, Dr Vikki Humphries, and Shelley Rundle, for their work on RNA quality control, library preparation, and sequencing. Thank you to Samantha Hill and Dr Peter Giles for their compilation of differentially-expressed genes lists and bioinformatics work and support.

I wish to thank Zoë Fuchs, Dana Valley, Dr Gabrielle Rushing, and Adam Bouwman, for their collaboration and coordination of plasma samples from the USA. I would also like to thank Daniel Robins for coordinating collection of biobanked plasma samples from the Cardiff University Biobank.

I would like to thank Dr Emer Bourke (University of Galway, Ireland) who gave me my first glimpse of cancer research as an undergraduate student and whose encouragement inspired my career today. I would also like to thank Christina Johnston and Ciara O'Shea, my former science teachers from secondary school, who instigated my passion for the sciences all those years ago.

I feel very lucky to have met and worked with some wonderful people in the Division of Cancer and Genetics. I would like to thank Marie Wiltshire specially, who went above and beyond her duty to ensure that PhD students could return to the lab safely and promptly following the COVID-19 lockdowns. Thank you for all your assistance and guidance on the Health and Safety matters, Marie. I would also like to thank the cleaning staff of the Tenovus building, whose diligence kept us safe in clean conditions particularly during our return-to-work periods. Thank you to Liz Husband and Ashley Dias, for making sure deliveries got to storage as quickly as possible. Thank you to Dr Alexandra Shephard and Dr Alex Cocks for helping me to get up to speed with extracellular vesicle lab techniques when I started in the lab. Thank you Thea and Sara V for your companionship and support, and continued willingness to discuss experiments! Thank you Amr for being a lovely person to chat to, especially during the late evenings on shift work. Thank you to Mariama, for always having a positive and encouraging word to say to perk me up. My thanks also to Kate, Andreia, Lauren, and TMEG members for chats that made the long days feel shorter.

The opportunity to move to Cardiff came to me at just the right time. I could have only dreamt to move somewhere that I would grow to love so much. To my dear Cardiff friends: I'm so grateful to have you in my life. Silvia, thank you for being one truly amazing friend. Ellie and Sophie, how lucky I was to take those first few steps together at Induction Week, making two beautiful friends on the very first week. Aisling, thank you for being my piece of home away from home, and a source of support, reassurance, and comfort being away all this time. To my fab friends Laura and Angharad C, thank you for always being there to listen and cheer me up. To Chantelle, Gwawr, Mafe, Franzi, Maddie, and Abby: thank you for all the great times shared across many houses in Cardiff. You all added a special something. To the CanGen crewzers: Angharad W, Becky, Jesse, Darius, and Naledi – I feel

so lucky that our paths crossed and I got to work surrounded by lovely friends. Thank you all for being there and for the evenings spent laughing in between busy work days. Sara S, thank you for looking out for me when I first started in the lab – and for introducing me to caramel coffees. Eileen, thank you for all your support as we started our lab journeys together, and for keeping a lovely friendship all these years. Harry, thank you for all the laughs and lovely words of encouragement when I needed to hear it the most. Sarah, Bríd, and Róisín: thank you for standing by me through all the ups and downs, and for always rooting for me. I can't wait to see where the next few years take us. To Ciara C, Hannah, Ciara G, Robert, India, Maggie, Tommy, and Aoife: thank you for keeping the light on.

Gabháim buíochas le mo theaghlach uilig a bhí in aice liom thar na blianta seo. Go speisialta, mo mhíle buíochas do mo thuistí, Maura agus Séamus, mo dheirfiúr Ríoghnach agus mo dhearthair Séimidh, a bhí uilig mar chrann taca dom le linn na tréimhse seo. Táim buíoch beannachtach as a bhfuil againn le chéile.

Muireann Ní Bhaoighill

September 2022

ORAL AND POSTER PRESENTATIONS

Ní Bhaoighill, M., Tee, A. R., Webber, J. P., Dunlop, E. A.. **Extracellular vesicles from mTORC1-driven tumours activate fibroblasts in the tumour microenvironment, but this is attenuated by rapamycin treatment.** United Kingdom Society of Extracellular Vesicles (UKEV) Forum 2021, December 2021. Oral presentation.

Ní Bhaoighill, M., Tee, A. R., Webber, J. P., Dunlop, E. A.. **Transcriptome profiling of extracellular vesicles from mTOR-driven tumours reveals a distinct RNA signature.** United Kingdom Society of Extracellular Vesicles (UKEV) Forum 2021, December 2021. Flash oral presentation.

Ní Bhaoighill, M., Tee, A. R., Webber, J. P., Dunlop, E. A.. **Extracellular vesicles (EVs) secreted by TSC2-deficient cells shuttle altered cargo to fibroblasts of the tumour microenvironment to promote pro-tumoral signalling**. International Tuberous Sclerosis Research Conference (ITSCRC2021), June 2021. Rapid-fire oral presentation and poster presentation.

Ní Bhaoighill, M., Tee, A. R., Webber, J. P., Dunlop, E. A.. **Altered cargo of EVs from mTORC1-driven tumours enhances pro-tumoral signalling in recipient fibroblasts of the tumour microenvironment.** International Society of Extracellular Vesicles (ISEV) Annual Conference, May 2021. Poster presentation.

Ní Bhaoighill, M., Tee, A. R., Webber, J. P., Dunlop, E. A.. **Altered cargo of EVs from mTORC1-driven tumours enhances pro-tumoral signalling in recipient fibroblasts of the tumour microenvironment.** Postgraduate School of Medicine and Dentistry Symposium, April 2021. Poster presentation.

Ní Bhaoighill, M. Tee, A. R., Webber, J. P., Dunlop, E. A.. **Characterising the role of extracellular vesicles from mTORC1-driven tumours**. Division of Cancer and Genetics Seminar Series, February 2021. Oral presentation.

Ní Bhaoighill, M., Tee, A. R., Webber, J. P., Dunlop, E. A.. **EV cargo is altered downstream of *TSC2* growth suppressor deficiency.** United Kingdom Society of Extracellular Vesicles (UKEV) Forum 2020, December 2020. Flash oral presentation.

Burton, C., Milward, K., Veiga, S., Ní Bhaoighill, M., Evans, L., de Almeida, A., Mikhaylov, R., Wu, F., Yang, C., Errington, R., Webber, J., Clayton, A.. **A 3D-printed model to represent the structure and nature of extracellular vesicles, for public engagement and education events**. International Society of Extracellular Vesicles (ISEV) 2020, July 2020. Philadelphia, Pennsylvania (virtual due to COVID-19 pandemic). Poster presentation.

Ní Bhaoighill, M., Tee, A. T., Webber, J. P., Dunlop, E. A.. **Profiling the molecular cargo of TSC extracellular vesicles.** Division of Cancer and Genetics Rare Disease Meeting, July 2020. Oral presentation.

Ní Bhaoighill, M., Tee, A. T., Webber, J. P., Dunlop, E. A.. **Characterising the role of extracellular vesicles in Tuberous Sclerosis Complex**. 34th Annual School of Medicine and Dentistry Postgraduate Research Day, January 2020. Poster presentation.

Ní Bhaoighill, M., Tee, A. T., Webber, J. P., Dunlop, E. A.. **Characterising the role of extracellular vesicles in Tuberous Sclerosis Complex**. United Kingdom Society of Extracellular Vesicles (UKEV) Forum 2019, December 2019. The Francis Crick Institute, London. Poster presentation.

Ní Bhaoighill, M., Tee, A. T., Webber, J. P., Dunlop, E. A.. **Characterising the role of extracellular vesicles in Tuberous Sclerosis Complex**. Division of Cancer and Genetics Postgraduate Researchers' Research Symposium. Oral presentation, October 2019.

Ní Bhaoighill, M., Tee, A. T., Webber, J. P., Dunlop, E. A.. **Understanding the TSC Tumour Environment.** Tuberous Sclerosis Association (TSA) Welsh Info Day, September 2019. University Hospital of Wales. Oral Presentation.

Ní Bhaoighill, M.. **Extracellular vesicles as personalised communicators**. 33rd Annual School of Medicine and Dentistry Postgraduate Research Day, January 2019. 3-Minute Thesis (3MT) Oral Presentation.

AWARDS

Early Career Researcher 2021
Awarded by United Kingdom Society of Extracellular Vesicles (UKEV)

Young Investigator Award and Scholarship 2021
Awarded by International Society of Extracellular Vesicles (ISEV)

Division of Cancer and Genetics Best Oral Presentation 2019
Second prize, awarded by Division of Cancer and Genetics, Cardiff University

GRANTS

William Morgan Thomas Travel Fund, December 2019

PUBLICATIONS

Ní Bhaoighill, M., Falcón-Pérez, J. M., Royo, F., Tee, A. R., Webber, J. P., Dunlop, E. A. **Extracellular vesicles from Tuberous Sclerosis Complex cells induce tumour-promoting signalling and have biomarker potential.** *Submitted.*

Ní Bhaoighill, M., Dunlop, E. A. (2019). **Mechanistic target of rapamycin inhibitors: successes and challenges as cancer therapeutics**. *Cancer Drug Resist*, 2, pp. 1069-85. DOI: 10.20517/cdr.2019.87

Dedicated to my parents, Maura & Séamus

CHAPTER 1

GENERAL INTRODUCTION

1.1. TUBEROUS SCLEROSIS COMPLEX (TSC)

1.1.1. Introduction

Tuberous Sclerosis Complex (TSC) is a rare autosomal-dominant tumour suppressor gene syndrome, caused by loss-of-function mutations in either of two genes - *TSC1* (OMIM 191100) or *TSC2* (OMIM 613254). It is a progressive, multi-system genetic disease with high penetrance and morbidity, and it manifests in a variable inter-patient phenotype (Orlova *et al*., 2010; Islam and Roach, 2015). TSC is characterised by the development of multi-organ hamartomas (benign growths) that cause impaired function in vital organs, including the kidneys, brain, lungs, heart, skin and eyes; and the onset of neurological conditions, including seizures, intellectual disability, autism, and developmental delay (as reviewed by Crino *et al.*, 2006; as reviewed by Henske *et al*., 2016). TSC features present and develop with varying severity (as reviewed by Caban *et al*., 2016). Due to its multi-system presentation, TSC requires a multi-disciplinary approach for optimal clinical management (as reviewed by Leung and Robson, 2007; Northup *et al*., 2020).

1.1.2. Incidence and prevalence

Approximately 2 million patients suffer from TSC worldwide (Curatolo *et al.*, 2008). Although the live-birth incidence of TSC is 1:6000-10000 (Osborne *et al*., 2000; Curatolo *et al.*, 2008), TSC can present differently between patients and symptoms and clinical signs can present and diversify at various time points in one's lifetime

(Wataya-Kaneda *et al*., 2013). The prevalence of TSC is estimated to be 8.8/100,000 in Europe, affecting multiple ethnic groups (Joinson *et al*., 2003).

1.1.3. TSC phenotypes

1.1.3.1. Major and minor clinical features

TSC clinical signs are defined as either major or minor clinical features and are summarised in **Table 1.1**. A definite diagnosis of TSC requires presentation of two or more major features, or one major feature with two or more minor features. Presentation of one major feature, or two or more minor features denotes a possible TSC diagnosis.

Table 1.1: Clinical diagnostic criteria for TSC diagnoses (as per recommendations of the 2020 International Tuberous Sclerosis Complex Consensus Conference).

Major Features	Minor Features
Hypomelanotic macules (≥3; ≥5mm diameter)	"Confetti" skin lesions
Angiofibromas (≥3) or fibrous cephalic plaque	Dental enamel pits (≥3)
Ungual fibromas (≥2)	Intraoral fibromas (≥2)
Shagreen patch	Retinal achromic patch
Multiple retinal hamartomas	Multiple renal cysts
Cortical dysplasia	Non-renal hamartomas
Subependymal nodules	
Subependymal giant cell astrocytoma (SEGA)	
Cardiac rhabdomyoma	
Lymphangioleiomyomatosis (LAM)	
Angiomyolipoma (AML) (≥2)	

In infancy and childhood, the most frequently seen TSC manifestations are brain hamartomas, epilepsy, skin lesions and cardiac rhabdomyomas (as reviewed by Crino *et al*., 2006). Observed trends of TSC manifestation with aging is summarised below in **Fig. 1.1**.

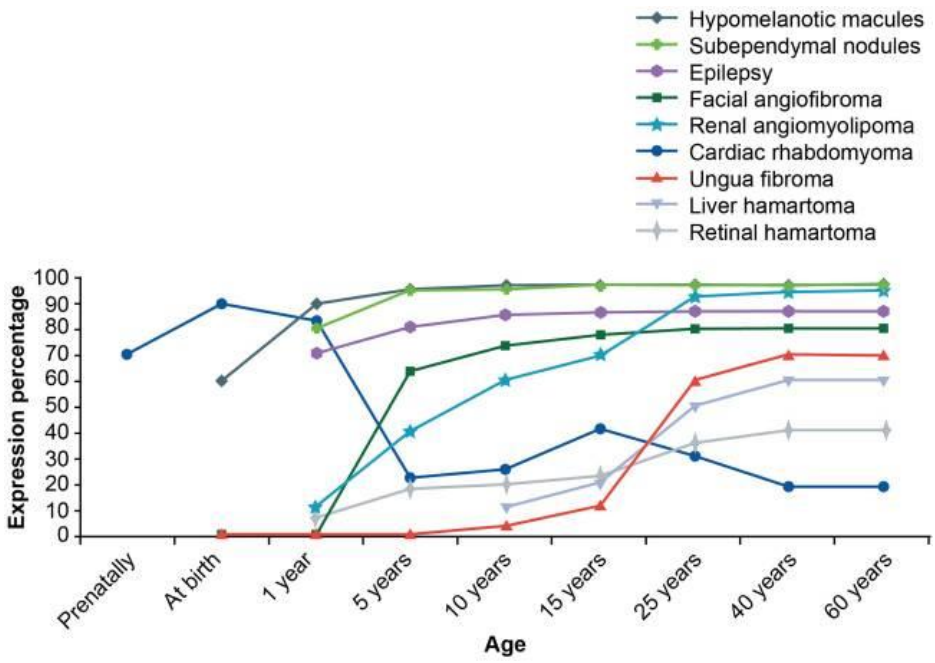

Figure 1.1: Age-dependent trends of TSC clinical manifestations. *(Graph from Curatolo et al., 2008; reprinted in Samueli et al., 2015).*

1.1.3.2. Renal angiomyolipoma (AML)

Renal disease is a leading cause of morbidity and mortality in TSC patients (Shepherd *et al.,* 1991; Bissler and Kingswood *et al*., 2004; Eijkemans *et al*., 2015;) and is the key tumour type of focus of this Thesis. Clinical management and surveillance of renal growths is particularly important (as reviewed by Lam *et al*., 2018). Typically, TSC-associated renal angiomyolipoma (AML) presents as bilateral, multifocal lesions in the 30-50-year age bracket and with no sex predominance (Caliò *et al*., 2021). AMLs are triphasic benign mesenchymal tumours and are comprised of varying amounts of dysplastic blood vessels, smooth muscle, and mature adipose tissue (as reviewed by Jinzaki *et al*., 2014). Over 80% of TSC patients develop multiple renal AML (Franz *et al*., 2010) and epithelial, fluid-filled renal cysts are reported in 14-32% TSC patients (Rakowski *et al*., 2006). This renal involvement can begin at a young age with an increasing incidence and

severity throughout adulthood, as shown in **Fig. 1.1**. Malignant AML and renal cell carcinoma (RCC) occur more commonly in TSC patients than in the general population (Borkowska *et al*., 2011). It is estimated that RCC develop typically at a young age (28–30-year age bracket) in between 2% and 5% of TSC patients (Northup *et al*., 2021). It is reported that TSC-AMLs tend to be larger and more rapidly growing than spontaneous AML (as reviewed by Nelson and Sanda, 2002). TSC-associated AML poses significant tumour burden to patients (O'Callaghan *et al*., 2004). AMLs of greater than 3cm diameter are vulnerable to bleeding or infiltration of the kidney, resulting in renal failure (Bissler and Kingswood, 2004). Up to 10% of TSC patients with AML suffer retroperitoneal haemorrhage, which can be fatal (Pradilla *et al*., 2017). An example computerised tomography (CT) scan is shown in **Fig. 1.2**.

Figure 1.2: Computerised tomography (CT) scan showing a right kidney AML with high adipose content. *Image published in Pradilla et al., 2017.*

1.1.4. Genotype

TSC has a defined genotype of loss-of-function mutations in tumour suppressor genes *TSC1* or *TSC2 (*Curatolo *et al*., 2008*)*. Since *TSC1* and *TSC2* are tumour suppressor genes, inactivation of both *TSC1/TSC2* alleles is said to be required for

tumour formation (as reviewed by Rosset *et al*., 2017), inkeeping with the *two-hit hypothesis* (Knudson, 1971). An inherited germline *TSC1/TSC2* mutation, found in approximately 85% of patients with clinical features associated with TSC, is the first hit, while the second hit is somatic (as reviewed by Rosset *et al*., 2017).

1.1.4.1. Tuberous Sclerosis Complex Subunit 1 (TSC1)

TSC1 is a protein-coding gene located at the chromosome 9q34.13 locus. It has 21 coding exons and an 8.6kb mRNA transcript, which contains a small 5' and a large 4kb 3' untranslated region. It encodes a 130kDa-sized growth-suppressing protein called TSC1 (also called *hamartin*; 1164 amino acids). TSC1 has an N-terminal α-helical core domain (Sun *et al*., 2013). It also possesses a large predicted coiled coil (CC) region (residues 726–988) (Santiago Lima *et al*., 2014). Tre2-Bub2-Cdc16 (TBC) 1 domain family member 7 (TBC1D7) is a known binding partner of TSC1, involving TSC1 residues 939–992, which are located at the C-terminal end of the CC region (Santiago Lima *et al.*, 2014).

With regards to its molecular function, TSC1 interacts with and stabilises protein TSC2 (also called *tuberin*) in the TSC1/TSC2/TBC1D7 cytosolic tumour suppressor complex. TSC1 also acts as a co-chaperone for heat shock protein 90 (Hsp90), inhibiting its adenosine triphosphate (ATP)ase activity, and accommodates Hsp90-mediated folding of kinase and non-kinase clients, including TSC2, to prevent their ubiquitation and proteosomal degradation (Chong-Kopera *et al*., 2006; Hu *et al*., 2008).

Approximately 26% of people with TSC and related family members with identified pathogenic mutations had a *TSC1* mutation in an analysis of over 10,000 people (Northup *et al.*, 2020, GeneReviews®). Approximately 9.9% of these were familial TSC, while approximately 16% were simplex cases. These mutations are most frequently small nonsense and insertion or deletion (indel) mutations, causing premature protein truncation, with only few functionally determined missense mutations (Northup *et al*., 2020).

1.1.4.2. Tuberous Sclerosis Complex Subunit 2 (TSC2)

TSC2 is a protein-coding tumour suppressor gene located at the chromosome 16p13.3 locus. It has 41 coding exons and a 5.5kb mRNA transcript. *TSC2* encodes 200kDa-sized TSC2 (also called *tuberin*; 1807 amino acids) that associates with TSC1 in a cytosolic tumour suppressor complex. TSC2 can stimulate specific GTPases. In mTORC1 signalling, TSC2 acts as a GTPase-activating protein by converting Rheb from its active GTP-bound state to its inactive GDP-bound state. This elicits controlled signals from Rheb in activating downstream mTORC1 (as reviewed by Saxton and Sabatini, 2017).

Approximately 69% of TSC cases reported have a *TSC2* pathogenic mutation (Northup *et al*., 2020; GeneReviews®), in over 10,000 people with TSC analysed. Approximately 14% of these are familial cases and approximately 55% of these are simplex cases (Jones *et al*., 1999; Dabora *et al*., 2001; Au *et al*., 2004; Sancak *et al.*, 2005; Au *et al*., 2007; Tyburczy *et al*., 2015; Northup *et al*., 2020). Twenty percent of *TSC2* mutations are missense or nonsense mutations. The most frequent *TSC2* mutations reported are missense changes in codons 611 and 1675,

and a 18bp in-frame deletion in exon 40 (< 5% of known *TSC2* mutations). *TSC2* pathogenic variants are associated with more severe disease manifestations than *TSC1* pathogenic variants (Hizawa *et al*., 1994; Gould, 1991; Jones *et al*., 1999; Dabora *et al*., 2001: Northup *et al*., 2021). Patients carrying a pathogenic *TSC2* variant are reported to be at increased risk of renal malignancy (Yang *et al*., 2014), intellectual disability (Kothare *et al*., 2014), and autism and infantile spasms (Numis *et al*., 2011).

A summary of *TSC1* and *TSC2* structures and key functions is shown in **Fig 1.3**.

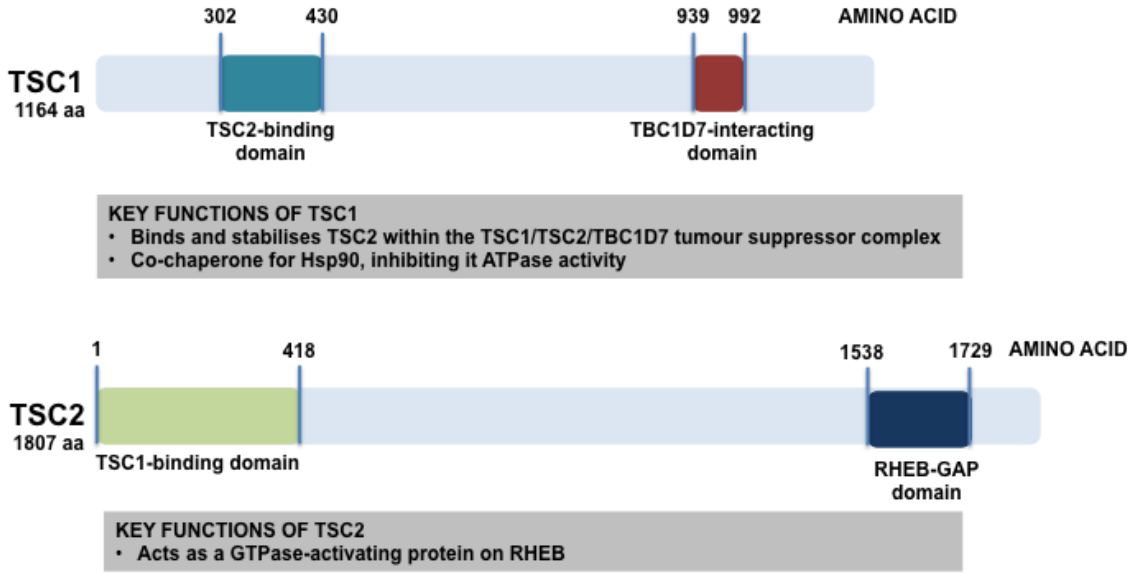

Figure 1.3: Graphical summary of TSC1 and TSC2 structure, domains, and functions. *Tuberous sclerosis complex subunit 1, TSC1; tuberous sclerosis complex subunit 2, TSC2; Tre2-Bub2-Cdc16 (TBC) 1 domain family member 7, TBC1D7; Ras homolog enriched in brain, Rheb; GTPase-activating protein, GAP; amino acid, aa. Relevant references: Yang et al., 2021; Natarajan et al., 2020.*

1.1.4.3. Inheritance

TSC hereditary occurs due to an autosomal dominant trait, although spontaneous/sporadic mutations are more common. It is approximated that one third of TSC cases are discovered to be familial while the other two thirds are sporadic and arise due to *de novo* mutations (as reviewed by Lam *et al*., 2018) in

either *TSC1* or *TSC2*. It is reported that a higher proportion of TSC patients with severe disease manifestations express a *de novo TSC2* pathogenic variant than a *de novo TSC1* pathogenic variant (Au *et al*., 2007). Simplex cases of TSC are more likely to express a *TSC2* pathogenic variant.

1.1.4.4. Penetrance and expressivity

Penetrance is defined as the number of individuals of a particular genotype that simultaneously express an associated phenotype. TSC is widely considered to have high penetrance of over 95% (Northup *et al*., 1993; as reviewed by Rosset *et al*., 2017). There was a case report of a subject with minimal symptomatic presentation and another subject with non-penetrance between a great-grandfather and his great grandson (Webb and Osborne, 1991; Treichel *et al*., 2019). Expressivity is defined as the degree to which individuals who have the same genotype exhibit a phenotype. TSC has variable expressivity, even within a given family (as reviewed by Leung and Robson, 2007; Northup *et al*., 1993).

1.1.4.5. Mosaicism and 'no mutation identified' (NMI)

TSC patients can also have somatic mosaic mutations in some cases but tend to have milder disease manifestations (Verkoef *et al*., 1995; Sampson *et al*., 1997). Germline mosaicism is not recommended for investigation unless a couple had multiple children with TSC. Parents with one affected child should be informed of a small chance (1-2%) of recurrence, even in parents with no genetic markers of TSC (Roach, Gomez, and Northup, 1998). Around 10% patients exhibiting clinical signs of TSC may have no identified mutation in *TSC1* or *TSC2*, leading to the hypothesis that there may be other pathogenic genes involved in TSC. For

example, another component of the functional mTORC1 complex is TBC1D7, though mutational status of this in TSC is currently unknown. Similarly, with improvements in next-generation sequencing (NGS) studies, additional alterations to TSC1 and TSC2 have also been detected that had originally missed on initial sequencing (Tyburczy *et al.*, 2015). Therefore, discovery of new mutations associated with TSC may become known that are relevant to diagnosis or associated with particular phenotypes.

1.1.4.6. Genotype-phenotype studies in TSC

Causative mutations are commonly identified in patients affected by TSC, with mosaicism and other gene mutations likely to be responsible for the 10% (approximate) patients exhibiting clinical signs of TSC but with NMI. Though *TSC2* mutations are commonly associated with more severe TSC tumour and neurological phenotypes, underpinning specific genotype-phenotype correlations is still a challenge at the individual level due to high expressivity (as reviewed by Curatolo *et al*., 2015). Work in establishing genotype-phenotype correlations in TSC is underway, taking both lab-based and case studies of affected patients and their families into account.

Other studies focus analysis at the gene level, where a study showed that *TSC2* mutations in exons 25 and 31 were not likely to cause clinical signs of TSC (Ekong *et al.*, 2016). Profiling functional pathogenicity of TSC1 and TSC2 is also insightful to gauge which mutations are truly pathogenic. In one study, functionality pathogenicity of four known *TSC2* mutations: E92V, R505Q, H597R, and L1624P; was analysed to find considerable variation in efficient control of mTORC1 and its

downstream substrates, highlighting the need for multiple functional assays to determine mutation pathogenicity at the patient level (Dunlop *et al*., 2011). Another study examined the phenotypic differences arising in thirty TSC patients, where analysis of both *TSC1* and *TSC2* mutations was divided between those with premature termination codons (PTCs), and missense mutations (Muto *et al.*, 2022). The authors report that in cases of mutations causing PTCs, patients had a significantly increased likelihood of developing more major features of TSC (as per **Table 1.1)**, particularly subependymal nodules and cortical tubers. When the analysis was conducted on patients with *TSC2* mutations with AML, patients with mutations with PTC exhibited a trend towards early age of onset and bilateral AML (Muto *et al*., 2022).

In TSC-associated AML, Li *et al.* report that a TSC mutation was detected in 80% of patient TSC-AML cases (20/25 unrelated patients), with a higher proportion of TSC2 mutations (68%; 17/25) compared to TSC1 mutation (12%; 3/25) (Li *et al*., 2018). Furthermore, this study identified 7 new mutation sites, and also reported that there were no differences in tumour size, haemoglobin, or serum creatinine by TSC mutation types ($p > 0.05$). The criteria for such pathogenic mutations include those that inactivate TSC1 or TSC2 (e.g. out-of-frame indel or nonsense mutation), hinder protein synthesis (e.g. large genomic deletion) or a missense mutation with an effect on the protein evident from functional assessment (www.lovd.ml/TSC1, www.lovd/TSC2; Hoogeveen-Westerveld *et al*., 2012; Hoogeveen-Westerveld *et al.*, 2013). In the literature that examines cohorts of TSC patients, one study found that *TSC1* and familial *TSC2* mutations were associated with less severe TSC phenotypes compared to *de novo TSC2* mutations (N=490) (Sancak *et al*., 2005).

In this same study, NMI patients were also found to have less severe TSC phenotypes than patients with *TSC1/TSC2* mutations detected. In another study of children (age range = 1.4-17.9) with TSC (*N*=64), inactivating mutations in *TSC2* was associated with severity of brain pathology, specifically: increased numbers of brain tubers, radial migration lines, and subependymal nodules compared to patients with *TSC1* mutation (Overwater *et al*., 2016).

1.1.4.7. TSC1 and TSC2 mutations in other diseases

Mutations in *TSC1* and *TSC2* are also reported in other diseases. *TSC1* alterations are reported in 2.15% of all cancers within *The AACR Project GENIE Consortium* (accessed via cbioportal.org). Cancer types having the greatest prevalence of *TSC1* mutation were found to include bladder urothelial carcinoma, colon adenocarcinoma, lung adenocarcinoma, endometrial endometrioid adenocarcinoma, breast invasive ductal carcinoma, and cutaneous melanoma (The AACR Project GENIE Consortium, 2017). *TSC2* mutations were reported in 3.39% of cancers within this consortium cohort, and many of the same cancer types implicated with *TSC1* mutations were also found implicated with *TSC2* mutations. These include lung adenocarcinoma, colon adenocarcinoma, breast invasive ductal carcinoma, and endometrial endometrioid adenocarcinoma. High-grade ovarian serous adenocarcinoma was also found as a cancer type with the greatest prevalence of *TSC2* alterations (The AACR Project GENIE Consortium, 2017). *TSC1* and *TSC2* mutation maps in cancer are provided in **Appendices B** and **C** (sourced from COSMIC; www.cancer.sanger.ac.uk/cosmic).

1.1.5. Mammalian target of rapamycin complex 1 (mTORC1) signalling

1.1.5.1. mTOR complexes: mTORC1 and mTORC2

In cell homeostasis, mammalian target of rapamycin (mTOR) functions as a central signalling node and coordinates an elaborate network of upstream signals, induced by extracellular factors such as insulin and growth factors, into important downstream cellular processes that regulate cell growth, cell size, cell cycle, and proliferation (as reviewed by Saxton and Sabatini, 2017). mTOR is an atypical serine/threonine kinase that functions as the catalytic subunit of two heteromeric protein complexes: mTOR Complex 1 (mTORC1) and mTORC2 (**Fig. 1.4**).

mTORC1 is comprised of mTOR, regulatory-associated protein of mammalian target of rapamycin (RAPTOR), DEP domain-containing mTOR interacting protein (DEPTOR), proline rich Akt substrate 40 (PRAS40), and mammalian lethal with SEC13 protein 8 (mLST8) (Aylett *et al.,* 2016). mTORC1 integrates various environmental and nutritional extracellular signals, including cellular stress, amino acids, growth factors and energy cues, in order to promote and coordinate cell growth. It achieves this by initiating phosphorylation of substrates involved in anabolic processes in mRNA translation and lipid synthesis, or hindering catabolic processes such as autophagy (as reviewed by Saxton and Sabatini, 2017).

mTORC2 is composed of mTOR, Rapamycin-insensitive companion of mammalian target of rapamycin (RICTOR), DEPTOR, mLST8, stress-activated protein kinase-interacting protein (SIN1), and PRotein Observed with RicTOR (Protor-1). mTORC2 is involved in cytoskeletal remodelling by activating protein kinase C α

(PKCα), promoting cell survival, via Akt activation, and mediating transport of ions and subsequent growth, via serum/glucocorticoid regulated kinase 1 (SGK1) phosphorylation (as reviewed by Saxton and Sabatini, 2017).

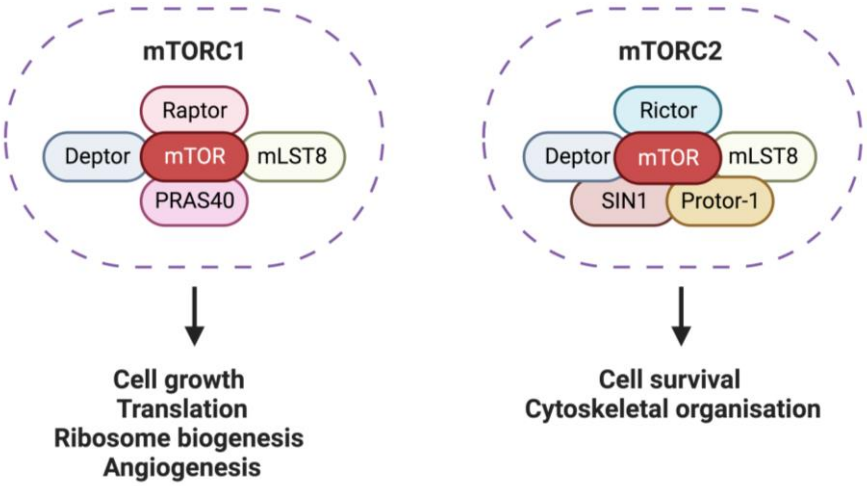

Figure 1.4: mTORC1 and mTORC2 complexes and their respective protein subunits, with downstream functions particular to each complex. *mTOR and mLST8 are common components between the two complexes. Image created using Biorender.com.*

1.1.5.2. mTORC1 signalling in normal physiological context

1.1.5.2.1. TSC1/TSC2/TBC1D7-mTORC1 axis

In normal cell physiology, stimulation from various extracellular and environmental signals including insulin, growth factors, glucose, hypoxia, and amino acids, initiates activation of a complex programme of signalling cascades that converge on the TSC1/TSC2/TBC1D7 heterotrimeric complex, which acts as a negative regulator on downstream mTORC1 (Dibble *et al*., 2012). Specifically, TSC2 acts as a GTPase-activating protein for a small GTPase protein called Rheb (as reviewed by Saxton and Sabatini, 2017). Active GTP-bound Rheb stimulates mTORC1

activity (Long *et al*., 2005; Sancak *et al*., 2007). The TSC1/TSC2/TBC1D7 complex is responsible for converting the active GTP-bound Rheb to inactive GDP-bound form, thereby controlling its downstream stimulation of mTORC1 activity (Inoki *et al*., 2003; Tee *et al*., 2003). An overview of physiological mTORC1 signalling is shown in **Fig. 1.5**.

1.1.5.2.2. Effectors upstream of mTORC1

Many pathways converge on the TSC1/TSC2/TBC1D7 complex, including components of the canonical Ras signalling pathway and different growth factors. In terms of receptor tyrosine kinase (RTK)-dependent Ras signalling, mitogen activated protein (MAP) Kinase ERK and its effector p90 ribosomal S6 kinase (p90RSK) cause phosphorylation and subsequent inhibition of TSC2 (Ma *et al*., 2005; Roux *et al*., 2004). Akt can also induce phosphorylation TSC2 causing its dissociation from and inactivation of the TSC1/TSC2/TBC1D7 complex, leaving Rheb in its active GTP-bound state signalling downstream to activate mTORC1 (Inoki *et al*., 2002). It has also been shown that Akt phosphorylates PRAS40 (component of the mTORC1 complex) which then dissociates from RAPTOR, revealing a mechanism by which Akt regulates mTORC1 activity independent of TSC1/TSC2/TBC1D7 (Sancak *et al*., 2007). Growth factors such as Wnt and Tumor Necrosis Factor α (TNFα) inhibit TSC1, which causes subsequent activation of mTORC1 (Inoki *et al*., 2006; Lee *et al*., 2007). Other extracellular environmental cues can affect intracellular mTORC1 signalling. For example, glucose deprivation activates AMPK, a metabolic regulator, induces an inhibitory effect on mTORC1 both directly and indirectly. Its direct mechanism of inhibiting mTORC1 arises from phosphorylating RAPTOR, while its indirect inhibition of mTORC1 comes via TSC2

phosphorylation and activation (Gwinn *et al.,* 2008; Inoki *et al*., 2003; Shaw *et al*., 2004). This glucose deprivation also can cause mTORC1 inhibition in cells deficient in AMPK, through inhibiting Rag GTPases (Efeyan *et al*., 2013). Hypoxia also exhibits its inhibitory effects on mTORC1 by a mechanism of activating AMPK and by inducing REDD1, which causes TSC1/TSC2/TBC1D7 activation (Brugarolas *et al*., 2004). Induction of p53 target genes, including AMPK-β, PTEN, and TSC2, also increases activity of the TSC1/TSC2/TBC1D7 complex (Feng *et al.,* 2007), indicating that also DNA damage-response pathways can also inhibit mTORC1.

1.1.5.2.3. Downstream effectors of activated mTORC1

mTORC1 mediates both anabolic processes, including cell growth, protein synthesis, and lipid synthesis; and catabolic processes including inhibiting autophagy via various downstream effectors. Downstream activation of S6K1 activity causes an increase in mRNA biogenesis, cap-dependent translation. Regulation of proteins such as ribosomal protein 6 (rpS6), S6K1 aly/REF-like target (SKAR), programmed cell death 4 (PDCD4), eukaryotic elongation factor 2 kinase (eEF2K) are involved in this process (as reviewed by Ma and Blenis, 2009). Ribosome biogenesis downstream of activated mTORC1 has also been shown to be promoted by transcription of ribosomal RNA, involving protein phosphatase 2A (PP2A) and transcription initiation factor IA (TIF-IA) (Mayer *et al*., 2004). Protein synthesis is enabled downstream of mTORC1 via the phosphorylation of the eukaryotic initiation factor 4E (eIF4E)-binding protein 1 (4EBP1) and the p70 ribosomal S6 kinase 1 (S6K1) (as reviewed by Saxton and Sabatini, 2017). Specifically, phosphorylation of 4EBP1 prevents 4EBP1-eIF4E binding, which releases eIF4E for cap-dependent translation (Sonenberg and Gingras, 1998).

Active mTORC1 also promote angiogenesis, via its mediation of hypoxia inducible factor-1 α (HIF-1α) following phosphorylation of STAT3 (under hypoxia) (Dodd *et al.,* 2015). Vascular endothelial growth factor A (VEGFA) can also be mediated downstream of this STAT3/HIF- 1α axis (Dodd *et al*., 2015).

Active mTORC1 acts as a positive regulator of glutamine metabolism by eliciting an inhibitory effect on sirtuin 4 (SIRT4) (Csibi *et al*., 2013). It is also involved in lipid synthesis via its signalling on sterol regulatory element binding protein 1 (SREBP-1) and its effect on the pentose phosphate pathway (Porstmann *et al*., 2008). mTORC1 also can regulate downstream processes involved in autophagy via ULK1 (Dunlop and Tee, 2014).

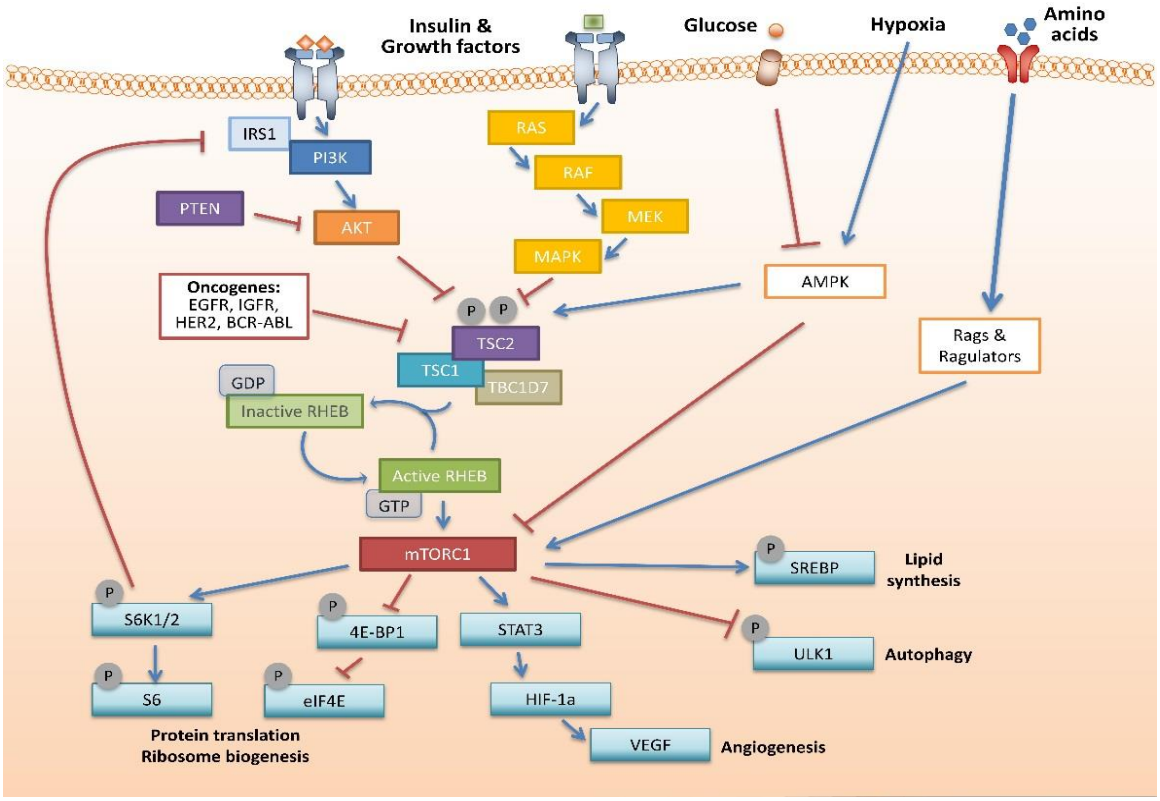

Figure 1.5: Schematic of physiological mTORC1 signalling cascade in a cell. *Published in Ní Bhaoighill and Dunlop, 2019.*

1.1.5.3. mTORC1 hyperactivity in TSC tumours

TSC1/TSC2/TBC1D7 heterotrimeric complex is an essential tumour suppressor complex, working in tandem to control cell growth and survival by negatively regulating mTORC1. Loss-of-function mutations in *TSC1* or *TSC2* causes destabilisation of the TSC1/TSC2/TBC1D7 complex, leading to failure of this tumour suppressor complex in acting as an essential negative regulator of mTORC1. These mutations cause the complex to lose its ability to act as a GTPase activity protein on Rheb, thereby leading to constitutive mTORC1 activity (Tee *et al*., 2003) and inappropriate signalling downstream of mTORC1, which promotes uncontrolled cell growth and proliferation, and protein translation (Northup *et al*., 2021). This mTORC1 hyperactivity is the hallmark intracellular driver of the development of TSC tumours (Schrötter *et al*., 2022).

TSC1 and TSC2 are also important regulators of downstream PI3K/mTOR/Akt signalling pathways, and are also implicated in MAPK, AMPK, β-catenin, and autophagy pathway modulation (as reviewed by Kozma and Thomas 2002; Astrinidis *et al*., 2003; El-Hashemite *et al*., 2003; as reviewed by Harris and Lawrence, 2003; as reviewed by Yeung, 2003; Au *et al*., 2004; Birchenall-Roberts *et al*., 2004; Mak & Yeung 2004; Zhang *et al*., 2013). The TSC1-TSC2 complex is also involved in the regulation of mTORC2 complex activity, which modulates Akt activation and cytoskeleton formation (as reviewed by Han and Sahin, 2011).

1.1.6. TSC diagnosis, management, and surveillance

1.1.6.1. Guidelines

In 1998, diagnostic criteria for TSC were first clarified (Roach, Gomez, and Northup, 1998) in accordance with updated medical knowledge and molecular understanding of the disease. This was the first to conclude that clinical signs once considered to be pathognomonic were less specific to TSC. In recognition of no single clinical feature being present in all TSC patients, and no clinical and radiographic sign being fully TSC-specific, the authors categorised TSC symptoms into major and minor criteria. This categorisation was based on the apparent extent of TSC specificity. A diagnosis of TSC could be given with clinical presentation of two or more distinct lesion types, instead of multi-growths in one organ (Roach, Gomez, and Northup, 1998). It is noteworthy that, at this time, the two genes *TSC2* (European Chromosome 16 Tuberous Sclerosis Consortium, 1993) and *TSC1* (van Slegtenhorst, deHoogt, Hermans *et al*., 1997) had been identified in TSC; but their molecular function had not been characterised.

Subsequently in 2012 and in 2020, these criteria were reviewed with the aim of introducing new recommendations for TSC diagnosis, surveillance, and management at the International Tuberous Sclerosis Complex Consensus Conference (Northup *et al*., 2013; Northup *et al*., 2020). Since TSC can manifest in variable inter-patient phenotypes, various permutations of features qualify for diagnosis. In the latest guidelines published by Northup *et al*., a definite clinical diagnosis of TSC is defined in a proband with presentation of two or more major features, or one major feature with two or more minor features (as summarised in

Table 1.1; Northup *et al*., 2020). It is important to note here that presentation of both LAM and AML does not constitute a definite clinical diagnosis of TSC. A possible TSC diagnosis is signified by presentation of one major feature, or two or more minor features. Given that clinical manifestations of TSC have high inter-patient variability, and present at various ages and progress at different rates, a molecular diagnosis is sufficient even in the absence of clinical symptoms. Molecular diagnosis of TSC occurs with the identification of a pathogenic variant in *TSC1* or *TSC2* by concurrent gene testing or the use a multi-gene panel (Northup *et al*., 2021). Detection of loss-of-function *TSC1* or *TSC2* mutations in somatic tissue is sufficient for a definitive diagnosis of TSC (as reviewed by Henske *et al*., 2016). However, failure to identify a mutation does not disqualify clinic-based diagnosis of TSC. With failure in mutation detection, clinicians can use a scoring system to diagnose disease from a combination of clinical and radiographic characteristics (as reviewed by Henske *et al*., 2016), against clinical diagnostic criteria consisting of major and minor disease features (as outlined in **Table 1.1**; adapted from Northup and Krueger *et al*., 2013).

1.1.6.2. Biomarkers

TSC1 or *TSC2* pathogenic mutations are the genetic biomarkers used for TSC diagnosis. However, there are currently no biofluid-based biomarkers for TSC, which is a major clinical need to enable earlier detection and diagnosis, monitoring of patients and family members that have tested genetically positive, therapeutic surveillance, and ultimately optimising patient outcomes. There is also a clinical need to have specific biomarkers per TSC phenotype, to help detect and predict

onset of the variability in TSC manifestations. Currently, serum VEGF-D expression of >800 pg/mL is used to diagnose TSC-LAM (Hirose *et al*., 2019).

1.1.6.3. Therapeutic strategies for TSC

1.1.6.3.1. Standard-of-care mTORC1 inhibition

Rapamycin, or rapalogs (e.g. everolimus/sirolimus) is the standard-of-care anti-tumour therapy for TSC (Northup *et al*., 2020). Its mechanism of action is in its allosteric binding to FK binding protein 12 (FKBP12) causing contraction of the mTORC1 dimer active site cleft from 20 Å to 10 Å (Aylett *et al*., 2016; Yuan and Guan, 2016). Therefore, rapamycin inhibits intracellular mTORC1 activity and shrinkage of certain types of TSC tumour is reported during the duration of its treatment regimen (Davies *et al*., 2011; Bissler *et al*., 2008). Everolimus was granted approval from the Food and Drug Administration (FDA) for TSC SEGAs and AML, and more recently a sirolimus-based topical gel was approved for TSC facial angiofibromas. AML tumour volume exhibited a mean (± S.D.) of 53.2 ± 26.6 % decrease with intravenous rapamycin treatment in serial magnetic resonance imaging (MRI) on TSC patients. However, AML tumours regrow to establish their pre-treatment volume with discontinuation of rapamycin treatment (Bissler *et al*., 2008; clinicaltrials.gov number: NCT00457808). As mTORC1 inhibition fails to have a cytotoxic effect on AML tumours with permanent eradication, investigating other signalling mechanisms that promote AML tumour growth could improve on anti-tumour therapy.

1.1.6.3.2. ATP competitive inhibitors and dual inhibitor therapy

Given the cytostatic limitations of rapamycin and rapalogs, some clinical trials have been conducted using drugs that target other oncogenic proteins that are activated as part of the compensatory mechanism to mTORC1 inhibition. For example, it is known that mTORC1 inhibition causes re-activation of Akt and MAPK signalling as a compensatory mechanism to sustain growth. One avenue of investigation is adenosine triphosphate (ATP) competitive inhibitors. These agents compete for the ATP binding pocket on both mTOR and PI3K, as they express high sequence homology within hinge domains of both protein kinases (as reviewed by Schenone *et al*., 2011; as reviewed by Laplante and Sabatini, 2012). The aim is to achieve a broader anti-tumour targeted treatment (as reviewed by Martellini *et al*., 2012). Trial results have been mixed (as reviewed by Ní Bhaoighill and Dunlop, 2019) and such dual targeting requires further pre-clinical development. However, since inhibiting various oncogenic intracellular drivers is limited in benefit, other in vitro findings may hold some promise clinically.

Other targetable mechanism in *TSC2*-deficient cells, such as their intrinsic elevated levels of endoplasmic reticulum (ER) stress due to increased protein translation and hindering of autophagy, Johnson *et al*. found that treating these cells with nelfinavir (increases ER stress) and bortezomib (proteosome inhibitor) combination therapy inhibited tumour formation in xenograft mouse models and had cytotoxic compared to rapamycin treatment alone (Johnson *et al.*, 2018). Another study showed cytotoxic effects with a nelfinavir/salinomyciin combination treatment regime at reducing tumour formation in TSC2-deficient models and in models of sporadic cancers with mTORC1 hyperactivity (Dunlop *et al*., 2017). Another study

found that treating *TSC2*-deficient cells with chloroquine (lysosomal/autophagy inhibitor) and Vps34 inhibitor reduced cell growth selectively in *TSC2*-deficient cells, and not in *TSC2*-expressing cells (Filippakis *et al*., 2017). Similarly, a clinical trial in LAM patients investigated the efficacy of combination therapy of an mTOR inhibitor with an autophagy inhibitor, hydroxychloroquine (El-Chemaly *et al*., 2017).
Another avenue of potential new targets may lie in elucidating the crosstalk networks between these tumour cells and their tumour microenvironment, an emerging feature of tumour biology therapy given its fundamental role in supplying the tumour with optimal environment to grow and develop. This key aspect of TSC tumour growth and development is largely unknown but may improve on current anti-tumour treatment limitations.

1.2. THE TUMOUR MICROENVIRONMENT (TME)

1.2.1. Introduction

A tumour biomass is comprised not only of a heterogeneous population of tumour cells, but also a dynamic milieu of resident and infiltrating host cells, secreted factors, and extracellular matrix components, collectively termed as the tumour microenvironment (TME) (Luga *et al*., 2012). The tumour microenvironment is typically defined as the surrounding proximal cells to a primary tumour biomass, and it is continually interacting with primary tumour cells to promote tumoral proliferation and vitality, and the pro-tumoral processes angiogenesis, invasiveness, and metastasis (as reviewed by Joyce and Pollard, 2009). Thus, the crosstalk between tumour cells and their TME is critical in ensuring tumour viability and metastatic potential, and ultimately tumour fate.

1.2.2. TME components

The TME is comprised of malignant tumour cells, extracellular matrix, cancer-associated fibroblasts, inflammatory immune cells, lymphatics, tumour-associated vasculature (Luga *et al*., 2012), pericytes and, in some cases, adipocytes (as reviewed by Balkwill *et al*., 2012). Components of the TME are typically identified by cell type-specific markers, which are usually expressed on the respective cell membranes (as reviewed by Balkwill *et al*., 2012). In particular, fibroblasts and cancer-associated fibroblasts have been widely implicated as a key TME component in tumour progression. Fibroblasts are spindle-like, elongated cells of mesenchymal origin, and are primarily characterised by positive expression of vimentin, an intermediate filament protein (Franke *et al*., 1978). Fibroblasts play a key role in tissue homeostasis by secreting collagen proteins and maintaining the extracellular matrix in order to preserve tissue architecture. They become activated in wound healing processes (Gabbiani *et al*., 1971) resulting in differentiation to a myofibroblast phenotype. Myofibroblasts deposit an altered extracellular matrix and facilitate angiogenesis. Furthermore, myofibroblasts are a contractile phenotype that eventually act to close the wound, before being removed from the site of injury. Cancer-associated fibroblasts are a highly differentiated and heterogeneous group of stromal cells that promote tumour proliferation, angiogenesis, and extracellular matrix remodelling (Pape *et al*., 2020). Activated fibroblasts are key drivers in stromal remodelling via collagen deposition and MMP secretion (as reviewed by Kalluri, 2016). They are known to be involved in many pro-tumoral processes including tumour growth, dissemination and metastasis, and resisting drug penetrance (Sahai *et al.,* 2020; as reviewed by Wu and Dai, 2017). Intercellular communication networks between tumour cells and cells of the surrounding

microenvironment are driven by signalling by growth factors, cytokines, chemokines, and immuno-modulating and matrix remodelling enzymes (Bawkwill *et al.*, 2012). CAF activation has been linked to EVs previously, in a study showing that EVs from ovarian cancer cells CABA I cell lines could activate normal fibroblasts to become more CAF-like in terms of both morphological and molecular features (Giusti *et al.*, 2022).

1.2.3. TME modifications by EVs

EVs mediate cell-cell communication between tumour cells and recipient cells within the tumour microenvironment and at distant sites, which ultimately plays an important role in promoting tumour-supporting processes to facilitate tumour growth and progression (Bao *et al*., 2022; as reviewed by Meehan and Vella, 2015). One mechanism by which tumour cell-derived EVs can achieve this is by activating signalling cascades in recipient cells. For example, epidermal growth factor receptor (EGFR)vIII associated with EVs were shown to merge with colorectal cells deficient in EGFRvIII, instigating signalling and subsequent invasion in a previously non-invasive cell line (Al-Nedawi *et al.*, 2008). Abd Elmageed et al. showed that EV-associated H-ras, N-ras, and Rab proteins could potentially downregulate tumour suppressors (Abd Elmageed *et al.*, 2014), while another study showed that EV-miRNAs could target tumour suppressors in recipient cells to silence them (Ostenfeld *et al.*, 2016). Another study by Grange and colleagues showed that EVs from renal cells could induce invasive phenotypes in pulmonary cancer ascites (Grange *et al*., 2011). EVs from tumour cells can mediate a pro-tumorigenic influence by aberrantly activating tumour stroma, via the delivery of TGF-β (Webber *et al*., 2010). This triggers stromal cell differentiation towards a myofibroblast-like

phenotype with pro-angiogenic function that can facilitate angiogenesis *in vitro* and tumour growth *in vivo* (Webber *et al.,* 2015). Other studies have also shown interactions of fibroblasts and EVs causing the secretion of various growth factors, such as HGF and VEGF, in response to EV treatment (Webber *et al.,* 2015).

1.2.4. TME in TSC tumour types

TSC2$^{-/-}$ cell morphology differs depending on the microenvironment. In renal AML, these cells appear as tri-phasic tumours of smooth muscle, densely vascularized, with adipose-rich components in various ratios. In LAM, these cells are spindle-shaped and epithelioid (Cai, Pacheco-Rodriguez, Fan *et al*., 2010). Little is known currently about how fibroblasts are modulated in these tumour types to promote tumour growth.

1.2.4.1. AML microenvironment

The crosstalk between TSC-associated tumour cells and their surrounding microenvironment is a key area of preclinical research (as reviewed by Lam *et al.,* 2018). There is evidence that shows some potential therapeutic benefit in targeting the microenvironment surrounding AML *TSC2*-deficient cells. Treatment with antibodies against PD1 and CTLA4 decreased AML tumour size in both subcutaneous allograft models and *Tsc2*$^{+/-}$ mice (Goncharova *et al*., 2011). The treated mice were found to have prolonged disease-free survival (>100 days) after treatment cessation (Goncharova *et al*., 2011), suggesting a potential targetable mechanism within the AML tumour microenvironment that could improve upon the cytostatic effects of standard-of-care mTORC1 inhibition.

1.2.5.2. LAM microenvironment

The LAM microenvironment has characteristic stromal alterations and lung destruction (Glasgow *et al*., 2010). It is hypothesised that multi-system spread of LAM could be caused by metastatic processes (Cai, Pacheco-Rodriguez, Fan *et al*., 2010; as reviewed by Henske, 2003; Grzegorek *et al*., 2013). It was found that LAM cells from *ex vivo* lungs (CD44v6/CD44), blood (CD235a), bronchoalveolar lavage fluid and urine had different proteins expressed of their surface (Cai, Pacheco-Rodriguez, Fan *et al*., 2010). This perhaps suggests that LAM cells arising from different microenvironments have different phenotypes, complementary to their known phenotypic heterogeneity in different tissues.

1.3. EXTRACELLULAR VESICLES (EVs)

1.3.1. Introduction

Extracellular vesicles (EVs) are a heterogeneous population of vesicles that are produced and secreted by virtually all prokaryotic and eukaryotic cell types (as reviewed by Veziroglu *et al*., 2020; Li *et al*., 2020) and are subcategorised based on their mode of biogenesis and secretion from their parental cell. EVs that originate from the endosomal compartment are *exosomes*, and EVs that arise from shedding of the plasma membrane are *microvesicles, oncosomes*, or *apoptotic bodies* (as reviewed by O'Brien *et al*., 2020). EVs are lipid bilayer-bound and luminal, which enables them to carry biological cargo from their parent cells. Once they are released from the parental cell membrane (as reviewed by Oggero *et al*., 2019), EVs carry this cargo into the extracellular space of the surrounding microenvironment and systemically in biofluids where they can elicit a variety of

biological processes and phenotypic modifications (as reviewed by Margolis and Sadovsky, 2019). Therefore, EVs embody a critical mechanism of intercellular communication between adjacent and distant cells and are implicated in numerous roles in both physiological and pathological settings (as reviewed by Beruman Sánchez *et al*., 2021).

1.3.2. Brief history of EV research

Determining vesicle characteristics and functionality was conducted subsequently to these initial biological observations of vesicles. A number of landmark studies, published in the 1980s, led to the coining of the term *exosome*. An ultrastructural study by Trams *et al*. described two distinct vesicle populations, becoming the first size-based classification of vesicle heterogeneity (Trams *et al*., 1981). Soon after, it was shown that maturing red blood cells could produce small vesicles to recycle transferrin and its cognate receptor (Harding *et al*., 1984). Johnstone *et al*. published a study based on multi-vesicular bodies (MVBs), containing intraluminal vesicles (ILVs) formed from the limiting membrane, which were then released from the cell when the MVB fuses with the plasma membrane (Johnstone *et al*., 1987). Later, exosomes from B lymphocytes were shown to be antigen-presenting and capable of T cell response induction (Raposo *et al*., 1996). Later discoveries of RNA content of EVs pioneered their status as mediators of intercellular communication (Valadi *et al*., 2007; Ratajczak *et al*., 2006). Taken together, these studies determined that cell-derived vesicles had functional implications in cell-cell communication and were not solely used as an extracellular waste disposal mechanism as previously thought.

1.3.3. EV structure

Exosomes are nanometre-sized luminal vesicles that, when viewed under transmission electron microscopy, are classically represented as spherical in configuration (as reviewed by Yellon and Davidson, 2014) though their shape is also malleable. Proteins on the surface of exosomes are used to characterise the vesicles, including families of tetraspanins (CD9, CD63, CD81), lysosomal proteins (LAMP2B), fusion proteins (CD9, annexin, flotillin), and heat shock proteins (Hsp90) (Conde-Vancells *et al*., 2008). The proteins are usually exclusive in expression on exosome surfaces, thereby serving as characterisation markers to distinguish exosomes from other EV subtypes (as reviewed by Lee *et al*., 2012). However, it is important to note that the existence of a single exosome-specific protein have not yet been identified, and a multi-parameter approach at characterising isolates is essential to best determining the likely nature of a particular EV subtype (Lässer *et al*., 2012; Théry *et al*., 2018).

1.3.4. EV biogenesis

Biogenesis of small vesicles of endosomal origin begins with the formation of the early endosome from the plasma membrane, which matures to become a late endosome (Stoorvogel *et al*., 1991). Invagination of the limiting membrane of this late endosome forms hundreds of ILVs. During this development of ILVs, certain proteins are integrated into the invaginating membrane, while other cytosolic components become encased within the ILVs (as reviewed by Johnsen *et al*., 2014). This ILV-containing endosome is referred to as a multivesicular body (MVB) (Trajkovic and Hsu *et al*., 2008) in the cell cytoplasm. With the process of

endosome maturation, MVBs can fuse with the plasma membrane in a Rab GTPase-dependent fashion to secrete their encased ILVs, now referred to as *exosomes*, into the extracellular space to interact with recipient cell populations. MVBs can also be translocate to the lysosome for degradation (as reviewed by Teng and Fussenegger, 2021). A summary of this EV biogenesis is shown in **Fig. 1.6**.

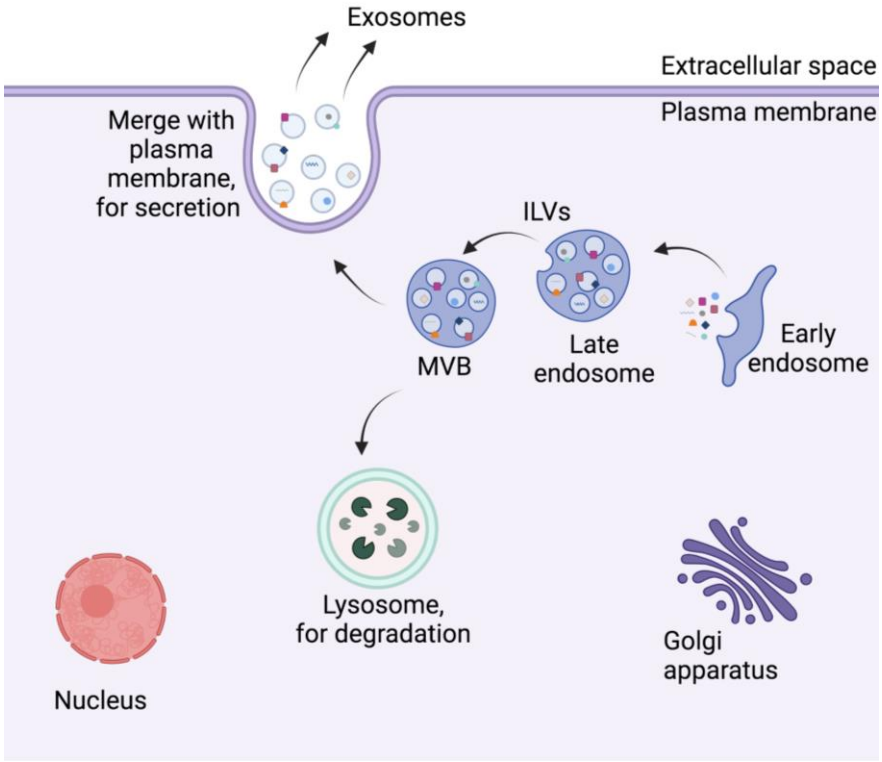

Figure 1.6: Schematic of exosome biogenesis in a eukaryotic cell. *Invagination of the early endosomal membrane generates ILVs, eventually forming MVBs as the endosome matures. This process is mediated by ESCRTs, syndecans, and tetraspanins. MBVs translocate in one of two directions: 1) to fuse with to plasma membrane, secreting the vesicles as exosomes into the extracellular space; or 2) to the lysosome for degradation. Fusion with the plasma membrane is facilitated by ESCRTs, SNARE proteins, and ARF6. Intraluminal vesicles, ILVs; multi-vesicular bodies, MVBs; endosomal-sorting complexes required for transport, ESCRT; ADP Ribosylation Factor 6; ARF6. Image created using Biorender.com.*

Various mechanisms for the formation of MVBs have been reported. This includes both endosomal-sorting complexes required for transport (ESCRT)-dependent and –independent mechanisms. The ESCRT machinery controls membrane budding at

cells membrane and late endosome membrane levels (as reviewed by Raiboug and Stenmark, 2009), and ESCRT-dependent MVB generation is the most extensively described mechanism for its responsibility of protein sorting into ILVs (as reviewed by Hurley *et al*., 2008; Schmidt *et al*., 2012). The ESCRT machinery is composed of early-acting complexes ESCRT-0, ESCRT-I, and ESCRT-II; and late-acting components ESCRT-III and vacuolar protein sorting 4 (Vps4). ESCRT-0, ESCRT-0, ESCRT-I, and ESCRT-II are involved in mediating the sorting of ubiquitinated cargo, while ESCRT-III and Vsp4 are involved in ending EV formation and budding. The ESCRT subunits ESCRT-0, ESCRT-I, and ESCRT-II have ubiquitin-binding subunits that mediate the sorting of ubiquitous membrane proteins onto specific domains of both the endosomes and also within the endosomal invaginations (Baietti *et al*., 2012). Specifically, ESCRT-0 holds ubiquitinated proteins within the membrane of the late endosome. ESCRT-I/II instigates the initial invagination of the limiting membrane of the MVB, allowing a spiral-shaped ESCRT-III to constrict the budding neck to encapsulate the vesicle (as reviewed by Frankel and Audhya, 2018). ATPase Vps4 is responsible for dissembly of the ESCRT-III complex (as reviewed by Mir and Goettsch, 2020). Even though ESCRT machinery-dependent mechanisms in MVB formation have been delineated, it is still elusive if the fate of MVBs formed by ubiquitin-dependent processes is lysosomal degradation or for membrane fusion to allow exosome release (as reviewed by Bebelman *et al*., 2018). It is also known that the ubiquitinated cargo loses their ubiquitin tags via the de-ubiquitinating enzyme-associated molecule with the SH3 domain of STAM (Agromayor and Martin-Serrano, 2006), before vesicle membrane scission.

Another mechanism for MVB formation involves sphingomyelin ceramide. Sphingomyelinase 2-induced hydrolysis of sphingomyelin generates ceramide, which was shown to induce negative MVB membrane curvature via its characteristic cone shape, causing ILV budding into MVBs (Trajkovic *et al*., 2008). Proteins from the tetraspanin family have also been implicated in ESCRT-independent processes of EV biogenesis.

Protein cargo sorting into ILV can also proceed by ubiquitination-independent processes. Syntenin, a small cytosolic adapter protein, is responsible for linking syndecan to ESCRT-III-associated protein ALIX (Baietti *et al.,* 2012). Heparanase-induced cleavage of heparin sulphate chains causes syndecan clustering to trigger syntenin-ALIX-ESCRT-mediated sorting and exosome formation (as reviewed by Bebelman *et al*., 2018). It was also shown that GTPase ADP ribosylation factor 6 (ARF6) and effector protein phospholipase D2 (PLD2) specifically regulates syntenin-mediated CD63 ILV budding (Ghossoub *et al*., 2014). Various transmembrane proteins are associated with EVs, including cluster of differentiation (CD) 9 (CD9), CD63, and CD81 (Kowal *et al*., 2016). These proteins are commonly used as markers for EVs, due to their enrichment in EVs compared to whole cell lysates (Mathieu *et al*., 2021).

RAS-related protein (Rab) GTPases mobilise MVBs towards the cell periphery, where they dock and fuse with the plasma membrane to secrete the ILVs, now exosomes, into the extracellular space. It has also been indicated that subpopulations of vesicles could be regulated by different Rab-related processes (Yeung *et al*., 2018), which could have diverging functional effects. Different Rabs

have also been implicated in different cell line models of EV secretion, but evidence of Rab27a and Rab27b (Ostrowski *et al*., 2010) involvement has been observed in many cancer cell *in vitro* and *in vivo* studies (Peinado *et al*., 2012), considered to have a stabilising effect on actin filaments of the MVB docking site (Sinha *et al*., 2016). Soluble Nethylmaleimide sensitive fusion attachment protein (SNAP) receptor (SNARE) complexes are important for the fusion and subsequent secretion of exosomes from the plasma membrane (Verweij *et al*., 2018). Various SNAREs, such as VAMP7, syntaxin 1A, and SNAP23, have been implicated in different models studying EV secretion (as reviewed by Teng and Fussennegger, 2021).

1.3.5. Defining and distinguishing EVs

As previously described, EVs are a heterogeneous group of vesicles consisting of various subtypes including exosomes, microvesicles, and apoptotic bodies (as reviewed by O'Brien *et al*., 2020). These EV subtypes are distinguishable based on the subcellular site of their biogenesis. Key differentiating characteristics of these EV subtypes are summarised below in **Table 1.2**. However, it is currently difficult experimentally to discriminate between EV subtypes due to technical limitations of several isolation methods and characterisation techniques. Furthermore, EV subtypes also have similar morphologies, overlapping ranges of size, and consensus on membrane and molecular markers is still to be reached. Therefore, a major focus of the EV research field is on advancing techniques to distinguish EV subtypes from one another. Given the difficulties in nomenclature, the term *extracellular vesicles* was encouraged for use and includes all secreted vesicles (Gould and Raposo, 2016; Théry *et al*., 2018). The International Society of

Extracellular Vesicles (ISEV) published a position paper in attempt to standardise EV studies in terms of distinctions between isolated EV populations and necessary information for reporting of EV isolation and characterisation steps (Théry *et al*., 2018).

Table 1.2: Summary of EV subtypes

EV subtype	Subcellular origin	Size	Centrifugal force for isolation (*x g*)	Proteins and protein classes required for biogenesis
Exosomes	Multivesicular bodies (MVBs)	20-150 nm	100,000	ESCRTs Rab proteins Tetraspanins Syndecan Syntenin ATG12 NSMase
Microvesicles	Plasma membrane	100-1000 nm	10,000	ASMase Flippase Scramblase ARF6
Apoptotic bodies	Apoptotic blebs	0.8-5.0 μm	2000	Annexin V Caspase 3

1.3.6. EV isolation

EVs can be isolated from cell-conditioned media and biofluids using a variety of techniques, including differential ultracentrifugation, ultrafiltration, size-exclusion chromatography (SEC), density gradient centrifugation, isolation using polymer precipitation e.g. poly-ethylene glycol precipitation (PEG) agents; immuno-affinity capture, and microfluidics. The key principles of these techniques in their use to isolate EVs is summarised in **Table 1.3**. Each technique has associated advantages and disadvantages that should be considered when selecting a method to isolate EVs, particularly when attributing cargo and/or interpreting function to particular EV isolates (Chiriacò *et al*., 2018; Zhang *et al*., 2018).

Table 1.3: EV isolation techniques and their associated advantages and disadvantages (adapted from Chiriacò *et al*., 2018).

EV isolation technique	Principle	Potential advantages	Potential disadvantages
Differential ultracentrifugation	Size	• Large source volume • Widely available equipment	• Co-pelleting of non-vesicular material with EVs • Not applicable to small volumes • Time-consuming • Differences in rotors/ ultracentrifugation times may affect reproducibility
Ultrafiltration	Weight or size	• High purity of EV isolate • Quick to conduct	• Contamination risk with non-vesicular material
Size-exclusion chromatography (SEC)	Size (gravity-dependent)	• Easy to conduct • High purity and reproducibility • Minimal disruption to EV structure and integrity • Sample not contaminated in process	• Time-consuming fractionation • Risk of low yield • Contamination of proteins of equal size
Density gradient centrifugation	Density	• Large source volume • Widely available equipment • High purity of EV isolate	• Contamination risk of gradient material in EV isolate • Not applicable to smaller source volumes • Time-consuming
Polymer precipitation e.g. polyethylene glycol (PEG)	Solubility or aggregation	• EV integrity maintained	• Contamination of EV isolate by polymer used
Immuno-affinity capture	Marker: vesicle surface proteins	• High purity of EV isolate • Easy and quick to conduct • Non-target vesicles remain unbound and so are removed	• Instability • Appropriate for small volume only • Low yield • Capture EVs with specified markers only
Microfluidics	Marker: vesicle surface markers Size Acoustics	• High purity of EV isolate, in shorter period of time • Quick to conduct • Small volume of sample required • More selective on parameters used to isolate EVs (e.g. specified size) • Contact-free	• Expensive • Specialised equipment may be expensive • Low yield • Capture EVs with specified markers only

Given the development of multiple techniques, and each with their associated considerations and caveats, there remains a lack of consensus on which one technique is optimal for EV isolation (Théry *et al*., 2018). Commonly used techniques for bulk EV isolation are differential centrifugation and ultracentrifugation (Johnstone *et al*., 1987; Gardiner *et al*., 2016; Théry *et al.*, 2018), which can be combined with further ultracentrifugation on a sucrose or iodixanol gradient (Raposo *et al*., 1996; Lamparski *et al*., 2002; Théry *et al*., 2006; Iwai *et al*., 2016). Though these techniques are widely used, they are time-consuming to complete and their application to larger sample volumes may limit their application to clinical settings. Thus, this affirms the importance of accurate reporting of used experimental parameters in EV isolation. EV-TRACK is an online knowledgebase platform that was created to collate experimental parameters of EV-related studies, in order to document the evolution of EV research and facilitate optimal reproducibility and interpretation of EV experimental results (van Deun *et al*., 2017).

1.3.7. EV characterisation

The 2018 ISEV position paper, titled *Minimal information for studies of extracellular vesicles 2018 (MISEV2018): a position statement of the International Society for Extracellular Vesicles and update of the MISEV2014 guidelines* (Théry *et al*., 2018) proposed recommended criteria for standardisation of EV characterisation. This includes assessment of key parameters such as size, molecular composition, and potential origin of EVs within an EV isolate. This includes the use of multiple complementary techniques to demonstrate presence or enrichment of EV markers, and the absence or depletion of non-vesicular contaminants, when attributing contents and/or function to the studied EV population. Although EVs derived from

human and mouse cells/subjects have been the primary models used in EV research to date, MISEV guidelines are considered to be applicable all species, cells, and conditions (Théry *et al*., 2018). Specific guidelines and recommendations for other species and experimental conditions will be developed with more investigations of EVs from different model origins. The MISEV authors established recommendations to be considered for bulk EV characterisation, that includes: i) reporting quantification of EV source (i.e. number of cells/total starting volume of biofluids); and EV preparation (i.e. a global quantification of EVs, including total protein and total particle number, and a purity measurement such as protein:particle ratio). These guidelines also detail molecular markers that are recommended for use in EV characterisation, and discussed in subsection ***1.3.8.2.1***.. General guidelines regarding EV markers specify the inclusion of at least three EV protein markers, and that these should include one transmembrane protein, one cytosolic protein, and one negative protein marker (Théry *et al*., 2018). In this Thesis, vesicles isolated and studied are referred to small extracellular vesicles (sEVs) and include a population of EVs that are enriched for endosomal-associated proteins and express tetraspanin surface markers and are between 20 and 150 nm in diameter.

1.3.8. EV cargo

Transmembrane trafficking of biological material is an evolutionarily conserved process and contributes to cell homeostasis and disease (as reviewed by Azmi *et al*., 2013). EVs traffick bioactive material, encased in their protective lipid bilayer, into the extracellular space, where they can make contact with surrounding and distant recipient cell populations. The functionality of EVs is dependent on their

packaged cargo and their secretion and uptake dynamics (as reviewed by Bebelman *et al*., 2018). EV cargo includes an assortment of nucleic acids, proteins, and lipids (as reviewed by Mathieu *et al*., 2019), representative of their parental cells (as reviewed by Kao and Papoutsakis, 2019). Many studies profile the impact of delivery of EV cargo as a whole (as reviewed by Mathieu *et al*., 2019), while others aim to specify EV cargo components that are responsible and essential for execution of specific biological functions in recipient cells. To date, the literature has been particularly focused on the functional roles of EV-RNAs and EV proteins in the cancer biology field, as discussed below. **Figure 1.7** depicts a representative schematic of EV composition and cargo.

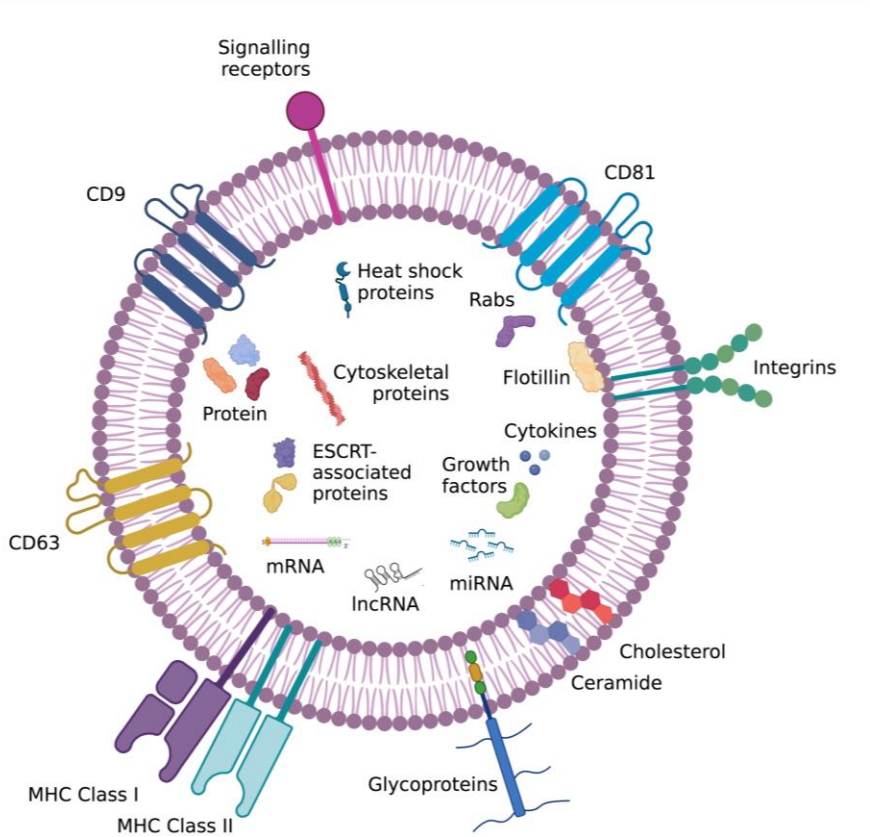

Figure 1.7: Representative schematic of EV composition and cargo. *Molecules represented at the bilayer membrane include tetraspanins CD9, CD63, and CD81; antigen-presenting molecules MHC Class-II and Class-II; signalling receptors, integrins, lipids cholesterol and ceramide; and glycoproteins. Intraluminal cargo shown represents various protein (cytosolic, cytoskeletal, ESCRT-associated, heat-shock proteins, Rabs, flotillin, growth factors, cytokines) and RNA species (mRNA, lncRNA, miRNA). Image created using Biorender.com. Relevant references: Šabanović et al., 2021.*

1.3.8.1. EV-RNA cargo

1.3.8.1.1. RNA biotypes in EVs

EVs contain a diversity of RNA biotypes, including protein-coding mRNAs; and both long non-coding RNA (lncRNA), and short non-coding RNAs, such as micro RNAs (miRNAs), circular RNAs, transfer RNA fragments, vault RNA, piwi-interacting RNA, and Y RNA (as reviewed in Li *et al*., 2018; as reviewed by O'Brien *et al*., 2020). Interestingly, it is thought that EVs secreted from a particular cell type tend to be enriched for a different RNA profile than their parental cells (Guduric-Fuchs et al.,

2012). Studies investigating how particular RNA biotypes are loaded into EVs are underway.

1.3.8.1.2. RNA loading into EVs

Differential enrichment of specific miRNAs in EVs has been reported in numerous studies (Skog *et al*., 2008; Valadi *et al*., 2007; as reviewed by Kosaka *et al*., 2010; Wei *et al*., 2017). While varying miRNA stability or passive packaging of miRNAs in EVs could explain this differential loading, uncovering the specific loading mechanisms that regulate miRNA loading into EVs remains a key focus within the EV community (Mateescu *et al*., 2017). In the literature to date, RNA sequence motifs and RNA-binding proteins were found to be largely responsible for RNA sorting and loading into EVs (as reviewed by Corrado *et al*., 2021). Mechanisms that describe endogenous miRNA loading into EVs are the best elucidated to date. Shurtleff *et al*. identified YBX1 as the RNA-binding protein responsible for packaging of miR-223 into EVs *in vitro* and subsequent secretion from its parental cells (Shurtleff *et al*., 2016). Villarroya-Beltri *et al*. identified the sequence motif GAGG, which is shared by a subset of miRNAs, which could control miRNA loading into EVs. The GAGG sequence binds to the protein called heterogeneous nuclear ribonucleoprotein A2B1 (hnRNPA2B1). This process appears to be regulated by the SUMOylation of hnRNPA2B1, a post-translational modification that can mediate protein stability and cellular trafficking (Villarroya-Beltri *et al*., 2013). Another RNA-binding protein called SYNCRIP was found to bind miRNAs sharing the short hEXO motif, enriched in EVs (Santangelo *et al*., 2016). In this study, the hEXO motif was shown to increase miRNA loading into EVs. The authors also published evidence of SUMOylation of SYNCRIP, suggesting that this post-translational modification

may be an important component of miRNA loading into EVs. One miRNA loading mechanism involves argonaute2 (AGO2), a protein associated with the RISC complex involved in RNA silencing, which was shown to mediate miRNA loading into EVs (Guduric-Fuchs *et al*., 2012) and ribonucleoproteins (Arroyo *et al*., 2011). It is important to note, though, that there is some contradiction as to whether AGO2 is associated with EVs (Li *et al*., 2012; as reviewed by Abels and Breakefield, 2016) or if it localises intracellularly (Gibbings *et al*., 2009).

In the case of mRNAs, it was found that a 3'UTR sequence motif for certain mRNAs enriched in EVs may serve as a 'zipcode' that can target mRNAs into EVs (as reviewed by Abels and Breakefield, 2016). For example, Bolukbasi *et al*. identified a 25-nucleotide sequence with a short CTGCC core domain on a stem-loop structure, which carries a miR-1289 binding site (Bolukbasi *et al*., 2012). It was proposed that interaction between this miRNA and the zipcode increases packaging of RNAs containing this sequence into EVs.

1.3.8.2. EV protein

1.3.8.2.1. Protein types in EVs

EV protein cargo can contain cytosolic proteins, transcription factors, receptors, enzymes, cytokines, metabolites, and growth factors. Analysis of EV-associated proteins can be divided into two strands: proteins that are associated with EV biogenesis, formation, secretion and docking; and proteins within the EV cargo that contribute to cellular processes when delivered to recipient cells. Proteins associated with mechanisms of EV biogenesis, such as ALIX and TSG101, and EV formation and release, including RAB27A, RAB11B, and ARF6, are commonly

found and enriched in EVs (as reviewed by Abels and Breakefield, 2016). Tetraspanins CD9, CD63, CD81 (Théry *et al*., 2018), and CD82 (Escola *et al*., 1998), proteins mediating signal transduction (Epithelial Growth Factor Receptor, EGFR), antigen presentation (MHC-1 and MHC-II), and transmembrane proteins such as LAMP1, are also detected in EVs (as reviewed by Abels and Breakefield, 2016; Simpson *et al*., 2012). Other protein families have also been found enriched in EVs, including a disintegrin and metalloproteinases (ADAMs) and lysosome-associated membrane proteins (LAMPs). These proteins can be used to characterise EVs to distinguish them from other vesicular components of the cell secretome. Other EV cargo proteins are known to induce both disease-protective (Jiang *et al*., 2022) and disease-promoting roles (Peinado *et al.,* 2012; Costa-Silva *et al*., 2015; Millimaggi *et al*., 2007; Clayton *et al*., 2007; Webber *et al*., 2015). Understanding how specific EV cargo functions is valuable in determining the mechanisms by which EVs promote disease processes and will highlight novel targets for improved therapies.

1.3.8.2.2. Protein loading into EVs

While there are several studies detailing different mechanisms of miRNA loading into EVs, there is currently much less understood about how proteins are selectively loaded into EVs. One study indicates that proteins associated with the plasma membrane as an oligomeric complex can be loaded into EVs (Yang and Gould, 2013). Other concepts for protein loading are EV subtype-dependent; for example, a blebbing ectosome (microvesicle type) will contain cytosolic and plasma membrane proteins that are not selectively loaded.

1.3.9. EV uptake by recipient target cells

Following their secretion from parental cells, EVs interact with recipient cells to activate intracellular signalling cascades and modify cell phenotypes. EVs can directly fuse with the plasma membrane of a recipient cells, enabling delivery of the EV cargo to the target cells to induce phenotypic modifications. EVs can also be internalised by recipient cells via endocytosis, pinocytosis/phagocytosis, and macropinocytosis (as reviewed by Johnsen *et al*., 2014; as reviewed by Kwok *et al*., 2021; as reviewed by Teng and Fussenegger, 2021). Endocytic uptake of EVs by recipient cells has been demonstrated in the literature, and can be mediated by several protein-protein interactions. Clathrin-mediated endocytosis is facilitated by clathrin-coated vesicles, which induce degradation of the membrane and generation of a vesicular bud that detaches from the cell membrane. Once internalised in the recipient cells, these clathrin-coated vesicles are uncoated so fusion with the endosome occurs with associated release of their contents (as reviewed by Kaksonen and Roux, 2018). Akin to clathrin-mediated endocytosis, endocytosis can also involve caveolin. Caveolin-dependent endocytosis takes place when small invaginations are created in the plasma membrane. These are known as caveolar vesicles that detach and are internalised by the cell. Caveolin proteins, such as caveolin-1, were previously found to induce this caveolae formation (Costa Verdera *et al*., 2017). Oligomerisation of caveolins via their oligomerisation domains is required for the assembly of caveolin-rich rafts in the plasma membrane (Parton *et al*., 2020). Lipid rafts are microdomains within the plasma membrane that have dynamic composition of phospholipids, sphingolipids, cholesterol, and glycophosphatidylinositol (GPI)-anchored proteins (as reviewed by Sezgin *et al*., 2017). These lipid rafts act as scaffolds for signalling complexes, and

are involved in membrane fluidity and trafficking of proteins (as reviewed by Lajoie and Nabi, 2010). Thus, lipid rafts are important in these clathrin-mediated and caveolin-dependent endocytic mechanisms and can be found in clathrin- and caveolar-coated vesicles (as reviewed by Kwok *et al.*, 2021). Furthermore, lipid rafts can be abundant in flotillin-enriched sections of the membrane, whereby they facilitate endocytosis (Frick *et al*., 2007; as reviewed by Meister and Tikkanen, 2014).

Macropinocytosis is another mechanism of EV uptake by recipient cells, and is a process dependent on the Na^+/H^+ exchanger and cholesterol. This enables activated rac1 GTPase to alter the actin cytoskeleton at the invaginating sites (as reviewed by Kerr and Teasdale, 2009; Grimmer *et al*., 2002). This invagination causes 'ruffled' extensions of the plasma membrane that pinch off to the intracellular space. EVs then become trapped and absorbed in fusion with these protrusions (as reviewed by Bloomfield and Kay, 2016). Alternatively to macropinocytosis, phagocytosis is another process of EV uptake in which membrane invaginations encase the material to be internalised (as reviewed by Feng and Levine, 2010), and does not require direct contact with internalised material or the use of membrane ruffles (as reviewed by Gordon, 2016).

Direct fusion of EV with the cell membrane of a recipient cell is also possible. This is facilitated by the close contact of the two lipid bilayers of both the EV and the cell, which in proximity forms a fusion stalk. This generates an expanded diaphragm layer, which causes a pore to form when the two hydrophobic cores come together (as reviewed by Jahn *et al*., 2003; Chernomordik *et al.*, 2008; as reviewed by Jahn

et al., 2006). SNARE proteins and Sec1/Munc-18 related proteins (SM-proteins) are known to be involved in this direct fusion (as reviewed by Südhof and Rothman, 2009).

1.3.10. EV functionality

1.3.10.1. EV-RNA function in cancer

Much of the interest in EV research actually began with the discovery of horizontal transfer of mRNAs and miRNAs between cells (Valadi *et al*., 2007). This has been supported by numerous subsequent publications on the horizontal transfer of EV cargo that can modulate and modify recipient cell behaviours (as reviewed by Corrado *et al.,* 2021). In the cancer setting, tumour-derived EV-RNAs have been implicated in promoting tumour growth, modifying the tumour microenvironment to optimise a tumour-supporting environment, and facilitating metastasis. RNA sorting into EVs is considered to be dependent not only on their size but also upon RNA origin. It is reported that RNA polymerase II transcripts are preferentially packaged into EVs (Mosbach *et al*., 2021). EV-associated RNAs have been shown to be implicated in many disease processes and clinical applications, such as promoting cancer cell phenotypes, facilitating disease progression, embody cell surrogates in regenerative medicine, and as a putative source of minimally-invasive molecular biomarkers (as reviewed by Fabbiano *et al*., 2020).

The advantage of EV-packaged RNA is the protective EV lipid bilayer membrane protects the RNA cargo from RNase digestion in the extracellular space (as reviewed by Prieto-Vila *et al.*, 2021; as reviewed by O'Brien *et al*., 2020). Furthermore, other EV contents can be used to stabilise RNA cargo. EV-

associated ribonucleoproteins (RNPs), such as argonaute 2, and high- and low-density lipoproteins, are enriched in EVs or artificially enriched in EV fractions, depending on EV isolation method (Arroyo *et al*., 2011; Vickers *et al*., 2011; as reviewed by Vickers and Remaley, 2012).

1.3.10.2. EV protein function in cancer

Tumour-derived EVs can promote many different tumour-supporting functions at both the local and distal levels. For example, tumour cell-derived EVs were found to promote angiogenesis in endothelial cells in many cancer types including chronic myeloid leukaemia (Mineo *et al*., 2012), glioma (Kucharzewska *et al.*, 2013), and squamous cell carcinoma (de Andrade *et al*., 2017). Additionally, prostate tumour-derived EVs were found to stimulate angiogenesis and invasion in mesenchymal stem cells (Chowdhury *et al.*, 2015). Furthermore, tumour-derived EVs displaying TGF-β on their surfaces can activate fibroblasts into a myofibroblast phenotype (Webber *et al*., 2010) capable of supporting tumour growth *in vivo* (Webber et al., 2015). Tumour-derived EVs have also been implicated in immunosuppressive mechanisms that support cancer progression. One study showed that vesicular TGF-β and IL-10 can promote immunosuppressive effects (Rong *et al*., 2016), and vesicular TGF-β is involved in downregulating NKG2D/KLRK1 to inhibit natural killer cells (Clayton *et al*., 2008; Szczepanski *et al*., 2011). Pre-metastatic niche formation can also be supported via EV-mediated mechanisms from the primary tumour cells. In melanoma models, EVs preferentially targeted to lymph nodes, induce a permissive environment for metastasis (Hood *et al*., 2011). Furthermore, melanoma EVs educate bone marrow progenitors, leading to their recruitment and development of an optimal pre-metastatic niche (Peinado *et al*., 2012). Tumour-

derived EVs have also been found to regulate organotropism specifically towards metastatic sites, which they target due to the distinct integrin combinations that they transport (Hoshino *et al*., 2015). Thus, determining how EVs function both in surrounding cells of the tumour microenvironment, and at distant sites can reveal important insights into disease development and progression.

1.3.10.3. EVs in TSC/mTORC1 signalling

Studies to examine the role of EVs in TSC tumour pathogenesis specifically are limited. One study showed that EVs from *Tsc1*-null cells induce a disease-like phenotype in neighbouring wild-type cells *in vivo* (Patel *et al*., 2016). This was found to be mediated by EV-associated Notch and Rheb mRNA delivery to recipient cells, which caused the reactivation of mTOR and Notch pathways (Patel *et al*., 2016). Another study described a link between mTOR signalling and exosome secretion, in which the authors identified Proline-rich Akt substrate 40 (PRAS40) as the first known regulator of stress-induced TGF-α-triggered exosome secretion (Guo *et al*., 2017). It was also shown to act as a common regulator of microenvironmental and oncogenic signalling-induced exosome secretion in both non-transformed and tumour cell types (Guo *et al*., 2017). Other studies have shown that exosome populations could activate mTOR signalling. Cardiac progenitor cell-derived exosomes stimulated H9C2 cell growth by Akt/mTOR activation, in a time-dependent manner (Li *et al*., 2018). Exosomes isolated from irradiated donor cells were cell growth-promoting due to increased Akt/mTOR signalling, with phosphorylated ribosomal S6 (p-rpS6) and MMP2/9 matrix metalloproteinase-2 (MMP-2) and –9 (MMP-9) activity as the underlying mechanism (Mutschelknaus *et al*., 2017). *PI3K/AKT/MTOR* gene expression was

reported to be significantly higher in both cervical cancer tissues and exosomes isolated from vaginal secretions, compared to non-transformed adjacent tissues, but the authors did not detect downstream mTOR signalling components or other global changes to EVs (Zhang *et al*., 2019). *PI3K/AKT/MTOR* gene expression increased positively with malignancy in the cervical cancer tissues, but it is not reported whether or not this was mirrored in isolated exosomes (Zhang *et al*., 2019). It was also previously shown that tailored mesenchymal stem cells, enriched for miR-17-92, increased axonal growth and activated PTEN/mTOR signalling in recipient neurons (Zhang *et al*., 2013). While mTOR signalling components have been detected in secreted EVs from various cell types, alterations to cargo and function of EVs from cells with aberrant mTORC1 activity is not well understood, despite altered mTORC1 expression impacting global protein networks within these cells.

Few studies that have investigated EVs from TSC cysts and tumours (driven by mTORC1 hyperactivity) have been published to date. The first of these studies revealed that Notch and Rheb mRNAs in EVs from *Tsc1*-deficient cells could activate Notch and Rheb signalling in recipient wild type cells (Patel *et al*., 2016). The authors also reported a similar mechanism in AML cells, where Rheb from TSC2-deficient AML cell-derived EVs could activate mTOR and Notch signalling in recipient AML cells depleted of Rheb (Patel *et al.*, 2016). Another study employed *Tsc2*-expressing and *Tsc2*-deficient mouse embryonic fibroblast (MEF) cells to investigate EV secretion and protein and miRNA cargoes alterations following rapamycin treatment, the standard-of-care therapy for TSC patients with AML (Zou *et al.*, 2019). This study showed that *Tsc2*-deficient MEFs secreted significantly

less EVs than the *Tsc2*-expressing MEFs *in vitro.* The same paper reports that rapamycin treatment caused an increase in EV secretion from HeLa cells finding some miRNAs with increased expression, namely hsa-miR-10b-3p, hsa-miR-409-3p, and 5 other miRNAs with unknown sequences; and decreased expression of hsa-let-7c-5p, hsa-miR-941, hsa-miR-328-3p, and hsa-miR-455-5p. EV protein cargo was found to be largely similar between control- and rapamycin-treated Hela cells, with approximately 1.5-fold increases in ENO1 and GAPDH proteins noted in rapamycin-treated cells (Zou *et al.*, 2019). Bissler and colleagues reported that intercalated cells (from renal epithelia) treated with EVs from *Tsc2*-deficient mouse inner medullary collecting duct (mIMCD3) cells had a higher phospho-S6/S6 ratio compared to cells treated with cells treated with media or *Tsc1*-deficient cell-derived EVs (Bissler *et al*., 2019). Another study published by Zadjali *et al*. demonstrated that *Tsc2*-deficient mIMCD3 cells secreted a two-fold increase in EVs compared to *Tsc2*-expressing mIMCD3 cells (Zadjali *et al*., 2020), and that these EVs are enriched for proteins involved in various pathways linked to proliferation, primary cilia, and stress responses (Zadjali *et al*., 2020). Using the same parental cell line, Kumar *et al*. investigated cells with CRISPR/Cas9-edited mIMCD3 *Tsc1* and *Tsc2* knockouts, to compare EV secretion and signalling activation capacity between the two TSC genotypes (Kumar *et al*., 2021). The authors report that *Tsc1*-deficient cells had reduced EV secretion compared to their *Tsc2*-deficient counterparts, while downregulation of various miRNAs in *Tsc2*-deficient compared to *Tsc1*-deficient cells. It was also shown in this study that EVs from *Tsc1*- and *Tsc2*-deficient cells had different capacities in activating various signalling pathways including mTORC1, autophagy, and β-catenin (Kumar *et al*., 2021). However, no studies to date have been conducted using a patient-derived

model of AML or comparing EVs from *TSC2*-expressing and *TSC2*-deficient AML cells, in a short- or long-term culture. Furthermore, cargo associated with these EVs patient-derived model and the differences that may come downstream of the different genotypes is also currently unknown. While rapamycin is the standard-of-care therapy for TSC patients with AML, little is known about how these rapamycin-treated AML cells may signal intercellularly in a different manner than parental AML cells, and whether this may have a pro- or anti-therapeutic impact. Lastly, the translational potential of TSC EV cargo into biomarkers for TSC has not been explored but could reveal novel biomarker candidates with increased stability and bioavailability.

1.3.11. Use of EVs as sources of biomarkers

Biological markers, coined *biomarkers*, are quantifiable indicators of a biological state, pathological state, or therapeutic response to a pharmacological treatment regimen (Biomarkers Definitions Working Group, 2001). Specifically, cancer biomarkers can be used for routine personalised screening, diagnosis and prognosis, treatment monitoring, and detection of relapse (Barnie *et al*., 2022). In translational medicine, EVs in systemic circulation are gaining traction as a candidate for 'liquid biopsy', as EVs contain a diverse and multi-faceted cargo containing proteins, lipids, and RNA species, that can reflect their parental cell of origin (as reviewed by Han *et al*., 2019; as reviewed by Fujita *et al*., 2016). EVs are an attractive source of potential biomarkers for disease states as they have many innate advantages that may be beneficial over soluble circulating biomarkers. The EV lipid bilayer entity is protective of its cargo from enzymatic degradation by proteases in circulation, which may increase stability of a biomarker over exposed

soluble factors (Zhou *et al*., 2020). Furthermore, EV cargo functionality is conserved by this lipid bilayer, and so this may serve as advantageous in terms of developing functional biomarkers for disease and response to treatment (Palviainen *et al*., 2020). In the cancer setting, the complex assortment of EV cargo could be used to gauge a multi-faceted 'omics' tumour profile, providing diagnostic and/or prognostic insight superior to that obtained by tissue needle biopsy alone (as reviewed by Pang *et al*., 2020). Furthermore, given that EVs can regulate various pro-tumoral processes and phenotypic modifications, EVs could also be considered in a longitudinal disease monitoring or therapeutic surveillance context (Zhou *et al*., 2021; as reviewed by Yekula *et al*., 2020).

As previously mentioned, EVs can be isolated from various biofluids, including plasma, serum, urine, cerebrospinal fluid, and saliva (as reviewed by Yekula *et al.,* 2020). Considerate selection of biofluid in the development of a tumour-associated EV biomarker is critical for accurate data interpretation. Plasma, serum, and urine are commonly selected due to their minimally invasive collection and favourable volumes of sample for EV isolation. Biofluid samples from which EVs are isolated are a fundamental component to characterise in any EV biomarker study. In light of the MISEV 2018 guidelines, it is encouraged to keep biofluid sample collection and analysis consistent so as to optimise reproducibility of downstream analysis and interpretation (Théry *et al*., 2018). Namely, it is important to report technical details pertaining to biofluid sample collections, such as: biofluid volume, anticoagulant used, orientation and any agitation to the collected tube following collection and in subsequent transportation, storage temperatures, exact EV isolation procedure, characterisation of isolated EVs, amongst others. These guidelines also encourage

the collation of accompanying clinical data to account for potential inter-patient variations. These may include factors such as age, biological sex, collection time, medication regimens and pre/post-prandial status (Théry *et al.*, 2018; as reviewed by Yekula *et al.*, 2020).

1.4. STUDY HYPOTHESES AND AIMS

Given the roles of small EVs in optimising tumour microenvironments to support tumour growth, examining the characteristics, cargo, and functionality of TSC-deficient small EVs, from AML cells, could provide valuable insight into this poorly understood aspect of TSC tumour biology.

This project tested the primary hypothesis that *TSC2*-deficient (AML-) tumour cells secrete small extracellular vesicles (sEVs), with RNA and protein cargo distinct from sEVs secreted from control *TSC2*-expressing (AML+) cells. The secondary hypothesis tested was that these AML- sEVs are capable of modifying fibroblasts of the tumour microenvironment to contribute to TSC tumour growth and development.

To understand how sEVs contribute to AML tumour biology in TSC, the overarching aims of this study are as follows:

I. To characterise TSC sEVs, in terms of their size, morphology, and molecular marker expression profiles
II. To profile the RNA cargo carried by TSC sEVs, followed by *in silico* exploration these RNA biotypes to aid prediction of the potential biological impact of delivery of these sEVs to recipient cells

III. To examine the protein cargo carried by TSC sEVs, and to determine if mTORC1 inhibition therapy may impact TSC sEV cargoes to have different intercellular consequences in the microenvironment

IV. To establish the application of TSC sEV cargo as blood-based biomarkers for TSC patients ± mTOR inhibitor therapy

CHAPTER 2

MATERIALS AND METHODS

2.1. CELL LINES

The cell lines used in this study are frequently used as *in vitro* TSC tumour cell models. The *TSC2*-null 621.101 angiomyolipoma (AML) cell line is derived from the kidney of a lymphangioleiomyomatosis (LAM) patient. 621.101 cells carry inactivating mutations in both *TSC2* alleles. The immortalised, stable cell lines, *TSC2*-deficient 621.102 and *TSC2*-re-expressing 621.103 cell lines were derived from 621.101 by transfection of an empty vector and a TSC2 encoding vector, respectively (Yu *et al*., 2004; Siroky *et al*., 2012). These lines are referred to as AML- (*TSC2*-deficient = tumour) and AML+ (*TSC2*-re-expressing = control) throughout this Thesis. Mouse embryonic fibroblast (MEF) cells lines (Zhang *et al*., 2003; Siroky *et al*., 2012) were also used for some initial EV characterisation work in **Chapter 3**. These cell lines are referred to as MEF- (*Tsc2*$^{-/-}$ *TP53*$^{-/-}$) and MEF+ (wild-type *Tsc2*$^{+/+}$ *TP53*$^{-/-}$) in this work.

The human pulmonary fibroblast (HPF-c) Z031 line is a primary cell line, derived from peripheral lung tissue (Promocell, Heidelberg, Germany). These HPF-c Z031 cells were used as an *in vitro* model of recipient fibroblasts of the tumour microenvironment.

2.1.1. Standard cell culture

Media requirements as per cell line are detailed in **Table 2.1**. Prior to media supplementation, fetal bovine serum (FBS) was centrifuged at 100,000 *x g* for 18 hours prior to serial filtration through a 0.22 µm and 0.1 µm vacuum filters to deplete EVs. This was done to avoid contamination of sample EV populations by bovine EVs (Théry *et al*., 2006). Cell cultures were incubated in a humidified environment with 5 % CO_2 at 37° Celsius. All tissue culture work was carried out in a Class II biosafety cabinet. Mycoplasma testing on cell-conditioned media was conducted once per month. Passage number of cell lines was recorded at each passage.

Table 2.1: Cell lines used, and their respective genotypes. Suppliers for all AML and MEF reagents were SIGMA-ALDRICH. Fibroblast Growth Medium 2 was supplied by PromoCell.

Cell line	Cell Culture Media	Media Supplements
AML+ and AML-	DMEM with 4500 mg/L glucose, L-glutamine, sodium pyruvate, and sodium bicarbonate	15% [v/v] EV-dep. FBS 1% [v/v] *Pen. Strep.* *10000 units penicillin 10 mg/strep*
MEF+ and MEF-	DMEM with 4500 mg/L glucose, L-glutamine, sodium pyruvate, and sodium bicarbonate	10% [v/v] EV-dep. FBS; 1% [v/v] *Pen. Strep.* *10000 units penicillin 10 mg/strep*
HPF-c Z031	Fibroblast Growth Medium 2	Manufacturer's FBS and supplements

Dulbecco's Modified Eagle's Media, ***DMEM****; EV-depleted Fetal Bovine Serum,* ***EV-dep. FBS.***

2.1.2. High-density bioreactor cell culture

EVs were isolated from high-density cell cultures, maintained in AD 1000 CELLine adhere bioreactor flasks (Merck, New Jersey, USA) for high-density cell culture for increased production of EVs (Mitchell *et al.,* 2008). These bioreactors are comprised of two separate compartments: a small internal chamber for holding cultured cells and a larger outer chamber for holding cell culture media. The compartments are separated by a 10 kDa semi-permeable membrane, which facilitates continuous diffusion of nutrients from the medium compartment to the cell compartment, and waste from the cell compartment to the medium compartment (Guerreiro *et al*., 2018). The membrane does not permit the passage of EVs from one compartment to another.

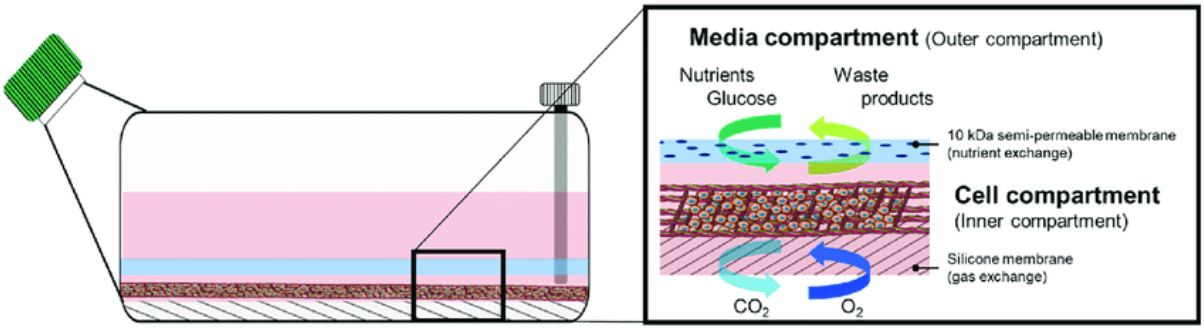

Figure 2.1: Diagram of CELLine AD 1000 bioreactor flask us as 3D-based culture for EV production*. Schematic created and published by Guerreiro et al., 2018.*

AML or MEF cells at low passage were seeded, as required, at a density of 2.0 x 10^7 cells in 15 mL of required supplemented culture media with 15 % EV-depleted FBS, as described above (**Table 2.1**). Within the compartment, cells attach to a woven, polyethylene terephthalate (PET) matrix and EVs are secreted into the small cell-conditioned media compartment for collection. The large media chamber was filled with 500 mL of supplemented culture media with 10 % FBS. The high

cell density within a low volume of culture media, within the cell compartment, allows collection of EV yields that are eight-ten times more concentrated (per mL) compared standard monolayer cultures (Mitchell *et al*., 2008). Media within the bioreactor flasks was replaced weekly, following collection of cell conditioned media from the cell compartment.

2.1.3. Rapamycin treatment in bioreactors

Rapamycin treatment of a high-density AML- bioreactor flask was established to generate EVs for experiments designed to examine the effect of standard-of-care mTORC1 inhibition on EV characteristics, count, cargo and functionality. A concentration of rapamycin of 10 ng/mL was selected to mimic patient serum trough levels consistently observed across multiple clinical trials investigating rapalog use in AML patients (Bissler *et al*., 2008; Davies *et al*., 2011; EXIST-2 trial, Bissler *et al*., 2013). Rapamycin (10 ng/mL) was added weekly at time of media replacement.

2.1.4. Pre-clearing cell-conditioned media

Prior to EV isolation, cell-conditioned media was harvested weekly from the cell compartment and subjected to differential centrifugation (400 *x g* for six minutes, twice; followed by 2000 *x g* for 15 minutes; all at 4° Celsius) to remove cell debris, protein aggregates, and apoptotic contaminants, followed by filtration to remove particles >0.22 μm (Théry *et al*., 2018). Processed cell-conditioned media was stored at -80° Celsius prior to pooling for EV isolation.

2.2. SUCROSE-BASED EV ISOLATION FROM CELL-CONDITIONED MEDIA

To isolate EVs, pre-cleared cell conditioned media samples were pooled and layered on top of 4 mL of 30% [w/v] sucrose/D2O (density of 1.2 g/mL) (protocol adapted from Lamparski *et al*., 2002), prior to ultracentrifugation at 100,000 *x g* (SW-32 rotor, Beckman Coulter, High Wycombe, UK) for 90 minutes. Given that EVs would float at the interface of the sucrose cushion and media supernatants, the sucrose cushion was carefully removed and washed in phosphate buffer saline (PBS) before a second ultracentrifugation at 100,000 *x g* (fixed angle 70Ti rotor, Beckman Coulter) for 90 minutes. A visible pellet of EVs was then isolated and resuspended in 500 µL PBS before aliquots were created for storage at -80° Celsius. This EV production pipeline is summarised in the schematic below (**Figure 2.2**).

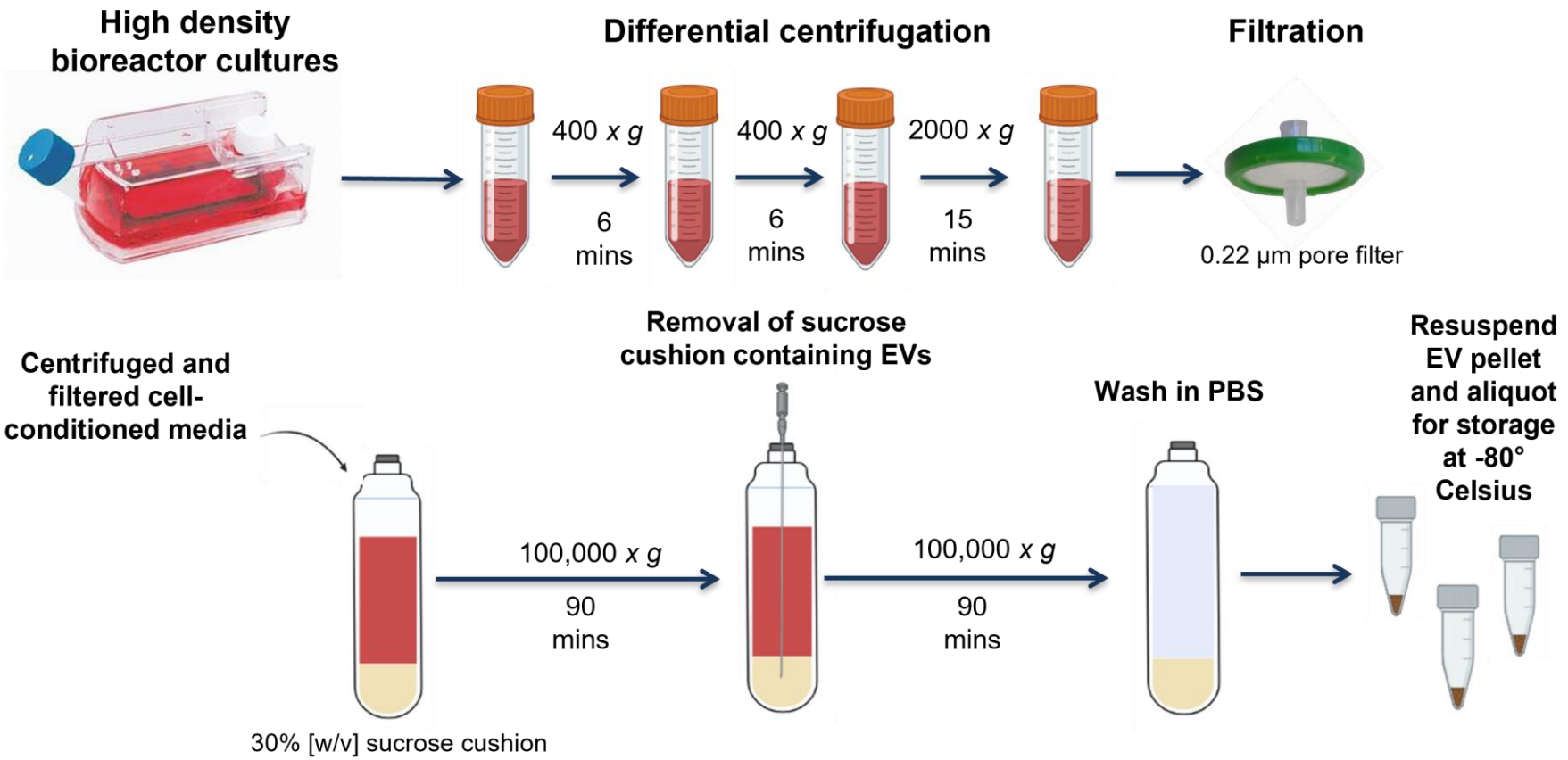

Figure 2.2: EV separation protocol workflow from high density bioreactor cultures. *Cell-conditioned media from the internal bioreactor chamber was extracted and subjected to 3 differential centrifugation steps before filtration through a 0.22 µm pore filter. Processed cell-conditioned media was pooled and EVs were separated based on their density via ultracentrifugation against a sucrose gradient. Pelleted EVs were washed in PBS and aliquoted for storage at -80° Celsius prior to experimentation. Schematic constructed using BioRender.com.*

2.2.1. Bicinchoninic acid (BCA) assay

The protein concentration of EV samples was determined using the MicroBCA Protein Assay (ThermoFisher Scientific). This bicinchoninic acid (BCA) assay relies on the classical biuret reaction, with reduction of protein cupric ion to a cuprous ion. Cuprous ions bind to two molecules of bicinchoninic acid to produce various intensities of purple, correlating with protein concentrations. 5 µL EV preparation was diluted in 35 µL PBS and plated in duplicate to read against a 12-point standard curve with a top standard of 2 mg/mL bovine serum albumin (BSA) and subsequent standards prepared in a two-fold serial dilution. Briefly, EVs were diluted 1:8 with PBS and absorbance values were calculated from the standard curve, to determine the protein content from EV preparations. Duplicate readings of each sample were taken and averaged to determine a total protein (µg/mL) measurement. Plates were incubated at 37° Celsius for 30 minutes before absorbance readings were measured using the PHERAstar® plate reader (BMG LABTECH). EV protein concentration was determined based on absorbance reading comparisons to the absorbance values of BSA standards of known concentration.

2.3. IMMUNOFLUORESCENCE MICROSCOPY

Immunofluorescence microscopy (IF) was used to characterise protein expression within monolayer-cultured cells. AML cells were grown to 80 % confluence on glass-bottomed 24-well plates (greiner bio-one, Stonehouse, UK), and fixed using ice-cold acetone:methanol (1:1 [v/v]) for 20 minutes. Non-specific sites were blocked by incubation with 1 % [w/v] bovine serum albumin (BSA) in Hank's

Balanced Salt Solution (HBSS, MERCK, Darmstadt, Germany) for two hours at room temperature. Fixed cells were washed twice, with 0.1 % [w/v] BSA in HBSS. Cells were then incubated with primary antibodies listed in **Table 2.2** (diluted in 0.1% BSA in HBSS) at room temperature for two hours. Cells were washed twice with 0.1% [v/v] BSA in HBSS before incubation with Alexa Fluor® 488 conjugated goat anti-mouse secondary antibody (10 µg/mL in 0.1% [v/v] BSA in HBSS; Catalogue # A11029 from Life Technologies) for one hour at room temperature. Cells were washed once with 0.1% [v/v] BSA in HBSS before staining with DAPI diluted in distilled H_20 (1 µg/mL; ThermoFisher Scientific) for one minute at room temperature. Cells were washed once with 0.1% [w/v] BSA in HBSS and then twice in HBSS. 500 µL HBSS was added to cells for imaging. Fluorescence microscopy was performed with structured illumination using the ZEISS ApoTome system, using a 63×/1.4 numerical aperture oil-immersion objective (Zeiss Z1 Observer, Cambridge, UK; running Zen Pro Software).

Table 2.2: Primary antibodies and respective isotypes used in IF.

Antibody	Isotype	Stock conc. (mg/mL)	Dilution to Working Conc. (1 µg/mL)	Catalogue #	Company
α-smooth muscle actin mouse	IgG_{2a}	0.2	1:200	sc-32251	Santa Cruz Biotechnology
Desmin mouse	IgG_{2b}	0.1	1:100	sc-70961	Santa Cruz Biotechnology
Cytokeratin 18 mouse	IgG_1	0.2	1:200	sc-32329	Santa Cruz Biotechnology
EEA1 mouse	IgG_1	0.2	1:200	sc-137130	Santa Cruz Biotechnology
LAMP2 mouse	IgG_1	0.2	1:200	sc-18822	Santa Cruz Biotechnology
CD9 mouse	IgG_{2b}	0.5	1:500	MAB1880	eBioscience
CD63 mouse	IgG_1	1	1:1000	MCA2142	Bio-rad Laboratories
CD81 mouse	IgG_1	1	1:1000	MCA1847EL	Bio-rad Laboratories
IgG_1	-	0.5	1:500	14-4714-84	eBioscience
IgG_{2a}	-	0.5	1:500	14-4724-85	eBioscience
IgG_{2b}	-	0.5	1:500	14-4732-85	eBioscience

2.4. IMMUNO-PHENOTYPING OF EVs

Plate-based immunofluorescent analysis of EV-associated proteins was performed using an established time-resolved fluorescence (TRF) assay (as described by Webber *et al*., 2014). 100 µL/well EV samples (0.5 µg/µL) were plated in triplicate in high-binding strip 96-well plates (Greiner bio-one) and incubated at 4° Celsius overnight. Samples were washed three times in 1X Delfia wash buffer (Kaivogen). Non-specific sites on EVs were blocked using 1% [v/v] BSA in PBS and incubated at room temperature for two hours. For sample lysis to examine EV-luminal proteins, 100 µL/well RIPA Lysis Buffer (Santa Cruz Biotechnology) was added to appropriate wells and incubated at room temperature for one hour. Samples were

washed three times in 1X Delfia wash buffer. Primary antibodies (**Table 2.3**) were diluted in 0.1% [v/v] BSA in PBS to give a working concentration of 1 µg/mL for the assay and used at a volume of 100 µL/well. Samples were incubated with primary antibodies at room temperature, for 2 hours, whilst under gentle agitation on a plate shaker. Samples were washed three times again using 1X Delfia wash buffer. Anti-mouse IgG (goat) biotin-labelled secondary antibody (Perkin Elmer) was diluted in 0.1% [v/v] BSA in PBS to provide a working concentration of 200 ng/mL. Samples were incubated with 100 µL/well secondary antibody at room temperature for one hour. Samples were washed three times with 1X Delfia wash buffer. Europium-conjugated strepavidin (Perkin Elmer) was diluted 1:1000 [v/v] in Assay Buffer (Kaivogen). Samples were incubated with 100 µL/well europium-conjugated strepavidin at room temperature for 45 minutes. Samples were washed six times with 1X Delfia wash buffer. 100 µL/well Europium Fluorescence Intensifier (Kaivogen) was added to each well and incubated at room temperature for five minutes. Europium signal per well was measured on the PHERAstar® plate reader (BMG LABTECH, Ortenberg, Germany). Data was plotted and statistically analysed in Microsoft Office Excel and GraphPad Prism (Version 8) software.

Table 2.3: Primary antibodies and respective isotype controls used in plate-based immunofluorescent analysis.

Primary antibody *specificity*	**Raised in:**	**Isotype**	**Stock conc. (mg/mL)**	**Dilution to working conc. (1 µg/mL)**	**Catalogue #**	**Company**
CD9 *Human*	Mouse	IgG_{2b}	0.5	1:500	MAB1880	eBioscience
CD63 *Human*	Mouse	IgG_1	1	1:1000	MCA2142	Bio-rad Laboratories
CD81 human	Mouse	IgG_1	1	1:1000	MCA1847EL	Bio-rad Laboratories
ALIX *Human*	Mouse	IgG_1	0.2	1:200	sc-166952	Santa Cruz Biotechnology
TSG101	Mouse	IgG_1	0.2	1:200	sc-7964	Invitrogen
IgG_1	Mouse	-	0.5	1:500	14-4714-84	eBioscience
IgG_{2a}	Mouse	-	0.5	1:500	14-4724-85	eBioscience
IgG_{2b}	Mouse	-	0.5	1:500	14-4732-85	eBioscience

2.5. NANOPARTICLE TRACKING ANALYSIS (NTA)

Nanoparticle tracking and size distribution analysis was conducted on cell-conditioned media samples post-serial centrifugation and filtration. Analysis was performed using NanoSight NS300 apparatus, configured with a temperature controlled 488 nm laser module and a high-sensitivity sCMOS Camera System (OrcaFlash 2.8, Hamamatsu C11440, Hamamatsu City, Japan) and a syringe-pump system (Malvern Instruments). Experimental samples were diluted using particle-free H_2O and loaded into a 1 mL syringe pump. Samples were syringed into the NS300 at a fixed speed infusion rate of 80 arbitary units, and temperature set at 25 °Celsius, while three two-minute videos were recorded for tracking and size distribution analysis. Camera level was set at 15 for all recordings. Screen gain was set at 1.0 for each recording. Samples were diluted in nanoparticle-free water (Fresenius Kabi, Runcorn, UK), so that the particle concentration (particles / ml) was within the linear range of the instrument. Camera focus was adjusted prior

to each recording to maximise observer visualisation of nanoparticle flow. Sample analysis was performed using NanoSight NTA software (version 3.1). NTA quantification of particles is based on two principles: Brownian motion, and the Stokes Einstein equation. Brownian motion describes the constant, random movement of particles in suspension. Temperature and viscosity of the suspension fluid is a factor of Brownian motion. These moving particles cause light scatter from the NS300 high-intensity laser beams to allow individual tracking. NTA software then calculates particle diameter using the Stokes Einstein equation:

$$Dt = TK_B / 3\pi \eta d$$

where, Dt = diffusion constant (D = diffusion coefficient; t = time), T = sample temperature, K_B = Boltzmann's constant, η = solvent viscosity, d = diameter of spherical particle.

NTA was conducted on each EV sample, where three video recordings represent technical triplicates. The mean of these triplicates were graphed as a mean in the resulting size distribution profiles.

2.6. CRYOGENIC ELECTRON MICROSCOPY (Cryo-EM)

Cryo-EM was conducted to visualise and characterise EV morphology and heterogeneity within and between AML+ and AML- samples. One AML+ and one AML- EV sample was subjected to cryo-EM analysis in this study. EVs isolated by density gradient ultracentrifugation were added to glow-discharged holey carbon grids (Quantifoil, Germany). A vitrobot (Maastricht Instruments BV, The Netherlands) was then used to vitrify the grids. To image the samples, a JEM-2200FS/CR transmission cryo-electron microscope (JEOL, Japan) was used.

Samples were imaged at -196° Celsius with an acceleration voltage of 200 kV. Cryo-EM was conducted in collaboration with Professor Juan Falcon-Perez (CIC bioGUNE, Bilbao). Morphological analysis of .tiff images was conducted using ImageJ (version 1.50i) software and data was plotted in GraphPad Prism (Version 8) software.

2.7. RNA ISOLATION AND REVERSE TRANSCRIPTION

RNA was extracted from EV samples (based on 200 µg of EV protein), using 1 mL TRI Reagent® per sample (Sigma-Aldrich). 200 µL of chloroform (Sigma-Aldrich) was added to the samples, before samples were mixed vigorously for 15 seconds to disperse the chloroform. This was followed by a 5-minute incubation on ice. The samples were centrifuged at 16,000 *x g* for 20 minutes at 4° Celsius, to allow the separation of both aqueous and phenol phases. The clear aqueous layer was removed carefully by pipette and added to 500 mL ice-cold isopropanol. Samples were then incubated at -20° Celsius overnight, to allow precipitation of RNA. Samples were centrifuged at 16,000 *x g* for 20 minutes at 4° Celsius, to pellet the RNA. RNA pellets were washed twice in 1 mL ice-cold 70% [v/v] ethanol. Tubes were then inverted, and RNA pellets air-dried for 1 hour. Pellets were resuspended in 12 µL DNase- and RNase-free H_2O. 1 µL of each RNA sample was assessed for RNA concentration using a NanoDrop™ 2000 Spectrometer (ThermoFisher Scientific), which provides ratios of absorbance measured at 260nm and 280nm. A 260nm:280nm ratio of >1.7 is generally accepted as *pure* RNA and was used as a threshold for further analysis in this study. If the ratio is considerably lower, it may indicate the presence of protein, phenol or other contaminants that absorb strongly

near 280nm. For nucleic acid quantification, the extinction coefficient for RNA is 40 and the modified Beer-Lambert equation (ThermoFisher Scientific) used is:

$$C = \frac{A\varepsilon}{b}$$

*where **C** = nucleic acid concentration in µg/ml, **A** = absorbance in Absorbance Units (AU), **ε** = wavelength-dependent extinction coefficient in ng-cm/µl, and **b** is pathway length in cm.*

Reverse transcription was performed using the random primer method in a final volume of 20 µL per reaction, containing 0.08 µg of RNA of the sample (as detailed in **Table 2.4**). A negative control was included, which substituted RNA sample for molecular biology grade H_2O. Reverse transcription was performed in an S1000 Thermal Cycler (Bio-Rad). This included incubation at 25° Celsius for 10 minutes to allow the primers to anneal to the RNA. The primers were then extended in the presence of dNTPs using reverse transcriptase at 37° Celsius for 2 hours, generating cDNA. The reaction mixture was then heated at 85° Celsius for 5 seconds to deactivate the RT. The resultant 20 µL cDNA samples were diluted in 80 µL H_2O and stored at -20° Celsius.

Table 2.4: List of constituents in master mix from Kit with RNase inhibitor (appliedbiosystems by Thermo Fisher Scientific)

Reagent	Volume (µL)
10X RT Buffer	2
25X dNTP Mix (100 mM)	0.8
10X RT Random Primers	2
MultiScribe™ Reverse Transcriptase	1
RNase inhibitor	1
Nuclease-free H_2O	3.2
Total per reaction	**10**

2.8. QUANTITATIVE POLYMERASE CHAIN REACTION (qPCR)

qPCR was carried out with 20 µL per reaction, containing 5 µL of pre-diluted sample cDNA (as above), 10 µL of TaqMan® Universal Master Mix (2X) (ThermoFisher Scientific), 4 µL H_2O and 1 µL TaqMan® gene expression assay primer and probe mix (all from ThermoFisher Scientific) (**Table 2.5**). Each sample was plated in duplicate, and a negative control was prepared using H_2O substituted for the cDNA. The PCR amplification was performed in a StepOnePlus™ Real-Time PCR System Thermocycler (ThermoFisher Scientific). Samples were amplified in stages, first by heating them to 50° Celsius for 2 minutes, followed by 95° Celsius for 10 minutes, then at 95° Celsius for 15 seconds, and finally at 60° Celsius for 1 minute, for a total of 40 cycles.

Table 2.5: List of constituents in master mix per primer tested by qPCR

Reagent	Volume (µL)
TaqMan® MasterMix	10
Primer & probe	1
H_20	4

The comparative CT method was used for relative quantification of target gene expression. The CT (cycle where amplification is in the linear range of the amplification curve and crosses the set threshold) for the standard reference gene (glyceraldehyde 3-phosphate dehydrogenase, GAPDH) was subtracted from the target gene CT to obtain the ΔCT for each sample. Target gene expression was calculated in each experimental sample relative to control samples by:

$$\textbf{Relative Expression} = 2^{-(\Delta CT \text{ of experimental sample}) - (\Delta CT \text{ of reference sample})}$$

$$\textbf{Relative Expression} = 2^{-((\Delta CT\ 1) - (\Delta CT\ 2))}$$

The “ΔCT1” is the mean ΔCT value calculated for the experimental samples (AML-), whereas the “ΔCT 2” is the mean ΔCT value calculated for the reference samples (AML+). The data was analysed using the StepOnePlus™ Software (Version 2.0, ThermoFisher Scientific).

2.9. RNA SEQUENCING (RNA-Seq)

2.9.1. Quality control

EV RNA samples, extracted as described above, were submitted for RNASeq to the Wales Gene Park, Heath Park Campus, Cardiff University. Quality and quantities of total RNA per sample were assessed using Agilent 4200 TapeStation and high-sensitivity ScreenTape (Agilent Technologies), conducted as per outlined in the manufacturer’s instructions. This quality control was conducted by Shelley Rundle and Vikki Humphries (Wales Gene Park), The DV200 method, that measures percentage of RNA fragments that are longer than 200 nucleotides in length, was used to assess RNA quality, and samples were graded and ranked in accordance with the Illumina® recommendations (too degraded = <30 % DV200; low = 30-50% DV200; medium = 50-70% DV200; high = > 70% DV200). The 6 top-ranking samples per group (AML+, AML-) were selected for sequencing.

2.9.2. Library preparation and sequencing

Libraries for sequencing were generated following Chapter 2 of the NEB® Ultra™ II Directional RNA Library Prep Kit for Illumina® (New England BioLabs, Massachusetts, USA) protocol. This was conducted by Vikki Humphries (Wales Gene Park). 5 ng of total RNA was depleted of ribosomal RNA using the NEBNext® rRNA Depletion Kit (Human/Mouse/Rat), (New England BioLabs,).

Library construction consisted of the following steps: RNA fragmentation and priming, cDNA synthesis (1st strand, then 2nd strand) adenylation of 3' ends, adapter ligation (1:199 dilution of adapter) and PCR amplification for 16 cycles. Samples with low DV200 readings were subjected to a short fragmentation period of 8 minutes at 94°C. Higher quality RNA was incubated at 94°C for 15 minutes. AMPure XP beads (Beckman Coulter®) were used as a replacement of RNAClean XP and SPRIselect beads listed in the manufacturer's instructions. Library validation was conducted using the Agilent 4200 TapeStation and high sensitivity ScreenTapes (Agilent Technologies) to determine insert size. Qubit® (Thermo Fisher Technologies) was used to carry out the fluorometric quantitation. The validated libraries were normalised to 4nM before pooling. The pooled libraries were then sequenced on an S1 (200 cycle) flow cell using XP workflow for a 2x100bp PE dual index format using the NovaSeq6000 sequencing system (**i**llumina®), as per the manufacturer's instructions.

RNASeq reads were trimmed using Trim Galore (Babraham Bioinformatics) and mapped against reference genome GRCh38 using STAR (Dobin *et al*., 2013). Expression counts were conducted using featureCounts against the GENCODE GFCh38.p10 gene annotation model, and differentially expressed genes (DEG) lists were generated using DeSeq2 (Love *et al*., 2014). In this analysis, RNA reads differentially expressed in AML- EVs compared to AML+ EVs were listed. Statistical significance was explored by filtering at various *p* value thresholds, adjusted for multiple corrections.

2.9.3. Downstream analysis of differentially expressed genes

DEG lists were subdivided into RNA biotypes using BioMart (Ensembl), by Samantha Hill (Wales Gene Park, Heath Park Campus, Cardiff University). RNA biodistribution in AML+ and AML- EVs were compared. Biotype classes found to be upregulated and downregulated in AML- EVs were assessed. The largest RNA biotypes – mRNA, lncRNA, and miRNA – were selected, and listed RNA reads were ranked by false-discovery rate adjusted *p (p.adj.)* values. An appropriate *p*.adj. value cut-off threshold per list was established for inclusion of the most statistically significant reads and taking size of dataset into account. A five-fold change threshold was also applied, which resulted in a final list of genes for downstream analysis. Functional enrichment gene ontology (GO) analysis on the RNA-Seq datasets was performed using online software programme GOliath (https://www.bioinformatics.babraham.ac.uk/goliath/goliath.cgi), and by literature review. Results were compiled in tables and graphs were created in GraphPad Prism (Version 8).

2.10. PROTEOME PROFILE ANTIBODY ARRAY

A proteome profiler antibody array (Human XL Oncology Array; R&D Systems) was conducted to compare the expression of 84 oncology-associated proteins within lysates from AML+ and AML- cells and cell-derived EVs. For cell lysates, AML+ and AML- cells were grown to confluence in 60mm-diameter plates and treated with 0.7 µg/mL GolgiStop™ and 1 µg/mL GolgiPlug™ Protein Transport Inhibitors (Thermo Fisher Scientific) for 18 hours to prevent cytokine release, prior to lysis

with 1X RIPA Lysis Buffer with phenylmethylsulfonyl fluoride (PMSF), sodium orthovanadate, and kit inhibitor cocktail (Bio-Rad Laboratories). EVs generated from bioreactor flasks were also lysed with the same 1X RIPA buffer and inhibitor cocktail before protein quantification. 180 µg protein from both cells and EVs was suspended in assay buffer and incubated on the supplied membrane (R&D Systems), dotted with capture antibodies for 84 oncology-associated proteins. Blots were then incubated with a cocktail of biotinylated detection antibodies and processed as per the manufacturer's instructions. Membranes were imaged by chemiluminence using C-DiGit® Blot Scanner (LI-COR) and analysed by densitometry using ImageJ software (version 1.50i).

2.10.1. Functional enrichment analysis

Functional enrichment analysis on proteins with elevated expression in AML- cells and EVs was conducted using FunRich: Functional Enrichment Analysis Tool (http://www.funrich.org/) software (version 3.1.3), as previously described (Kalra *et al*., 2012; Pathan *et al*., 2015; Fonseka *et al.,* 2021). The encoding gene for each candidate protein was retrieved from NCBI Gene Nomenclature, tabulated in **Table 2.6**. Upregulated protein lists were inputted into FunRich software and analysed for gene oncology annotation *Biological pathway* within installed background FunRich datasets Gene Ontology database, Human Protein Reference Database (Keshava Prasad *et al*., 2009), Entrez Gene (Maglott *et al*., 2007), and UniProt (UniProt-Consortium, 2010). Percentage gene set coverage per biological pathway within the datasets was determined, with matched fold enrichment. Hypergeometric *p* values were used to analyse statistical significance. Percentage gene set coverage was ranked in descending order, and biological pathway annotated with less than

three gene hits in any category were omitted. The ten top-ranking percentage gene coverage/enrichment scores were selected and compiled in a bar chart.

Table 2.6: Genes corresponding to proteins analysed by proteome profiler antibody array. Gene names were obtained from the NCBI Gene Nomenclature prior for functional enrichment gene ontology analysis.

Protein	*Encoding Gene*	Protein	*Encoding Gene*	Protein	*Encoding Gene*
α-fetoprotein	*AFP*	**ErbB4**	*ERBB4*	**MMP-2**	*MMP2*
amphiregulin	*AREG*	**FGF basic**	*FGF2*	**MMP-3**	*MMP3*
Angiopoietin-1	*ANGPT1*	**FoxC2**	*FOXC2*	**MMP-9**	*MMP9*
Angiopoietin-like 4	*ANGPTL4*	**Fox01/FKHR**	*FOXO1*	**MSP/MST1**	*MST1*
ENNP-2/Autotaxin	*ENNP2*	**Galectin-3**	*LGALS3*	**MUC-1**	*MUC1*
Axl	*AXL*	**GM-CSF**	*CSF2*	**Nestin-4**	*NES*
BCL-x	*BCL2L1*	**CG α/β (HCG)**	*CGB3*	**Osteopontin (OPN)**	*OPN*
CA125/MUC16	*MUC16*	**HGF/c-Met**	*HGF*	**p27/Kip1**	*CDKN1B*
E-cadherin	*CDH1*	**HIF-1α**	*HIF1A*	**p53**	*TP53*
VE-cadherin	*CDH5*	**HNF-3β**	*FOXA2*	**PDGF-AA**	*PDGFA*
CapG	*CAPG*	**H0-1/HMOX1**	*HMOX1*	**CD31/PECAM-1**	*PECAM1*
Carbonic anhydrase IX	*CA9*	**ICAM-1/CD54**	*ICAM1*	**Progesterone R/NR3C3**	*PGR*
Cathepsin B	*CTSB*	**IL-2 Rα**	*IL2RA*	**Progranulin**	*GRN*
Cathepsin D	*CTSD*	**IL-6**	*IL6*	**Prolactin**	*PRL*
Cathepsin S	*CTSS*	**CXCL8/IL-8**	*IL8*	**Prostasin/Prss8**	*PRSS8*
CEACAM-5	*CEACAM5*	**IL-18 BPa**	*IL18BP*	**E-Selectin/CD62E**	*SELE*
Decorin	*DCN*	**Kallikrein 3/PSA**	*KLK3*	**Serpin B5/Maspin**	*SERPINB5*
Dkk1	*DKK1*	**Kallikrein 5**	*KLK5*	**Serpin E1/PAI-1**	*SERPINE1*
DLL1	*DLL1*	**Kallikrein 6**	*KLK6*	**Snail**	*SNAI1*
EGFR/ErbB1	*EGFR*	**Leptin**	*LEP*	**SPARC**	*SPARC*
Endoglin/CD105	*ENG*	**Lumican**	*LUM*	**Survivin**	*BIRC5*
Endostatin	*COL18A1*	**CCL2/MCP-1**	*CCL2*	**Tenascin C**	*TNC*
Enolase 2	*ENO2*	**CCL8/MCP-2**	*CCL8*	**Thrombospondin-1**	THBS1
eNOS	*NOS3*	**CCL7/MCP-3**	*CCL7*	**Tie-2**	*TEK*
EpCAM/TROP1	*EPCAM*	**M-CSF**	*CSF1*	***U-plasminogen activator/urokinase***	*PLAU*
ER α/NR3A1	*ESR1*	**Mesothelin**	*MSLN*	***VCAM-1/CD106***	*VCAM1*
ErbB2	*ERBB2*	**CCL3/MIP-1α**	*CCL3*	***VEGF***	*VEGFA*
ErbB3/Her3	*ERBB3*	**CCL20/MIP-3α**	*CCL20*	***Vimentin***	*VIM*

2.11. ENZYME-LINKED IMMUNO-SORBANT ASSAY (ELISA)

Quantification of selected protein targets was conducted using commercially available ELISA kits (DuoSet ELISA Development System, R&D Systems, Minneapolis, USA). EVs (normalised for total protein levels) were lysed using 1X RIPA lysis buffer (Santa Cruz Biotechnology) with PMSF, sodium orthovanadate, and kit inhibitor cocktail on ice for 30 minutes. The protocol outlined by R&D Systems was followed with amendments to the conjugate used for signal detection. Samples were plated in duplicate or triplicate, specified in respective figure legends. Europium-labelled streptavidin (Perkin Elmer) was diluted 1:1000 [v/v] in Assay Buffer RED (Kaivogen), allowing for more sensitive detection. Samples were incubated with 100 µL/well europium-labelled strepavidin at room temperature for 45 minutes. Samples were washed 6 times with 1X Delfia wash buffer. 100 µL/well Europium Fluorescence Intensifier (Kaivogen) was added to each well and incubated at room temperature for five minutes. Europium signal in wells was measured on the PHERAstar® plate reader (BMG LABTECH). Statistical analysis by two-way ANOVA and Tukey's multiple comparisons correction was performed using GraphPad Prism (Version 8) software. Identical experiments were conducted three times.

ELISA was also used to measure growth factor secretion in cell-conditioned media from non-transformed Z031 lung fibroblasts following EV treatment. Cells were treated with EVs for four days and cell-conditioned media was removed and subjected to a high-speed ultracentrifugation at 100,000 *x g* for two hours to deplete EVs. Then, ELISA, as described above, was performed to detect VEGF, FGF, and HGF in cell-conditioned media. Note that lysis using 1X RIPA buffer with

added protease inhibitor cocktail (PIC) was not necessary here as growth factors secreted were not EV-associated. Samples were plated in duplicate and this experiment was repeated three times.

2.10. SODIUM DODECYL SULPHATE-POLYACRYLAMIDE GEL ELECTROPHORESIS (SDS-PAGE) AND WESTERN BLOT

Cells were lysed in lysis buffer (20nM Tris, pH 7.5, 135 mM NaCl, 5% [v/v] glycerol, 50 mM NaF, 0.1% [v/v] Triton X-100) (as described by Dunlop *et al*., 2014), with protease and phosphatase inhibitors pepstatin, antipain, benzamidine, phenylmethylsulfonyl fluoride, sodium orthovanadate, leupeptin and dithiothreitol (DTT). Cells were sonicated with three 30 second pulses in Bioruptor® (diagenode), and then centrifuged at 17,000 *x g* at 4° Celsius for eight minutes to remove insoluble debris. Protein quantification was conducted as described previously. 4X LDS sample buffer (Invitrogen) and 25 mM DTT was then added to samples (cell lysates and EVs). Samples were then heated at 70° Celsius for ten minutes. Lysates and EVs were separated on a 4-12% Bis-Tris gradient gel (ThermoFisher Scientific) and run at 150 V for 65 min alongside a molecular weight marker. Protein bands were blotted onto methanol-activated polyvinylidene difluoride (PVDF) membranes (Millipore) at 25 V for 130 min. The membrane was blocked in 5% [w/v] non-fat dried milk in Tris-buffered Saline (TBS) containing 0.1% [v/v] Tween-20 (TBST) for one hour. The membrane was washed in TBST in three 5-minute washes before being divided into sections to maximise data yield. Respective sections (based on their predicted size ranges) were incubated individually overnight at 4° Celsius with primary antibodies (**Table 2.7**), diluted to manufacturer's recommended dilution, in 2% [w/v] BSA. After incubation, blots

were subjected to three five-minute washes each in TBST before a one-hour incubation at room temperature in corresponding secondary goat anti-mouse (sc-2302, Santa Cruz Biotechnologies)/goat anti-rabbit (sc-2004, Santa Cruz Biotechnologies) antibodies diluted to 1:10000 [v/v] in 5% non-fat milk/TBST. Blots were washed again three times for five minutes per wash. Blots were subsequently analysed by chemiluminescence using Immobilon Classico Western Horse Radish Peroxidase (HRP) substrate (Millipore) and developed on film (Hyperfilm). Blots for proteins under investigation were repeated three times on three cell or EV lysates prepared identically as described here.

Due to COVID-19 lab restrictions, access to equipment to develop blots using film was not possible. Therefore, for the latter period of this project, blot development was conducted using WesternSure® PREMIUM Chemiluminescent Substrate and C-DiGit® Chemiluminescence Western Blot Scanner (LI-COR Biosciences, Biotechnology).

Table 2.7: Primary antibodies using for protein detection by western blot

Primary antibody specific for:	Stock Conc. (mg/mL)	Dilution to Working Conc. (1 µg/mL)	Catalogue #	Company
mTOR rabbit	1	1:1000	CST 2972	Cell Signalling Technology
TSC2 rabbit	1	1:1000	CST 3990	Cell Signalling Technology
Notch1 rat	1	1:1000	CST 3447	Cell Signalling Technology
ALIX mouse	0.2	1:200	sc-166952	Santa Cruz Biotechnologies
GRP94 mouse	0.2	1:200	sc-393402	Santa Cruz Biotechnologies
S6K1 rabbit	1	1:1000	CST 9202	Cell Signalling Technology
Akt rabbit	1	1:1000	CST 9272	Cell Signalling Technology
TSG101 mouse	0.2	1:200	sc-7964	Santa Cruz Biotechnologies
4eBP1 rabbit	1	1:1000	CST 9644	Cell Signalling Technology
elf4E rabbit	1	1:1000	CST 9742	Cell Signalling Technology
Rheb sheep	1	1:1000	5483B	University of Dundee
GAPDH mouse	10	1:10000	NBP1-47339	Novus Biologicals

2.11. PHOSPHO-PROTEIN SIGNALLING ACTIVATION

Non-transformed lung fibroblasts, Z031, were grown to 100 % confluence in 60mm diameter plates and serum-starved for 24 hours, as described above. Cells were treated with 200 µg of either AML+, AML- , or rapaAML- EVs resuspended in serum-free media and incubated for one hour. Serum-free media was added to another plate as a negative control. After incubation, cells were lysed with 1X RIPA Lysis Buffer with added protease inhibitor cocktail (Bio-rad Laboratories) and total protein per lysate was quantified by BCA assay, as described above. 3 µg protein lysates were loaded into wells and subjected to SDS-PAGE and western blot as described above, except here the western blots were blocked in 2% [w/v] BSA

instead of 5% [w/v] non-fat milk to avoid contamination by phospho-casein.

Membranes were then probed for phosphorylated proteins listed in **Table 2.8**.

Table 2.8: Primary antibodies used for phospho-protein signalling experiments.

Primary antibody specific for:	Stock Conc. (mg/mL)	Dilution to Working Conc. (1 µg/mL)	Catalogue #	Company
p44/42 pMAPK (ERK1/2) Thr202/Tyr204 rabbit	2	1:2000	CST 4370	Cell Signalling Technology
pS6 Ser235/236 rabbit	1	1:1000	CST 2211L	Cell Signalling Technology
pIRS Ser636/639 rabbit	1	1:1000	CST 2388	Cell Signalling Technology

2.13. ANALYSIS OF PLASMA SAMPLES

2.13.1. Plasma samples

Three adult (>18yo) cohorts of plasma samples were utilised in this study, namely: healthy donor (labelled HD) samples; TSC patients with identified *TSC2* mutations (labelled TSC); and TSC patients with a *TSC2* mutation receiving mTOR inhibition therapy (labelled TSC+mTORi). HD samples were obtained from Cardiff University Biobank (Heath Park Campus, Dental Drive, Cardiff, CF14 4AX, Application Number 21-0002; REC No 18/WA/0089). TSC and TSC+mTORi samples were obtained from the TSC Alliance Biosample Repository (Van Andel Institute, Michigan, USA; IRB Study Number 15039-05). Analysis of plasma samples in this study was approved by Cardiff University School of Medicine Research Ethics Committee (SMREC reference: 19.84). Written informed consent was received

before precipitation. Samples were age- and sex-matched between groups, as summarised in **Table 2.9**.

Table 2.9: Summary of plasma sample cohorts.

	Healthy donor		TSC patient with *TSC2* mutation		TSC patient with *TSC2* mutation + mTOR inhibitor treatment	
Age (years)	**Male**	**Female**	**Male**	**Female**	**Male**	**Female**
30-39	1	3	1	3	1	3
40-49	2	2	2	2	2	2
50-59	1	0	1	0	1	0

2.13.2. Size-exclusion chromatography (SEC) for EV isolation from plasma

EVs were isolated from donor or patient plasma samples by size exclusion chromatography, using Exo-spin midi columns (CELL Guidance Systems, Cambridge, UK) following our established protocol (Welton *et al*., 2015). The SEC method was chosen as plasma is viscous and not suitable for flotation- or density gradient-based EV separation. Specifically, three treatment groups were processed to analyse if their EV cargo contained selected target proteins, and whether expression of these target proteins were differential between these groups. SEC was performed in accordance with the manufacturer's instructions. Briefly, SEC columns were clamped onto retort stands and washed through with 20 mL PBS + 6 mM EDTA to equilibrate the column. 1 mL plasma samples were loaded, 500 µL at a time, onto the top of the SEC column, and 500 µL fractions were collected at the bottom of the SEC column as it drained under gravity. Subsequently, 500 µL PBS + 6 mM EDTA was loaded onto the top of the columns and resulting 500 uL fractions were collected until 21 fractions had been collected in total.

2.13.2. TRIFic™ detection assays on plasma SEC fractions

Following fraction pooling, TRIFic™ detection assays (CELL guidance systems), a type of TRF assay, were used to quantify CD9 and CD63 expression levels in SEC fractions from plasma samples to further confirm EV enrichment in the expected pooled samples. This was conducted in accordance with the manufacturer's protocol. Specifically, 2 ng/µL biotinylated CD9/CD63 antibody was made up in 100 µL and added to each well of the high-binding plate and incubated on plate shaker at room temperature for one hour. The plate was washed in wash buffer using an automatic plate washer. 100 µL of the pooled SEC groups – pre-EV, EV-rich, and post-EV – were added to the plate and incubated on a plate shaker at room temperature for one hour. Given the restrictions in number of wells per assay kit, samples were plated in singlate. The wash step was repeated as above, and Europium-conjugated CD9/CD63/CD81 antibody (concentrations indicated in the manufacturer's guidebook) was added to each well. The plate was again incubated at room temperature on a plate shaker for one hour. The plate was washed again as above, and 100 µL Europium Fluorescence Intensifier was added to each well. This was incubated on the plate for 15 minutes on a plate shaker at room temperature, and TRF was measured from the bottom optic using PHERAstar® plate reader (BMG LABTECH).

2.14. STATISTICAL ANALYSIS

Statistical analyses were performed using GraphPad Prism (version 8). Statistical tests used are detailed in respective figures legends. *p* values less than 0.05 were considered statistically significant. Throughout this Thesis, *statistical significance*

was annotated using astericks as follows: ns = non-statistical significance (i.e., $p>0.05$); * = $p<0.05$; ** = $p<0.01$; *** = $p<0.001$; **** = $p<0.0001$. Graphs depict mean±standard deviation (SD), from one representative experiment of at least three similar independent experiments shown, unless stated otherwise. Employed statistical tests per experiment are denoted in figure legends throughout.

CHAPTER 3

CHARACTERISING TSC SMALL EVs

3.1. INTRODUCTION

3.1.1. Rationale

Extracellular vesicles (EVs) are a group of lipid bilayer-bound luminal structures secreted from cells into the extracellular space (as reviewed by van Niel *et al*., 2018; as reviewed by Cheng and Hill, 2022). EVs consist of three main subtypes: microvesicles (MVs), apoptotic bodies, and exosomes, which are differentiated based on various physical and molecular parameters including their mode of biogenesis, size, cargo, and function (as reviewed by Zaborowski *et al*., 2015; as reviewed by Yáñez-Mó *et al*., 2015). At present, there are some difficulties in isolating specific subtypes from others co-secreted from the biosource being examined, and a critical focus of the EV research is in developing EV subtype-specific markers and technologies to isolate subtypes accurately and purely (Kowal *et al.*, 2016; as reviewed by Willms *et al*., 2018). In light of these challenges, the most widely studied are small EVs, and are the focus of this Thesis.

3.1.1.2. Small extracellular vesicles (sEVs)

Small extracellular vesicles (sEVs) are a key component of the cell secretome in both normal physiology and disease. Along with other EV subpopulations, cells secrete sEVs – cargo-filled nanometre-sized vesicles – into the surrounding microenvironment and systemic circulation to modulate important roles in intercellular signalling and biological processes. In the cancer setting, parental tumour cells specifically package tumour biomolecules into sEVs prior to secretion,

which has important implications in what disease phenotypes can be promoted beyond the boundaries of the primary tumour. In many cancers, tumour cells have been found to secrete elevated quantities of sEVs (Logozzi *et al*., 2009; Riches *et al*., 2014), indicating that export of tumour-derived biomolecules in sEVs could be important to tumour growth and development. Knowing that sEVs induce a wide range of phenotypic modifications to recipient cell populations, uncovering EV-specific effects underpinning the pathology is key.

3.1.2. EVs in Tuberous Sclerosis Complex (TSC)

Tuberous Sclerosis Complex (TSC) is a rare multi-organ tumour syndrome, driven by hyperactivated mammalian target of rapamycin complex 1 (mTORC1) signalling. Inhibiting mTORC1 is the only current pharmacological treatment, and the observed therapeutic effects are inconsistent. Understanding how the tumours function within the context of the tumour microenvironment could be key to uncovering improved therapeutic options. Research into soluble factors in TSC tumour biology has been published, which focused on soluble factors secreted by TSC cells (Li *et al*., 2005; Clements *et al*., 2022; Hirose *et al*., 2019). This includes soluble VEGF-D that is currently used as a clinical biomarker for LAM (TSC-associated and sporadic). Yet much less is known about the vesicular component of TSC tumour cell secretomes. Characterising EVs secreted by TSC tumour cells will add considerable knowledge to this area, helping to close the knowledge gap, and will enhance our knowledge about how TSC tumour cells signal intercellularly to promote growth and development. Specifically, in TSC AML, it is currently unknown if these tumour cells have signature sEV exports which facilitate tumour-supporting intercellular signalling.

3.1.3. sEV characterisation

This Chapter sets out a comprehensive characterisation of sEVs from AML+ (*TSC2*-expressing) control and AML- (*TSC2*-deficient) tumour cells grown in standard cell culture following guidelines recommended by the International Society of Extracellular Vesicles (ISEV) (Lötvall *et al*., 2014; Théry *et al.*, 2018). To aid generation of sufficient quantities of sEVs for further analysis throughout this project, *TSC2*-expressing and *TSC2*-deficient cell cultures were maintained using an established high-density culture bioreactor system (Mitchell *et al*., 2008). Characteristics of sEVs generated from cells high density cultures were also profiled to determine whether these sEVs from a long-term based culture have the same characteristics as sEVs from standard monolayer culture.

3.1.4. Challenges with EV characterisation

sEVs were characterised using a multi-technique approach in-keeping with that outlined and recommended for cell lines in the published Minimal Information for Studies of Extracellular Vesicles (MISEV) guidelines (Théry *et al*., 2018). MISEV sets out important recommendations and minimal information required for studies reporting on EV biology (summarised in **Chapter 1**). EV characterisation is important for inter-laboratory standardisation of EV research. Many different types of vesicles are secreted by cells into the extracellular space and discriminating these EV subtypes from one another is important for appropriate comparisons of EV data. Furthermore, the characterisation of sEVs isolated from cell-conditioned media and biological fluids is crucial in attributing phenotypic modifications and tumour biomarkers to EVs correctly. Consensus has not yet been reached in regard to exclusive markers of EV subtypes (Théry *et al*., 2018), though this

remains a pressing aim of the research field. Ultimately, specific markers that indicate a vesicle's cell of origin and biogenesis pathway will discriminate EV subpopulations. Given this is obscured by experimental limitations, ISEV recommend that vesicles should be characterised by a multitude of complimentary techniques, highlighting various characteristics. These include: i) physical characteristics, including diameter or density; ii) biochemical composition, determining if the vesicles are CD9+/CD63+/CD81+; and whether they express luminal ALIX and TSG101; iii) indication of the biosource from which the EVs are derived. The research presented in this Chapter offers a good basis to standardise subsequent studies in TSC AML EV research. Furthermore, being a rare disease, EV characterisation is important to ensure that research is not made more difficult to interpret or translate due to lack of standardisation.

For this work, I isolated EVs by differential ultracentrifugation on a 30% [w/v] sucrose cushion (protocol adapted from Lamparski *et al*., 2002) to ensure an isolation of EVs with specific buoyant density, thereby increasing the specificity of isolated EVs, with further characterisation to examine EV size, surface protein expression (CD9, CD63, CD81) by plate-based immune-fluorescent analysis using both in-house established assays and a commercially available assay (TRIFic™ detection assays, Cell Guidance Systems, Cambridge, UK). Detection of ALIX and TSG101, proteins associated with ESCRT-mediated endosomal maturation and therefore endosomal origin, were assessed by western blot. Isolated EVs were then characterised based on their diameters by nanoparticle tracking analysis (NTA).

Determining the purity of EV preparations is important in monitoring the quality of preparations, and more broadly in establishing an international standard for pure EV preparations separate from co-existing soluble biomaterial (Webber and Clayton, 2013). This is particularly important to attribute cargo and particular phenotypic modifications to the correct and specific class and preparation of EVs. Purity of EV preparations, therefore, was estimated by comparing the nano-vesicle counts, as per NTA, to protein concentration, as per BCA protein assay, which generated a particle:protein ratio (P:P ratio), as defined previously (Webber and Clayton, 2013).

Research presented in this Thesis aims to characterise a novel aspect of TSC tumour pathology, by investigating the effect of TSC AML EVs on cells of the tumour microenvironment. Work presented in this Chapter aims to characterise EVs secreted from TSC AML cells. To date, only two research groups have published on TSC renal EVs (Zadjali *et al*., 2020; Kumar *et al*., 2021; Patel *et al.*, 2016). Given that the subsequent Chapters aim to profile EV cargo and EV-induced signalling and phenotypic changes in recipient cells, and that the cell secretome is comprised of many different vesicular components, ensuring that EV isolation has been successful, reproducible, and pure was important for correct attribution of disease pathology to these AML EVs.

3.1.5. Hypothesis and aims

The overarching hypothesis for this Chapter was that TSC cell lines secrete vesicles that have the characteristics associated with sEVs of endosomal origin.

Specifically, work presented in this Chapter aims:

I. To determine that *TSC2*-deficient (AML- and MEF-) and *TSC2*-expressing (AML+ and MEF+) cell lines secrete EVs expressing classic biophysical and molecular markers
II. To determine if expansion of TSC cell line cultures to high-density bioreactor cultures affects EV characteristics
III. To determine that EV isolates are pure for experimental use

3.2. RESULTS

3.2.1. Cell and endosomal characterisation

The *TSC2*-expressing (AML+) and *TSC2*-deficient (AML-) cell lines are widely used pre-clinical models in TSC research (Vaughan *et al*., 2022; Wang *et al*., 2021; Yue *et al.,* 2016). An advantage to using these AML+ and AML- cells owes to their patient origin, as described in **Table 2.1**. Other cell lines commonly used as preclinical TSC models include MEF- (*Tsc2*-deficient) and MEF+ (*Tsc2*-expressing) cell lines, which are of murine origin; and ELT3 *Tsc2*-null cells, derived from rat.

To examine cell morphology, a monolayer of AML+ and AML- cells were grown to confluence in glass-bottomed 24-well plates and fixed before staining. Given a shortage of published data on characterisation of these AML+ and AML- cell lines, I conducted basic characterisation to identify cell origin in these cell lines using IF microscopy (**Fig. 3.1**). Isotype controls were stained as imaging experiment controls. Mesenchymal marker vimentin stained positively in both AML+ and AML- cell lines. Staining for muscle-specific marker desmin and epithelial marker cytokeratin 18 was negative in both cell lines (**Fig. 3.1**).

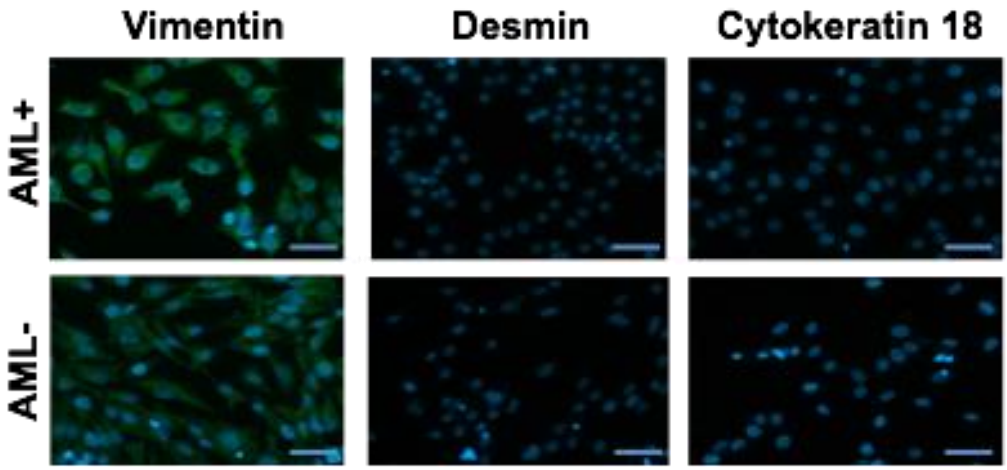

Figure 3.1: Characterisation of AML cell lines reveals a mesenchymal origin. *IF was used to determine expression of vimentin, desmin, and cytokeratin 18. Fluorescent green staining indicates expression. Nuclei stained using DAPI. Representative images of 10 fields of view per well, from 3 independent experiments. Scale bar = 50 μm.*

Cells were also stained for markers associated with endosomes and potential EV biogenesis (**Fig. 3.2** and **3.3**). Lysosome-associated membrane protein (LAMP) 1 and LAMP2 appeared to cluster at some cell peripheries in AML+ cells, while their expression was more diffuse and ubiquitous throughout the cytosol of AML- cells with LAMP2 appearing more prevalent compared to LAMP1 (**Fig. 3.2**). Early endosomal marker, early endosome antigen 1 (EEA1) appeared to cluster at both AML+ and AML- cell peripheries, and staining appeared more widespread in AML+ cells (**Fig. 3.2**).

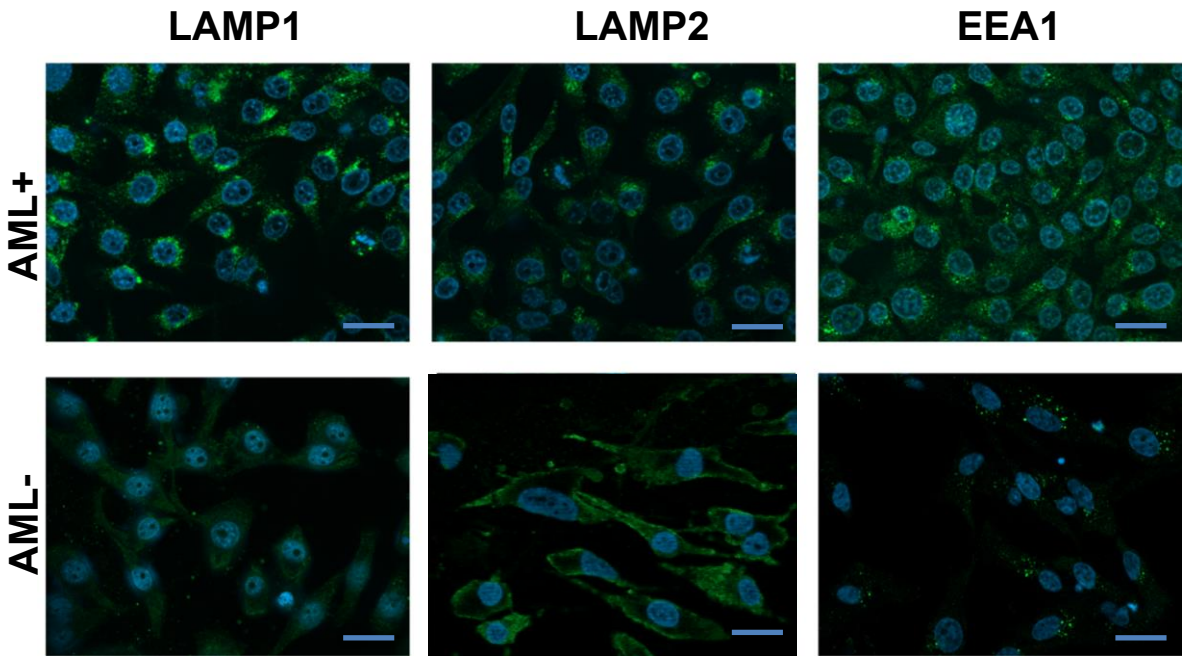

Figure 3.2: Endosomal characterisation reveals some localisation differences in AML+ and AML- cells. *Cell localisation of lysosome- and endosome-associated markers was determined by immunofluorescent microscopy. Lysosomal-associated Membrane Protein 1, LAMP1; Lysosomal-associated Membrane Protein 2, LAMP2; Early Endosome Antigen 1; EEA1 Scale bar = 25 µm.*

CD9 appears faint in both AML+ and AML- cell lines and appears more widespread in AML+ cells (**Fig. 3.3**). CD63 expression was seen to be punctate in AML+ cells and appears to localise towards the AML- cell peripheries (**Fig. 3.3**). A similar pattern is seen with CD81. CD81 expression appeared more ubiquitous throughout the cytoplasm of AML+ cells, while it appears to localise towards the AML- cell peripheries (**Fig. 3.3**).

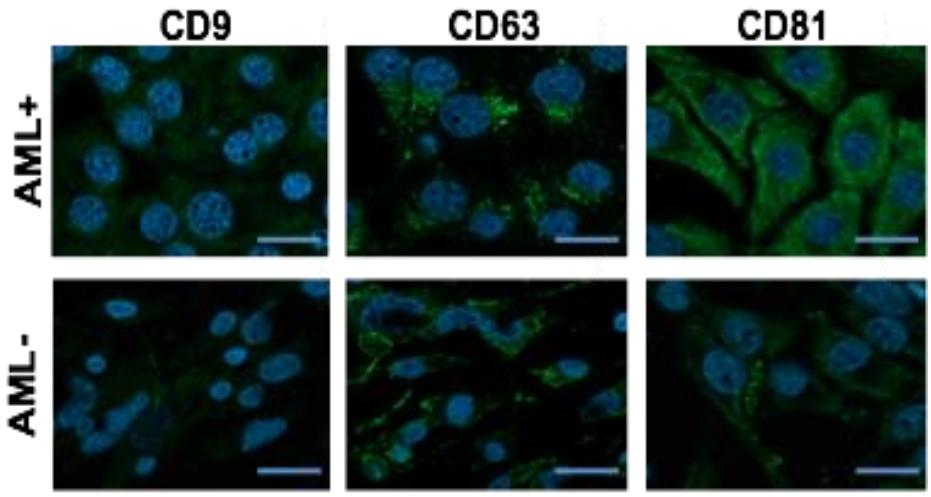

Figure 3.3: Expression of tetraspanins CD63, and CD81 appear more prominent at AML+ and AML- cell peripheries. *Marker expression determined by immunofluorescence imaging. Cluster of differentiation, CD. Scale bar = 20 µm.*

3.2.2. Characterisation of EVs from 2D monolayer culture

In this work, AML cell- and MEF cell-derived EVs were isolated from cell-conditioned media, once cells cultured in T-75cm^2 flasks reached confluence. EVs were isolated by ultracentrifugation onto a sucrose cushion, as described in detail in **Chapter 2.**

3.2.2.1. AML and MEF cells secrete EVs that express CD9, CD63, and CD81

Immuno-affinity-based microplate assays, as described in **Chapter 2,** were used to detect and quantify relative expression levels of tetraspanins: CD9, CD63, and CD81. Three tetraspanins CD9, CD63, and CD81, were detected on the surfaces of control and disease AML and MEF EVs, to varying expression levels (**Fig. 3.4**). Expression levels also varied between AML and MEF cell lines (**Fig. 3.4**). Higher levels of CD9 were detected in AML+ EVs compared to AML- EVs, while higher levels of CD63 and CD81 were detected in AML- EVs versus their AML+ EV control

counterparts (**Fig. 3.4**). The only significantly elevated tetraspanin found in AML- EVs compared to AML+ EVs was CD81. Expression of isotype controls IgG_1 and IgG_{2b} were low relative to the expression levels of the three tetraspanins. When examining expression in the MEF EV groups, CD9, CD63, and CD81 expression was found to be higher in the MEF- EVs compared to the MEF+ EVs (**Fig. 3.4**). this elevated expression of CD9 and CD63 in MEF- EVs was found to be statistically significant, though CD9, CD63, and CD81 expression in MEF+ EVs were detected levels similar to the isotype controls (**Fig. 3.4**). CD81 expression in MEF- EVs was seen to be highly variable compared to expression of CD9 and CD63 in MEF- EVs.

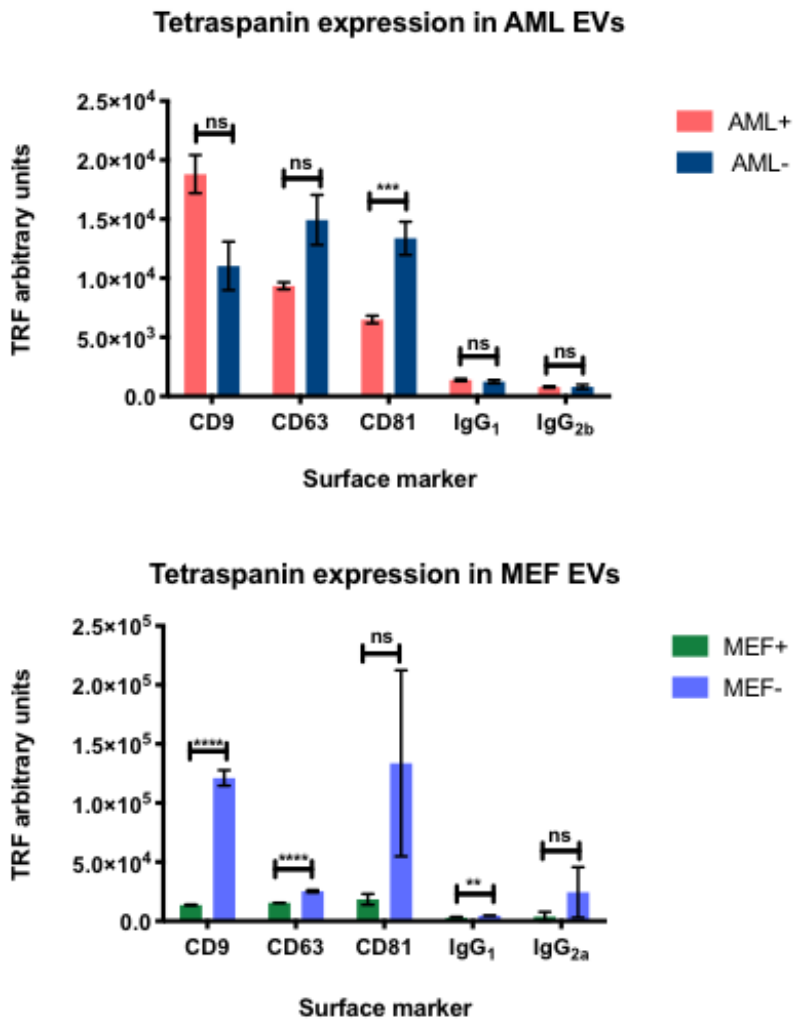

Figure 3.4: Detection of tetraspanins CD9, CD63, and CD81, on the surface of AML and MEF cell-derived EVs. *Total protein of 0.5 µg/mL per well was used as a surrogate for vesicle loading. CD9, CD63, and CD81 expression, and respective IgG_1, IgG_{2b}, IgG_{2a} isotype control expression was quantified on vesicles using an immuno-affinity-based microplate-based assay. Error bars indicate mean+SD of three technical repeats. Representative graph of three independent experiments. Non-parametric multiple t-tests used for statistical analysis. Ns, non-statsitically significant; * = p<0.05; ** = p<0.01; *** = p<0.001; **** = p<0.0001. Time-resolved fluorescence, TRF.*

3.2.2.2 Nanoparticle tracking analysis (NTA) of AML and MEF cell-derived EVs from monolayer culture

NTA was performed to define particle size distribution profiles within a given preparation of EVs from 2D monolayer culture, isolated by ultracentrifugation against a sucrose cushion (as described in **Chapter 2**). Typical volumes of 2D

monolayer culture-derived cell-conditioned media used was 90 mL, taken at passage of confluent T-75cm^2 flasks, per EV isolation via sucrose cushion. A majority of particle isolated from AML+, AML-, MEF+, and MEF- samples were within the diameter size range of 20-150 nm, which is the size range typically associated with small EVs, such as exosomes (**Fig. 3.5A+C**). Mean particle sizes did not differ significantly between AML+ and AML- (**Fig.3.5A**) EV samples, or MEF+ and MEF- EV samples (**Fig. 3.5D**).

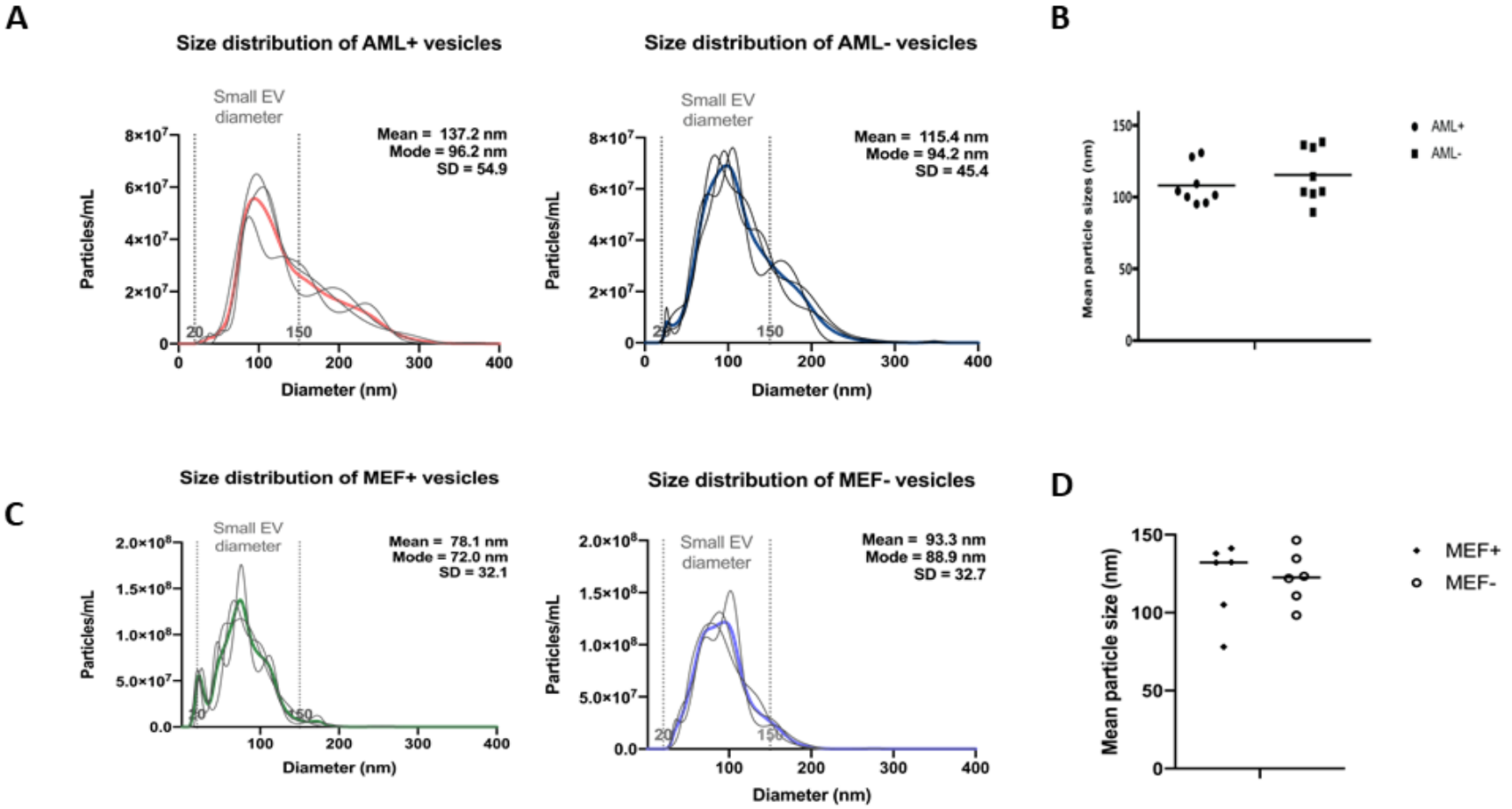

Figure 3.5: NTA-based assessment of AML and MEF cell-derived EVs. *AML and MEF cell-conditioned media post-differential centrifugation and filtration was diluted in particle-free H_20 and loaded at a fixed infusion rate for NTA analysis (A+C) with one biological replicate shown as an example. Three two-minute videos were recorded (plotted in grey lines) and mean concentrations were determined (plotted in thicker coloured lines). Mean diameter sizes (nm) of AML and MEF particles were compiled and compared from various n=8 AML and n=6 MEF biological replicates (B+D).*

3.2.2.3 Concentration of EVs secreted is elevated from AML- and MEF- cells compared to their counterpart control cells

To further assess EV secretion and to determine if control and disease cells release different quantities of EVs, EV secretion from both AML and MEF cells was quantified by NTA. Cell-conditioned media was subjected to differential centrifugation and filtering using 0.22 µm pore filter on day 4 post-cell seeding. Concentration per mL of particles remaining in the supernatant were assessed by NTA. These counts were normalised to cell number, counted using a haemocytometer. EV secretion per cell was increased from AML- cells compared to AML+ cells (**Fig. 3.6A).** In MEF cell-conditioned media, EV secretion was elevated from MEF- cells compared to MEF+ cells (**Fig. 3.6B).** Inter-experimental variation was large, as seen with large error bars below, thereby hindering a conclusive trend in EV secretion to be detected. Mean differences were not significantly different between the AML+ and AML- cells, and MEF+ and MEF- cells.

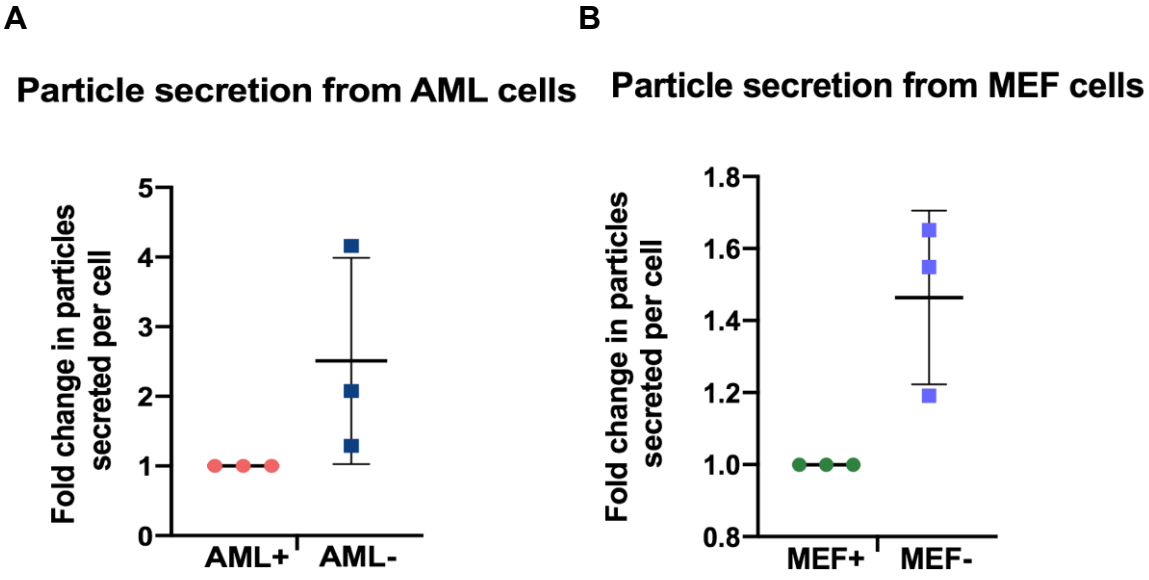

Figure 3.6: Secretion of small EVs from AML and MEF cells in 2D culture is variable. *EV count was determined by NTA and normalised to cell count. Graph shows n=3 independent biological repeats. Fold changes normalised to respective AML+ and MEF+ particles/cell count. Error bars indicate mean±SD.*

At this point, the AML+ and AML- cell lines were selected as the primary model for upscaling to high-density bioreactor culture. This decision was informed by variability in MEF data shown in expression of CD9, CD63, and CD81 (**Fig. 3.4)**, and the human origin of the AML cell line.

3.2.3. Analysis of AML EVs from high-density bioreactor-based culture

To generate a higher yield of EVs for downstream analysis, high-density cell cultures were established in CELLine adherent bioreactor flasks (Merck), as described in **Chapter 2**. Characterisation of bioreactor EVs, in addition to that done on EVs from 2D cultures, was conducted to ensure that upscaling production did not affect EV characteristics.

3.2.3.1. AML cell-derived EVs are enriched for ESCRT-associated proteins ALIX and TSG101, and lack expression of ER-association protein GRP94

CD9, CD63, and CD81 tetraspanin expression on the surface of AML EVs isolated from bioreactor-derived cultures reflected that detected in EVs isolated from monolayer culture using the immuno-affinity-based microplate assay. Both AML+ and AML- EVs expressed all three tetraspanins CD9, CD63, and CD81 on their surfaces (**Fig. 3.7A**). Expression of these tetraspanins was found to be significantly higher in AML- EVs compared to AML+ EVs. This is largely similar to that observed in 2D monolayer culture-derived AML EVs (**Fig. 3.3A**), except for CD9 expression which had different findings. CD9 expression was elevated in AML+ EVs versus AML- EVs from 2D monolayer culture but had elevated expression in AML- EVs compared to AML+ EVs generated from high-density bioreactor culture (**Fig. 3.7A**).

Western blot was used to assess the presence of ALIX and TSG101, proteins associated with the ESCRT complex and, therefore, EV biogenesis, in both cell and EV lysates. ALIX and TSG101 were enriched in both AML+ EVs and AML- EVs, in comparison to their parental cells (**Fig. 3.7B**). As a negative control, cell and EV lysates were also assessed for the endoplasmic reticulum (ER)-associated protein GRP94. GRP94 was enriched within both the AML+ and AML- cell lysates, with no detectable expression with AML+ or AML- EVs (**Fig. 3.7B**). This data highlights enrichment of specific proteins within EVs and indicates there are EVs present that are of endosomal origin.

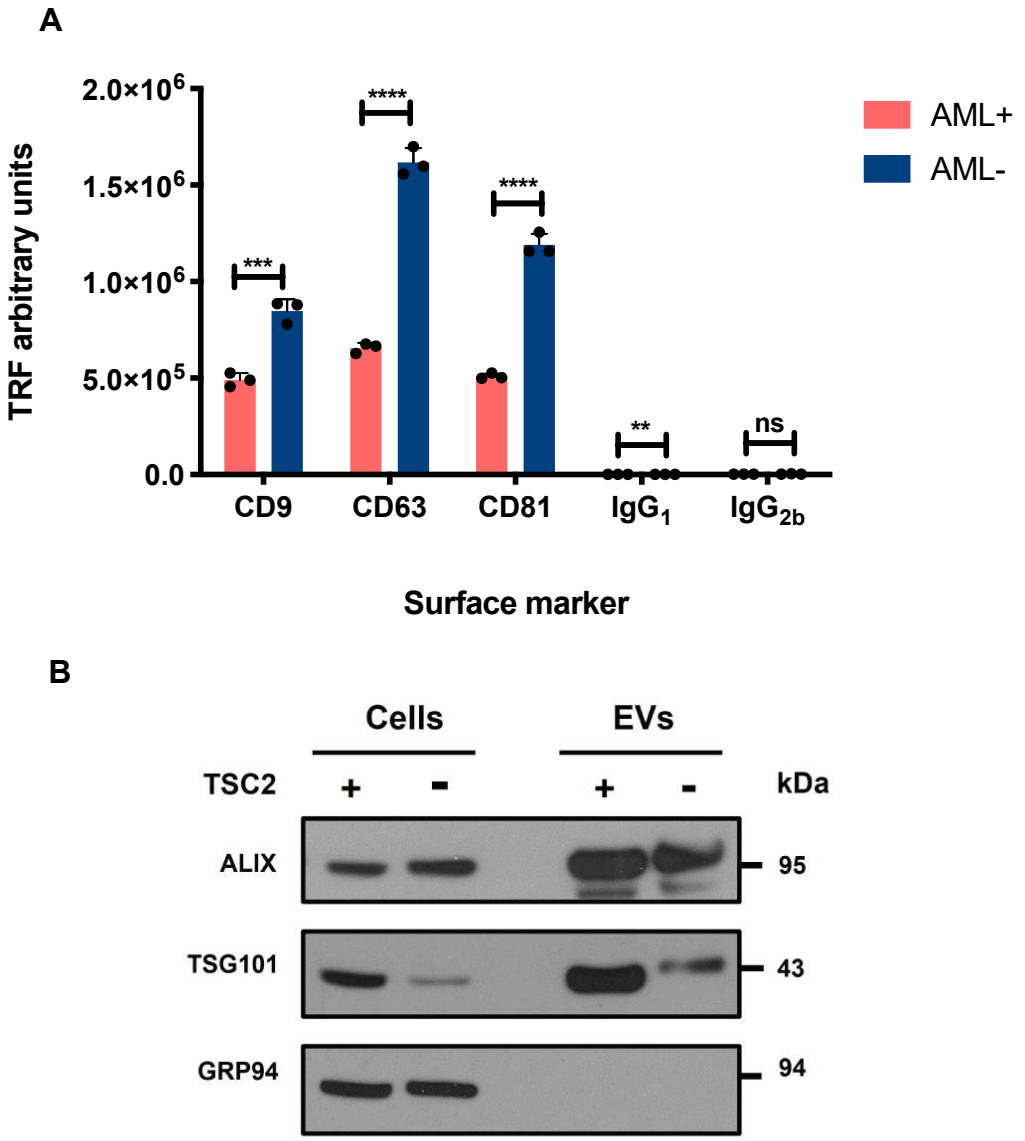

Figure. 3.7: AML EVs express tetraspanins and are enriched in ALIX and TSG-101 protein expression, compared to parental cell lysates. *EVs secreted from AML cells in bioreactors express tetraspanins CD9, CD81 and CD63 on their surfaces, examined by TRF-plate based assay (A). Enriched expression of ALIX and TSG101 was detected in EV lysates compared to cell lysates, by western blot. GRP94 was detected only in cell lysates (B). Non-parametric multiple t-test used as statistical analysis. Ns = non-statistical significance; * = p<0.05; ** = p<0.01; *** = p<0.001; **** = p<0.0001. Immunoglobulin G1, IgG_1; Immunoglobulin G (2a allele), $IgG2_a$; Immunoglobulin G (2b allele), IgG_{2b}); ALG-interacting protein protein X, ALIX; Tumor susceptibility gene 101 protein, TSG101; ER-associated glucose-regulated protein 94, GRP94.*

Taking the evidence of enriched expression of these three tetraspanins and the EV biogenesis-associated proteins, and quantities of EVs being generated, a more thorough characterisation was performed that included NTA and cryo-EM.

NTA was used to determine size distribution profiles of vesicles secreted from cultured cell lines. A majority of particles in AML+ and AML- EV preparations had a diameter of between 30 and 150 nm (**Fig. 3.8A,B**). Furthermore, NTA provided evidence that EVs isolated from high-density bioreactor cultures were a higher abundance (in the order of 10^8 particles/mL for AML+ 2D monolayer culture versus order of 10^{11} for AML+ bioreactor culture, and 10^8 AML- 2D vs. 10^{11} AML- bioreactor culture). Mean particle sizes from NTA experiments were compiled to examine reproducibility of a small EV-rich preparation from AML+ and AML- samples. Mean particle sizes between several different experiments showed that the mean diameter of particles observed were of small EV size, with a mean size less than 150 nm, and did not significantly differ between AML+ and AML- EV preparations (**Fig. 3.8C**), like that observed in EVs from 2D monolayer culture (**Fig. 3.5)**.

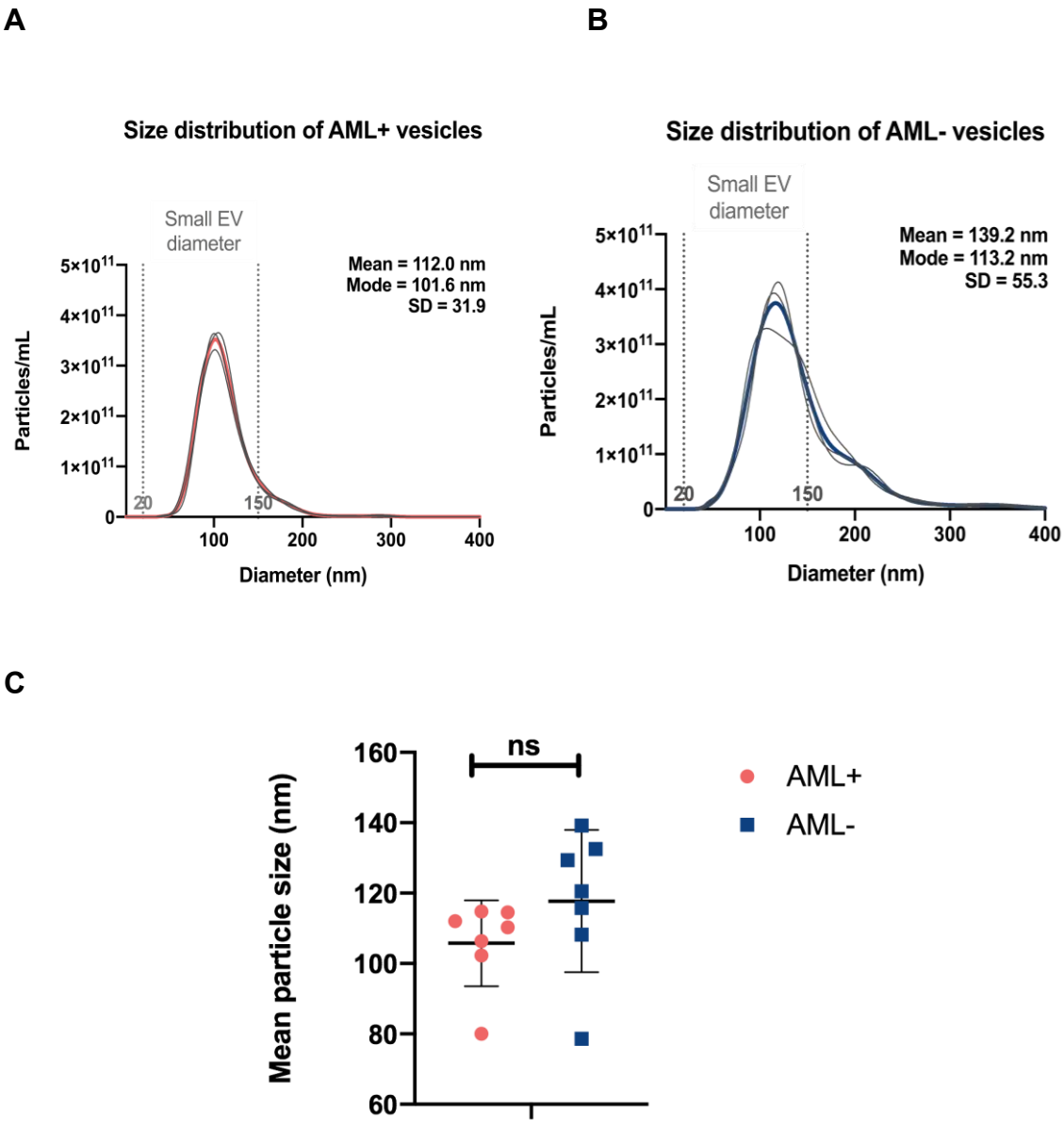

Figure 3.8: EVs generated from AML+ and AML- cell bioreactors are predominantly of classical small EV size. *Particle size and concentration were measured by NTA using NanoSight 3.1 accompanying software. Samples were diluted in particle-free H_2O and loaded for imaging via a syringe pump set at a fixed rate. Three 2-minute videos (shown in grey lines) were recorded and mean concentrations were plotted in coloured lines; representative graph shown of seven independent biological repeats (A,B). Mean particle sizes from various NTA experiments were compiled (C). Statistical analysis was performed using a two-tailed Mann Whitney non-parametric test, where threshold of statistical significance was set at p value of less than 0.05. non-statistical significance, ns.*

3.2.3.2. AML+ and AML- bioreactor cultures secrete a majority of vesicles with diameter and morphology consistent with that of small EVs

Cryo-electron microscopy (cryo-EM) was performed to assess vesicle morphology and heterogeneity within samples (Sokolova *et al*., 2011), and was done in collaboration with Professor Juan Falcón-Pérez (CIC bioGUNE, Bilbao). AML+ and AML- EVs, derived from high-density bioreactor cultures, were visualised as described in **Chapter 2.** Diameters of the vesicles in each image were measured using ImageJ software (version 6). In AML+ and AML- samples, the majority of vesicles had a diameter between 30-150 nm, qualifying them as being classical small EV size (**Fig. 3.9A** and **3.9B**). Other morphologies were also observed, categorised below as: electron-dense, bi-membrane, multi-membrane, irregular sacs, and budding morphologies. These were present in much lower quantities, compared to those within the classic small EV size category, in both AML+ and AML- samples (**Fig. 3.9A** and **3.9B)**. Multi-membrane and budding morphologies were not detected in AML+ samples. Mean diameters of the morphologies were also recorded (**Fig. 3.9C**). Classic small EVs, bi-membrane, multi-membrane, and electron dense categories had similar average diameters, while irregular sacs and budding morphologies had larger diameters (**Fig. 3.9C**). In terms of relative proportions of these vesicle categories, a large majority of vesicles in both AML+ (97.8%) and AML- (95.6%) were classified as a small EV (**Fig. 3.8D,E**). Findings of electron dense vesicles were similar between both groups (2.0% in AML+ vs. 2.1% in AML-). Bi-membranes were found to represent 0.1% of the AML+ group versus 1.1% in AML- samples. Irregular sacs made up 0.1% of the AML+ sample versus making up 0.8% in the AML- sample. Multi-membrane and budding morphologies were found only in AML- and not AML+ (**Fig. 3.8D,E**).

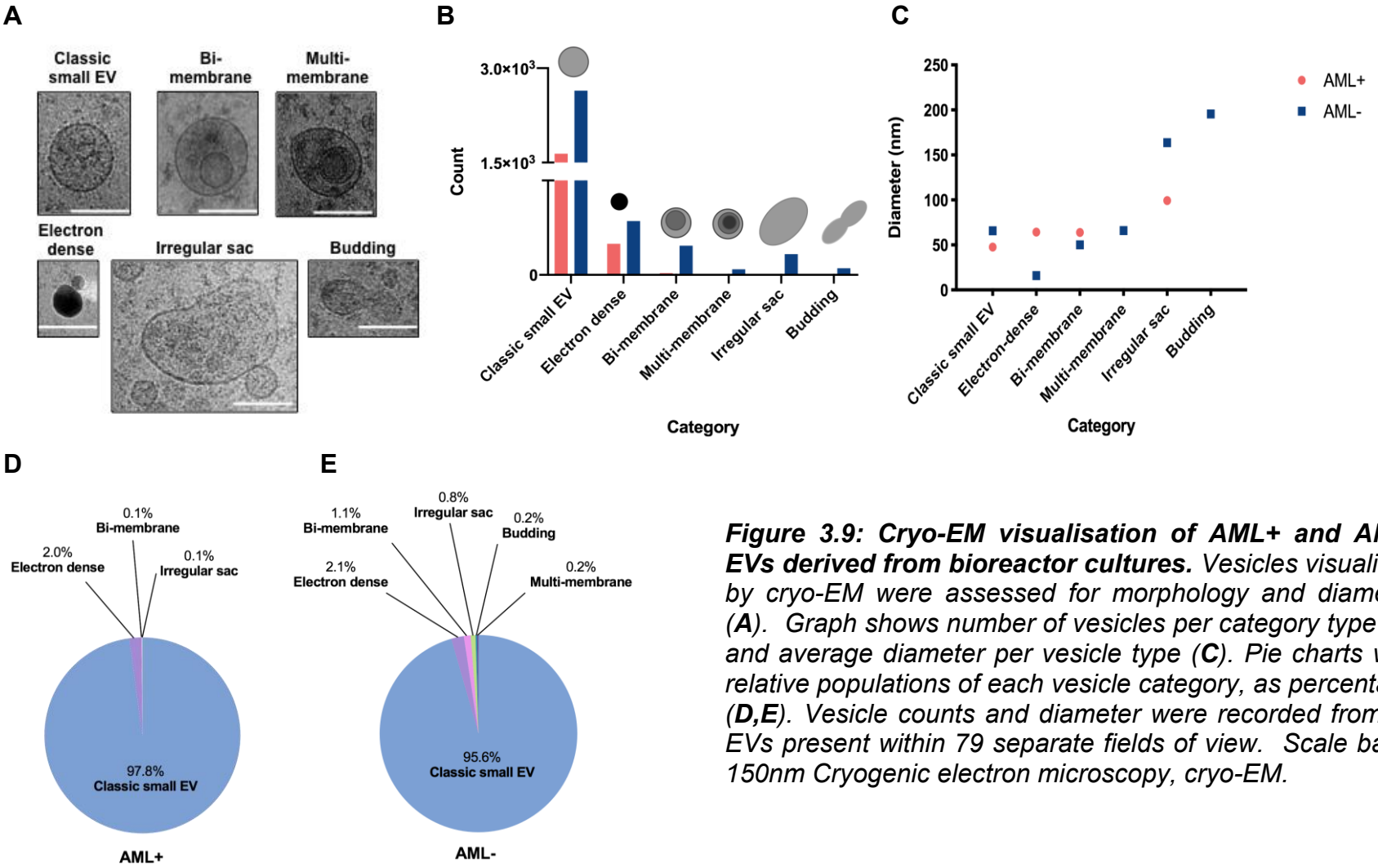

Figure 3.9: Cryo-EM visualisation of AML+ and AML- EVs derived from bioreactor cultures. *Vesicles visualised by cryo-EM were assessed for morphology and diameter (**A**). Graph shows number of vesicles per category type (B) and average diameter per vesicle type (**C**). Pie charts with relative populations of each vesicle category, as percentage (**D,E**). Vesicle counts and diameter were recorded from all EVs present within 79 separate fields of view. Scale bar = 150nm Cryogenic electron microscopy, cryo-EM.*

3.2.3.3. EVs generated from high-density bioreactor-based cultures are pure

Purity of EVs isolated from high-density bioreactor cultures was assessed using the P:P ratio, published by Webber and Clayton. A P:P ratio of > 2.0 x 10^9 denotes a pure preparation of EVs from a given isolation technique (Webber and Clayton, 2013). EVs isolated from AML+ and AML- bioreactors had a P:P ratio of > 2.0 x 10^9 (**Fig. 3.10**), indicating a pure preparation of EVs isolated using our pipeline (outlined in **Chapter 2)** and isolated using differential centrifugation against a sucrose gradient. This pipeline is also reliably reproducible between preparations.

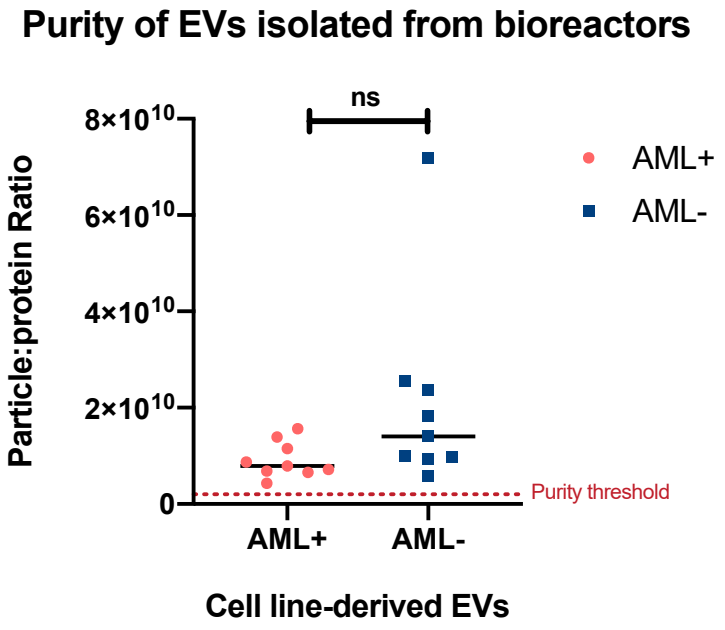

Figure 3.10: EVs separated by sucrose density gradient are pure. *Particles/mL by NTA and protein (µg/mL) by BCA assay were recorded, and P:P ratios calculated for n=9 independent EV preparations from both AML+ and AML- bioreactor cultures. Non-parametric Mann Whitney statistical analysis conducted. ns = non-statistically significant.*

Taken together, these data highlight that a higher yield of EVs can be generated from both AML+ and AML- cells when cells are maintained in high-density bioreactor cultures. Furthermore, culture of cells in bioreactors did not appear to impact vesicle morphology or cargo. Consequently, AML+ and AML- cells were

maintained in bioreactor cultures to generate larger yields of EVs thereby facilitating further analysis, reported in subsequent chapters.

3.3. DISCUSSION

EVs are key mediators of cell-cell communication, and profiling EVs separately from other components of the cell secretome unveils important knowledge about the role of EVs in physiology and how they may promote different disease phenotypes. Research presented in this Chapter aimed to address a key knowledge gap in characterising TSC EVs and determining if they could be isolated from TSC *in vitro* cultures. This work is the first to characterise EVs derived from the AML+ and AML- cell lines and is also the first to report successful expansion of TSC EV production to high-density bioreactor cultures to enhance EV generation for an in-depth, multi-faceted, downstream analysis of EV cargo and subsequent function.

The mesenchymal origin of TSC cells was validated by IF microscopy. The current literature on characterisation of AML cells is limited, despite AML cells being used frequently *in vitro* cell line in TSC tumour biology research. Whilst imaging techniques have previously been used to compare AML cells derived from male and female LAM patients (Bertolini *et al.,* 2018) and formalin-fixed paraffin-embedded tissue (Stone *et al*., 2001) literature which compares the TSC genotype (*TSC2*-deficient) to the rescue control (*TSC2*-expressing) has not yet been published. Positive vimentin stains indicated a mesenchymal origin of both AML+ and AML- cell lines. Negative cytokeratin 18 staining suggests that these cell lines are not of epithelial origin, as expected. The negative staining observed in both

AML+ and AML- cells (**Fig. 3.1**) was complimentary to that observed in the literature. In one study, desmin is documented to stain positively in 20% AML cases only (L'Hostis *et al*., 1999), again potentially due to the variable triphasic composition of AML tumours.

Endolysosomal staining shows some expression of both LAMP1 and LAMP2 in AML cells, although in apparently distinctive patterns. AML+ cells have more clustered expression and potentially larger lysosomes, while LAMP1 and LAMP2 expression appears more ubiquitously throughout the cytoplasm of AML- cells (**Fig. 3.2**). This ubiquitous expression of LAMP1 and LAMP2 could indicate more mobility of the late endosomes in AML- cells. EEA1, a marker for the early endosome, is also visible in AML+ cells and to a lesser extent in AML- cells. EEA1 is implicated in various endocytic processes and vesicle mobility through the cell, suggesting some differences in endocytic processes and vesicle mobility between AML+ cell and AML- cells, though this is difficult to conclude upon from this basic characterisation panel. Furthermore, markers typical of EV surfaces were examined by IF in the parental cells. CD63 and CD81 expression appeared to localise towards the AML- cell peripheries, seen via IF imaging (**Fig. 3.3**). This could indicate readiness for EV secretion from the AML- cells compared to the control AML+ cells, although interpretation of the true meaning of this data would be improved by quantification of expression in repeat experiments. How the cell expression corresponds to EV secretion or expression on EVs, in the case of tetraspanins, is difficult to ascertain.

Characterisation of TSC EVs is currently limited to a few published studies (Patel *et al*., 2016; Zadjali *et al*., 2020; Kumar *et al*., 2021; Bissler *et al*., 2019; Zou *et al*., 2019). EVs in this study were isolated from cell-conditioned media, first from 2D standard cell culture of AML and MEF cells, by serial centrifugation of cell conditioned media underlaid with a 30% sucrose:dH_20 cushion, prior to subsequent PBS wash. Although there is no optimal technique to isolate EVs absolutely and purely from source biomaterial, differential ultracentrifugation is the recommended and most widely used method of EV separation from cell-conditioned media (Théry *et al*., 2018; Gardiner *et al*., 2016). However, differential ultracentrifugation alone does not distinguish EVs from other vesicle types or contaminants, therefore incorporating a sucrose cushion integrates another defining characteristic of EVs – floatation – thereby refining the isolation to EVs only and as specifically as possible. Some, but not all, published studies of TSC EVs use the same sucrose gradient isolation technique (Zou *et al*., 2019), while some also use size-exclusion chromatography (Zadjali *et al*., 2020; Kumar *et al*., 2021). Hence, subsequent analysis of additional molecular characteristics of isolated EVs is important to confirm a pure EV isolation. Additionally, considering that EVs are malleable and mobile in fluid, EVs may also be contaminated by the sucrose, which may affect the purity of the EVs isolated. Therefore, steady handling of apparatus is also required but may be variable between individuals.

While it is the ultimate goal to identify an EV-specific marker, probably based on their unique biogenesis, in order to characterise EVs, the use of a multi-technique approach which classifies EVs based on several characteristics is currently recommended (Théry *et al*., 2018). In this way, researchers can conclude from

multiple complimentary methods that EVs have been isolated for their experiments. This also aims to ensure inter-laboratory standardisation and interpretation of EV-mediated biological effects. In 2D culture-derived EVs, all three tetraspanins were expressed to varying quantities between 1.0 x 10^4 and 2.0 x 10^4 (TRF arbitrary units) in both AML+ and AML- samples (**Fig. 3.4**). Tetraspanin expression is less convincing in MEF+ EVs from 2D culture, with low expression levels similar to that of the isotype controls. This may be indicative of insufficient antibody binding, specificity, or difficulty in isolating EVs from the MEF+ cell line in particular. CD9 and CD81 expression in MEF- is higher but variable in the case of CD81, while CD63 expression is again low and similar to that of the isotypes (**Fig. 3.4**). Both AML and MEF cell lines had a majority of particles that had a diameter classical of a small EV, according to NTA size distribution analysis, which suggests that all cell lines secrete small EVs (**Fig. 3.5**).

Trends in EV secretion over time were analysed and compared between *TSC2*-deficient and control cell types (**Fig. 3.6**). Both AML- and MEF- cell lines showed a trend of increased EV secretion respective to AML+ and MEF+ control cell lines, though neither cell line was found to have a statistically significant increase in EV secretion. This may reflect a sporadic nature of EV secretion, especially when taking findings of other relevant studies into account. One study reported that *Tsc2*-deficient T2J cells had significantly increased EV secretion compared to parental control cell lines from mouse renal inner medullary duct cells (Zadjali *et al*., 2020). Another study by Zou and colleagues reported decreased EV secretion from *Tsc2*-deficient MEF- cells compared to *Tsc2*-expressing MEF+ cells (Zou *et al*., 2019), though expression of other EV-associated markers (namely ALIX, CD63, and

TSG101) were also found to be markedly lower in MEF- EVs compared to the MEF+ EVs in the same study. There is also the argument that it may be, in fact, the cargo of EVs secreted, not necessarily their elevated secretion, that may be most significant in promoting disease progression. Moreover, the destination of EVs secreted from tumour cells and the disease-supporting phenotypes that they promote is also a key factor in how EVs contribute to disease, which remains largely unknown in TSC.

AML+ and AML- cells grown in bioreactors secrete EVs that displayed similar characteristics to the EVs isolated from 2D cultures. Tetraspanin expression was also expressed on AML+ and AML- EVs generated from high-density bioreactor cultures (**Fig. 3.7A**). It is also notable that all three tetraspanins were expressed more highly in AML- EVs compared to AML+ EVs. However, one limitation of this TRF-based plate assay is that it cannot distinguish tetraspanin expression per EV. Instead, it detects total expression of a particular tetraspanin within a sample, which uses total protein as a surrogate for EV loading. Therefore, single EV tetraspanin expression cannot be reliably interpreted. Furthermore, a larger yield of EVs, as provided by bioreactor cultures, was required to have enough protein to perform SDS-PAGE and western blot for detection of ESCRT proteins ALIX and TSG101, associated with EV biogenesis. ALIX and TSG101 expression were evident in parental cell lysates, but their enrichment in the AML+ and AML- EV lysates is clear, as expected, and indicates their likely association with the late endosome. Both EV lysates were devoid of ER protein GRP94 expression, which would suggest that the EV isolations were not contaminated with cellular components such as the ER (**Fig. 3.7B**). NTA data also showed that the majority of EVs from AML+ and AML-

bioreactors were of small EV size (**Fig. 3.8**). This data, together with size distribution profiles of AML+ and AML- samples indicates that AML+ and AML- cells secrete small EVs of endosomal origin. It is important to note that protein markers named do not represent EV-specific markers, but rather markers that are EV-enriched proteins (Mathivanan and Simpson, 2009; Kalra *et al*., 2012). It is equally important to remember that these EV preparations are not without EV subpopulations, though most of those in EV isolates in this study were found to be of endosomal origin. Another point to consider is the culture media of these cells contained high glucose levels (as described in **Table 2.1**). High glucose levels have been shown to increase mTORC1 phosphorylation and activation (as reviewed by Sangüesa *et al*., 2019). For example, high glucose levels *in vitro* were shown to elevate glycolytic flux and decrease Rheb-GAPDH interactions, thereby causing an increased bioavailability to Rheb to activate mTORC1 (Lee *et al.*, 2009). This may elicit some effects on the mTORC1 activity status of cells grown both in 2D and in 3D-based bioreactor cultures. Furthermore, potential caveats in bioreactor cultures are important to consider. Maintenance of cell lines in bioreactors in long term culture may pose some issues and it is important to assess stability of these cell lines overtime. This could be achieved, for example, by assessing TSC2 expression or TSC2 deficiency by western blot in cells pelleted in the clearing centrifugation steps in weekly isolation of EVs from cell-conditioned media. Hypoxic environments may also be generated in long-term cultures, which may impact results particularly regarding HIF-1α or VEGF expression, for example. Importantly, while secreted EVs are removed for processing on a weekly basis, there may be some cellular effects caused by EVs within the inner chamber interacting with the resident cells within the bioreactor. This could induce

stimulation of biological pathways or processes, or phenotypic modifications to the cells, which may in turn altered secreted EV cargo and functionality over time. This poses challenges in terms for these long term cultures, but it is also worth pointing out that this could be also more indicative of a long-term tumour model that could recapitulate dynamic interactions of tumour cells with EVs *in vivo.*

Cryo-EM is commonly used technology to analyse the architecture of cells and cell-derived vesicles (as reviewed by Dubochet *et al*., 2012). The key advantage of cryo-EM is that EVs can be analysed in their native spherical morphology, and samples are not subject to dehydration or chemical fixatives used in other EM techniques which may change the morphology of the EVs. This enables the broad repertoire of vesicles secreted from cells to be visualised (Arraud *et al*., 2014). Cryo-EM images in this study revealed several different structures defined by lipid bilayer boundaries (**Fig. 3.9A**). EV samples from TSC cells have not been previously published, nor have EVs secreted from mTORC1-driven cells, indicating the novelty of this finding. The analysis shows a heterogeneity of vesicles, with a large majority of both AML+ and AML- samples containing small vesicles with a diameter ranging from 20 to 150 nm (**Fig. 3.9**). The detection of vesicles larger than 200 nm was rare but not unexpected, however vesicles and particles may become distorted through the pressure-driven filtration in processing. It is also important to note that while separation of EVs using a sucrose-based cushion is biased towards EVs that float at 1.1 and 1.2 g/mL, it is not without risk of isolating other vesicular matter. No one technique for isolating EVs ensures an entirely pure EV population. Cryo-EM analysis supported NTA data, with a majority of EVs secreted having a diameter that would qualify them as a small EV. However, NTA

is not with its own limitations as a technique. Dilution of samples, light scattering from any detected particulate matter, some variability between subsequent runs using the same sample, all may cloud the ability to distinguish small EVs, which are the key focus of this study, and other nanoparticulate matter. Hence, the importance of analysis of molecular markers associated with EVs and EV biogenesis as previously discussed in order to demonstrate enrichment of ESCRT-associated proteins and tetraspanins on the surface.

Assessment of EV purity was conducted using the P:P ratio which calculates a purity measurement based on particles divided by total protein content detected (**Fig. 3.10**). Acceptable P:P ratio thresholds are published by the authors (Webber and Clayton, 2013) and P:P ratios were calculated for each EV preparation using a sucrose density gradient. As previously discussed, the reliance on NTA to generate accurate and reproducible measurements of particles/mL can be limiting. Total protein quantification was measured using the BCA Protein Assay Kit. This is a widely used colorimetric assay that can measure a broad range of protein concentrations and is highly sensitive. However, although EVs were isolated using a recommended method, there is no guarantee of total protein concentration of a particular sample being solely vesicular and contaminant-free. However, throughout this study, EV isolations and subsequent P:P ratio calculations did indicate that our EV production was producing EVs that were suitably pure for use.

3.4. CONCLUDING REMARKS

In this Chapter, I have shown that TSC cells secrete vesicles that exhibit molecular characteristics of a small EV of endosomal origin. These EVs were found to

express tetraspanins on their surfaces, and were enriched for EV biogenesis proteins, compared to their parental cells. The majority of EVs isolated in our preparation had diameter sizes within the range of 20-150 nm, which qualifies them as small EVs (sEVs). Visualisation of EVs by cryo-EM also showed a majority of EVs from both AML+ and AML- cells had diameters customary of a small EV. This study also showed, for the first time, that AML cell lines cultured in high-density bioreactor cultures produced high yields of sEVs, with the same characteristics as those generated from 2D monolayer culture. sEVs generated using our high-density bioreactor pipeline were also found to be pure, according to P:P ratio calculations, and thereby this TSC EV production was deemed suitable for EV cargo and functional analysis. Profiling the molecular cargo of AML cell-derived EVs is the next step in understanding their contribution to disease, and comprises the work laid out in **Chapters 4** and **5.**

CHAPTER 4

PROFILING TSC sEV RNA CARGO

4.1. INTRODUCTION

4.1.1. Rationale

Understanding the function of sEV-RNA is critical to a holistic insight into a particular disease state due to the ability of these intercellular RNA messengers to alter gene expression and phenotypes of recipient cells (as reviewed by O'Brien *et al*., 2020). The RNA cargo of sEVs can include an assortment of RNA sequences that represent many RNA biotypes, including protein-coding components such as messenger RNA (mRNAs) and non-coding RNAs such long non-coding RNAs (lncRNAs) and micro RNA (miRNAs) (as reviewed by O'Brien *et al*., 2020). Determining the RNA signature of sEVs from TSC AML cells could reveal important biological insights into drivers of AML tumour progression and development, and may reveal potential biomarkers of disease status.

4.1.2. RNA biotypes

RNA biotypes of focus in this study were mRNAs, lncRNAs, and miRNAs. These RNA biotypes have unique biological roles and have potential biological relevance to a disease state given their intercellular delivery by sEVs, and are described in more detail below.

4.1.2.1. Coding RNA biotype: mRNA

The coding component of the EV RNA cargo involves mRNA, a single-stranded RNA molecule that has a complementary sequence to one strand of DNA of a gene. mRNAs conduct the intermediate step between DNA transcription and protein production by cytoplasmic ribosomes (as reviewed by Pardi *et al.,* 2018). EV-mRNA-mediated translation of proteins in recipient cells has been reported (Valadi *et al*., 2007; Skog *et al*., 2008). EV-associated mRNAs have been implicated in many cancer types, promoting various pro-tumoral biological processes and signalling cascades.

However, knowledge of how EV-mRNA functions in the context of TSC tumours is limited. Studies relating to TSC EV-RNA are few, where one focused on mRNAs (Patel *et al*., 2016) and others investigated miRNAs and their predicted mRNA targets (Kumar *et al*., 2021; Cukovic *et al*., 2021) and so profiling the mRNAs shuttled intercellularly from AML cells could reveal important insight into EV-induced protein translation in the microenvironment. Attributing functions to mRNA is aided by extensive online platforms that perform gene ontology and functional enrichment analysis, to determine molecular functions and biological networks encompassed by these EV-mRNAs.

4.1.2.2. Non-coding RNA biotypes

4.1.2.2.1. micro RNA (miRNA)

miRNAs are 20-24 nucleotide-long, conserved single-stranded RNA molecules that do not encode functional proteins as products (as reviewed by Ambros *et al*., 2004).

Instead, miRNAs regulate gene expression post-transcriptionally. Specifically, miRNAs anneal to complementary sites in the 3' untranslated region (3'UTR) on target transcripts of mRNA, to cause mRNA transcript downregulation via destabilisation or inhibition of protein translation (as reviewed by Huntzinger and Izaurralde, 2011; Rizzuti *et al*., 2018). Complete annealing of the miRNA to its target mRNA causes degradation of the transcript, while incomplete miRNA-mRNA base-pairing causes translational repression, mRNA degradation or sequestration into cytoplasmic P-bodies (as reviewed by Paez-Colasante *et al*., 2015).

In TSC, miRNA research has been focused in the context of TSC cortical tubers and epilepsy. In these studies, differentially expressed miRNAs were found to be involved in activating IL-1R/Toll-like receptor pathway signalling (van Scheppingen *et al*., 2016). Another study identified twelve differentially expressed EV-associated miRNAs from epileptogenic TSC tubers that were involved in targeting neuroinflammatory cascades (Cukovic *et al*., 2021). Additionally, another study found overexpression of miR-23a, miR-34a, miR-34b, and miR-532-5p in epileptogenic tubers versus neighbouring non-tuberous tissue (Dombkowski *et al*., 2016). It is also noteworthy that miR-23a and miR-34a were found to target the *TSC1* 3' UTR, in the same study. Few studies have reported on the role of miRNAs in AMLs to date. One reported that miR-9-5p, miR-124-3p, and miR-132-3p targeted *BCL2L11* to regulate apoptosis and proliferation in a *Tsc2*$^{-/-}$ MEF cell model of TSC (Cai *et al.,* 2018). Another group revealed that miR-212a-3p and miR-99a-5p were downregulated in EVs from *Tsc2*-mutant cells compared to *Tsc1*-mutant cells (Kumar *et al*., 2021), yet their expression in control cells is unclear. Understanding what miRNAs are carried by EVs from *TSC2*-deficient cells (AML-

cells) compared to *TSC2*-expressing counterparts (AML+ cells) could reveal more differences in what role miRNAs play in regulating gene expression and how this governs AML versus normal renal physiology.

4.1.2.2.2. Long non-coding RNA (lncRNA)

Transcription of the genome generates lncRNA, a large and diverse subclass of RNA transcripts. LncRNAs are defined as RNA transcripts that are longer than 200 nucleotides, and that are not translated to functional proteins (as reviewed by Statello *et al*., 2021). The functions of lncRNAs are wide-ranging, with roles in regulating gene expression at the epigenetic, transcriptional, and post-transcriptional level (as reviewed by Fang and Fullwood, 2016). LncRNAs can function as miRNA *sponges* when they act as negative regulators of miRNAs or tag mRNAs for degradation processes (Usman et al., 2018), or in mediating transcriptional regulation of genes (as reviewed by Long *et al.,* 2017). LncRNAs can also encode hidden polypeptides via translation of small open reading frames (smORFs) (Matsumoto *et al*., 2017; Ruiz-Orera *et al.*, 2014). However, it is still difficult to ascertain how lncRNA function in disease. Many lncRNAs are included in prognostic signature panels for different cancer settings (Mohankumar and Patel, 2016; Zhang and Gao, 2019; Li *et al*., 2018).

The role of lncRNAs in TSC is currently not well documented. Some research has been conducted revealing some insights into the lncRNA regulation of the mTOR signalling pathway. For example, one study showed the lncRNA *MEG3* was involved in regulating Akt/TSC/mTOR pathway-mediated autophagy, causing increased cisplatin-induced nephrotoxicity (Jing *et al*., 2021). Another lncRNA *MALAT1* was found to inhibit autophagy by regulating TSC2/mTOR signalling,

thereby promoting apoptosis in cardiomyocytes (Hu *et al*., 2019). LncRNAs are also noted to have many advantages as biomarkers, as they are highly stable in biodistribution, particularly so when associated with EVs (as reviewed by Akers *et al*., 2013), and are considered as tissue-specific. Secondly, lncRNA detection is reliable across many body fluids (as reviewed by Pardini *et al.*, 2019), permitting their application to non-invasive patient sampling, which is more easily tolerated than traditional tissue biopsies. Knowing which lncRNA are highly differential between AML- sEVs and AML+ sEVs could point towards those with relevance to TSC biology or indeed which may have an application as biomarkers.

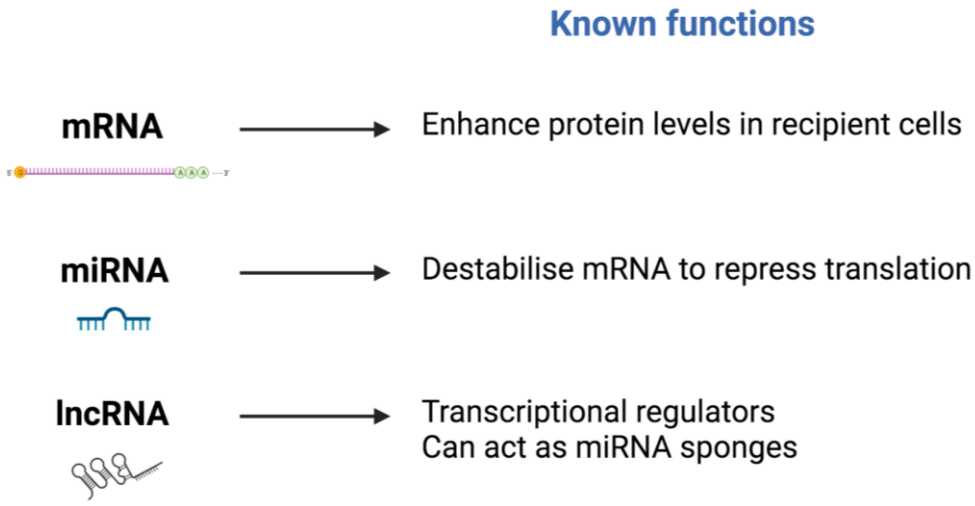

Figure 4.1: mRNA, miRNA, and lncRNAs functions. *Examples of known functions of RNA species commonly associated with EV cargoes. Ribonucleic acid, RNA; Messenger RNA, mRNA; microRNA, miRNA; long non-coding RNA, lncRNA.*

4.1.3. Standardisation and sequencing of EV-RNA

In recent years, a position paper outlining the challenges and opportunities to be considered to standardise functional analysis of EV RNA was published (Mateescu *et al.*, 2017). An important consideration prior to EV-RNA profiling is in assessment

of RNA quality within EVs. EV samples are thought to be largely absent of intact large and small ribosomal RNA (rRNA) subunits (Mateescu *et al*., 2017), differing that of cellular RNA. RNA quality is typically measured by generating a RNA Integrity Number (RIN) score. However, RIN scores are not suitable when analysing EV-RNA as this score measures the major 18S and 28S ribosomal RNA peaks which are commonly abundant in cell-derived RNA but not EV-RNA (Hill *et al.*, 2013).

RNA sequencing (RNA-Seq) is a high-throughput technology that profiles the transcriptome of a particular biological sample (Yalamanchili *et al*., 2017). To do so, RNA-Seq uses next-generation sequencing (NGS) platforms to determine the presence and quantity of RNA within query samples. Prior to library generation and subsequent RNA-Seq, ribosomal RNA depletion takes place by one of two methods: rRNA depletion or polyadenylated (poly-A) mRNA tail enrichment. Depletion of rRNA is an essential step when sequencing cell-derived RNA, as it is said to make up over 90% of RNA from cells (Eaves *et al*., 2020). Conducting rRNA depletion from EV-derived RNA is still recommended, as though EVs are not thought to carry rRNA, some evidence suggests that rRNA fragments may be contained in EVs (as reviewed by Turchinovich *et al.*, 2019). Next, remaining RNA fragments are incubated at high temperatures before hybridising to random hexamer primers for RNA transcript to be reverse transcribed into cDNA (Kadakkuzha *et al*., 2015). First strand cDNA occurs when a reverse transcriptase from the random primer extends the entire length of the strand, with actinomycin D added to prevent synthesis of the second strand at this point. Second strand synthesis succeeds this step with the addition of uracils along the length of the

second strand, creating strandedness. This method is known as the deoxyuridine triphosphate (dUTP) method. A clean-up step follows before the addition of phosphorylated ends to both ends of the DNA molecule. An adenine overhang is added to the 3' end. Hairpin-shaped adapters with thymine overhangs then bind the DNA molecule. The added uracil to the second strand is enzymatically degraded, leaving only the first strand still intact with the adapters, and as a single strand for the final library. Size selection for particular RNA fragments can also take place after this step, followed by PCR amplification. PCR amplification selects for molecules that have two adapters at each end, and molecules are compiled in a library ready for sequencing. The library is aligned to a reference database to identify the unknown transcripts, to generating a genome-wide expression profile. The resultant dataset is used to assess the transcriptome, to analyse its complexities and to interpret its relevance to a particular pathology. This technology offers some advantages over the traditional hybridisation-based microarray or Sanger-sequencing based methods with its higher resolution and less background noise (as reviewed by Wang *et al*., 2009). RNA-Seq can be used to examine differential gene expression between the transcriptomes of different samples or treatment groups (as reviewed by Wang *et al*., 2009). Differential expression of genes associated with certain biological processes or pathways, or molecular functions can be used to predict differences in mechanisms between different samples, and so RNA-Seq contributes to predicting novel mechanisms in many pathologies. It also generates larger datasets in a much more efficient manner, not just those pre-selected in microarrays or primers designed for Sanger sequencing.

Following an RNA-Seq experiment, pathway analysis is commonly conducted to establish insights into potential mechanisms of disease generated from comparing different experimental groups in a genome-scale omics experiment (Reimand *et al*., 2019). Pathway analysis uses existing knowledge of related or interacting biomolecules, and tests hypotheses about relationships between a set of these biomolecules, called the pathway, and a particular experimental condition (Pomyen *et al*., 2015). Analysis of these gene lists can be conducted using two main methods: over-representation analysis (ORA) and its extension gene set enrichment analysis (GSEA). ORA categorises genes into those that are differentially expressed or not, based on their *p* values. Then, the number of differentially expressed genes in each annotated pathway is established. Finally, a p value for each pathway is determined by getting the number of differentially expressed genes against the background list of all genes, this is calculated used a hypergeometric distribution. There are some limitations to consider when employing ORA, such as its handling of data in binary terms only and not on a continuous measurement. ORA also is based on the assumption that genes are exclusive from one another, which is a simplification due to the complex network of interacting genes particularly within the same given gene pathway. GSEA aims to mitigate *ad hoc* thresholds, instead determining if an annotated gene set is unexpectedly low or high via running-sum statistic (Liu and Ruan, 2014). Potential biases in pathway analysis are important to consider when interpreting results. These include *length bias*, *GC content bias*, and *chromosome bias*. *Length bias* can arise when long genes result in more fragments being generated in cDNA fragmentation, which can result in higher numbers of counts and increase power when differential expression is being assessed (Oshlack and Wakefield, 2009;

Phipson *et al*., 2017). This results in GO analysis bias towards GO categories with longer genes (Young *et al.,* 2010). *GC content bias* refers to the number of guanine and cytosine bases occurring within a particular genomic region, and how this affect read coverage across a genome. Studies have reported that GC-rich genomic regions are amplified with less efficiency (Arezi *et al*., 2003) and that GC bias increases with more PCR cycles (Chen *et al*., 2013). *Chromosome bias* in gene sets points to the bias caused by large chromosomal duplication or deletion. In these cases, there could be increased or decreased expression of genes from the affected chromosome, which could affect sequencing reads. Determining which biases could play into the reading of the sequences of the data is important for a fair judgement of potential mechanisms or functions.

4.1.4. TSC RNA profiling

To date, research about RNA in TSC has largely focused on intracellular RNA. A recent landmark study by Martin *et al.* used a comprehensive genomic screen of 111 TSC-associated tissues from various organs (Martin *et al*., 2017). The authors reported decreased *TSC2* mRNA transcripts in TSC tissues compared to non-TSC tissues in the case of one or two truncating *TSC2* mutations, and tumours with two truncating *TSC1* mutations resulted in reduced *TSC1* mRNA expression compared to non-TSC tissue. Importantly, this study also reports an identified 1395 genes differentially expressed in AMLs compared to non-TSC normal kidneys. Differentially expressed genes (DEGs) found most decreased were associated with normal kidney function, including transmembrane transport, ion transport, and excretion (Martin et al., 2017), uncovered in GO analysis. Primarily, TSC RNA

research has used models of TSC brain-associated clinical signs, such as cortical tubers (Mills *et al*., 2017) and TSC SEGAs (Zordan *et al*., 2018). Zordan *et al*. identified matched upregulation of *Gpnmb, Mpeg1*, *Ltf*, and *Sln* genes in both mouse SEGAs and human TSC lesions by RNA-Seq. Another study reported differential expression of 11 miRNAs in serum of TSC patients compared to age- and sex-matched healthy donors (Trelinska *et al*., 2016).

4.1.2.1. TSC EV-RNA profiling

Knowledge of the RNA cargo carried by TSC sEVs is currently limited. Mouse work showed *Rheb* and *Notch* mRNAs in *Tsc1*-deficient EVs (Patel *et al*., 2016), while other studies showed that EVs from *Tsc1*-deficient and *Tsc2*-deficient cell lines could mediate miRNA/mTORC1 axes differentially (Kumar *et al*., 2021). Cukovic *et al.* discovered the elevated expression of twelve miRNAs in EVs isolated from epileptogenic tubers, compared to EVs from non-epileptogenic tubers, with an enrichment for innate immune signalling via toll-like receptors 7/8 and inflammatory responses (Cukovic *et al*., 2021). To date, no studies have been published based on the sEV-RNA cargo or function from TSC tumours, or TSC-AML sEVs, specifically despite AML being associated with significant morbidity and mortality. Determining RNA biotypes and predicted functions upon delivery could reveal novel mechanisms which promote tumour growth and that could be applicable to new anti-tumour therapy. Such knowledge may also uncover novel RNA candidates that could act as TSC biomarkers.

Work presented in this Chapter expands on this smaller scale work, addressing the gaps in human TSC EV knowledge using an unbiased RNA-Seq approach.
The Chapter presents the first comprehensive screen of human TSC sEV-RNA cargo focusing on RNA from AML+ sEVs and AML- sEVs analysed by next-generation sequencing. This RNA-sequencing culminated in a list of differentially-expressed genes between the two sEV groups. RNA biotypes were identified in both AML+ sEV and AML- sEV sample groups, and those with the largest coverages were subjected to gene ontology (GO) enrichment analysis using multiple online GO platforms, to predict networks of mRNAs packaged into TSC sEVs and signalling that could be propagated by delivery of these sEV groups to recipient cells.

4.1.6. Hypothesis and aims

Work presented in this Chapter aims to profile the circulating sEV-RNA secreted from AML cells. I also wanted to investigate how the predominant sEV-RNA biotypes found could be contributing to TSC tumour progression. Analysis of the TSC EV transcriptome is limited to a few studies (Cukovic *et al*., 2021), but profiling the transcriptome of AML sEVs has not been conducted comprehensively to date.

The overarching hypothesis for this Chapter is that AML- sEVs have a transcriptome of various RNA biotype species that may be implicated in regulating gene expression and modulating phenotypes and cell signalling in recipient cells of the tumour microenvironment.

Specifically, work presented in this Chapter aims:

I. To isolate RNA in detectable quantities (ng/µL) from AML+ and AML- sEVs
II. To identify RNA biotypes and differentially expressed genes (DEGs), including components of the mTORC1 signalling pathway, in AML- sEVs versus AML+ sEVs
III. To conduct functional enrichment gene ontology (GO) analysis on DEGs in AML- sEVs versus AML+ sEVs using online platform GOliath (www.bioinformatics.babraham.ac.uk/projects/goliath/) to aid prediction of potential phenotypic and cell signalling modifications in recipient cells post sEV delivery

4.2. RESULTS

4.2.1. AML+ and AML- sEVs for RNA-Seq contain detectable quantities of RNA

RNA was isolated from bulk AML+ and AML- sEVs from bioreactor cultures. RNA quantities (determined using NanoDrop™ *2000/2000c Spectrophotometer)* were normalised to number of particles per sample, as determined by NTA using NanoSight NS300. Both AML+ and AML- sEV samples contained detectable quantities for RNA, within the range of 6.79×10^{-11} and 7.93×10^{-10} ng per particle (**Fig. 4.2**).

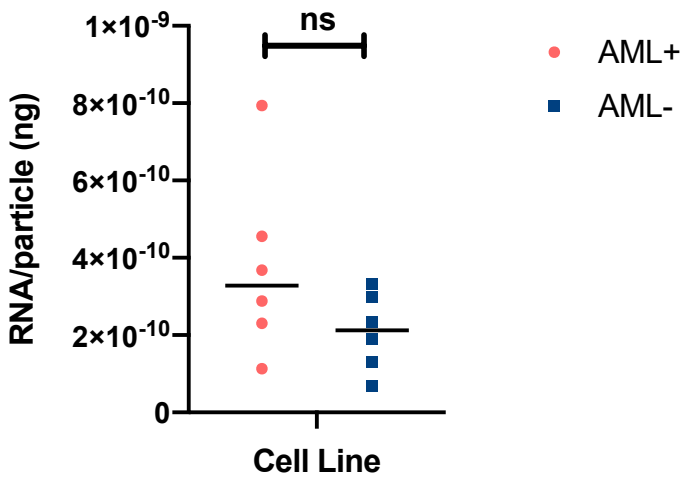

Figure 4.2: AML+ and AML- sEVs contain detectable quantities of RNA. *sEV-RNA was extracted using a TRIzol®-chloroform-based extraction method. Air-dried RNA pellets were resuspended in PCR grade H_20 and RNA (µg/µL) per sample was quantified using NanoDrop™ 2000/2000c Spectrophotometer. Graph represents RNA quantities from n=6 separate sEV isolations from AML+ and AML- cell line bioreactor cultures. Non-parametric Mann Whitney statistical test used; ns = non-statistical significance.*

4.2.2. Selection of sEV-RNA samples for RNA-Seq

Seventeen RNA samples were submitted for quality control using the % DV200 method, which was conducted by Shelley Rundle (Wales Gene Park, Heath Park Campus, Cardiff University, Wales, UK). The % DV200 method indicates the percentage of RNA fragments that are >200 nucleotides in length. This method of assessing purity was used given the lack of rRNA associated with EVs and, hence, the inability to generate an RNA Integrity Number (RIN) score. Using this parameter, samples were categorised by quality rating in accordance with illumina® guidelines (**Table 4.1**). Top-ranking AML+ sEV and AML- sEV samples were selected, shown shaded in **Table 4.1**, and submitted for sequencing. The NEBNext® Ultra™ II DNA library Prep Kit for Illumina® was used to prepare the DNA libraries for next-generation sequencing on Novaseq. Library preparation and

subsequent sequencing was conducted by Dr Vikki Humphries (Wales Gene Park) in accordance with illumina® manual protocols.

Table 4.1: Sample selection was determined by top-ranking % DV200 scores. % DV200 was assessed using TapeStation. Samples were ranked in accordance with illumina quality guidelines (>70 % = high quality; 50-69.99 % = medium quality; 45-49.99 % = medium/low quality; 30-44.99 % = low quality; < 30 % = not suitable for sequencing, denoted by a red-coloured "X"). Shaded rows indicate quality-approved samples (n=6 bulk AML+ sEVs; n=6 bulk AML sEVs-) sequenced on NovaSeq.

Sample	RNA conc. (ng/µL)	Total RNA in aliquot (ng/12 µL)	% Total (DV200)	illumina Quality category
AML+	24.3	291.6	59.82	Medium
AML+	6.2	155	57.68	Medium
AML+	11.6	139.2	57.07	Medium
AML+	5.9	70.8	46.19	Low/Medium
AML+	9.5	114	41.17	Low
AML+	224.8	2697.6	39.98	Low
AML+	16.9	202.8	37.17	Low
AML+	5.1	61.2	30.21	Low
AML+	61.1	733.2	19.11	X
AML-	6.1	73.2	70.56	High
AML-	4.2	50.4	66.15	Medium
AML-	7.8	93.6	56.85	Medium
AML-	7.6	91.2	49.01	Low/Medium
AML-	5.2	62.4	47.14	Low/Medium
AML-	24.2	290.4	38.87	Low
AML-	4.8	57.6	36.96	Low
AML-	4.5	54	28.13	X

4.2.3. mRNAs associated with mTORC1 signalling are differentially expressed between AML+ sEVs and AML- sEVs

Given the known role of mTOR hyperactive signalling in TSC tumour development, expression of a small panel of mTOR-related mRNAs in AML+ sEVs and AML- sEVs was conducted by qPCR. Trend of *TSC2* mRNA expression was lower in AML- sEVs compared to AML+ sEVs (**Fig. 4.3A**), though with not statistical significance. *RHEB* (**Fig. 4.3B**), *4EBP1* (**Fig. 4.3D**) and *AKT* (**Fig. 4.3E**) mRNA

expression appeared to be elevated in AML- sEVs compared to control AML+ sEVs, though this difference was not found to be statistically significant. *MTOR* (**Fig. 4.3C**) and *NOTCH* (**Fig. 4.3F**) mRNA expression was variable in AML- sEVs, but not significantly differentially expressed on average compared to AML+ sEVs. Some similar findings were seen in the RNA-Seq data, with *TSC2* expression found to be lower in sequenced AML- sEVs compared to AML+ sEVs, and *MTOR* was found variably expressed across samples of both AML+ and AML- sEVs groups (data not shown). Some opposite trends were observed between the findings generated by the two techniques. *RHEB* was found comparably expressed in sequenced AML+ and AML- sEVs, while *NOTCH1* was found to be expressed higher in AML+ sEVs compared to AML- sEVs analysed by RNA-Seq (data not shown).

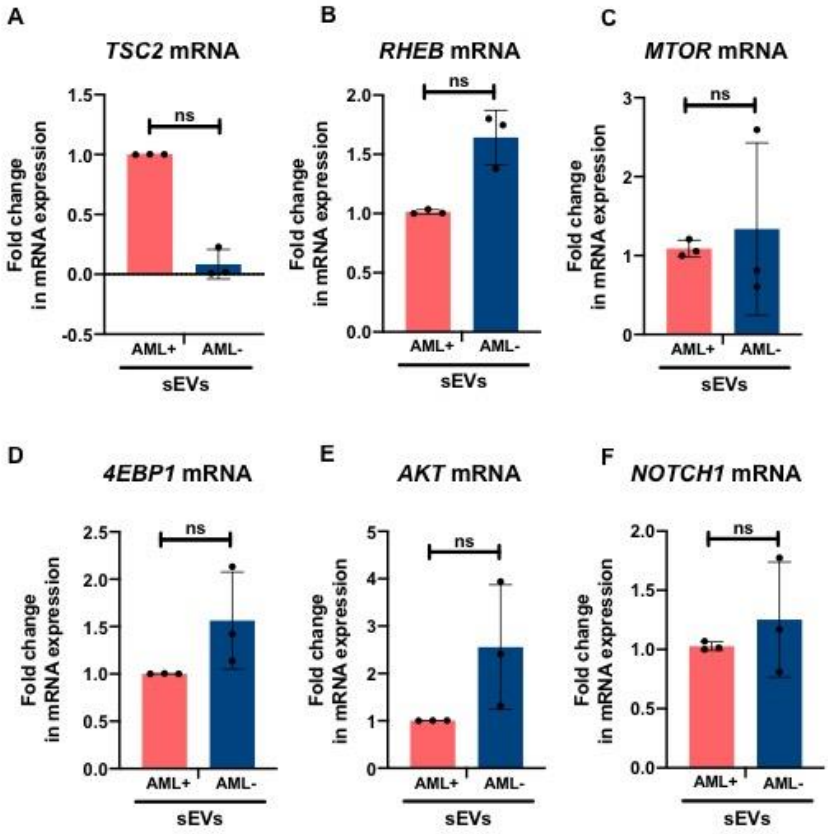

Figure 4.3: mRNAs associated with mTORC1 signalling are differentially incorporated in AML+ and AML- sEVs. *RNA was isolated from sEVs using a Trizol-chloroform method anwas conducted using TaqMan gene expression assays. Graphs show fold changes in three independent repeats. Non-parametric Mann Whitney statistical analysis conducted, ns = non-statistical significance.*

4.2.4. Differential gene expression (DEGs) analysis in AML- sEVs versus AML+ sEVs

The DEGs list, comparing RNA expression in AML- sEVs versus AML+ sEVs, was curated by Samantha Hill and Dr Peter Giles (Wales Gene Park). Using DeSeq2, initial analysis revealed statistically significant (FDR-adj. *p* value < 0.05) differential expression of 11584 RNAs between AML- sEVs and AML+ sEVs. This DEGs list was subdivided into different RNA biotypes using BioMart (Ensembl) by Samantha Hill (Wales Gene Park). Biotype classes found to be upregulated and downregulated in AML- sEVs were assessed. mRNA (89.25%), lncRNA (10.73%)

and miRNA (0.02%) were the RNA biotype classes upregulated in AML- sEVs compared to AML+ sEVs. mRNA, lncRNA, and miRNA were the largest downregulated biotype classes (74.4%, 23.7%, and 1.12%, respectively) in AML- sEVs compared to AML+ sEV controls (**Fig. 4.3A** and **B**). Small nuclear RNAs (snoRNA), small non-coding RNAs (scaRNA), mitochondrial RNA (mtRNA), and small conditional RNA (scRNA) were also found to be downregulated in small percentages in AML- sEVs, but no candidates in these biotype classes were found to be upregulated in AML- sEVs (**Fig. 4.4B**). Given their prominence, these protein-coding (mRNA) and non-coding (lncRNA and miRNA) biotypes were selected for gene ontology analysis.

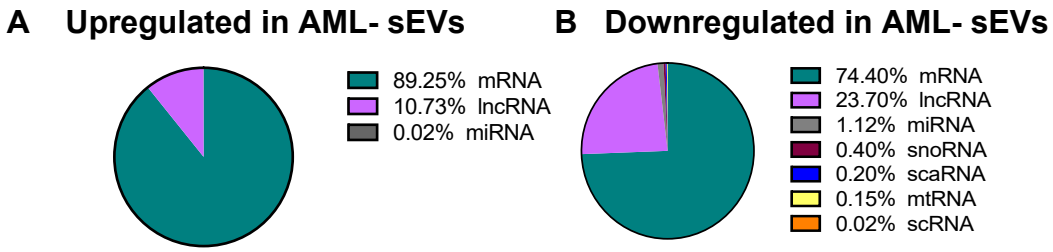

Figure 4.4: Pie charts representing RNA biotypes upregulated and downregulated in AML- sEVs compared to AML+ sEVs. *Differentially expressed genes (DEGs) list in AML+ and AML- sEVs was divided into RNA biotypes using BioMart (Ensembl). RNAs qualifying statistical significance (i.e. FDR-adj. p value < 0.05) were tallied per biotype.*

4.2.5. mRNAs in AML- sEVs

mRNAs were the largest class of differentially expressed RNAs in AML- sEVs versus AML+ sEVs (**Fig. 4.5**). This mRNA list was ranked by descending FDR-adjusted *p* value, and genes with a *p* value greater than 0.05 were omitted. 4316 mRNAs were found to be upregulated in AML- sEVs compared to AML+ sEVs (**Fig. 4.5**) beyond a statistical significance FDR-adj. *p* value of threshold of 0.05. 4038

mRNAs were downregulated in AML- sEVs versus AML+ sEVs, to the same statistical significance threshold.

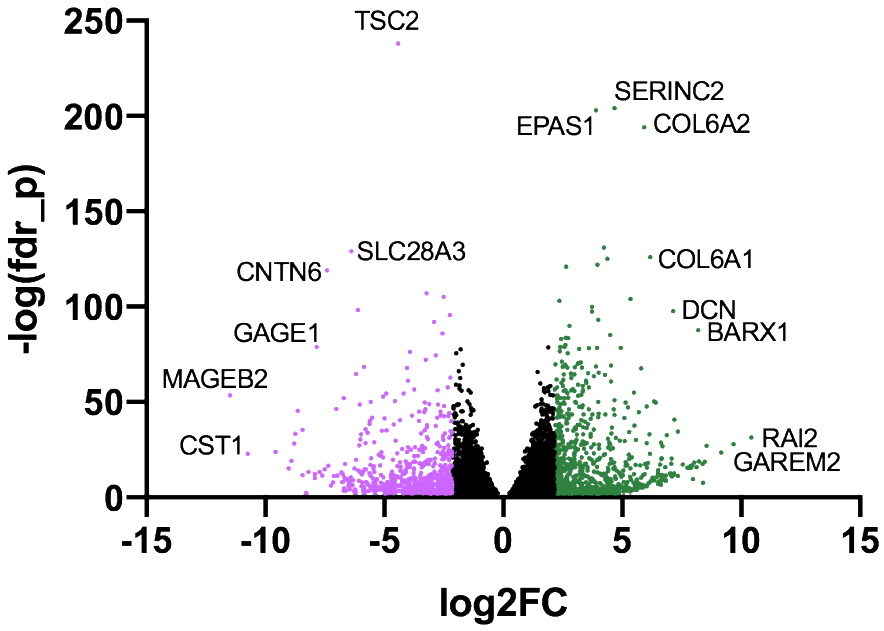

Figure 4.5: Distribution of differentially expressed mRNA between AML- sEVs and AML+ sEVs. *Green dots represent statistically significantly expressed genes FDR-corrected p value of < 0.05, with Benjamini Hochberg (multiple test) correction. Names of top-ranking genes with most significant FDR_p and largest fold changes labelled.*

GO analysis was conducted on differentially expressed genes with greater than 5-fold change, to determine which networks could be most important to examine functionally with delivery of these AML- sEVs to recipient cells. 778 mRNAs were found to be upregulated in AML- sEVs. The identified upregulated mRNAs in AML- sEVs were inputted into GOliath Gene Ontology Search System. Given the aim to investigate potential biological phenotypes and pathways that may be promoted with delivery of these sEVs to recipient cells, analysis was focused on GO annotations *Molecular function* and *Biological processes* and respective enrichment scores were generated. Potential biases to the GO analysis were also listed by GOliath to consider when interpreting the data.

4.2.5.1. AML- sEVS are enriched for mRNAs associated with tumour-supporting molecular functions, involving extracellular matrix remodelling, growth factor and receptor activity, and ion channels

From GOliath, the twenty top-ranking *Molecular function* categories, with FDR-adj. *p* value < 0.05 and greater than 5-fold change are graphed in **Figure 4.6** with accompanying enrichment scores in **Table 4.2**. *Extracellular matrix structural constituent* is the GO term that is significantly enriched and has with the widest % gene coverage (**Fig. 4.6**). Other top-ranking molecular functions involve growth factor signalling – namely, *Growth factor activity*, *Growth factor receptor binding*, and *growth factor binding*. Other molecular functions flagged as top-ranking involve ion channels, including *potassium channel activity*, *ion channel regulator activity*, *cation channel activity, metal ion transmembrane transporter activity*, and *passive transmembrane transporter activity*, amongst others. *Receptor regulator activity* and *Receptor ligand activity* also appear the highest statistical significance. **Table 4.2** details the enrichment of each list category. *Length* bias was flagged in 14 of the top-ranking molecular functions (**Table 4.2**). 12 molecular functions had 'very_long' as a flagged length bias in associated genes while one molecular function had 'vv_long' and another had 'very_short' flagged as a potential bias to consider.

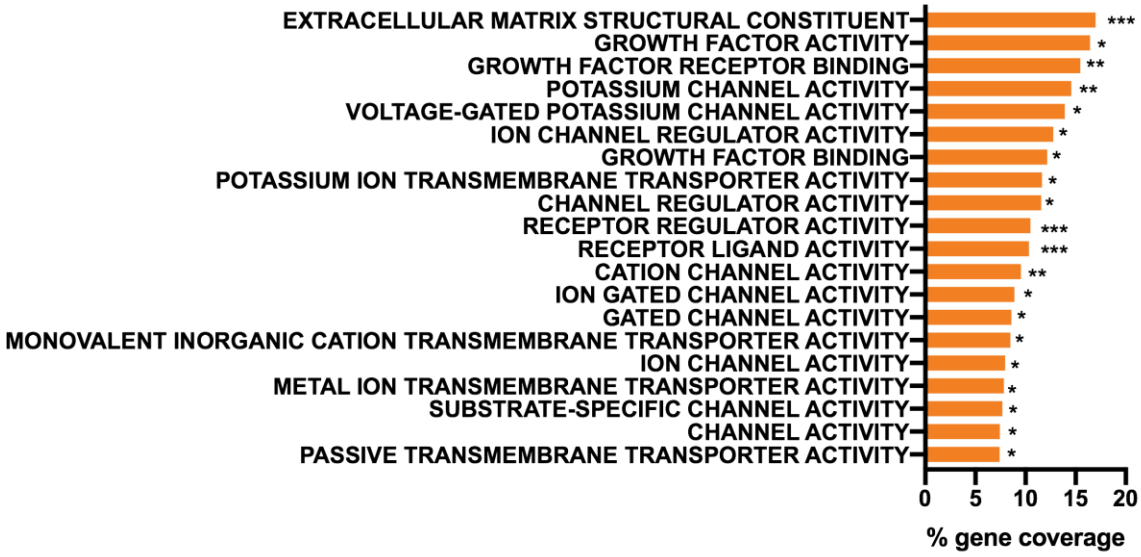

Figure 4.6: Twenty top-ranking Molecular function hits enriched in upregulated AML- sEV mRNAs. *Differentially expressed genes (DEGs) with significant FDR-adj. p value of less than 0.05 and the greatest % gene coverage were ranked in descending order. Enrichment scores in corresponding Table 4.6. False discovery rate adjusted p value, FDR-adj. p.*

As larger queries tend to match with more general GO categories, I also conducted analysis based on GO terms with less than or equal to 200 genes in the background set count. Nine *Molecular function* categories were significantly enriched in amongst these smaller background sets (data not shown). This included the same MF categories with the greatest % gene coverage as listed above, resolving potential bias with very large background datasets.

Table 4.2: Top-ranking molecular function hits in upregulated mRNAs in AML- sEVs. Statistically significant molecular functions with corresponding enrichment scores, based on the number of relevant genes upregulated in AML- sEVs against the total number of genes in the background dataset of each molecular function. Potential biases denoted.

Top 20 *Molecular function* hits in AML- sEVs mRNAs	FDR	Enrichment	Potential bias
EXTRACELLULAR MATRIX STRUCTURAL CONSTITUENT	0.001	4.298	
GROWTH FACTOR ACTIVITY	0.011	4.161	
GROWTH FACTOR RECEPTOR BINDING	0.005	3.914	
POTASSIUM CHANNEL ACTIVITY	0.005	3.682	very_long
VOLTAGE-GATED POTASSIUM CHANNEL ACTIVITY	0.038	3.524	very_long
ION CHANNEL REGULATOR ACTIVITY	0.039	3.231	very-long
GROWTH FACTOR BINDING	0.027	3.081	
POTASSIUM ION TRANSMEMBRANE TRANSPORTER ACTIVITY	0.014	2.947	very_long
CHANNEL REGULATOR ACTIVITY	0.034	2.928	very_long
RECEPTOR REGULATOR ACTIVITY	0.000	2.654	very_short
RECEPTOR LIGAND ACTIVITY	0.001	2.616	
CATION CHANNEL ACTIVITY	0.007	2.415	
ION GATED CHANNEL ACTIVITY	0.026	2.248	very_long
GATED CHANNEL ACTIVITY	0.034	2.172	very_long
MONOVALENT INORGANIC CATION TRANSMEMBRANE TRANSPORTER ACTIVITY	0.013	2.146	vv_long
ION CHANNEL ACTIVITY	0.025	2.017	very_long
METAL ION TRANSMEMBRANE TRANSPORTER ACTIVITY	0.025	1.988	very_long
SUBSTRATE-SPECIFIC CHANNEL ACTIVITY	0.034	1.947	very_long
CHANNEL ACTIVITY	0.041	1.88	very-long
PASSIVE TRANSMEMBRANE TRANSPORTER ACTIVITY	0.042	1.875	very_long

4.2.5.2. AML- sEVs are enriched for mRNAs involved in regulating fat cell differentiation, angiogenesis, ossification, and inflammatory pathways

Similarly, the twenty top-ranking *Biological process* categories with statistically enriched coverage in AML- sEV mRNAs were compiled in **Fig. 4.7,** with corresponding **Table 4.3**. Two biological processes *Extracellular matrix organisation* and *Extracellular structure organisation* were found to be the most statistically significant, followed by *Axon guidance*, *Skeletal system development*, *Circulatory system development*, and *Inflammatory response*. It is also important to note the biological processes with the largest % gene coverage – namely: *Regulation of fat cell differentiation*, *Regulation of signalling receptor activity*, and *Regulation of endothelial cell proliferation* – may also be important in terms of sEV functionality when delivered to the microenvironment. There are also some statistically significant hits pertaining to angiogenesis processes (a known feature of AML tumours), including *Positive regulation of vasculature development* and *Positive regulation of angiogenesis*. It is also noted that *Negative regulation of canonical Wnt signalling pathway* is significantly enriched in AML- sEVs mRNAs, previously implicated downstream of mTORC1 signalling (Heng *et al*., 2018). Length bias ‘very long’ was also denoted in seven of these top-ranking biological processes.

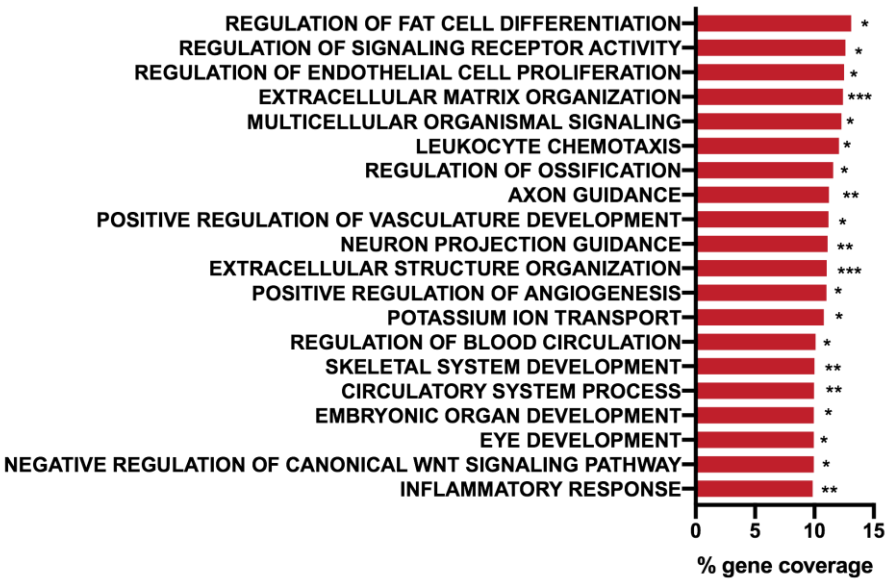

Figure 4.7: Twenty top-ranking Biological processes in AML- sEVs mRNAs. *Differentially expressed genes (DEGs) with significant FDR-adj. p value of less than 0.05 and the greatest % gene coverage were ranked in descending order. Enrichment scores in corresponding Table 4.3. False discovery rate adjusted p value, FDR-adj. p.*

Table 4.3: Top-ranking biological pathways upregulated mRNAs in AML- sEVs. Statistically significant biological pathways with corresponding enrichment scores, based on the number of relevant genes upregulated in AML- sEVs against the total number of genes in the background dataset of each biological function. Potential biases denoted.

Top 20 *Biological process* hits in AML- sEVs mRNAs	**FDR**	**Enrichment**	**Potential bias**
REGULATION OF FAT CELL DIFFERENTIATION	0.047	3.314	
REGULATION OF ENDOTHELIAL CELL PROLIFERATION	0.023	3.192	
REGULATION OF SIGNALING RECEPTOR ACTIVITY	0.024	3.164	very_long
EXTRACELLULAR MATRIX ORGANIZATION	7.491e-05	3.14	
MULTICELLULAR ORGANISMAL SIGNALING	0.025	3.108	very_long
LEUKOCYTE CHEMOTAXIS	0.028	3.055	
REGULATION OF OSSIFICATION	0.034	2.928	
AXON GUIDANCE	0.007	2.842	very_long
POSITIVE REGULATION OF VASCULATURE DEVELOPMENT	0.025	2.832	
NEURON PROJECTION GUIDANCE	0.008	2.812	very_long
EXTRACELLULAR STRUCTURE ORGANIZATION	0.000	2.794	
POSITIVE REGULATION OF ANGIOGENESIS	0.044	2.79	
POTASSIUM ION TRANSPORT	0.038	2.731	very_long
REGULATION OF BLOOD CIRCULATION	0.011	2.554	very_long
SKELETAL SYSTEM DEVELOPMENT	0.005	2.531	
CIRCULATORY SYSTEM PROCESS	0.006	2.521	very_long
EMBRYONIC ORGAN DEVELOPMENT	0.025	2.518	
EYE DEVELOPMENT	0.047	2.515	
NEGATIVE REGULATION OF CANONICAL WNT SIGNALING PATHWAY	0.047	2.515	
INFLAMMATORY RESPONSE	0.005	2.495	

4.2.6. miRNAs in AML- sEVs

Analysis and RNA biotypes revealed that there were a number of differentially expressed miRNAs between AML- sEVs and AML+ sEVs. A statistical significance cut-off of FDR-adjusted *p* value of less than 0.05 was applied and fold change threshold of 5. The distribution of up- and down-regulated miRNAs in AML- sEVs is shown in **Fig. 4.8**. There was a greater number of significantly downregulated miRNAs than upregulated miRNAs in AML- sEVs (**Fig. 4.8**).

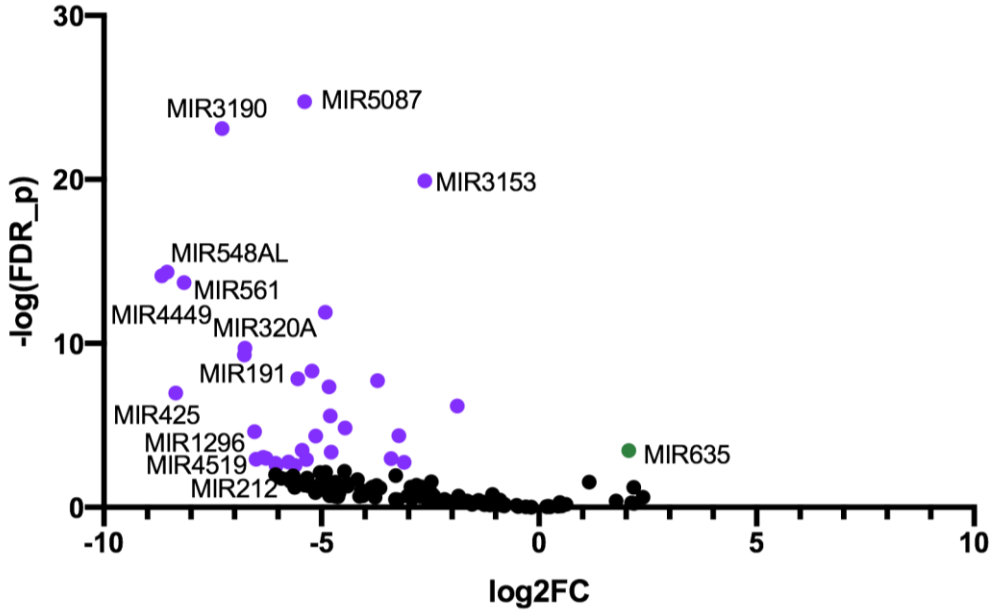

Figure 4.8: Distribution of differentially-expressed miRNAs in AML- sEVs vs. AML+ sEVs. *Green and purple dots represent differentially-expressed genes with FDR-adjusted p value of less than 0.05, with Benjamini Hochberg multiple test correction. Names of top-ranking genes with most significant FDR_p labelled.*

4.2.6.1. miR-635 upregulated in AML- sEVs has evidence of many tumour suppressive properties in various cancer settings

One miRNA, *miR-635,* was found to be upregulated in AML- sEVs (**Fig. 4.8)**, with statistical significance (FDR-adj. *p* value) less than 0.05. Functions associated with *miR-635* were collated via literature review and compiled in summary in **Table 4.4**.

Table 4.4.: Published studies of miR635 interactions, and functions in cancer settings

miRNA	Known interactions	Function	Disease setting	References
miR-635	Regulates KIFC1	Inhibits proliferation, migration and invasion	Gastric cancer	Cao *et al*., 2020
	Targets YY1	Inhibits cell invasion without affecting viability *in vitro* Inhibits solid tumour growth *in vivo*	Non-small cell lung cancer	Zhang *et al*., 2016
	Not reported	Inhibits proliferation and migration; Induces apoptosis	Downregulated in osteosarcoma tissues	Tian *et al*., 2017
	LncRNA DUXAP8 regulates miR635/ topoisomerase α 2 axis	Inhibits proliferation, migration, and invasion	Osteosarcoma	Yang *et al*., 2021
	Not reported	Increases invasive properties	A375 melanoma cells	Weber *et al.*, 2016
	Potentially targets ICAM1, CCL22, AQP4	Regulating key molecular pathways, e.g. glutamatergic/GABAergic transmission, the immune response, and glial K^+ and water homeostasis	Mesial temporal lobe epilepsy	Kan *et al.*, 2012

4.2.6.2. Most miRNAs were found downregulated in AML- sEVs, with varying reported functions in many cancer settings

Sixty-one miRNAs were found downregulated in AML- sEVs (**Fig. 4.8**) with statistical significance (FDR-adjusted *p* value) of less than 0.05. The ten differentially expressed miRNAs with the greatest fold changes were investigated for functional associations by literature review. Findings are summarised in **Table 4.5.** miR-3190 and miR-4519 have no reported interactors and functions reported in the literature and so were omitted from **Table 4.5.**

Table 4.5: Published studies of downregulated miRNAs' interactions, and functions in cancer settings. Multiple myeloma, MM; Colorectal cancer, CRC; Non-small cell lung cancer, NSCLC; Hepatocellular carcinoma, HCC; Breast cancer, BC; Hepatitis B, Hep B; Triple negative breast cancer, TNBC. Log transformation of gene expression fold change of 2, Log2FC.

miRNA	Log2FC	Known interactions	Function	Disease setting	Reference
miR-4449	-8.670	Not reported	Elevated in patient sera	MM	Shen *et al*., 2016
miR-548ai	-8.545	Not reported	Molecular protective mechanism against smooth muscle cell/exosome-induced dysfunction in epithelial cells	Vasculopathy	Xie *et al*., 2021
miR-425	-8.349	PTEN/PI3K/AKT signalling axis	miR-425-5p promotes cell growth	CRC	Zhou *et al*., 2020
		Targeting KLF3 via PI3K/AKT pathway	Increases proliferation and migration	CRC	Lv *et al*., 2021
miR-561	-8.160	PTEN/AKT pathway via targeting P-REX2a	Regulating proliferation and cell cycle	NSCLC	Liao, Zheng, Wei *et al.*, 2020
			Dysregulated expression	MM cell lines	Ronchetti *et al*., 2008
miR-191	-6.769		Use as reference gene	Colorectal adenocarcinoma Exosome fractions from HCC patient and Hep B sera	Zheng *et al.*, 2013 Li *et al*., 2015
		BDNF3 MPM4 CDK6 and CCND2	BDNF3 in proliferation MPM4 in apoptosis CDK6 and CCND2 in cell cycle		Nagpal, N. and Kulshreshtha, 2014
miR-320A	-6.757	PI3K/TSC/mTOR	Promotes myocardial fibroblast differentiation	Chronic heart failure	Wang *et al*., 2021
miR-1296	-6.535	SRPK1- PTEN/AKT pathway	Inhibits EMT and metastasis Reported tumour suppressor function	HCC	Xu *et al*., 2017

miR-212	-6.342		Downregulated in neural plasma exosomes	Alzheimer's Disease	Cha *et al*., 2019
		PRRX2	Suppresses EMT	TNBC	Lv *et al*., 2017
		Sp1 and VEGFA	212-3p regulates angiogenesis	BC	Li *et al*., 2020

4.2.7. lncRNAs in AML- sEVs

Differential expression of lncRNAs in AML- sEVs vs. AML+ sEVs was also examined. 518 lncRNAs were found to be upregulated while 1288 lncRNAs were found to be downregulated in AML- sEVs compared to AML+ sEVs, both sets with statistical significance *FDR-adj. p* value of less than 0.05. The ten significantly upregulated lncRNAs with the greatest fold changes were selected as candidates (**Table 4.6**) and their associated functions and/or use as cancer biomarkers was assessed by literature review, given the lack of functional enrichment GO analysis for lncRNAs.

Table 4.6: Ten lncRNAs upregulated in AML- sEVs with the greatest fold change. Log transformation of gene expression fold change of 2, Log2FC.

lncRNA	Log2FC
LINC00374	9.372
RP11-100E13.1	8.674
AC010127.3	8.388
CTD-3157E16.2	7.558
C20orf166-AS1	7.391
C18orf65	7.297
RP11-352D13.6	6.796
LINC00900	6.388
LINC00051	6.384
KCNJ2-AS1	6.188

4.2.7.1. lncRNAs in AML- sEVs with no previously published studies

RP11-100E13.1 and *AC010127.3* were identified as the next two most upregulated lncRNAs in AML- sEVs. No studies have been published, to date, that have investigated or attributed function to *RP11-100E13.1* or *AC010127.3*. Similarly, *C20orf166-A1S, C18orf65,* and *RP11-352D13.6* were highly increased in expression in AML- sEVs but have no published literature to date of known function.

C18orf65 is an alias of the ZNF516 Divergent Transcript (*ZNF516-DT*) gene (GeneCards® THE HUMAN GENE DATABASE). *ZNF516-DT* has limited literature supporting its function.

4.2.7.2. lncRNAs upregulated in AML- sEVs with reported function or biomarker potential in other cancers

LINC00374 displayed the greatest fold increase in AML- sEVs versus AML+ sEVs (**Table. 4.6)**. One study showed that *LINC00374* was a high-frequency HPV integration site into cervical cancer cell genome in a Chinese Uygyr population (Yang-chun and Sen-yu *et al*., 2020). It is difficult to interpret what this indicates about LINC00374 functionality. *CTD-3157E16.2* is an alias of *MEIS3P1* (*Meis homeobox 3 pseudogene 1*). *CTD-3157E16.2* is reported to be a retrotransposed pseudogene, based on its lack of exons compared to related gene family members, including *MEIS3* (on chromosome 19). It contains an open reading frame that may encode a protein of similar sequence and size to that of *MEIS3* (RefSeq 2008, NCBI ENTREZ gene 4213).

LINC00900 is upregulated in AML- sEVs, and has been previously identified in one study of patients with primary glioblastoma (Wang *et al*., 2021), and one study of prostate cancer patients (Gong *et al*., 2020). *LINC00900* has been included in a prognostic 4-part lncRNA biomarker panel for oesophageal carcinoma and could stratify low- and high-risk patients with differing overall survival (Liu *et al.,* 2020). It also forms part of an epithelial-to-mesenchymal signature in glioma (Tao *et al*., 2021). The functional role of *LINC00900* is yet unclear in these disease settings but it has been used as a biomarker for many cancers. *LINC00051* is also upregulated

in AML- sEVs but does not have a published function or role as a biomarker. *KCNJ2-AS1* (*KCNJ2 antisense RNA 1*) is a lncRNA that is upregulated in AML-EVs. *KCNJ2-AS1* has been previously included in a thirteen-marker prognostic panel that predicts disease-free survival in gastric cancer patients (Cheng *et al*., 2019). *KCNJ2-AS1* is also reported as part of a risk-score system to correlate and so predict with recurrence of colon adenocarcinoma (Yang *et al*., 2020). The same study also reported the correlation of PPAR and Hedgehog signalling pathway with recurrence, but the mechanistic link between the lncRNA and these signalling pathways is unclear.

Other upregulated lncRNAs found in AML- sEVs are included in prognostic signature panels for different cancer settings. *LINC01537* was previously found to be downregulated in lung cancer and was significantly associated with lung cancer survival and in inhibiting tumour growth and progression in an analysis of RNA sequencing and TCGA datasets validated in a patient cohort of 243 lung cancer patients (Gong *et al.*, 2019). Two studies have been published with results associating the involvement of *LINC01537* in lung cancer progression (Gong *et al*., 2019; Lu *et al*., 2021) and energy metabolism (*Gong et al.*, 2019). *RNF144A-A1S* is 48-fold upregulated in AML- sEVs, and has been widely associated with promoting tumour progression in many settings, including glioma (Tong *et al*., 2021), gastric (Li *et al*., 2021) and bladder (Wang *et al*., 2020) cancers. This lncRNA also has been included in a panel of lncRNAs as a prognostic signature of renal cell carcinoma, a disease state that has been associated to develop in a subset of TSC-patients with AMLs. Functionally, *RNF144-A1S* has been previously associated with chondrogenesis (Huynh *et al*., 2020). *PAX8AS1* is another lncRNA

upregulated in AML- sEVs, and has been included in a survival prediction model for paediatric acute myeloid leukemia (Guo *et al*., 2020). Functionally, *PAX8AS1* is aberrantly expressed in papillary thyroid carcinoma and has been reported to have an inhibitory effect on tumour growth due to its MYC-induced suppression (Zhang and Li *et al*., 2019). It has also been reported in another study in the breast cancer setting. *PAX8-AS1-N* was found to bind to miR-17-5p and upregulated targets of this miRNA such as *PTEN, CDKN1A*, and *ZBTB4* (Yu *et al*., 2018). *PTEN* also contributes to constitutive mTOR signalling (Seront *et al*., 2013).
Given the limited knowledge on the function of lncRNAs in disease, downregulated lncRNAs were not analysed by literature review.

4.3. DISCUSSION

sEV-RNA has a unique role in intercellular communication, regulating gene expression and modulating signalling cascades and biological pathways in recipient cells. Determining differential incorporation of RNAs in sEVs provides new important knowledge about the role of the sEV transcriptome in contributing to TSC tumour growth, development, and progression. This Chapter entails the first study of the AML sEV RNA landscape, with a focus on key coding mRNAs and non-coding miRNAs and lncRNAs, and provides an understanding of how these sEVs may mediate tumour-supporting and tumour-promoting processes in the AML microenvironment and at other recipient sites in the body. The research presented shows upregulated mTORC1 signalling-associated mRNAs and many other novel differentially expressed mRNAs, miRNAs, and lncRNAs in AML- sEVs compared to their AML+ control sEV counterparts. Examination of what these upregulated RNAs might execute in recipient cells was conducted using functional enrichment

GO analysis GOliath and literature reviews, revealing potential new mechanisms of TSC tumour growth and development. RNA was successfully isolated from bulk AML+ and AML- sEVs (**Fig. 4.2**), providing enough RNA isolate to conduct both qPCR and RNA-Seq experiments. Various RNA biotypes were identified in both AML+ and AML- sEVs (**Fig. 4.4**). Differential expression of genes between two groups can reveal important underlying biological mechanisms.

With a central role of mTORC1 signalling in TSC tumour growth and development, it was important to investigate if RNAs associated with this tumour-driving pathway also associated with TSC sEVs. I showed that *TSC2* mRNA was incorporated into AML+ sEVs, but absent from sEVs derived from AML- cells (**Fig. 4.3**), meaning that TSC2 protein would not be translated in the case of AML- sEVs delivery to recipient cells. However, TSC2 protein may be translated with delivery of AML+ sEVs. These results also showed that several mTORC1-signalling associated mRNAs – namely: *RHEB, 4EBP1, AKT* – had trends of elevated expression in AML- sEVs compared to AML+ sEVs (**Fig. 4.3**). With delivery of these AML- sEV cargo to recipient cells, there is the potential that increased bioavailability of *RHEB* mRNA may contribute to increased mTOR signalling in these recipient cells. However, as mRNA levels cannot be used as surrogates for corresponding protein expression, and transcription of sEV-delivered RNAs by recipient cells remain unclear, validation of the protein expression *in vitro* is required to determine the functional impact of these more highly incorporated mRNAs. Furthermore, probing cells which are either untreated or AML- sEV-treated for mTORC1 signalling pathway markers could further elucidate the functional impact of these sEVs on propagating mTORC1 signalling extracellularly. *NOTCH1* mRNA expression was not found to

be differentially expressed in AML+ sEVs and AML- sEVs, which contrasts with that reported previously (Patel *et al*., 2016). Differences here could be explained by different models used.

Knowing that mRNAs are implicated in encoding protein, it was important to prioritise this biotype in downstream analysis to determine what disease mechanisms or biological pathways and phenotypes could be induced with delivery of AML- sEV mRNA cargo to recipient cells. mRNAs expressed within AML- and AML+ sEVs were found to be strikingly different (**Fig. 4.5**). Functional enrichment GO software GOliath was utilised to analyse enriched molecular functions and biological processes in upregulated AML- sEVs mRNAs. Top-ranking significantly enriched *molecular functions* and *biological pathways* were identified in AML- sEVs (**Figs. 4.6** and **4.7**). Of the molecular functions identified, the top-ranking hit was *Extracellular matrix structural constituent* (**Fig. 4.6**), which could reveal important players in AML- sEV-mediated regulation of the ECM. Given the known role of the ECM in modulating important tumour-supporting processes, such as cell proliferation, migration and invasion, and adhesion (as reviewed by Hynes *et al*., 2009), understanding how AML- sEVs could encode alterations in the ECM could reveal important insight into novel anti-tumour treatments for TSC tumours. *TSC2* deficiency has been previously reported to modulate ECM processes in a LAM model (Moir *et al*., 2012), involving integrin receptors. Further to this, the second and third highest hits deal with growth factor activity and growth receptor binding Growth factors are important short-range mediators of various extracellular processes, including promotion of tumour growth and cell proliferation and modifications to the tumour microenvironment (as reviewed by Witsch *et al*., 2010).

Therefore, understanding more about the growth factor activity and signalling could reveal important insights into how AML tumours interact with their microenvironment to grow and develop. Importantly, this is supported by significantly enriched *Receptor regulator activity* and *receptor ligand activity*. *Potassium channel activity* and *Cation channel activity* are also identified as being highly significant (**Fig. 4.6**), along with various molecular functions involving ion channel activity and transmembrane transporter activity. Interpretation of this largely points towards kidney function, mirroring that reported from AML tissues (Martin *et al*., 2017), and TSC neural manifestations. Potassium channels are important and recognised determinants of seizure susceptibility (as reviewed by D'Adamo *et al*., 2013). One study showed that reduced absorption of potassium via astrocyte inward rectifier potassium channels could play a role in epileptogenesis in a *Tsc1*-deficient mouse model (Jansen *et al*., 2005). A recent study reported complex changes in epileptogenesis in TSC being associated with changes in several ion channels (Koene and Niggl *et al*., 2021). The first step in understanding the mechanisms behind these results is to establish which mRNAs are involved in these processes by assessing their expression levels using qPCR, on the presumption that those mRNAs more differentially expressed could be more central to TSC tumour growth and progression.

The analysis of enriched biological processes networks shows some interesting findings that could be involved in the various multi-organ manifestations of TSC. The biological processes with the widest coverage (%) was found to be *Regulation of fat cell differentiation* (**Fig. 4.7**). Given the triphasic histology of AMLs, and the varying extent of the fat components to their composition, understanding the mRNA

targets secreted by AML- sEVs into the microenvironment could help elucidate the biological mechanisms behind this fat component formation. Similarly, *Regulation of endothelial cell proliferation* is also flagged as a biological process with high coverage, which may have important implications in the blood vessel component development of these AML tumours. Biological functions pertaining to ECM are also highlighted in this analysis, which affirms the need to validate some targets involved in the structure and composition of this tumour feature, given the finding of ECM destruction in the lung component, LAM. Further biological processes found to be enriched in AML- sEV mRNAs were linked to vasculature and blood circulation. Enriched networks also involved in the *negative regulation of canonical Wnt signalling pathway* in these AML- sEV mRNAs. This is of interest as the TSC1/TSC2/mTORC1 signalling axis has been previously associated with mediating Wnt signalling (Zeng *et al*., 2018; Mak *et al*., 2005). *Regulation of ossification* and *Skeletal system development* could be of interest in revealing novel treatment targets as TSC can cause various bone defects, such as sclerotic bone lesions (Avila *et al*., 2010) and pitting of dental enamel. *Axon guidance* and *Neuron projection guidance* are also found with high coverage in these upregulated AML-sEV mRNAs, which could reveal important multi-organ communication pathways which modulate the neural manifestations of TSC. *Inflammatory response* has been widely implicated in TSC previously, both in the neural and tumour manifestations. While it is difficult to underpin the exact mechanisms from this data, determining key players in regulating the inflammatory aspect of these clinical signs could offer additional therapy options. *Length bias* was flagged in many of the top-ranking molecular function and biological processes in AML- sEV mRNAs, which was to be expected given the large number of DEGs identified in AML- sEVs.

miRNAs play an important role in gene regulation by annealing to mRNAs in order to inhibit translation. In this current study, miR-635 was the only miRNA found to be significantly upregulated in AML- sEVs compared to AML+ sEVs (**Fig. 4.8**). It is important to note that the RNA-Seq employed here was not specific for small RNAs, with some purification processes in the procedure actively removing them, so this list is not likely to be comprehensive. Some studies suggest a role of miR635 in inhibition of cancer-promoting processes, albeit processes that involve demonstrated interacting partners KIFC1 in gastric cancer (Cao *et al*., 2020) and Yin Yang 1 (YY1) targeting in non-small cell lung cancer (Zhang *et al*., 2016). As protein interactors for miR635 are known in these tumour contexts, it is plausible to question if the function of miR635 from sEVs may depend on expression of these known interacting partners in recipient cells or if other targets exist. Verification of these targets in recipient cells of the TSC tumour microenvironment would strengthen evidence of miRNA inhibiting tumour-promoting functions in TSC cells. Furthermore, targets of other dysregulated miRNAs in TSC EVs could be examined using miRNA target predicting software, such as *MicroRNA Target Prediction Database* (www.mirdb.org) or *TargetScanHuman* (www.targetscan.org), to establish potential functional mechanisms of this dysregulated miRNA. Additionally, function could be examined using reporter assays (Ritchie *et al*., 2013; Clément *et al.*, 2015). Most miRNAs with differential expression in AML- sEVs were found to be downregulated in this study (**Fig. 4.8**). Roles of these miRNAs were collated in **Table 4.5**, though interpreting the role of downregulated miRNAs may prove difficult, given that their innate role is in inhibiting translation of certain protein targets. Unless these miRNAs when downregulated permit tumour-supporting

processes, it is currently difficult to ascertain fully what these miRNAs contribute to TSC tumour pathology.

Publications detailing the biomarker or functional roles of these lncRNAs are scarce. Therefore, understanding how these lncRNAs in sEVs would function in the TSC tumour setting is difficult to determine with current scope of the understanding of biological roles of lncRNAs. However, some mentioned lncRNAs listed in AML-sEVs have been used in prognostic signature panels for various cancers (**Table 4.6**). Validation of their expression is necessary to determine their potential utility as biomarkers in TSC, in the first instance.

There is discussion about what it takes to have success delivery of EV-RNA to recipient cells, to elicit a functional impact intercellularly. There is literature highlighting that RNA amounts in a single EV are low, and indeed one vesicle will not contain all the RNAs identified within an RNA-Seq experiment. Taking the predicted functions from functional enrichment GO analysis to assess functional consequences of EV-RNA, there is a requirement to have sufficient numbers of EVs containing all the RNAs necessary as per highlighted in the functional enrichment analysis. Furthermore, it is also necessary to ensure that EVs and their RNAs successfully escape lysosomal degradation. Therefore, it is clear that there are factors to consider when discussing successful EV-RNA delivery to recipient cells.

4.4. CONCLUDING REMARKS

In this Chapter, I have reported the first isolation of RNA from bulk AML+ and AML- sEVs, in detectable quantities for RNA-Seq. Insight into mechanistic changes induced by largely divergent RNAs in AML+ and AML- sEVs have opened some hypotheses for AML tumour development with potential phenotypic and cell signalling modifications induced by AML- sEV RNAs.

CHAPTER 5

PROFILING TSC sEV PROTEIN CARGO AND RESPONSE TO RAPAMYCIN TREATMENT

5.1. INTRODUCTION

5.1.1. Rationale

Understanding new disease mechanisms that promote and support tumour growth in Tuberous Sclerosis Complex (TSC) is critical for the development of additional anti-tumour therapies. A key contributor to tumour progression is the tumour microenvironment (Luga *et al*., 2012; as reviewed by Maia *et al*., 2018; Truffi *et al*., 2019), which is primed by tumour cells to support tumour proliferation and to promote structural integrity and vitality of the tumour (as reviewed by Lazar *et al*., 2018). To establish this optimal tumour microenvironment, tumour cells will communicate intercellularly with their surroundings via various mechanisms, one of which is the secretion and subsequent uptake of extracellular vesicles (EVs). The major known role of EVs is in the intercellular transportation and delivery of their bioactive cargo material from parent tumour cells to recipient cells of the tumour microenvironment (TME) (as reviewed by Raposo and Stoorvogel, 2013). This bioactive EV cargo can stimulate tumour-supporting processes to ensure tumour growth and survival. The exact mechanisms of intercellular communication mediated by EVs and their cargo that is required for TSC tumour development and progression remains unclear, making it a key area of research.

5.1.2. Profiling EV protein cargo from tumour cells

One focus of EV biological research has been in profiling protein cargo. Previously, specific cargo from tumour-derived EVs was shown to play important roles in promoting primary tumour growth (as reviewed by Tomasetti *et al*., 2018), regulating angiogenesis (Grange *et al*., 2011; Mineo *et al*., 2012; Feng *et al*., 2017; Pakravan *et al*., 2017), regulating immune responses (as reviewed by Tomasetti *et al.,* 2018), and modifying surrounding parenchymal and stromal tissue (Patel *et al*., 2016; Webber *et al*., 2010; Webber *et al*., 2015) in various cancer settings. The diverse assortment of EV-mediated functions is responsible for modulation of the local tumour microenvironment resulting in enhanced tumour growth and survival. Biodistribution of EVs in blood and other bodily fluids also extends the bioavailability and function of the tumour-derived cargo beyond the primary tumour environment, contributing to pre-metastatic niche formation (Peinado *et al*., 2012). How the TSC microenvironment is modulated by EVs remains unclear, but knowledge of this potential tumour-promoting mechanism could highlight new targets that could improve on current anti-tumour therapy. Therefore, profiling the protein cargo associated with TSC sEVs could provide mechanistic information on how these sEVs may optimise their tumour microenvironment for tumour growth and progression.

5.1.2.1. EV cargo from TSC cells

While the roles of mTORC1 hyperactivity and its downstream signalling programme in driving TSC tumour growth are well characterised as aspects of intracellular TSC pathology, the mechanisms behind the intercellular regulation of the tumour microenvironment and stromal activation, necessary for growth, are unknown. Specifically, the mechanisms behind tumour-associated changes within the

microenvironment of AML, the TSC tumour type characterised by aberrant vascularisation and patient proneness to repeated aneurysm, severe haemorrhage or renal failure (as reviewed by Crino *et al*., 2006; as reviewed by Lam *et al*., 2018), remains unclear. Furthermore, the mechanisms contributing to cystic destruction of lung parenchyma in TSC-associated lymphangioleiomyomatosis (LAM), remain elusive (Walkup *et al*., 2019). Some published studies detail the knowledge already known in relation to TSC EVs. One study demonstrated that *Tsc1*-deficient (tumour) cell-derived EVs could induce TSC neural phenotypes in neighbouring wild-type cells, based on an EV *Notch* and *Rheb* mRNA delivery mechanism (Patel *et al*., 2016). Another study examining proteomic signatures of EVs from *Tsc2*-deficient mouse inner medullary collecting duct cells showed that these EVs had enriched networks involved in cell proliferation, primary cilia, and stress responses (Zadjali *et al*., 2020). However, no studies have been published to date on the protein cargo or function of AML patient cell line-derived sEVs derived from long-term bioreactor cultures.

5.1.3. Rapamycin effects on TSC EVs

Another avenue of exploration in this Chapter was to investigate how standard-of-care mTORC1 inhibitor rapamycin treatment could affect EV secretion and cargo loading. As mTORC1 is a central signalling hub in intracellular signalling, its inhibition poses some challenges in terms of retro-activating other tumour drivers or proteins involved in pro-tumoral signalling (as reviewed by Saxton and Sabatini, 2017), which is thought to contribute to the therapeutic limitations of rapamycin in the long term. Some studies report alterations in EV secretion *in vitro* by anti-cancer and antibiotic compounds (Loghry *et al*., 2020; Im *et al*., 2019, Fonseka *et*

al., 2021). One study showed evidence that mTORC1 was a potent regulator of EV proteomes, in an aging astrocyte *in vitro* model, where rapamycin treatment altered the EV proteome and improved downstream EV function to resemble those enacted by EVs derived from younger astrocytes (Willis *et al*., 2020). However, in the context of TSC, there are no published studies that investigate the cargo of sEVs secreted from rapamycin-treated AML cells. Furthermore, how mTORC1-active cells treated with an mTORC1 inhibitor signal extracellularly is currently unknown but may have significant effects in propagating or hindering anti-tumour therapy.

5.1.4. EV functionality in the tumour microenvironment

The heterogeneous tumour microenvironment (TME) is recognised as both a contributor and facilitator of tumour growth and progression in many cancers (as reviewed by Hanahan and Weinberg, 2011). It is known that sEVs from tumour cells can integrate with recipient cells in the TME to promote tumour-supporting processes, such as signalling mediation, inflammatory responses, cancer development, tumour microenvironment priming and angiogenesis, amongst others (Valadi *et al*., 2007; as reviewed by Zhang *et al*., 2021; as reviewed by Chang and Pauklin, 2021). Previously, *Tsc1*-deficient EVs were shown to induce accelerated neural differentiation in surrounding wild-type cells within the neural parenchyme microenvironment in a TSC mouse model (Patel *et al*., 2016). Other studies investigated the *Tsc2*-deficient cell-derived EV mechanisms of TSC renal cytogenesis (Kumar *et al*., 2021; Bissler *et al*., 2017). However, no studies have been published that examine the impact of TSC EVs on fibroblasts, a prominent cell type within the tumour microenvironment. Fibroblasts are recognised as

central to the tumour architecture, providing structural support and many extracellular features that benefit tumour growth and development, such as extracellular matrix remodelling, angiogenesis, and facilitating immune escape (as reviewed by Monteran and Erez, 2019). Published studies show that prostate cancer sEVs are capable of stimulating fibroblasts to an activated myofibroblast phenotype, to drive tumour growth *in vitro* and facilitate angiogenesis *in vivo* (Webber *et al*., 2014). Studying how TSC tumours signal intercellularly to optimise their microenvironment for tumour growth and development is important and may help uncover novel anti-tumour targeting strategies.

5.1.4.1. EV effects on growth factor secretion

Growth factors (GFs) are secreted-regulatory molecules that can facilitate short-range crosstalk between tumour cells and surrounding extracellular matrix and cells of the microenvironment, in order to optimise the microenvironment for supporting tumour growth (Yuan *et al*., 2016). It has been previously shown that prostate cancer cell line-derived sEVs can promote growth factor (GF) secretion in significantly elevated quantities compared to soluble Transforming Growth Factor β (TGF-β) (Webber *et al*., 2015). Given that several TSC tumours have an altered microenvironment, with renal AML being highly vascularised and lung LAM having stromal alterations, I wanted to understand if GF secretion from parental tumour cells may play a role in these microenvironmental features.

5.1.4.2. EV effects on signalling activation

Phosphorylation is one of the most well-studied post-translational modifications in molecular biology and is a major regulatory mechanism for biological processes

and signalling pathways. Phosphorylation is critical to protein function (Carnino *et al*., 2020), and it has previously been documented that EVs can stimulate phosphoprotein signalling cascades in recipient cells. For example, mast cell-derived EVs induced phosphorylation of epithelial-to-mesenchymal (EMT)-associated proteins in lung carcinoma epithelial cells (Yin *et al*., 2020). Another proteomics study showed that breast cancer cell line MDA-MB-231-derived EVs carry proteins capable of phosphorylating PKM2, crucial for aerobic glycolysis and tumorigenesis (Kang *et al*., 2021). One study showed that EGFRvIII-containing microvesicles could activate pERK (also known as pMAPK) and pAkt in recipient cells post EV stimulation and that these cells had an EV dose-dependent secretion of Vascular Endothelial Growth Factor (VEGF), a known protein in angiogenesis and target of Epithelial Growth Factor Receptor (EGFR) (Al-Nedawi *et al*., 2008). However, it remains unclear yet as to whether AML EVs could execute phosphorylation of proteins in recipient cells, and whether this provides a tumour-promoting advantage for the AML microenvironment.

5.1.5. Hypotheses and aims

I hypothesise that AML- sEVs have a distinct protein cargo, enriched for protein networks that could elicit different downstream functions in recipient cells. Secondly, I hypothesise that rapamycin treatment affects sEV secretion and cargo loading from AML- cells, with different intercellular signalling capacity compared to AML+ and AML- sEVs.

The specific aims of this Chapter were:

I. To determine differentially expressed proteins expressed in AML+ and AML- cells and AML+ and AML- sEV cargo
II. To investigate the impact of rapamycin treatment on sEV secretion, characteristics, and protein cargo loading into sEVs
III. To assess functional impact on signalling activation with delivery of AML+, AML-, and rapaAML- sEVs to recipient fibroblasts

5.2. RESULTS

5.2.1. TSC cells and sEVs are enriched for a distinct set of proteins with tumour-promoting potential

To undertake a broad investigation of protein cargo linked to tumour progression, the expression of 84 oncology-associated proteins in AML+ and AML- cells and their cell-derived sEVs was assessed using a commercially available proteome profiler antibody array (R&D Systems). Of the 84 oncology-associated proteins covered by the array, 42 showed altered expression in AML- cells, relative to AML+ cells (**Fig. 5.1**). 39 of these proteins had elevated expression in AML- cells, while 3 had reduced expression in AML- cells, relative to AML+ control counterparts. Some of these proteins with elevated expression have been previously associated with TSC, including HIF-1α, MMPs, VE-cadherin, IL-6, and VEGF (Dodd *et al*., 2015; Lee *et al*., 2010; Bertolini *et al*., 2018, Shu *et al*., 2010; Young *et al*., 2013; Wang *et al*., 2021), thus supporting the validity of our findings in the TSC disease context. However, the majority of the identified protein changes have not previously been linked to TSC tumours and so are novel findings.

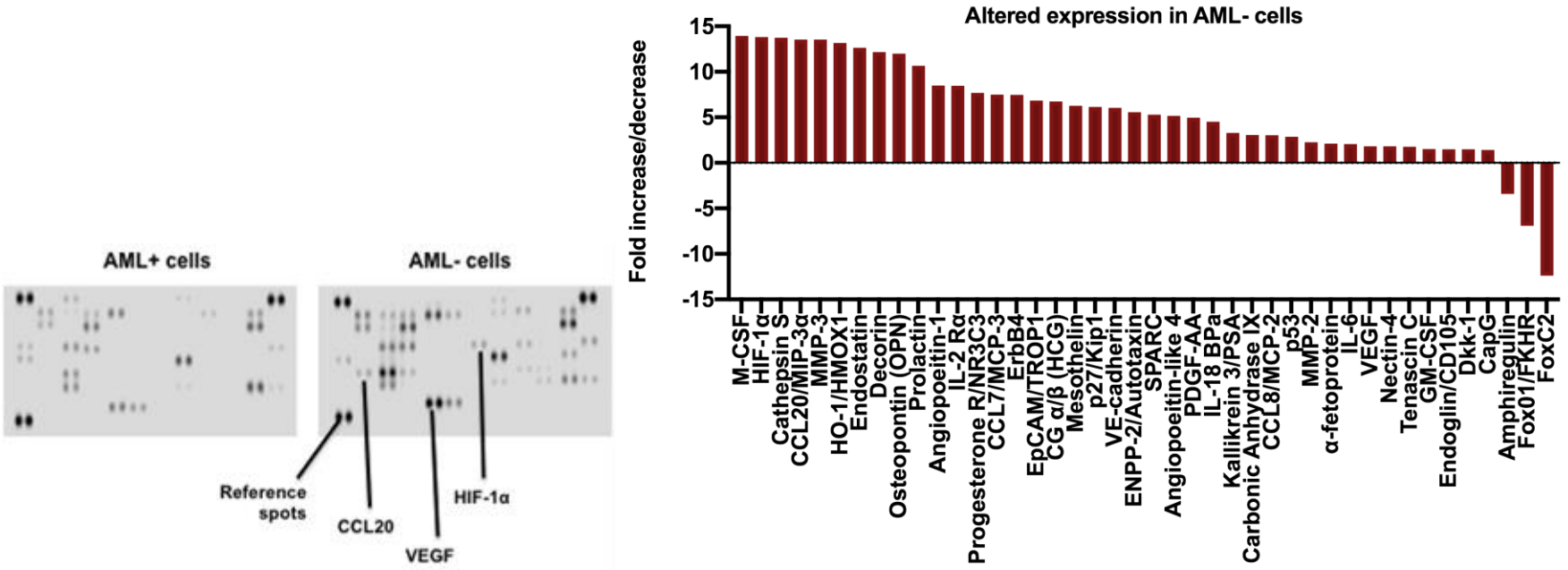

Figure 5.1: Altered expression of 42 oncology-associated proteins in AML- cells. *AML whole cell lysates (180 µg) were diluted and incubated overnight with nitrocellulose membranes dotted with capture antibodies for 84 oncology-associated proteins. Blots were then incubated with a cocktail of biotinylated detection antibodies, before visualisation by chemiluminescence and analysis by densitometry. Data graphed as waterfall plot to show fold change of > 2-fold increase/decrease (n=1).*

On analysing the sEV protein cargoes, 29 oncology-associated proteins were found to have altered expression in AML- sEVs, compared to the control AML+ sEVs (**Fig. 5.2**). The 21 proteins with elevated expression in AML- sEVs contained proteins previously implicated in TSC pathology, including IL-6, MMPs, VEGF, Galectin-3 (Dodd *et al*., 2015; Lee *et al*., 2010; Shu *et al*., 2010; Young *et al*., 2013; Klover *et al*., 2017) although their association with EVs released in TSC has not been previously reported. Another eight proteins were found to be present at reduced levels in AML- sEVs compared to the AML+ sEV controls.

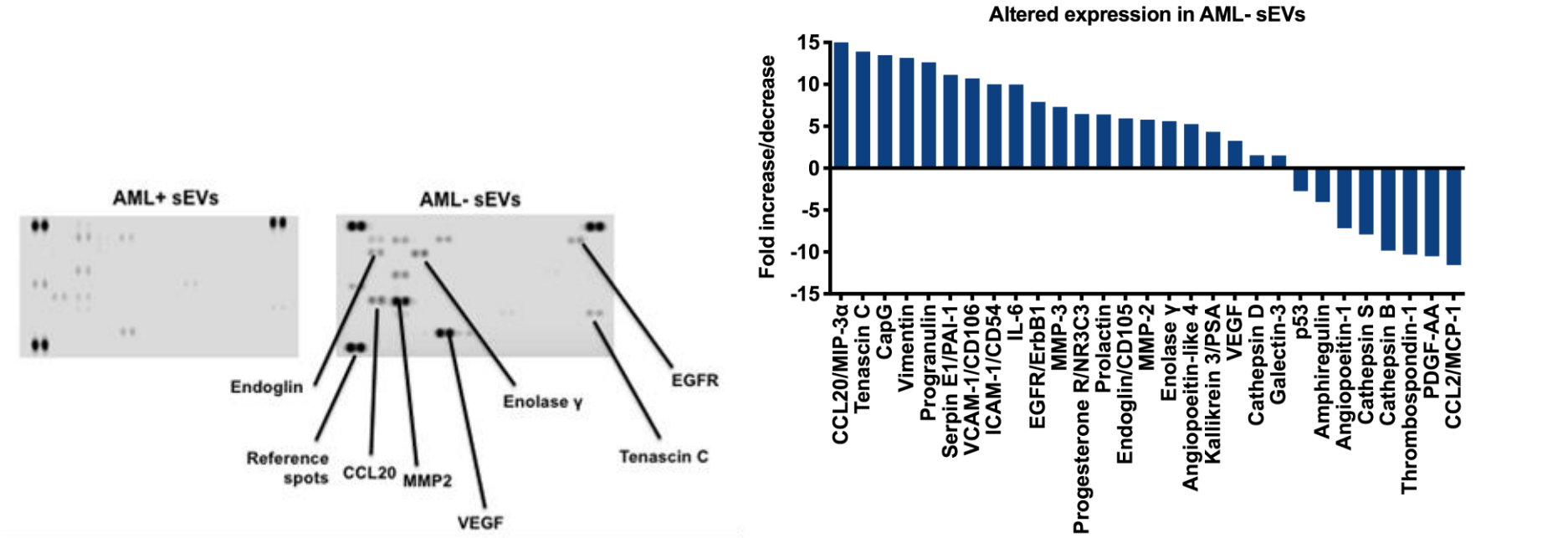

Figure 5.2: Altered expression of 29 oncology-associated proteins in AML- sEVs. *sEVs (based on 180 µg protein) derived from AML+ and AML- cells were lysed, diluted and incubated overnight with nitrocellulose membranes dotted with capture antibodies for 84 oncology-associated proteins. Blots were then incubated with a cocktail of biotinylated detection antibodies, before visualisation by chemiluminescence and analysis by densitometry. Data graphed as waterfall plot to show fold changes, with threshold of > 2-fold increase/decrease (n=1).*

To predict potential alterations in function of AML- cells, and their secreted EVs, compared to AML+ controls functional enrichment analysis was performed using FunRich software on TSC cell and sEV protein sets. Enriched protein networks within TSC cell and sEV cargo under the gene ontology (GO) annotation *Biological pathways* was assessed, and would be used to predict potential disease phenotypes induced by delivery of this sEV cargo to recipient cells. Specifically, genes corresponding to proteins with increased expression in AML- cells and EVs (**Table 2.6**) were submitted to FunRich software and functional enrichment was conducted on these gene sets. Since sEVs are thought to contain cargo specially-packaged by their parent cells to alter tumour microenvironment cell phenotype and function, target selection (for validation) was focused within the panel of 21 proteins that had elevated expression in AML- sEVs. This would inform subsequent design of functional assays to assess sEV mediation of tumour-supporting cell signalling in the tumour microenvironment. In this analysis, enriched biological pathways in proteins upregulated in AML- cells and sEVs were identified, and this also revealed the protein sets in common and distinct between AML- cells and sEVs. It is important to note that input data set (n=21) was very small, compared to that employed in proteomics studies, in this analysis. Consideration is due when interpreting enriched biological processes within this small input data set given the power limitations of this experiment.

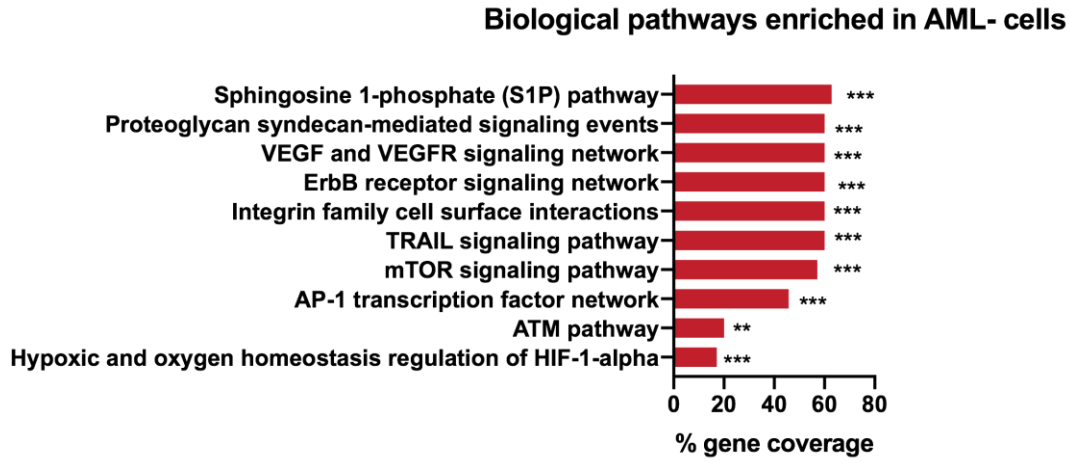

Figure 5.3: Top-ranking biological pathways enriched in AML- cell proteome. *Upregulated proteins found in AML- cells were analysed using FunRich functional enrichment software. Threshold of at least 3 proteins were selected. Statistical significance was assessed using hypergeometric p values, * = $p < 0.05$; ** = $p < 0.01$; *** = $p < 0.001$.*

Table 5.1: Fold enrichment scores of top-ranking gene networks mapped in AML- cell proteomes.

Biological pathway	Fold enrichment	Genes mapped
Sphingosine 1-phosphate (S1P) pathway	3.023	*CSF1; HIF1A; MMP3; HMOX1; COL18A1; DCN; SPP1; PRL; IL2RA; CDKN1B; CDH5; PDGFA; KLK3; CA9; TP53; MMP2; AFP; IL6; VEGFA; CSF2; ENG; DKK1;*
Proteoglycan syndecan-mediated signaling events	2.813	*CSF1; HIF1A; MMP3; HMOX1; COL18A1; DCN; SPP1; PRL; IL2RA; CDKN1B; KLK3; CA9; TP53; MMP2; AFP; IL6; VEGFA; TNC; CSF2; ENG; DKK1;*
VEGF and VEGFR signaling network	2.901	*CSF1; HIF1A; MMP3; HMOX1; COL18A1; DCN; SPP1; PRL; IL2RA; CDKN1B; CDH5; KLK3; CA9; TP53; MMP2; AFP; IL6; VEGFA; CSF2; ENG; DKK1;*
ErbB receptor signaling network	2.886	*CSF1; HIF1A; MMP3; HMOX1; COL18A1; DCN; SPP1; PRL; IL2RA; ERBB4; CDKN1B; KLK3; CA9; TP53; MMP2; AFP; IL6; VEGFA; CSF2; ENG; DKK1;*
Integrin family cell surface interactions	2.745	*CSF1; HIF1A; MMP3; HMOX1; COL18A1; DCN; SPP1; PRL; IL2RA; CDKN1B; KLK3; CA9; TP53; MMP2; AFP; IL6; VEGFA; TNC; CSF2; ENG; DKK1;*
TRAIL signaling pathway	2.849	*CSF1; HIF1A; MMP3;HMOX1; COL18A1; DCN; SPP1; PRL; IL2RA; CDKN1B; PDGFA; KLK3; CA9; TP53; MMP2; AFP; IL6; VEGFA; CSF2; ENG; DKK1;*
mTOR signaling pathway	2.798	*CSF1; HIF1A; MMP3; HMOX1; COL18A1; DCN; SPP1; PRL; IL2RA; CDKN1B; KLK3; CA9; TP53; MMP2; AFP; IL6; VEGFA; CSF2; ENG; DKK1;*
AP-1 transcription factor network	4.632	*HIF1A; HMOX1; DCN; PRL; IL2RA; CDKN1B; KLK3; CA9; TP53; MMP2; AFP; IL6; VEGFA; CSF2; ENG; DKK1;*
ATM pathway	4.102	*COL18A1; SPP1; CDKN1B; TP53; MMP2; AFP; DKK1;*
Hypoxic and oxygen homeostasis regulation of HIF-1-alpha	13.496	*HIF1A; HMOX1; CA9; TP53; VEGFA; ENG;*

In proteins with elevated expression in AML- cells, a number of biological pathways were identified with statistically significant enrichment. The top 10 biological pathways with the widest protein coverage within our dataset are graphed in **Fig.**

5.3, with accompanying enrichment values in **Table 5.1**. The top hit *Sphingosine 1 phosphate (S1P) pathway* is a known activator of mTOR signalling (Maeurer *et al.,* 2009). mTOR signalling is also a top-ranking biological pathway in AML- cells, which is not surprising due to its known role as intracellular driver of TSC tumours. Several top-ranking biological pathways with enrichment in AML- cell proteomes are involved in vesicle biogenesis and docking, including *proteoglycan-syndecan-mediated signaling events* and *Integrin family cell surface interactions.* Others biological pathways with enriched expression are known to be involved in angiogenesis, such as *VEGF and VEGFR signalling networks* and *hypoxic and oxygen homeostasis regulation of HIF-1-alpha.* As predicting functions of enriched protein cargo in AML- sEVs is a more central aim to this Thesis, emphasis has been placed on data presented in **Fig. 5.4** and **Table 5.2,** and enrichment scores are compared to that seen in AML- cells.

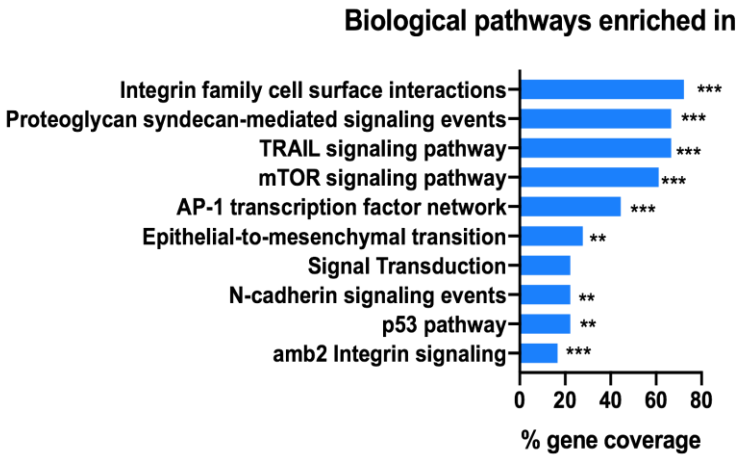

Figure 5.4: Top-ranking biological pathways enriched in AML- sEV protein cargo. *Upregulated proteins found in AML- sEVs were analysed using FunRich functional enrichment software. Threshold of at least 3 proteins were selected. Statistical significance was assessed using hypergeometric p values, * = p < 0.05; ** = p < 0.01; *** = p < 0.001.*

Table 5.2: Fold enrichment scores of top-ranking gene networks mapped in AML- sEV protein cargo.

Biological pathway	*Fold enrichment*	*Genes mapped*
Integrin family cell surface interactions	*3.30*	*TNC; SERPINE1; VCAM1; ICAM1; IL6; EGFR; MMP3; PRL; ENG; MMP2; KLK3; VEGFA; CTSD;*
TRAIL signalling pathway	*3.166*	*VIM; SERPINE1; ICAM1; IL6; EGFR; MMP3; PRL; ENG; MMP2; KLK3; VEGFA; CTSD*
Proteoglycan syndecan-mediated signaling events	*3.13*	*TNC; SERPINE1; ICAM1; IL6; EGFR; MMP3; PRL; ENG; MMP2; KLK3; VEGFA; CTSD;*
mTOR signaling pathway	*2.99*	*SERPINE1; ICAM1; IL6; EGFR; MMP3; PRL; ENG; MMP2; KLK3; VEGFA; CTSD;*
AP-1 transcription factor network	*4.505*	*SERPINE1; ICAM1; IL6; PRL; ENG; MMP2; KLK3; VEGFA;*
Epithelial-to-mesenchymal transition	*9.458*	*TNC; VIM; SERPINE1; VCAM1; MMP2*
P53 pathway	*7.410*	*SERPINE1; EGFR; MMP2; CTSD*
N-cadherin signalling events	*5.579*	*EGFR; MMP3; MMP2; KLK3*
Signalling transduction	*1.159*	*CCL20; TNC; VCAM1; EGFR*
AMB2 integrin signalling	*26.275*	*ICAM1; IL6; MMP2*

In proteins with elevated expression in AML- sEVs, GO analysis revealed that *Integrin family cell surface interactions* had the broadest percentage gene list in AML- sEVs, and was found to have a wider percentage gene coverage and higher fold enrichment than the same biological pathway observed in the cell dataset (72.2% > 60.0%; 3.305 > 2.745) (**Fig. 5.4** and **Table 5.2**). *TRAIL signalling pathway* (*p*=0.000038) and *Proteoglycan-syndecan mediated signalling events (p=0.000043)* were the next top-ranking hits in AML- sEVs for widest percentage gene coverage (both 66.67% > 60.0%), again having wider coverage and enrichment compared to that found in the AML- cell dataset (*TRAIL signalling pathway*...= 3.116 > 2.849; *Proteoglycan*... = 3.126 > 2.813). *mTOR signalling* also had wider percentage gene coverage (61.11% > 57.14%) and higher enrichment

(2.992 > 2.798) in the AML- sEVs compared to the AML- cells. *AP-1 transcription factor network* is slightly less enriched in AML- sEVs compared to the AML- cell counterparts (4.505 < 4.632). The remaining significantly enriched biological pathways – *Epithelial-to-mesenchymal transition, N-cadherin signalling events, p53 pathway,* and *amb2 integrin signalling* – were exclusive to AML- sEV protein cargo and not found to be enriched in the AML- cells.

5.2.2. Validation of selected protein enrichment in sEVs by ELISA

Proteins were selected for validation based on enrichment biological pathway analysis, focussing on those previously reported to have particular biological relevance to TSC (**Table 5.3**).

Table 5.3: Enriched proteins in AML- sEVs selected for validation

Protein	Known role in cancer	References
Endoglin	Co-receptor of TGF-β1 and TGF- β3; promotes TGF-β-BMP signalling cascade to activate SMAD signalling; Links with HIF-1α signalling Roles in angiogenesis	Chen *et al*., 2018 Sánchez-Elsner *et al.,* 2002 Nogués *et al*., 2020
Enolase γ	Energy-sensing Enolase 1 downregulates AMPK and activates mTOR; induce migration, proliferation, and migration; mitigated by rapamycin	Zhan *et al*., 2017
VEGF	Driver of angiogenesis downstream of hyperactive mTOR signalling VEGF-D a serum marker for TSC-LAM	Dodd *et al.,* 2015 Hirose *et al*., 2019
IL-6	Pro-inflammatory and anti-inflammatory cytokine; downstream to mTOR/JAK-Stat/VEGF Can activate mTOR signalling Rapamycin can reduce IL-6 effect on cell invasiveness Role in TSC-LAM microenvironment Overexpressed in many tumour microenvironments	Ekshyyan *et al*., 2016 Wang *et al*., 2021 Chonov *et al*., 2019
CCL20	Promotes cell migration Immune cell recruitment to promote cell death evasion	Marsigliante *et al*., 2013; Dolhman *et al.,* 2017; Geisman *et al*., 2017

Commercially-available ELISAs (DuoSet ELISAs, R&D Systems) were used to validate and quantify protein expression levels in AML- sEVs and AML+ sEVs. 5 target proteins, endoglin, enolase-y, VEGF, IL-6, and CCL20 had significantly elevated protein levels in AML- sEVs, compared to AML+ sEV controls (**Fig. 5.6**). This was consistent across 2 µg, 4 µg, and 8 µg doses of EVs, validating the proteome profiler results.

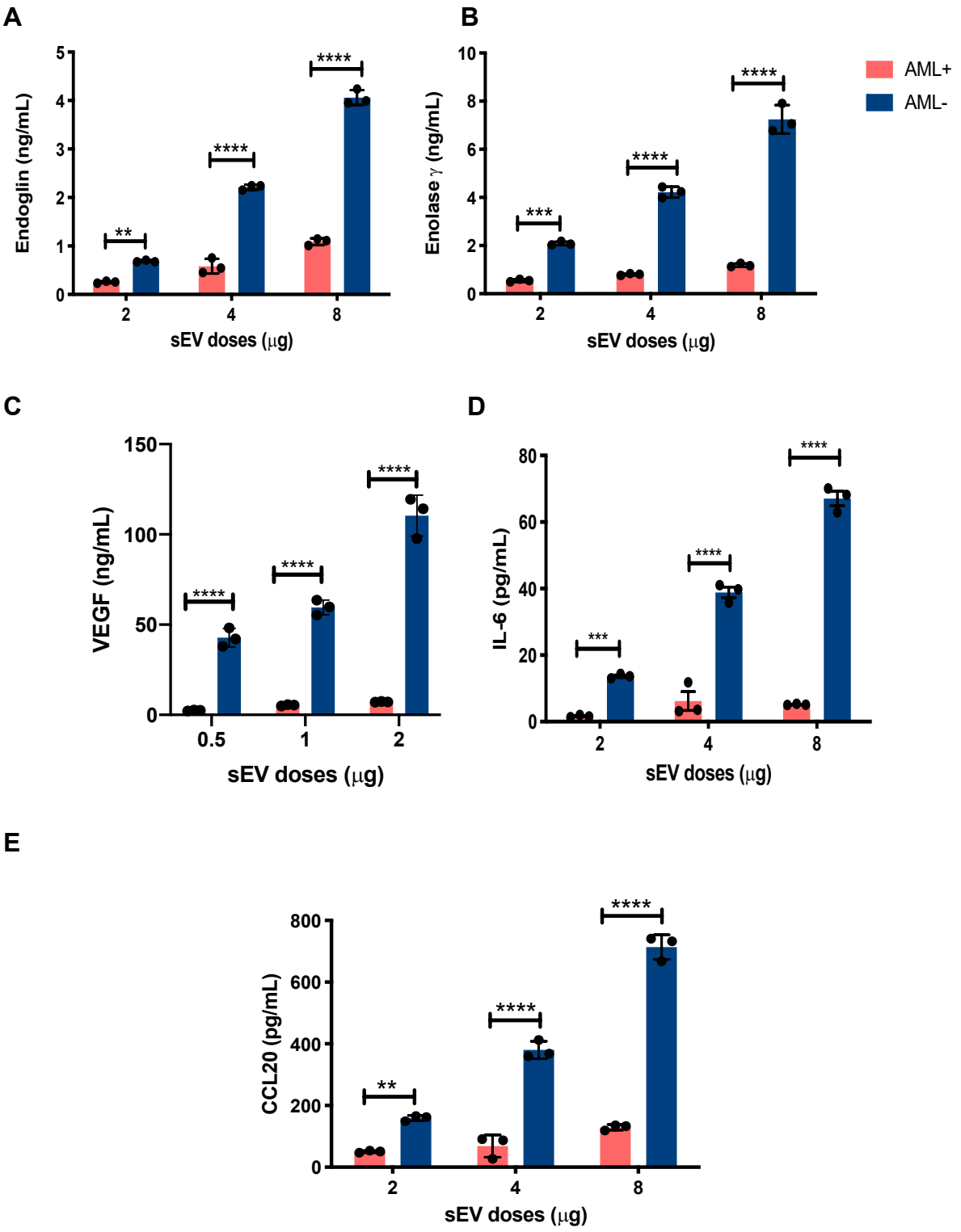

Figure 5.5: Endoglin, enolase γ, VEGF, IL-6 and CCL20 protein expression is elevated in AML- sEVs compared to AML+ sEVs. *Protein quantification of targets in lysed sEVs was determined by ELISA. Error bars represent mean±standard deviation, technical triplicates. ** p ≤ 0.01, *** p ≤ 0.001, **** p ≤ 0.0001 from two-way ANOVA with Tukey's multiple comparisons test. Representative graph of three independent experiments.*

Previously, work from our lab demonstrated that EV-associated Transforming Growth Factor β (TGF-β) plays a key role in facilitating tumour progression. EV-associated TGF-b was shown to drive differentiation of stromal fibroblast (Webber et al., 2010) to a disease-associated phenotype with pro-angiogenic function that is capable of promoting tumour growth *in vivo* (Webber *et al*., 2015). Furthermore, our selected protein target endoglin is a TGF-β co-receptor with involvement reported in both stimulating and repressing fibrotic signalling due to its association with various TGF-β family members (Finnson *et al*., 2010; as reviewed by Maring, Trojanowska, and ten Dijke, 2012). Involvement of TGF-β has also been linked to metalloproteinase-2 modulation and collagen synthesis in TSC tumour microenvironment remodelling (Lee *et al*., 2010; Woodcock *et al.,* 2019), but there are no previous reports of EV-TGF-β in TSC or whether it can modulate the tumour microenvironment in this genetic condition. Therefore, despite not being included within the proteome profiler, I chose to investigate whether TGF-β was altered in TSC EVs compared to controls EVs. Total TGF-β was assessed by ELISA and was found to be significantly elevated in all three AML- sEV doses, relative to their AML+ sEV controls (**Fig. 5.6**).

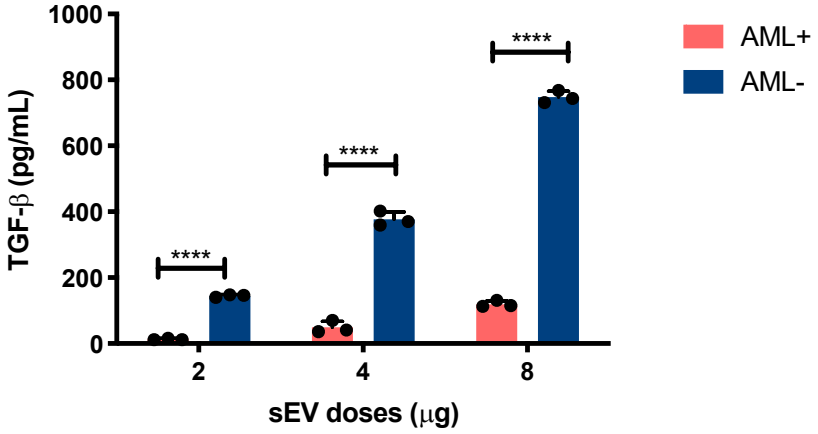

Figure 5.6: TGF-β protein expression is elevated in AML- sEVs compared to AML+ sEVs. *Lysed EVs were probed for TGF-β expression using ELISA. Error bars represent standard deviation between technical triplicates. **** $p \leq 0.0001$ from two-way ANOVA with Tukey's multiple comparisons correction. Representative graph of n=3 independent experiments.*

5.2.3. mTORC1 signalling markers are enriched in AML- EVs at a protein level

Since mTORC1 hyperactivation is the key pathogenic driver of TSC tumour growth, I wanted to map the expression of a panel of mTORC1 pathway-associated proteins in TSC cell-derived EVs to determine if mTORC1 pathway proteins are being packaged in EVs and could therefore be transferred to recipient cells.

Protein analysis by western blot showed TSC2 to be lost in AML- cells when compared to the AML+ cells, as expected (**Fig. 5.7**). Interestingly, this was also true in sEVs; there was no TSC2 expression detected in AML- sEVs while TSC2 was present in AML+ sEVs. Rheb was detected in both AML+ and AML- cells to similar levels, but Rheb expression appeared to be enriched in AML- sEVs compared to AML+ sEVs (**Fig. 5.7**). Expression of mTOR was detected in both AML+ and AML- cells and EVs. Opposing trends of 4e-BP1 expression were observed between AML cells and EVs, as 4e-BP1 appeared to be enriched in

AML+ cells versus AML- cells, but enriched in AML- sEVs compared to AML+ sEVs (**Fig. 5.7)**. Akt expression was detected in AML+ cells and to a slightly lower level in AML- cells. Interestingly, Akt expression was detected in AML- sEVs and not AML+ sEVs (**Fig. 5.7)**. GAPDH expression was found to be expressed consistently between AML+ and AML- cells, and again in AML+ and AML- sEVs. GAPDH expression was elevated within EVs compared to cells due to the selective enrichment of selected proteins within EVs compared to their parental cells (**Fig. 5.7)**.

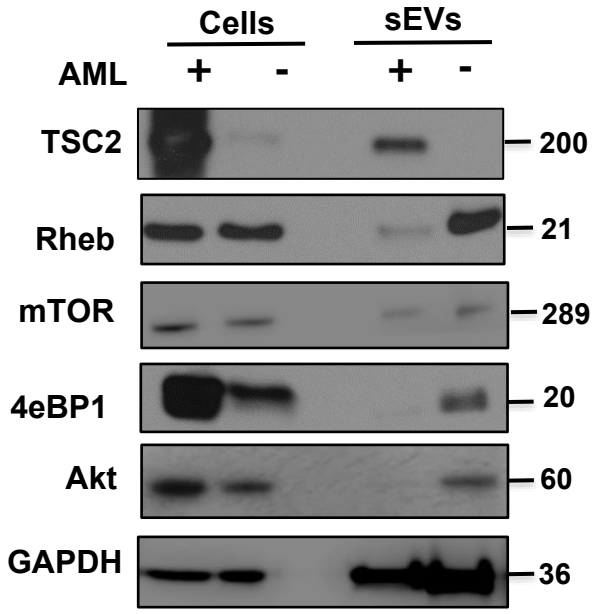

Figure 5.7: mTORC1 signalling pathway proteins are differentially expressed in AML+ and AML- cells and sEVs*. AML whole cell lysates and sEV lysates (10 µg/lane) were subjected to SDS-PAGE and western blot to probe for expression of proteins associated with mTORC1 signalling. Representative blots of n=3 independent experiments.*

5.2.4. Rapamycin treatment affects EV secretion and cargo loading

Given the differences in mTOR signalling related proteins between AML+ and AML- sEV protein cargo, I wanted to examine if mTORC1 inhibition in cells would affect sEV secretion and sEV cargo. Rapamycin, as the standard-of-care mTORC1 inhibitor, was chosen for this. The impact of rapamycin on sEV secretion was assessed from AML- cells treated with rapamycin (10 ng/mL) and compared to that from both AML+ cells and AML- cells cultured in the absence of rapamycin. Measurements of particles within serially centrifuged and filtered cell conditioned media, assessed by nanoparticle tracking analysis (NTA). Negative controls basal media and DMSO were also assessed by NTA (**Fig. 5.8A**). I show that AML- cell-conditioned media contained an elevated level of particles/mL with statistical significance in comparison to AML+ cells (**Fig. 5.8A**). Rapamycin-treated AML- (rapaAML-) cells appeared to secrete significantly fewer particles compared to AML- cells, and an amount of particles comparable with that of AML+ control cells (**Fig. 5.8A**). A similar trend is observed when these particles/mL are normalised to respective cell counts, although differences between all groups are non-statistically significant when normalised (**Fig. 5.8B**).

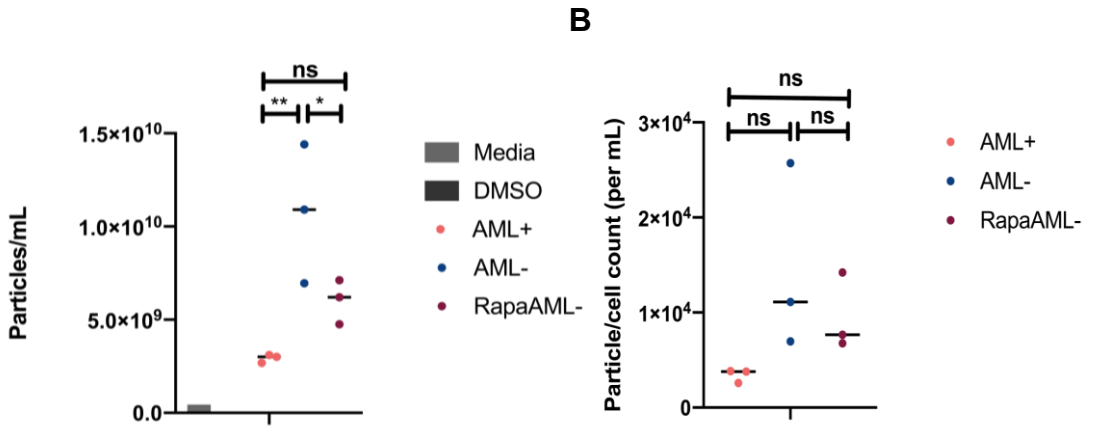

Figure 5.8: Rapamycin treatment reduces sEV secretion towards levels similar to that secreted by AML+ cells. *Cells were grown to confluence and media was replaced with fresh media or fresh media + rapamycin (10 ng/mL). Cell-conditioned media was collected after a 4-day incubation and processed to remove cell debris and particles > 0.22 µm before particles/mL was assessed by NTA (A). Particles/mL measurements were normalised to respective cell counts and plotted (B). Graphs show n=3 biological repeats. Statistical analysis was conducted using one-way ANOVA with Tukey's multiple corrections test, where ns = non significance; * = p < 0.05; ** = p < 0.01.*

Characterisation of rapaAML- sEVs was conducted to determine if rapamycin treatment would affect typical EV characteristics such as protein expression and size, as described in **Chapter 3.** Lysates from rapaAML- sEVs were found to express endosome-associated proteins ALIX and TSG101, to similar levels as to that expressed in AML+ and AML- sEVs (**Fig. 5.9A).** These rapaAML- sEVs were also found to express all three tetraspanins on their surfaces, to similar levels as that observed on AML+ sEVs and AML- sEVs (**Fig. 5.9B**). On analysing the size distribution profiles, rapaAML- cells secreted a majority of vesicles that qualify as a small EV, based on a measurement of their diameters (**Fig. 5.9C**), resembling the profiles of sEVs secreted from AML+ and AML- cells. From this characterisation, rapamycin-treated AML- cells appear to secrete sEVs of endosomal origin, and that these sEVs have similar molecular and size characteristics as AML+ and AML- sEVs.

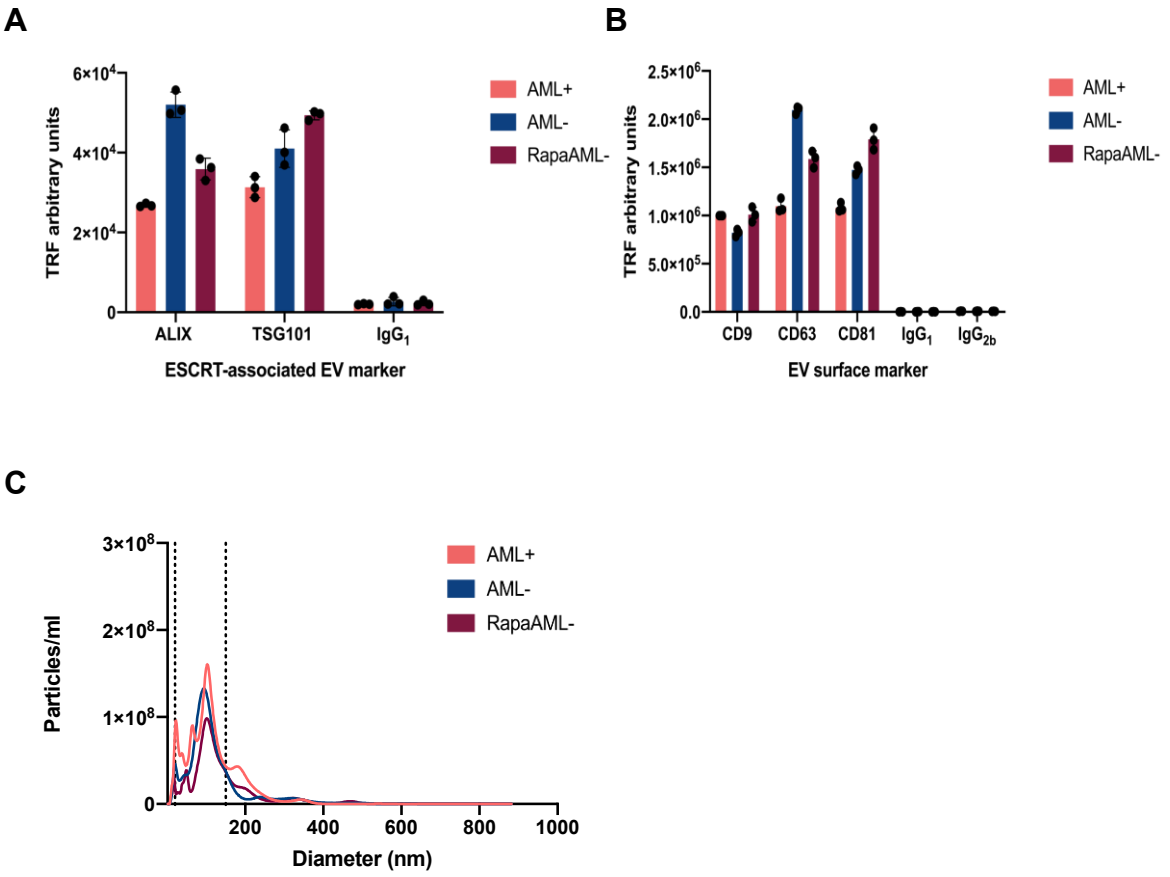

Figure 5.9: Rapamycin-treated AML- cells secrete sEVs with similar molecular characteristics as those secreted by AML+ and AML- cells*. RapaAML- sEVs were lysed and probed for ALIX and TSG101 (A) and sEV surface markers CD9, CD63, and CD81 (B) using an immunofluorescent plate assay; Size distribution profiles of EVs secreted by AML+, AML-, and rapamycin-treated AML- cells were plotted following NTA (C). Representative of three independent experiments.*

To investigate if treatment with an mTORC1 inhibitor could affect sEV cargo, I probed rapaAML- sEVs for expression of my previously selected protein targets – endoglin, enolase γ, VEGF, IL-6, and CCL20. Elevated expression of the selected target proteins was observed in AML- sEVs again, similar to results previously shown, apart from IL-6 expression found to not be differentially expressed in AML+ versus AML- sEVs at the 2μg dose (**Fig. 5.10A-E)**. Interestingly, rapaAML- sEVs

had significantly less endoglin (**Fig. 5.10A**), enolase γ (**Fig. 5.10B**) and CCL20 (**Fig. 5.10E**) protein expression in their cargo compared to AML- sEVs, observed at both 2μg and 4μg sEV doses. RapaAML- sEVs were found to have significantly less IL-6 (**Fig. 5.10D)** compared to AML- sEVs at the 4μg sEV dose only. VEGF expression was statistically elevated in rapaAML- sEVs (**Fig. 5.10C**) compared to AML- sEVs at the 4μg sEV dose, while VEGF expression was similar when comparing AML- sEVs and rapaAML- sEVs at the 2μg sEV dose. Endoglin expression in rapaAML- sEVs was similar to that of AML+ sEVs at the same 2μg sEV dose (**Fig. 5.10A**), but the relative expression between the control and drug-treated sEV groups at the 4μg sEV dose was statistically different. Enolase γ and IL-6 expression was similar in AML+ and rapaAML- sEVs at both the 2μg and 4μg sEV doses (**Fig. 5.10B+D**). IL-6 expression is significantly reduced in rapaAML- sEVs compared to AML- sEVs at the 4μg EV dose only. In contrast, VEGF protein expression is not reduced in rapaAML- EVs (**Fig. 5.10C**). Instead, VEGF is expressed at a similar or even a higher level than in AML- sEVs.

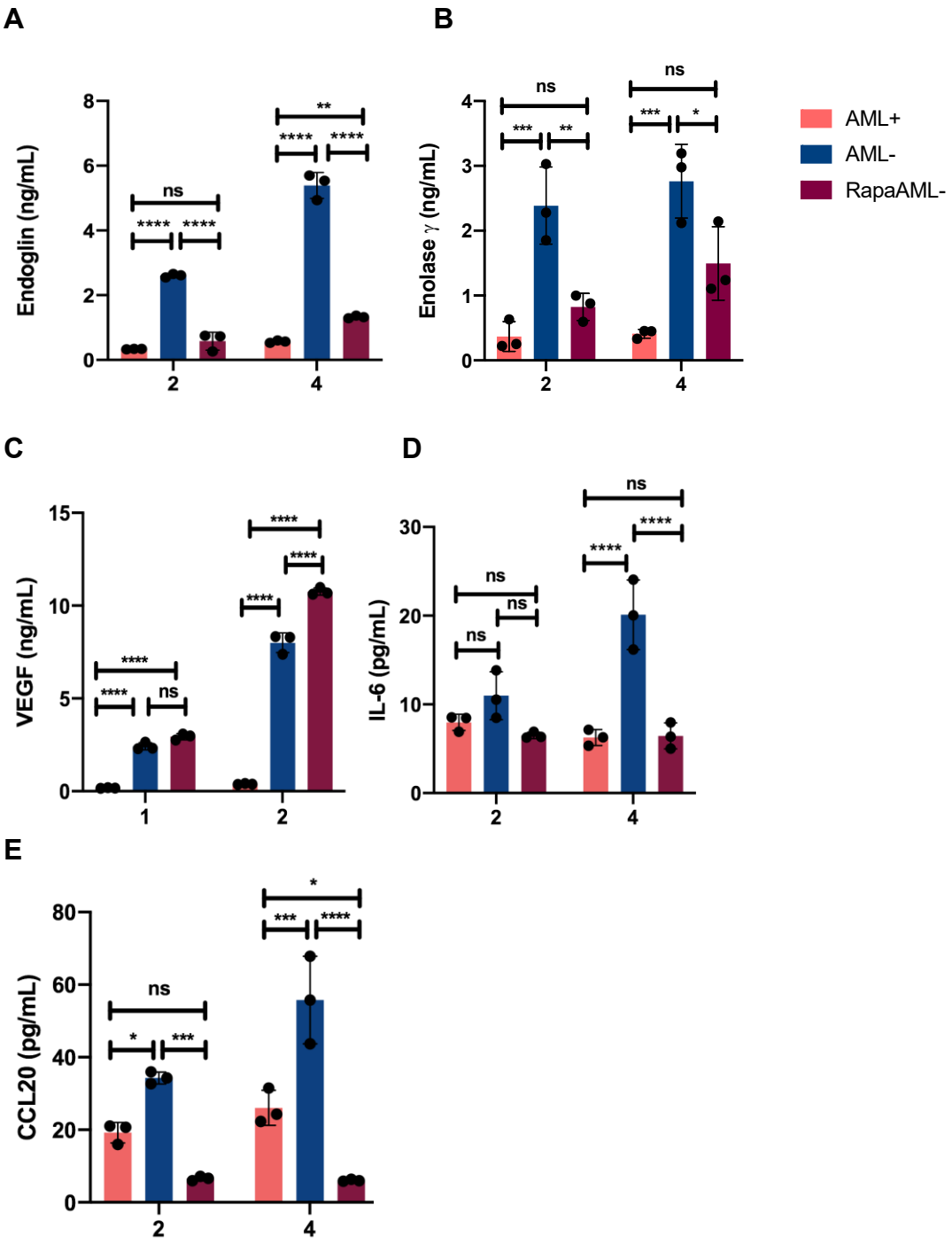

Figure 5.10: Expression of protein targets in sEVs secreted by rapamycin-treated cells. *sEVs (normalised by total protein in µg) were lysed and quantified for protein targets using ELISA. Error bars represent standard deviation between technical triplicates. Representative graph of n=3. Non-statistical significance, ns; ** = p ≤ 0.01; *** = p ≤ 0.001; **** = p ≤ 0.0001 from two-way ANOVA with Tukey's multiple comparisons correction.*

5.2.5. AML- EVs enhance growth factor secretion from normal fibroblasts

Understanding sEV-induced functional effects at cellular destination sites is perhaps most crucial in understanding the role of sEVs in contributing to disease phenotypes and progression. To determine if sEVs promote GF secretion from recipient cells, VEGF and HGF expression were quantified in EV-depleted cell-conditioned media taken from healthy lung fibroblast cells following a 4-day treatment with 200 µg of AML+ sEVs, AML- sEVs, or rapaAML- EVs. Both VEGF and HGF expression were significantly elevated in cell-conditioned media from fibroblasts treated with AML- sEVs and similarly so post-treatment with rapaAML-EVs, compared to that secreted following treatment with AML+ sEVs (**Fig. 5.11**).

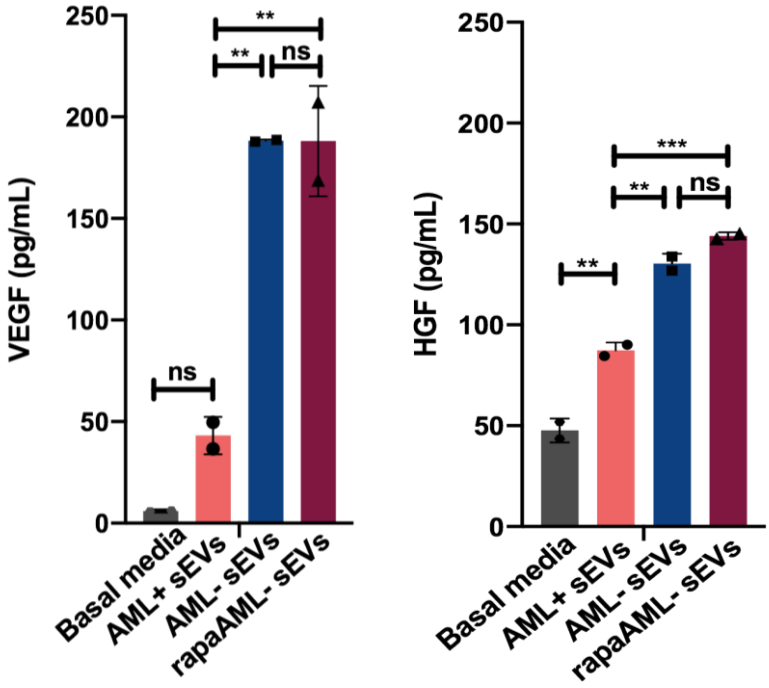

Figure 5.11: VEGF and HGF secretion is elevated in recipient fibroblasts post AML- EV and rapaAML- EV treatment. *Serum-starved fibroblasts Z031 were treated with 200µg EVs and incubated for 4 days. Cell-conditioned media was collected was subjected to ultracentrifugation to pellet and deplete EVs. Resulting cell-conditioned media was probed for VEGF and HGF expression using commercially-available ELISAs. Graphs shown are representative of three independent experiments. Statistical analysis was performed using one-way ANOVA with Tukey's multiple comparison's test. $p < 0.05$, * ; $p < 0.01$, ** ; $p < 0.001$, ***; non-statistical significance, ns. Vascular Endothelial Growth Factor, VEGF; Hepatocyte Growth Factor, HGF.*

5.2.6. Signalling activation induced by AML+ and AML- sEVs is ameliorated by rapamycin treatment

Knowing the role of mTORC1 signalling in TSC disease and reported evidence of phenotypic spread reported in *Tsc1*-deficient mouse models (Patel et al., 2016), I wanted to investigate if AML sEVs could alter mTORC1 signalling in recipient cells. Lysates from fibroblasts treated with AML+ sEVs, AML- sEVs, and rapaAML- sEVs were generated and expression of phosphorylated MAPK (pMAPK), an activator of mTORC1, and phosphorylated S6 (pS6), which is a downstream marker of

activated mTORC1, was analysed by western blot. Phosphorylation of MAPK was more prominent in fibroblasts treated with AML- sEVs compared to AML+ sEVs (**Fig. 5.12**). RapaAML- sEV treatment did not stimulate MAPK phosphorylation as much as AML- sEV treatment. S6 phosphorylation was observed in comparable amounts in fibroblasts treated with AML+ sEVs and AML- sEVs (**Fig. 5.12**). Similarly as with pMAPK, phosphorylation of S6 was reduced with treatment of rapaAML- sEVs.

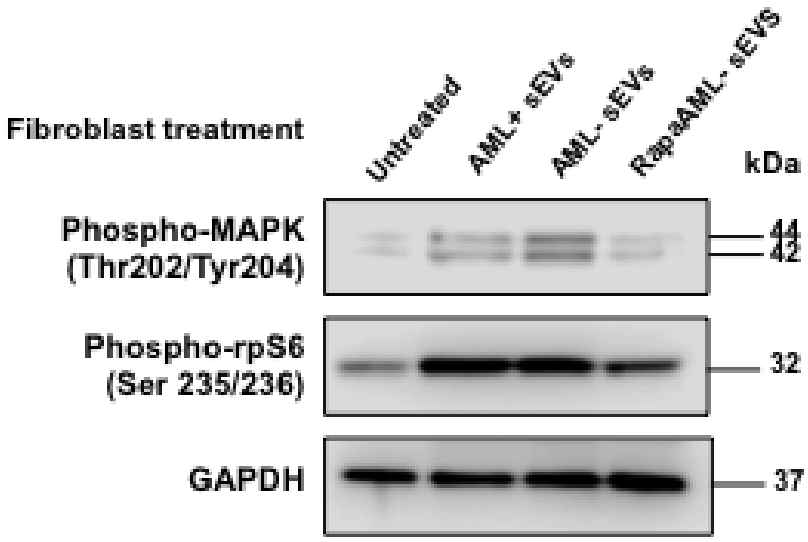

Figure 5.12: AML+ and AML- EVs can activate MAPK and S6 in recipient fibroblasts, but this is attenuated by rapamycin treatment*. Serum-starved fibroblasts Z031 were stimulated with 200 µg EVs for 1 hour. Lysates were collected and pMAPK (Thr202/Tyr204) and rpS6 (Ser 235/236) expression were probed using western blot. Blots shown representative of three indepdendent repeats. Phosphorylated Mitogen-activated Protein Kinase, pMAPK; Threonine, Thr; Tyrosine, Tyr; serine, ser; phosphorylated Ribosomal Protein S6, pS6; Glyceraldehyde-3-Phosphate Dehydrogenase, GAPDH.*

5.3. DISCUSSION

The mechanisms by which TSC tumours prime their microenvironment to support their growth are unknown. Uncovering how AML cells communicate with their tumour microenvironment could reveal important insights into how TSC tumours establish effective intercellular communication to regulate their proliferation and survival. More specifically, profiling sEV cargo could identify specific bioactive molecules that have the capacity to promote a tumour-supportive microenvironment, improving our understanding of disease progression whilst revealing potential therapeutic targets.

In this Chapter, I profiled protein cargo in TSC patient-derived AML cell line-derived sEVs to identify differentially expressed proteins that could potentially mediate tumour-supporting processes in recipient cells of a TSC tumour microenvironment. Using a combination of a protein profiler antibody array, western blots, and ELISAs, I have defined a distinct protein cargo carried by AML- sEVs, encompassing both oncology-associated and mTORC1 signalling proteins. This has revealed numerous new candidate targets that may contribute to mechanisms of EV-mediated tumour growth and survival. My investigation of 84 oncology-associated proteins in TSC AML cells and cell-derived sEVs aimed to identify potential novel players in TSC tumour growth and survival. Data from this profiler showed altered expression of 42 oncology-associated proteins in AML- cells (**Fig. 5.1**), and 29 proteins in AML- sEVs (**Fig. 5.2**), relative to AML+ cell and sEV controls respectively. In both cases, the majority of proteins identified have had no previous association to TSC tumour biology. To stratify the 21 proteins that were elevated in

AML- sEVs, functional enrichment analysis based on the gene ontology annotation *Biological pathways* was performed. Identifying that two of the top-ranking enriched networks were centred around integrin interactions and proteoglycan-syndecan mediated signalling (**Fig. 5.4, Table 5.2**) was perhaps to be expected considering their well-known roles in mediating EV-induced cell migration and adhesion (as reviewed by Hurwitz *et al.,* 2019), and EV biogenesis and uptake respectively (as reviewed by Cerezo-Magaña *et al*., 2020). The increased enrichment of *TRAIL signalling* in AML- sEVs, compared to AML- cells, may have important implications in the ability of these sEVs to activate apoptosis cascades in recipient cells upon delivery. It was also interesting to see that *mTOR signalling* was significantly enriched in AML- sEV cargo compared to the parental AML- cells. Investigating activation of this mTOR signalling-associated proteins may highlight a potential mechanism of how TSC sEVs drive anabolic signalling extracellularly. There were also a number of enriched biological pathways that were exclusive to AML- sEVs (and not the parental AML- cells), such as *epithelial-to-mesenchymal transition, N-cadherin signalling networks, p53 pathway*, and *amb2 integrin signalling*. These could have important implications in EV-induced alterations in the TSC tumour microenvironment. It is also important to note that, typically, functional enrichment analysis is employed in proteomic studies with typically much larger datasets to analyse (Tomczak *et al*., 2018). Input datasets in this study were small (*n*=39 for AML- cells; *n*=21 in AML- sEVs); hence, the results are simply a prediction of sEV function and should be used as a guide for further downstream analysis.

sEV cargo proteins to validate were selected with consideration of known pro-tumoral mechanisms at play in TSC, and specifically AML, namely pro-angiogenic signalling and inflammation, and by considering interesting novel mechanisms of biological relevance that have been under-explored in the context of TSC, including stromal modification and intercellular signal transduction (see **Table 5.3**). Selected proteins – endoglin, enolase γ, VEGF, IL-6, and CCL20 – were validated for differential protein amounts between AML+ and AML- sEVs by ELISA. Quantification revealed statistically significant elevation of these protein targets in all three doses of AML- sEVs examined, compared to their AML+ sEV counterparts (**Fig. 5.5**). Investigating known disease-promoting roles of these proteins could inform design of functional experiments to investigate sEV-mediated cell phenotypic changes in the TME.

Enolase γ is a glycolytic enzyme involved in the catabolic conversion of glucose to pyruvate that allows for the production of high-energy ATP and NADH (as reviewed by Vizin and Kos, 2015; Clayton *et al*., 2011). In the cancer setting, enolase γ is frequently upregulated and its major contribution is in the acceleration of intratumoral glycolysis (as reviewed by Kroemer and Pouyssegur, 2008), facilitating the phenomenon of the tumoral Warburg effect. Though research on EV-derived enolases is limited, links between this glycolytic enzyme and mTOR signalling have been previously explored. Zhan *et al.* describe that overexpressed enolase α leads to impaired AMPK signalling and activation of mTOR signalling. Furthermore, rapamycin could reduce enolase α overexpression-induced migration, proliferation, and invasion in colorectal cancer tissues (Zhan *et al*., 2017).

VEGF is a well-known pro-angiogenic protein that signals downstream of mTORC1 (Dodd *et al*., 2015). Knowing now that VEGF has elevated expression in AML- sEVs, compared to AML+ sEVs, and knowing that AML tumours are characterised by dense angiogenic networks (as reviewed by Vos and Oyen, 2019), this highlights a potential capacity of AML sEVs to stimulate angiogenesis when internalised by cells of the tumour microenvironment. EV-associated VEGF, both luminally and on the surface, has been associated with promoting angiogenesis in cancer settings (Feng *et al*., 2017; Ko *et al*., 2019). Therefore, investigating if these AML- sEVs can promote vessel formation would clarify their pro-angiogenic function in TSC, and more specifically TSC-associated AML. It has been shown that VEGF-C and VEGF-D promote metastatic spread of TSC-associated LAM. Currently, VEGF-D is used as a diagnostic and predictive serum biomarker for TSC-associated LAM (Young *et al*., 2008; Young *et al*., 2010; Goldberg *et al*., 2015; Hirose *et al*., 2019; Radzikowska *et al*., 2015) and is regarded as being highly sensitive. However, the suitability of VEGF-D as being a prognostic biomarker for LAM has not yet been characterised, despite there being a clinical need to stratify patients more prone to fatal outcomes or transplantation due to LAM (Gupta *et al*., 2019). It is also unknown if VEGF or its isoforms associate with sEVs, and whether this would improve on its wide range of that used for clinical diagnostics (Hirose *et al*., 2019; Radzikowska *et al*., 2015). Another VEGF isoform, VEGFA, stimulates the Akt/mTOR pathway via its activation of VEGF receptor 2 (VEGFR2) on endothelial cells (Trinh *et al*., 2009). Activation of this VEGFR2/Akt/mTOR pathway was found to associated with increased incidence of ascites and reduced overall survival (OS) of patients receiving cisplatin-taxane regimens, in the same study. Here the authors propose this as a potential

targetable mechanism using VEGFA inhibitors. Understanding if EV-associated VEGFA isoforms also promote intercellular activation of this tumour-promoting pathway could be beneficial in determining a microenvironmental dimension of these tumours with targeting potential.

IL-6 is known to play roles as both a pro- and anti-inflammatory cytokine. Several studies to date have explored EV-induced secretion of IL-6 from different cell populations to achieve both pro- and anti-tumour effects. For example, EVs from heat-stressed tumour cells can potently induce secretion of IL-6 from dendritic cells to facilitate preferential regulatory T cell to T helper type cell differentiation in order to establish an anti-tumour effect (Guo *et al*., 2018). Contrastingly, EV miR-1247-3p promotes release of pro-inflammatory IL-6 from cancer-associated fibroblasts via β1-integrin-NF-κB signalling in hepatocellular carcinoma (Fang *et al*., 2018). However, functionality of sEV-delivered IL-6 to cells of the tumour microenvironment is currently unknown. As this cytokine has potent and varied microenvironmental effects and has also been linked to TSC (Wang *et al*., 2021), it becomes an interesting candidate for further exploration. Furthermore, IL-6 is a known activator of the mTOR signalling pathway, and additionally stimulates Januskinases (Jak), which sequentially activates the Jak/STAT, MAPK, and PI3K pathways (Pinno *et al*., 2016). EV-associated IL-6 could potentially activate these key pathways in recipient cells, which could affect treatment efficacy of some targeted anti-tumour treatments.

CCL20 (also known as Macrophage Inflammatory Protein 3α) has well characterised roles in cell signalling and inflammatory cell recruitment. Intracellular

CCL20 can promote cell migration and proliferation via ERK and PI3K signalling activation (Wang *et al*., 2016). As proliferative drivers are a key focus for new therapeutic avenues to inhibit TSC tumour growth, EV-derived CCL20 may be a potential target. Mesenchymal stromal cell EV-derived CCL20 has been previously implicated in migration, inflammation suppression, and regenerative properties (Mardpour *et al*., 2019). It has also been shown that CCL20-CCR6 binding can attract tumour-promoting immune-suppressive cells within the tumour microenvironment (as reviewed by Chen *et al*., 2020) and facilitate extracellular matrix modification in a breast cancer setting (Marsigliante *et al*., 2013). Interestingly, a previous study showed that the mTORC1 inhibitor rapamycin mitigated CCL20-induced upregulation of N-cadherin and vimentin protein synthesis (Marsigliante *et al*., 2016). Although it was previously seen that AML is mesenchymal in origin (vimentin-positive as shown in **Chapter 3**; also, as demonstrated by Bertolini *et al*., 2018), it is unclear if EV-derived CCL20 could play a role in establishing mesenchymal cell phenotypes, and by extension if mTORC1 inhibition could ameliorate its vimentin-positive mesenchymal characteristics.

The glycoprotein, endoglin, is a recognised co-receptor of TGF-β, specifically interacting with type I and II TGF-β receptors (as reviewed by Pérez-Gómez *et al*., 2010). Endoglin has been implicated in regulating angiogenesis and neovascularisation, and is required for VEGF-induced angiogenesis (Tian *et al*., 2018). It has been previously shown that microvesicles derived from endoglin-expressing cancer stem cells stimulate blood vessel formation and growth *in vivo* (Grange *et al*., 2011). However, endoglin has not previously been linked to TSC pathogenesis. Given that AMLs are characterised by a dense vascular network,

understanding the pro-angiogenic processes is a major focus, making endoglin an interesting target.

It is also interesting that TGF-β was found to be significantly elevated in AML- sEVs versus AML+ sEVs (**Fig. 5.6**). The role of TGF-β has been extensively studied in the cancer setting. Previous work from our lab has demonstrated that EV-derived TGF-β can drive fibroblast differentiation to an activated myofibroblast phenotype with pro-angiogenic function, thereby activating tumour stroma to drive angiogenesis *in vitro* and tumour growth *in vivo*, in interesting contrast to soluble TGF-β that did not elicit these pro-tumoral effects (Webber *et al*., 2015). Uncovering the role that TGF-β and its co-receptor endoglin play in TSC-associated angiogenesis and stromal activation will provide interesting insight into TSC tumour growth and survival.

As TSC tumours are driven by hyperactived mTORC1 signalling, I probed for expression of a panel of mTORC1 signalling proteins to determine if TSC EVs contain mTORC1 components and whether or not their expression was mirrored or differed from that of their parent cells (**Fig. 5.7**). It is interesting that TSC2 is expressed in sEVs from AML+ (TSC2-expressing) cells, while its expression is lost in sEVs secreted from AML- (TSC2-deficient) cells. This could suggest a maintained tumour suppressor TSC1/TSC2 complex in control AML+ sEVs. In AML- sEVs, absent TSC2 protein would suggest that Rheb could be present in its active GTP-bound state. Rheb protein was found to be elevated in AML- EVs (**Fig. 5.7**). Rheb is activated downstream of a loss of TSC2 expression in the protein signalling pathway. Enrichment of Rheb protein in AML- sEVs is different from that

seen in cells, as Rheb expression appears to be relatively equal in both AML+ and AML- cell lysates. Furthermore, loading of Rheb protein within EVs complements previous EV-mRNA work in *Tsc1*-deficient neural cell-derived EVs (Patel *et al*., 2016). Together with the enhanced levels of Rheb protein observed in AML- EVs, could delivery of this EV-derived Rheb contribute to mTOR activation within recipient cell populations? By probing next for TSC1 and phosphorylated TSC2 expression, I could investigate if sEV-derived TSC2 could still maintain its GTPase-activating capacity, as it does in an intracellular context, to regulate Rheb activation in control AML+ EVs to sustain it in its GDP-bound inactive state. mTOR protein expression appears relatively equal in AML+ and AML- cells, though I would expect it to be hyperactivated in AML- cells given its key role in driving TSC tumour growth. Several antibodies for mTOR were trialled to address the specificity issues with little success. Additional probing for mTOR or phospho-mTOR in cell lysates could aid in clearer interpretation of this result. Despite this, mTOR expression appears to be slightly higher in expression in AML- sEVs compared to AML+ sEVs (**Fig. 5.7**). This may suggest that these disease sEVs carry mTOR into cells of the microenvironment, extending the impact of this intracellular driver hallmark of these tumours in the extracellularly domain. This compliments that observed in my GO analysis, with enrichment of proteins associated with mTOR signalling in AML- sEVs, as discussed above. Determining the phosphorylation network surrounding mTOR in recipient cells post-sEV delivery will help determine a clearer understanding of this mechanism, which inspired the subsequent functional work. It was also observed that opposite patterns of expression of 4E-BP1 in cells and sEVs. 4E-BP1 expression was higher in AML+ cells than in AML- cells, while 4E-BP1 is found to be expressed in AML- sEVs, but not in AML+ sEVs (**Fig. 5.7**). In a

normal physiological context, a hypophosphorylated 4E-BP1-eIF4E complex impedes ribosomal recruitment to prevent initiation of mRNA translation, as eIF4E does not interact with eIF4G. When mTOR is hyperactivated, cellular 4E-BP1 becomes phosphorylated at multiple sites, thereby instigating dissociation of the 4E-BP1-eIF4E complex. This allows eIF4E to form the eIF4F complex and so permits consequent initiation of cap-dependent translation (Chong *et al*., 2009). It is unclear why 4E-BP1 would have altered expression in AML- sEVs. Probing for phosphorylated 4E-BP1 and eIF4E complexes could shed further light on this mechanism. Delivery of these translation initiation factors, and inhibitors of the process, to a recipient cell could have important implications in the translation of proteins within the recipient cell population. I also saw that Akt is expressed slightly higher in AML+ cells compared to AML- cells, while Akt is expressed only in AML- sEVs and not in AML+ sEVs (**Fig. 5.7**). This is an interesting observation, as Akt is a known activator of mTORC1 via its phosphorylation of TSC2 and PRAS40 (Dan *et al*., 2014). mTOR and its downstream substrate S6K repress Akt intracellularly, so it may be more feasible biologically to package Akt in sEVs for intercellular export to optimise its ability to activate mTORC1 signalling cascades. Given its smaller size, it may be more efficient to package Akt into sEVs, compared to bigger proteins such as mTOR. Furthermore, determining if phospho-Akt expression is enriched with rapaAML- sEV treatment would indicate if retro-activation of Akt by mTORC1 inhibition could also be propagated by sEVs.

The effect of rapamycin, the standard-of-care anti-tumour therapy for TSC AML, on sEV secretion and sEV cargo was investigated. Previous studies indicate contrasting trends in EV secretion from TSC cells. *Tsc2*-deficient cell T2J were

found to promote EV secretion *in vitro* (Zadjali *et al*., 2020), while another study showed reduced secretion of EVs from *Tsc2*-deficient compared to *Tsc2*-expressing MEF cells (Zou *et al*., 2019). Finding that there was a trend showing that rapamycin-treated AML- cells secreted fewer particles/mL compared to AML- cells (**Fig. 5.8**) may suggest that *TSC2* deficiency or mTORC1 could play a role in regulating sEV secretion, aligning with some published literature (Zou *et al*., 2019; Ryskalin *et al*., 2020). This study also revealed that rapamycin treatment did not affect EV characteristics (**Fig. 5.9**). Furthermore, my selected protein candidates for validation, namely: endoglin, enolase γ, and CCL20; had significantly reduced incorporation into rapaAML- sEVs compared to AML- sEVs (**Fig. 5.10**). This suggests that these markers could have potential as predictive biomarkers or for therapeutic monitoring, and so were candidates for validation in patient plasma samples. Contrastingly, VEGF expression was not reduced in rapaAML- sEVs compared to AML- sEVs *in vitro* (**Fig. 5.10C)**. Instead, it was found to be expressed at a level comparable or significantly higher than AML- sEVs.

EV-mediated intercellular crosstalk is a contributing factor to the development and progression of many tumours, as EVs from parental tumour cells are delivered to surrounding cells of the tumour microenvironment to stimulate tumour-supporting processes. This work is the first study to profile the microenvironmental modifications induced by delivery of AML sEVs to fibroblasts of the tumour microenvironment, and the comparison of AML- sEV-induced effects to AML+ sEV effects is also unique to this study. Furthermore, inclusion of rapaAML- sEVs is also unique and provides interesting insight into how EVs in treated AML tumours may promote different functions to that of the tumour-derived AML- sEVs. While

some studies have been published regarding the role of mTOR in mediating EV biogenesis and secretion (Zou *et al*., 2019; Ryskalin *et al*., 2020), none have specifically examined the effect of sEVs on recipient cells. This allows us to gain perspective, for the first time, on how mTORC1-active tumours may signal intercellularly, and how inhibiting mTORC1 with rapamycin may affect how sEVs promote tumour-supporting processes intercellularly.

EVs have been reported to stimulate GF secretion from cancer cells/fibroblasts (Al-Newadi *et al.,* 2008; Webber *et al*., 2015), but this has not been investigated in relation to TSC or mTOR-driven tumour microenvironments. Elevated expression of VEGF, a known angiogenic driver; and HGF, a mesenchymal marker with known roles in promoting migration and metastasis; is of note with treatment with AML- sEVs compared to AML+ sEVs (**Fig. 5.11**). Knowing that AML- sEVs are derived from mTORC1-active cells, and that VEGF acts downstream of mTORC1 in a key angiogenesis-driving pathway, this data suggests that these AML- sEVs may also prime cells of the tumour microenvironment to stimulate blood vessel sprouting. HGF is also elevated with treatment of AML- sEVs, which suggest an EV-stimulated mechanism to promote a variety of tumour-promoting processes such as proliferation, migration, and invasion (as reviewed by Xiang *et al*., 2017). HGF has also been previously implicated in activation of mTOR and its downstream markers S6 and 4EBP1 (Moumen *et al*., 2007), leading me to hypothesise that elevated HGF may in fact activate mTOR signalling in recipient cells. Interestingly, I also observed that VEGF and HGF is also elevated in secretion, compared to AML+ sEVs, with treatment with rapaAML- sEVs (**Fig. 5.11**). This appears to be an intercellular tumour-supporting mechanism by rapaAML- sEVs, which may

suggests a limitation of rapamycin in an anti-tumour response. The limitations of rapamycin treatment, as previously discussed here, have been widely reported (as reviewed by Ní Bhaoighill and Dunlop, 2019). Thus, given these treatment shortcomings, these results suggest a potential treatment resistance mechanism induced by rapamycin treatment via sEVs. It is known that efficacy of rapamycin treatment can be limited due to mTORC1 inhibition compensatory mechanisms via feedback loops or mTORC1-independent pathways. This may be explained by sEVs from rapamycin-treated cells promoting a pro-survival tumour state as it stimulates VEGF and HGF secretion. Knowing of the expression and status of cognate receptors of VEGF and HGF in recipient cells of the microenvironment, both locally to AML tumours and also in other TSC tumour manifestations, will shed more light onto the exact mechanism by which this elevated GF secretion may be contributing to TSC tumour biology.

Given the hallmark role of mTORC1 hyperactivity in this disease, examining if mTORC1 signalling may be promoted by AML- sEVs in recipient fibroblasts representing the tumour microenvironment. EVs have been previously shown to activate tumour-supporting signalling in recipient cells, yet knowledge in the field of TSC or mTORC1-active tumours is currently elusive. pMAPK, an upstream activator of mTORC1; and pS6, a downstream readout of pmTORC1 were selected to elucidate potential mTORC1 activation pathway. Seeing that AML- sEVs stimulated activation of pMAPK and pS6 (**Fig. 5.12**) may indicate that these tumour cell-derived sEVs could activate mTORC1 signalling in recipient cells, meaning that the hallmark mTOR-active state also extends to the tumour microenvironment. Similar is reported by Patel *et al*., where EVs from cells with highly levels of Rheb

were shown to activate components of mTOR signalling in recipient Rheb-depleted AML cells (Patel *et al*., 2016). However, it was also seen that AML+ sEVs could activate pMAPK, to a lesser extend than did AML- sEVs, and pS6, to a similar extend to AML- sEVs. This suggests that also AML+ sEVs may also can activate mTORC1, despite having cargo distinct from that of AML- sEVs. It is noteworthy here that sEVs used in these experiments were derived from high-density bioreactor cultures, and so the parental cells were not serum-starved. This could affect signalling mediation intrinsic to these sEVs. Similarly, as sEVs carry a diverse cargo, I did not identify the specific sEV-associated cargo that could activate pMAPK and pS6. Both phosphoproteins are involved in an elaborate signalling network with feedback loops involving mTOR, a key signalling node in normal and disease cell physiology. Also, a more extensive panel spanning additional mTORC1 mediators and downstream readout markers could further elucidate this mechanism and create a clearer picture as to the mechanisms by which AML+ and AML- sEV mediate mTORC1 signalling in recipient cells. It is also of interest here that rapaAML- sEVs also had reduced levels of pMAPK and pS6 compared to that induced by AML- sEV treatment (**Fig. 5.13**). This is contrasting to the previous data, as it highlights a reduced ability of sEVs from rapamycin-treated cells to activate phospho-proteins associated with mTORC1 signalling in the tumour microenvironment, suggesting a previously unknown intercellular therapeutic effect of rapamycin. It is important to note here that it was not examined if rapamycin itself had been packaged into the sEVs. In this case, sEVs may have acted as drug carriers of rapamycin to extracellular sites to enact in mTORC1 in those recipient cells. It is also reasonable to question if administering rapamycin in combination with MAPK or S6 inhibitors would improve anti-tumour treatment of a

TSC tumour. Furthermore, our model was designed to mimic the AML microenvironment and the AML-LAM axis, two TSC manifestations which are speculated to have cells-of-origin in common (Yu *et al*., 2004). Use of co-culture *in vitro* models would expand upon this model to include a more representative model of the tumour microenvironment. Furthermore, *in vivo* models would provide systemic application of these sEVs on TSC tumour development as a multi-organ disease.

5.4. CONCLUDING REMARKS

The results presented in this Chapter reveal a distinct protein profile within AML- cells and cell-derived EVs, relative to their respective AML+ controls. Enrichment of protein networks involved in various tumour-supporting processes in AML- sEVs informed selection of protein candidates that could be relevant to TSC tumour biology and used as potential disease biomarkers. Components of mTORC1 signalling were also found to be carried by AML- sEVs, and not in AML+ sEVs, which could indicate mechanisms by which mTORC1 signalling is promoted intercellularly. Treatment with the mTORC1 inhibitor rapamycin did not alter secreted EV characteristics, but expression of selected sEVs proteins were found reduced. The effect of rapamycin treatment on sEVs from AML- cells was further highlighted by their reduced capacity to activate tumour-supporting signalling, associated with MAPK, compared to AML+ and AML- sEVs.

CHAPTER 6

EXPLORING sEV PROTEINS AS BIOFLUID-BASED BIOMARKERS FOR TSC

6.1. INTRODUCTION

6.1.1. Rationale

Tumour cell-derived sEVs carry a diverse assortment of biomolecules from the parental tumour into biodistribution (as reviewed by van Niel *et al*., 2018). Thus, sEVs facilitate the shuttling of a unique molecular signature, reflective of the parental tumour's underlying genetic and molecular complexity, into the extracellular space and systemic circulation in biofluids (as reviewed by Mathew *et al*., 2020). Given the stability and protection of this circulating molecular cargo within the encapsulating lipid bilayer, sEVs and their associated cargo are becoming attractive sources of 'liquid biopsy' disease biomarkers (as reviewed by Fujita *et al*., 2016; as reviewed by Ciferri *et al*., 2021). Determining specific cargo enriched in sEVs in patients with a particular disease or disease phenotype could significantly improve diagnostic, disease monitoring, or therapeutic surveillance strategies.

6.1.2. Tuberous Sclerosis Complex (TSC) biomarkers and clinical need for new developments

As described in **Chapter 1**, Tuberous Sclerosis Complex (TSC) is a genetic disease with a variable inter-patient multi-organ and neurological phenotype (as

reviewed by Crino *et al*., 2006). Diagnosis of TSC is made with identification of a pathogenic mutation in either *TSC1* or *TSC2* genes (www.lovd.nl/TSC1, www.lovd/TSC2). Following genetic diagnosis, there is an extensive programme of surveillance and management recommendations set out for these newly diagnosed or suspected TSC cases (Northup *et al*., 2020; on behalf of the International Tuberous Sclerosis Complex Consensus Group). Current knowledge of how specific *TSC1/2* pathogenic genotypes correlate to TSC tumour and other TSC phenotypes is limited (as reviewed by Curatolo *et al*., 2015), resulting in patients undergoing extensive routine testing and scans for each organ system potentially affected by TSC. As TSC manifestations arise independent of age (Northup *et al*., 2021) and are progressive, careful monitoring of these patients post-genetic diagnosis is central to optimising treatment and implementing best management. It is also important to mention that clinical signs of TSC can also be employed diagnostically in the absence of a *TSC1/2* pathogenic mutation, which is observed in up to 15% of patients (Tyburczy *et al*., 2015). In this cohort, identification of either 2 major features, or 1 major feature and 2 minor features (See **Table 6.1)** is sufficient for a diagnosis of TSC (Northup *et al*., 2021). In these patients with no mutation identified, biomarkers that signify specific TSC phenotypes could help to improve individualised detection, surveillance and monitoring.

Elevated expression of VEGF-D is the clinically used serum-based soluble biomarker for TSC-associated and sporadic lymphangioleiomyomatosis (LAM) (Young *et al*., 2008; Young *et al*., 2010), which also has some demonstrated evidence that it correlates with disease severity and treatment response (Young *et al*., 2013). However, this does not inform of other TSC manifestations, and not all

TSC patients with LAM have elevated serum VEGF-D (Verwer *et al*., 2018). Despite patients being predisposed to grow multi-organ tumours, there is currently no biofluid-based biomarker for monitoring TSC whole-body tumour burden or progression, or surveillance of response to rapamycin/rapalog therapy. Developing such a blood-based biomarker(s) could improve upon monitoring efficiency and reduce the cost of multiple routine tests and scans currently used for tumour monitoring and surveillance. It may also inform more strategically on personalised dosage and length of rapamycin/rapalog regimens for individual patients.

Previously, I showed that AML- sEVs have a distinct transcriptome (**Chapter 4**) and proteome (**Chapter 5**) compared to their AML+ sEVs counterparts *in vitro*. An altered sEV cargo may therefore provide a source of biomarkers for TSC or AML within these AML- sEVs. Specifically, I identified significant elevated expression of 5 sEV cargo proteins, endoglin, enolase γ, VEGF, IL-6, and CCL20, in AML- sEVs compared to AML+ sEVs isolated from *in vitro* AML cell cultures (**Chapter 5**). I also observed that the elevated expression of these proteins was reduced in sEVs from rapamycin-treated cells (rapaAML- sEVs) (**Chapter 5**). The potential of these sEVs or their cargo to be used as biomarkers of either detecting TSC tumours, or monitoring rapamycin treatment, remains unclear.

6.1.3. Considerations for sEV biomarker studies from biofluids

EVs have been detected in a variety of bodily fluids, including plasma, serum, urine, saliva, amniotic fluid, semen, malignant ascites, and breast milk (as reviewed by Raposo and Stoorvogel, 2013). Each biospecimen has associated advantages and disadvantages with regard to their application to EV research, as described in

Chapter 1, but the majority of biomarker discovery studies have isolated bulk EVs from serum and plasma samples (Muraoka *et al*., 2022; as reviewed by Johnsen *et al*., 2019).

Though blood is already a popular biosample used clinically and in research, it is important to contend with the potential contaminants and drawbacks of these biofluids in collection and processing for sEV isolation. Plasma and serum are viscous and also contain high concentrations of non-vesicular matter, such as soluble proteins and lipoproteins, which may impair the accurate isolation and subsequent detection of sEVs (Clayton *et al*., 2019). Thus, optimal collection and processing of biosamples, in light of EV research, is critical to translation of preclinical findings.

In this study, plasma samples collected in EDTA tubes, to minimise platelet activation, were available for use. Size-exclusion chromatography (SEC) fractionation is a recognised technique for separation of sEVs from bulk soluble protein (Welton *et al*., 2015). In addition, this technique avoids potential contamination of plasma with other material, e.g. sucrose as in a density gradient ultracentrifugation method (Baranyai *et al*., 2015). Liquid biopsy-based bulk EV analysis is advantageous as it can provide an overall representation of disease status within the patient, whilst also avoiding the complications associated with heterogeneity of multiple tumour foci, which is theoretically favourable for biomarkers aimed at diagnosis or detection of a multi-system genetic disease such as TSC. If sEVs can be reliably and specifically isolated from TSC plasma samples,

they could provide a means of stable blood-based biomarkers to support disease diagnosis, assess tumour burden and for therapeutic surveillance.

Research presented in this Thesis aimed to characterise the role of TSC cell-derived sEVs in tumour pathology. Work presented in this Chapter aims to assess the utility of five sEV cargo proteins as biofluid-based biomarkers for TSC. If successful, further studies would then be required to test and validate these biomarkers. Nonetheless, determining if the findings from earlier chapters of this Thesis translate to patient plasma has the potential to lead to new TSC biomarkers for either diagnosis, monitoring or therapeutic surveillance in the case of TSC patients receiving mTOR inhibitor treatment.

6.1.4. Hypothesis and aims

The overarching hypothesis for this Chapter is that circulating sEV-associated proteins have potential as a blood-based biomarker for TSC.

Specifically, work presented in this Chapter aims:

I. To isolate and characterise sEVs from TSC plasma samples
II. To determine if the TSC plasma sEVs have differential expression of five cargo proteins: endoglin, enolase γ, VEGF, IL-6, and CCL20; compared to that expressed in healthy donor plasma sEVs
III. To examine if mTOR inhibitor rapalog treatment could result in differential expression of these sEV cargo proteins, compared to plasma sEVs from untreated TSC patients

6.2. RESULTS

6.2.1. Characterisation of EVs from plasma samples

Using an established protocol (Welton *et al*., 2015), healthy donor (HD), TSC patient (TSC), and TSC patient receiving rapalog treatment (TSC+mTORi) plasma samples were fractionated into twenty-one fractions by SEC, using commercially available columns (Exo-spin™; Cell Guidance Systems), to separate EVs from bulk soluble protein. To determine which SEC fractions contain EVs, the immuno-affinity-based microplate assay (as described in **Chapter 2**) was used to determine expression of the EV surface marker CD81 in a number of fractions of 1 sample per treatment group. CD81 expression seemed to increase at Fraction 9 in all three samples (**Fig. 6.1**). Peaks of highest CD81 expression appeared between Fraction 10 and 13 within all three samples, suggesting that these fractions could be enriched for EVs (**Fig. 6.1**). NTA analysis was done on Fractions 8-14, alongside a selection of earlier and later SEC fractions as an alternative way of estimating EV counts. Fractions 8-14 had a majority of particles within the classical size range of a small EV (20-150 nm), while no particles were observed in Fractions 1-7 (**Fig. 6.1**). Fractions 14, 15, and 20 did contain some vesicle-sized particles but these fractions are likely to be contaminated with soluble prote

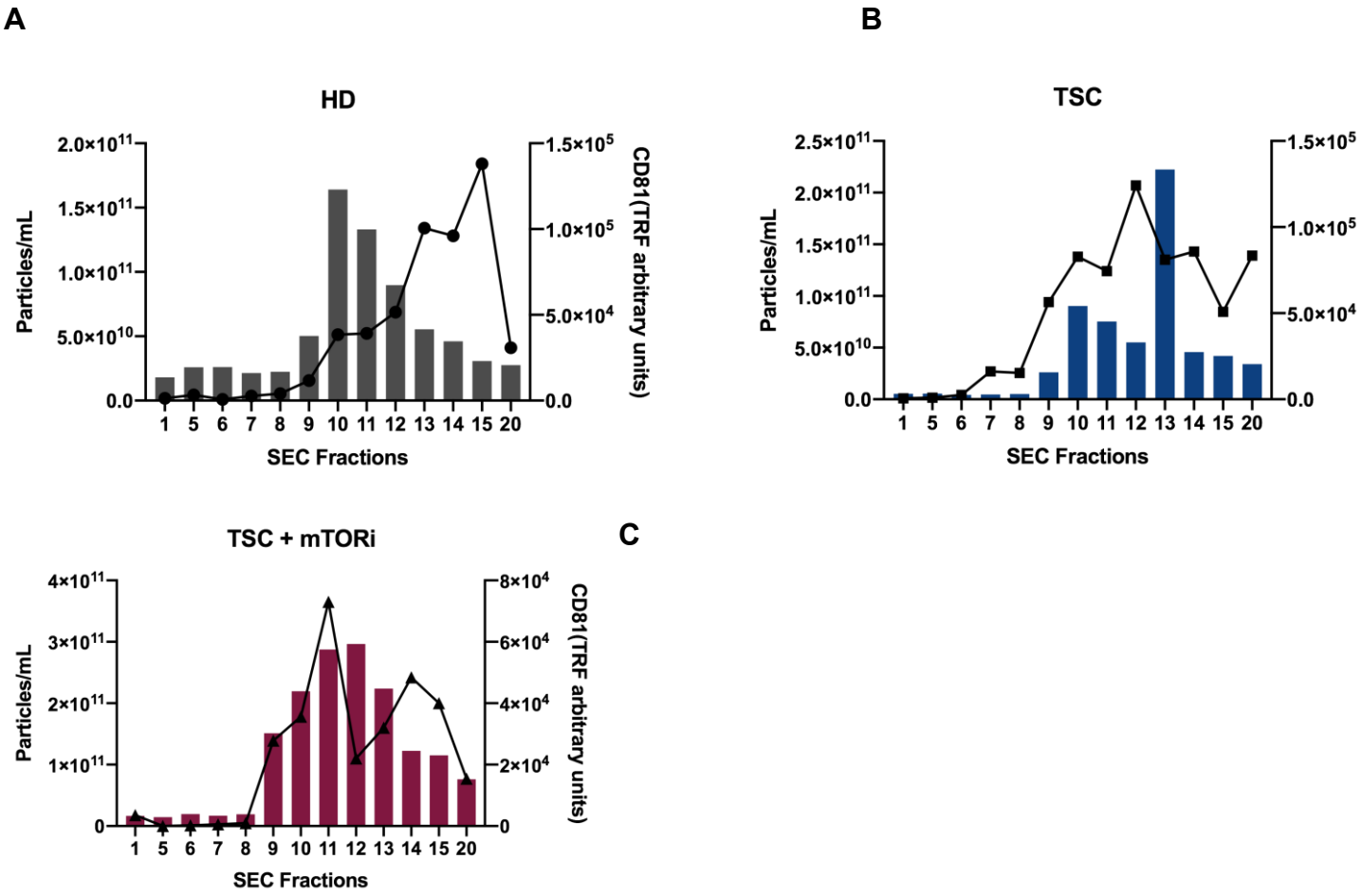

Figure 6.1: Particles/mL and CD81 expression were highest in fractions 8-14*. Immuno-affinity-based microplate assays (represented as bars; left-hand x axes) was used to quantify CD81 expression (bars) in SEC fractions. NTA (line graph; right-hand x axes) was used to assess particle counts within each fraction. Healthy donor, HD; Tuberous Sclerosis Complex patient, TSC; Tuberous Sclerosis Complex patient receiving mTOR inhibitor, TSC + mTORi, Size-exclusion chromatography, SEC. N=1/treatment group.*

Using this data, the remaining samples within each treatment group were fractionated by SEC, and then the fractions were pooled into three groups for EV cargo analysis: Fractions 1-7 were pooled to make up the '*pre-EV*' group; Fractions 8-14 were pooled to form the '*EV-rich'* group; and Fractions 15-21 were pooled to create the 'post-EV'. Additional quality control to ensure enrichment of EVs in the EV-rich group was performed by means of the TRIFic™ detection assays (Cell guidance systems) to assess the expression of EV surface markers CD9 and CD63. Expression of CD9 and CD63 was quantified in pre-EV, EV-rich, and post-EV groups. CD9 and CD63 expression was found to be significantly enriched in the EV-rich fractions compared to pre-EV fractions across all three treatment groups (**Fig. 6.2**), suggesting that EVs were likely contained within this pooled group. There seemed to be a decrease in CD9 and CD63 expression in EV-rich versus post-EV fractions across all treatment groups, though this was not found to be statistically significant (**Fig. 6.2**). CD9 and CD63 expression was not found to be significantly different when comparing pre-EV and post-EV groups in most treatment groups, apart from CD9 expression in HD fractions and CD63 expression in TSC+mTORi treatment group (**Fig. 6.2**).

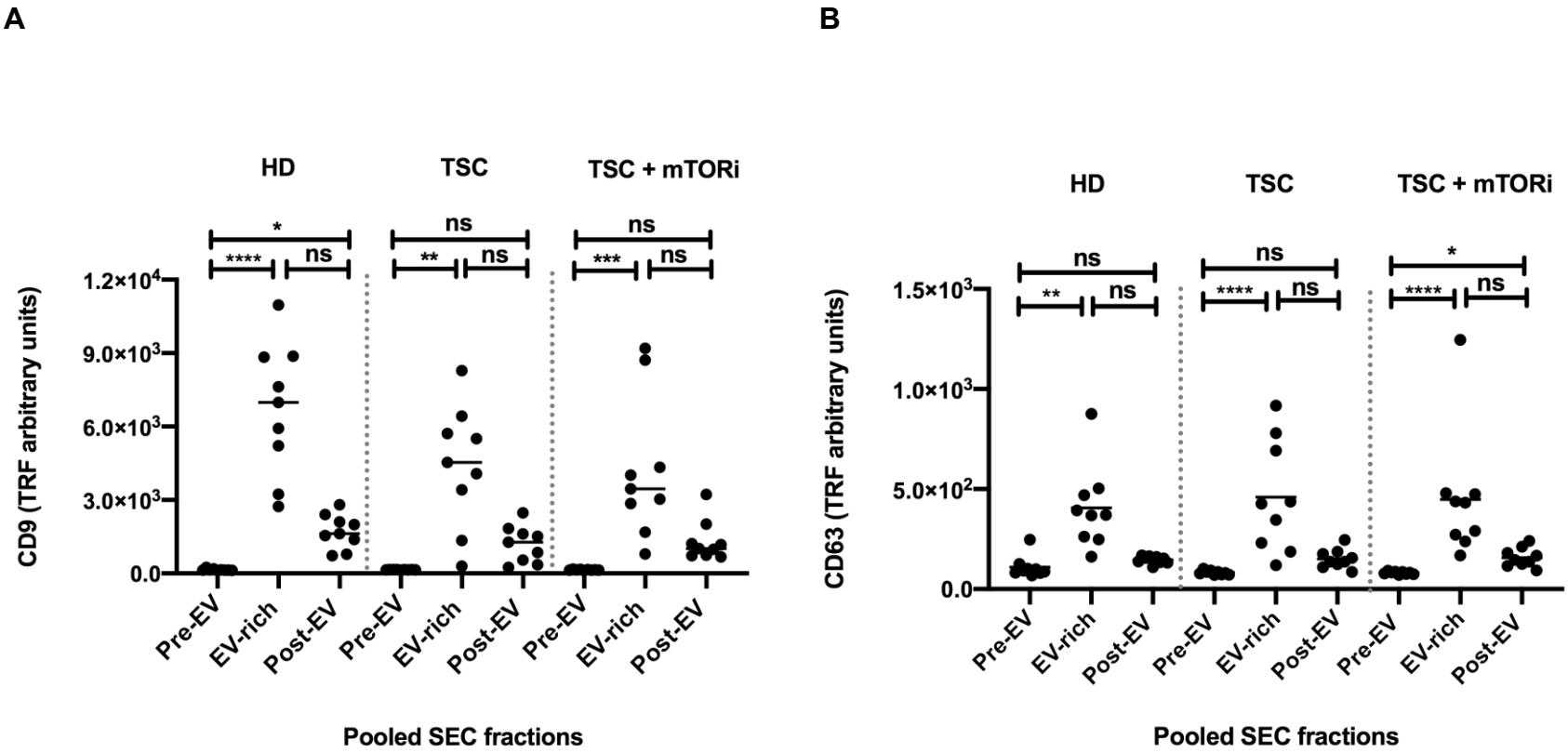

Figure 6.2: CD9 and CD63 expression is elevated in pooled SEC Fractions 8-14 ('EV-rich'). *TRIFic™ detection assays were used to quantify expression of EV surface tetraspanin markers in pooled SEC fractions. Samples were loaded volumetrically and individual values are plotted. Statistical analysis was conducted using a non-parametric Kruskal-Wallis test. N=9/treatment group. non-stastictal significance, ns; * = p < 0.05; ** p < 0.01; *** p < 0.001; **** p < 0.0001. Time-resolved fluorescence, TRF; Size-exclusion chromatography, SEC.*

6.2.2. Three novel sEV cargo proteins have significantly elevated expression in TSC plasma compared to healthy donor plasma

Previously, I identified 5 proteins had elevated expression in AML- sEVs, compared to AML+ sEVs *in vitro* (**Chapter 5**). To determine if these sEV-associated proteins: endoglin, enolase γ, VEGF, IL-6, and CCL20; may have potential as EV-associated biofluid-based biomarkers for TSC, their expression in sEVs isolated from TSC plasma sEVs were assessed using commercially available ELISAs and compared to that expressed in HD plasma sEVs. Given that CD9 expression, an EV surface marker, was variable across samples, potentially indicating different EV levels in different patients (**Fig. 6.3**), protein expression of target proteins was adjusted for CD9 expression and this normalised expression was compared between sample cohorts. When normalised to CD9, endoglin, enolase γ, and VEGF expression was elevated in the TSC patient sEVs compared to the HD control sEVs with statistical significance (**Fig. 6.3**). IL-6 and CCL20 exhibited very low expression and were not differentially expressed in the TSC patient sEVs group compared to the HD control sEVs (**Fig. 6.3**).

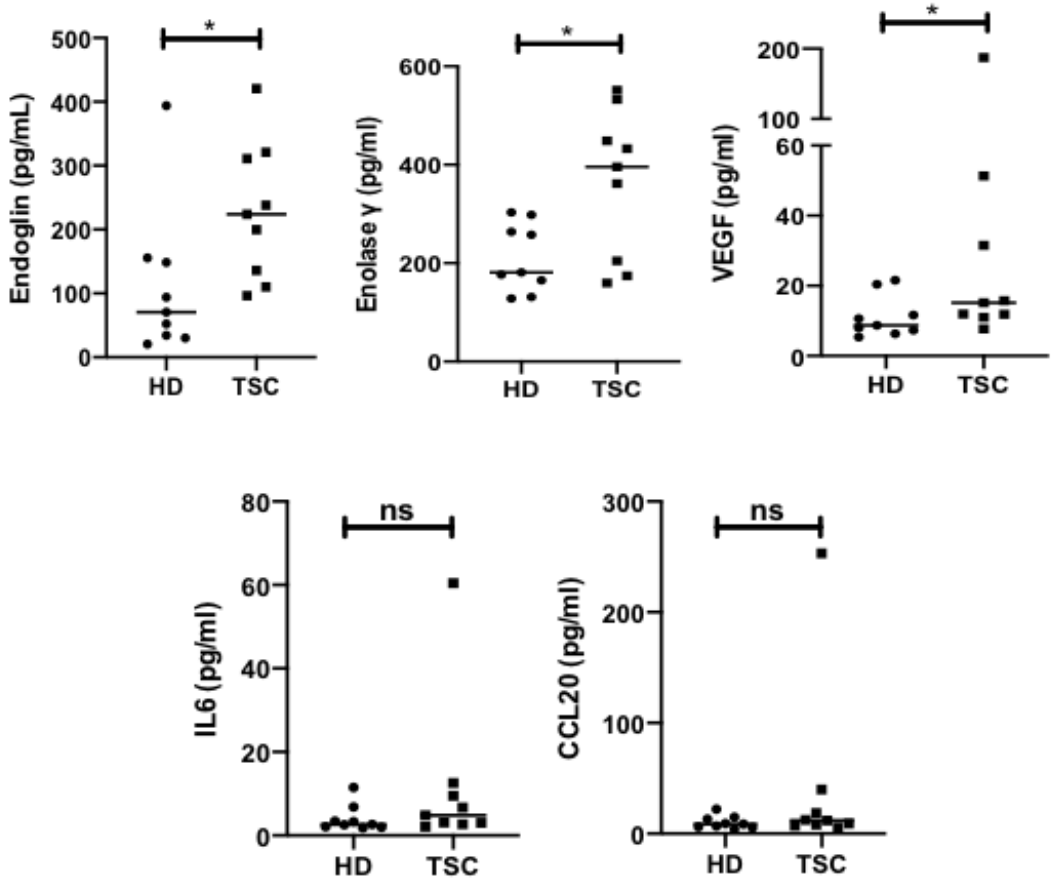

Figure 6.3: Endoglin, enolase γ, and VEGF are elevated in TSC patient plasma EVs compared to healthy donors. *EV-rich fractions were lysed and probed for expression of target proteins found elevated in AML- sEVs in vitro. Statistical analysis was conducted using unpaired two-tailed t-test. N=9/group. $p < 0.05$, * ; non-statistical significance, ns.*

6.2.3. Examination of sEV proteins as biomarkers in TSC patients treated with rapamycin

Previously, I also showed that endoglin and enolase γ protein expression was reduced in sEVs from rapamycin-treated AML- cells (rapaAML-) compared to AML- sEVs *in vitro*. VEGF protein expression was found to have comparable levels of expression in AML- sEVs and rapaAML- sEVs *in vitro* (**Chapter 5**). Thus, I wanted to examine if sEVs from rapalog-treated TSC patients had altered expression of these proteins compared to that found in plasma sEVs from TSC patients not receiving treatment. Endoglin, enolase γ, and VEGF protein expression was

detected in TSC+mTORi plasma sEVs to similar levels as that found in the TSC plasma sEVs. Statistically significant differential expression of these sEV proteins between treatment groups was not observed (**Fig. 6.4**).

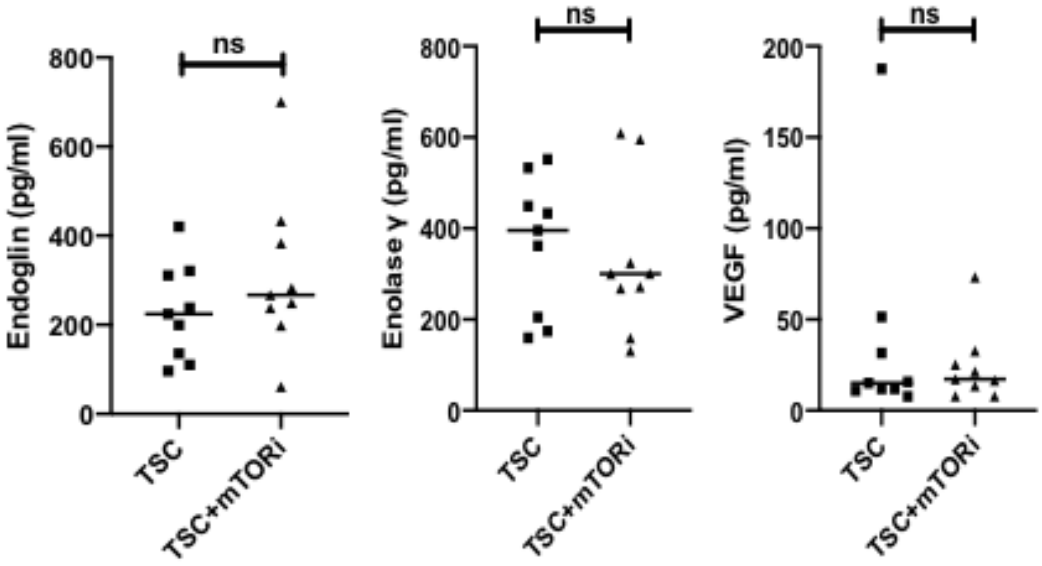

Figure 6.4: Endoglin, enolase γ and VEGF proteins were found in similar levels all TSC patient plasma*. EV-rich fractions were lysed and probed for expression of target proteins. Statistical analysis was conducted using unpaired two-tailed t-test. N=9/group. p < 0.05, * ; non-statistical significance, ns.*

6.3. DISCUSSION

Tumour cell-derived sEVs are key facilitators of intercellular distribution of biomolecules from their parental tumour cells. These sEVs are highly abundant in many biofluids (as reviewed by Sadovska *et al*., 2015) and have innate characteristics that protect of their cargo from enzymatic degradation while in systemic circulation in biofluids. Thus, given the stability of their cargo, sEVs have become attractive sources of biomarkers for tumour detection and monitoring. Currently, there is a lack of biofluid-based biomarkers for TSC, and patients rely on routine MRI scans for tumour detection, monitoring, and therapeutic surveillance (Northup *et al*., 2021). To address this unmet clinical need, I report the first

successful isolation and characterisation of sEVs from TSC patient plasma (**Figs. 6.1-6.2**). I also present three potential sEV-associated biomarkers for TSC patients, namely endoglin, enolase γ, and VEGF; that were found to have elevated expression in TSC plasma sEVs compared to healthy donor plasma sEVs (**Fig. 6.3**). I also investigated expression of these sEVs proteins in TSC patients receiving mTOR inhibition therapy, to investigate their potential as a therapeutic surveillance strategy (**Fig. 6.4**).

Isolating sEVs from plasma samples was important in this study for two reasons: first, to know if sEVs could be isolated from TSC patient plasma; and secondly, to investigate if the *in vitro* sEV characterisation (**Chapter 3**) and cargo findings (**Chapter 5**) would translate to TSC patient plasma. Isolating sEVs for EV biomarker discovery from a complex biofluid such as plasma can be challenging, as attempted isolations may be contaminated with non-vesicular matter that may obscure antibody binding and make EV detection (and subsequent detection of EV-associated proteins) more challenging. This contamination risk also may obscure what is truly EV-associated, making interpretation of clinical data difficult. Three treatment groups – healthy donor, TSC patient (with an identified *TSC2* mutation), and TSC patients (again with identified *TSC2* mutations) receiving mTOR inhibition rapalog treatment – were used in this study, and EVs were isolated from all samples by commercially-available SEC columns (Exo-spin™; CELL guidance systems). These columns have been examined previously for suitable and effective use in isolating EVs from plasma and serum (Welton *et al*., 2015), and also were successfully used in fractionating plasma samples in this study. Probing eluted fractions for CD81, a surface marker of EVs, and determining particles/mL present

by NTA provided a means of assessing which fractions were likely to contain sEVs. This characterisation was conducted in 1 sample per patient group, that were age- and sex-matched across treatment groups to ensure a fair comparison, though it is difficult to gauge how representative these selected samples truly are of this small cohort with wide age range and samples from both males and females. Taken both the CD81 and NTA measurements together, sEVs were found to be likely clustered in Fractions 8-14 in all treatment groups (**Fig. 6.1**), similar to that shown in other studies (Shephard *et al*., 2021). It is worth addressing that this initial characterisation assessed only one sEV surface marker CD81 (and not CD9 or CD63), which may bias towards a subset of sEVs within these samples. When fractions were pooled, confirmation of sEV enrichment in the sEV-rich groups was validated by TRIFic™ detection assays, which showed that all samples also had enriched CD9 and CD63 expression in the EV-rich pooled fraction groups (**Fig. 6.2**). Measurement of my selected EV protein biomarker candidates was conducted using a sandwich ELISA, whereby each assay used matched capture and detection antibodies for the specified EV protein. Plasma samples were lysed and loaded volumetrically (i.e. 100 µL per well, as opposed to loading per EV total protein). This does pose the risk of unequal EV loading per well, so candidate biomarker measurements (pg/mL) were normalised to a mean CD9 measurement for each treatment cohort. Repeats of further biomarker validation work could aim to incorporate the use of an EV-specific capture antibody such as CD9, and subsequent use of the EV-biomarker detection antibody. This opens the technical challenge when dealing with EV luminal proteins, as addition of a lysis buffer would be necessary on CD9 capture antibody-bound EVs. Careful examination of EV protein topology would also be beneficial in determining if lysis is necessary for

detection in the lumen or if these biomarker candidates could be associated with the EV surface. There is a risk of reducing the detected signal of sEV cargo by pooling the SEC fractions into groups. However, fraction pooling provided a more manageable sample set for subsequent sEV cargo analysis, and the ability to compare cargo expression most fairly between treatment groups. Fraction pooling also ensures that close to all sEVs within a particular sample would be lysed for collective cargo analysis, which also would be more applicable to a clinical laboratory setting.

Plasma has been previously used as a biofluid of choice in validating EV biomarker studies (Holcar *et al*., 2020; Luchetti *et al*., 2018) with the addition with an anti-coagulant. Accurate reporting of the anti-coagulation process is critical for fair study comparisons and sample selection from biobanks. However, it is worth noting that plasmatic proteins may be difficult to separate from EV-associated material. Another blood-based component serum is also frequently used in EV biomarker studies, but serum samples have a contamination risk of platelet-derived EVs (Zhang *et al*., 2022; Palviainen *et al*., 2020). Urinary EVs have been previously used as sources of biomarkers for certain kidney diseases, such as polycystic kidney disease (Hogan *et al*., 2009) and renal cell carcinoma (Raimondo *et al.,* 2013), and may also be applicable to determining an AML-specific biomarker. It is worth remembering that urinary EV processing poses some unique considerations, such as best time-of-day to collect urine, if the urine should be first pass. Urinary EVs can also be diluted in a large volume, which may reduce signal of biomarker detection or be difficult to store.

There are several caveats that are important to mention in the interpretation of these data. Firstly, the TSC plasma samples used had identified *TSC2* pathogenic mutations; however, corresponding clinical signs were not disclosed. Thus, correlating these candidate biomarkers with TSC phenotypes is not possible from this pilot study. Preclinical varibles could be affecting candidate biomarker levels, so provision of these characteristics could be useful in stratifying these biomarkers. It is known that sEVs can also carry specific molecular signatures indicative of disease phenotypes (as reviewed by Sadovska *et al*., 2015). Retrieving this clinical information in a future validation cohort would help discriminate if these biomarkers correlated with TSC whole-body or specific TSC tumour manifestations. Secondly, despite there being statistically significant differential expression between TSC and HD samples, there is notable overlap in expression ranges between the two groups for endoglin, enolase γ, and VEGF (**Fig. 6.3**). As this was a pilot study for EV biomarker discovery (*N*=9/group), these findings require validation using a larger sample set and an additional validation cohort, which could also help determine expression ranges or thresholds signifying elevated expression in TSC versus HD samples. Some studies publishing EV discovery biomarker data have analysed small cohorts of less than twenty patients/treatment group (Shephard *et al.*, 2021; Ko *et al*., 2020); however, other studies have analysed larger patient cohorts, such as *N*=100 (Melo *et al*., 2015) in their EV biomarkers investigations. It is also important to consider that there are some challenges to contend with with regard to patient recruitment or cohort sizes, given that TSC is a rare disease, when designing follow-up studies.

I also examined if these sEV biomarkers would discriminate TSC patients receiving mTOR inhibition therapy from TSC patients receiving no treatment, as a potential means of assessing response to therapy or as a therapeutic surveillance strategy. However, a significant difference in expression of endoglin, enolase γ, or VEGF in TSC+mTORi plasma sEVs compared to the TSC plasma sEVs was not detected (**Fig. 6.4**). Validating these findings in a larger patient cohort again would give a clearer indication whether these sEVs proteins are applicable to predicting response to therapy or as a means of monitoring existing anti-tumour therapy for TSC. Furthermore, requesting additional details regarding the rapalog treatment regimen or rapalog trough levels of these patients, to conduct a fairer analysis as a therapeutic surveillance biomarker for TSC tumours.

There could also be benefit in identifying if these biomarkers could be used to monitor AML specifically, as AMLs are the TSC tumour types associated with greatest mortality and morbidity. With standard-of-care rapalog treatment, AMLs reduce in size (Bissler *et al*., 2008; Davies *et al*., 2011). In patients with an identified pathogenic mutation in *TSC1* or *TSC2* genes, monitoring of kidney involvement is conducted using abdominal MRI every one to three years for the course of a patient's lifetime (Northup *et al*., 2020). Blood pressure of these patients is also monitored to detect hypertension, and kidney function is assessed by measuring the glomerular filtration rate (GFR) once every year (Northup *et al*., 2020). Given that AML manifests in over 80% of TSC patients, having an AML specific biomarker with a defined threshold and expression range profile would also be beneficial both as a disease monitoring and therapeutic surveillance tool.

6.4. CONCLUDING REMARKS

In this Chapter, I have identified three sEV cargo proteins that may have potential to be the first EV-associated blood-based biomarkers for TSC. Three sEV-associated proteins, endoglin, enolase γ, and VEGF, were discovered to be significantly elevated in TSC patient plasma sEVs compared to HD plasma sEVs in a small pilot study (*N*=9/group). With this, their potential application as TSC biomarkers, for TSC or for specific manifestations of TSC, requires further validation in additional, ideally larger, cohorts of patients and correlated with corresponding clinical information.

CHAPTER 7

GENERAL DISCUSSION

7.1. SUMMARY

Research presented in this Thesis tested the primary hypothesis that AML- tumour cells secrete sEVs, with RNA and protein cargo distinct from AML+ sEVs. The secondary hypothesis tested was that AML- sEVs capable of modifying fibroblasts of the tumour microenvironment in order to contribute to TSC tumour growth and development. In **Chapter 3**, populations of sEVs secreted from AML+ and AML- cells were characterised based on their biophysical and molecular properties. In **Chapter 4**, a comprehensive screen of RNA cargo in both AML+ and AML- sEVs was conducted using RNA-Seq, with additional qPCR used to assess if AML- sEVs carry mTORC1-signalling components. Functional enrichment of differentially expressed genes between these AML+ and AML- sEVs was performed using GOliath and REACTOME functional enrichment GO software programmes. In **Chapter 5**, AML- sEV protein cargo with tumour-promoting potential was investigated using a proteome profiler antibody array and functional enrichment analysis, using FunRich functional enrichment GO software, was used to aid prediction of functional consequences to signalling with delivery of AML- sEVs to recipient cells. The effect of rapamycin, the standard-of-care mTORC1 inhibitor, on sEV secretion and selected sEV cargo was examined, and differences between signalling capacities of AML+, AML- and rapaAML- sEVs was assessed *in vitro*. In **Chapter 6**, five proteins that were found elevated in AML- sEVs *in vitro* were evaluated as potential biofluid-based biomarkers in TSC patient plasma sEVs.

This Thesis presents work addressing key knowledge gaps regarding the intercellular perspective of TSC tumour biology, revealing important new knowledge about TSC sEVs, in terms of their characteristics, and their RNA and protein cargoes. This work highlights the role of sEVs in promoting tumour growth while also showing the potential utility of plasma-derived sEVs as biomarkers of disease. Thus, the key findings of this work are: **I.** TSC cells secrete sEVs of endosomal origin; **II.** AML- sEVs have an altered RNA cargo compared to that carried by AML+ sEVs; **III.** AML- sEVs have a distinct protein profile with tumour-promoting potential, and rapamycin treatment affects selected sEV cargo loading and signalling activation potential; **IV.** Plasma-derived sEVs represent a potential source of biomarkers for detection of patients with TSC.

7.2. DISCUSSION OF KEY FINDINGS

7.2.1. TSC cells secrete sEVs of endosomal origin

TSC patients are more frequently found to have a *TSC2* mutation compared to a *TSC1* mutation (Northup *et al*., 2021). AML (*TSC2*-deficient and their add-back controls) and MEF (*Tsc2*-deficient and *Tsc2* wild-type) are two well-known and frequently used cell line models of TSC, and were selected as *in vitro* models for this study. sEVs from AML and MEF cell lines were comprehensively characterised in accordance with published guidelines (Théry *et al*., 2018) in **Chapter 3**. AML and MEF cell lines secreted EVs (**Fig. 3.4**) that expressed surface tetraspanins typically associated with EV surfaces, namely CD9, CD63, and CD81. However, it is also important to note that reliability of my tetraspanin detection on MEF+ and MEF- sEVs was less convincing than that of the AML+ and AML- sEVs, potentially due to issues with antibody specificity (**Fig. 3.4**). Given the TSC patient-derived

origin and better tetraspanin detection, AML+ and AML- sEVs were selected as my primary *in vitro* model for sEV isolation. Focusing on one cell line model for preclinical investigation brings a risk of bias and using numerous models is considered to be beneficial to strengthen hypotheses prior to *in vivo* studies. However, most TSC EV studies to date (Patel *et al*., 2016; Kumar *et al*., 2021; Bissler *et al*., 2019) have not compared EVs from human-derived *TSC2*-deficient cells to EVs from *TSC2*-re-expressing control cells, bringing novelty of this selected model. One published study characterised EVs from the $Tsc2^{+/+}$ and $Tsc2^{-/-}$ MEF cell line model (Zou *et al*., 2019), reporting variations between $Tsc2^{+/+}$ and $Tsc2^{-/-}$ EV characteristics that contrast with the findings in this study. This could be due to differences in EV isolation methods used, purity of EV isolates, or number of molecular markers included in the characterisation panels. Another study isolated EVs from a *TSC2*-deficient AML cell line (621-101) using aldehyde beads incubated with CD9 and CD63 antibodies and FACS analysis (Patel *et al*., 2016), which likely has a bias towards certain EV subpopulations based on their tetraspanin expression. Furthermore, technical difficulty in eluting bound EVs from the aldehyde beads to allow their use in further experiments adds further challenge. I also observed that upscaling EV production from monolayer to bioreactor cultures did not impact their molecular characteristics. No studies to date have used long-term bioreactor cultures, which may recapitulate tumour growth and subsequent treatment (relevant in **Chapter 5**) better, to generate and study EVs in TSC research. Furthermore, significant expense is required for the maintenance of bioreactor cultures over the course of a three-year project; hence, the need to select one cell line for the primary model. EVs from these bioreactor-grown AML+ and AML- cells had a similar size distribution (**Fig. 3.8A** and **B**) and surface marker

expression (**Fig. 3.7A**) as they did when grown in monolayer cultures. I also established that at least some of the sEVs in these lysates are likely to be of endosomal origin (**Fig. 3.7B**), making sEV characterisation in this study the most comprehensive in the relevant published literature. Gauging that these sEVs preparations were reliably pure across all preparations using the Particle:Protein ratio (**Fig. 3.10**) as a guide, and routine characterisation of EV isolates, allowed for the fairest course of experimentation through this project.

It is also important to note that my characterisation was conducted on bulk sEV isolates, and the molecular characteristics do not inform of expression of sEV-associated markers on a single sEV level. There are some emerging technologies of note that could improve resolution of EV characterisation. Fluorescent-based imaging of immobilised EVs is one example, with technologies such as EVQuant (Erasmus MC, The Netherlands). EVQuant is a microscopy-based high-throughput sensitive assay that can be used to detect, quantify and characterise EVs of as small as 35 nm in diameter that have been immobilised within a gel (Hartjes *et al*., 2020). This technology can also be used to examine sEV subpopulations, such as CD9-negative/CD63-positive EVs, which could shed light on the subpopulation differences in tetraspanin expression between AML+ and AML- sEVs (**Fig. 3.7A**). Another option could be super-resolution imaging of EVs, such as that offered by NanoImager microscopy by ONI (Oxford, United Kingdom). This technology detects simultaneous immunofluorescent signals from two labelled biomarkers, e.g., CD9, CD63, and CD81; to determine EV size and frequency within a sample. Resultant plots visualise clearly the variations in biomarker frequencies across the size-distribution profile of EVs detected. ExoView® R200 (NanoView BioSciences,

Brighton, Massachusetts, USA) is another new sophisticated technology using multiplex fluorescence-based detection of EVs, with the capacity to identify as many as five co-localised sEV-associated markers at the single sEV level. This use of fluorescence for EV quantification would be considered advantageous compared to the non-specific detection of particles by light scattering techniques, as employed in NTA used in this study.

7.2.2. Profiling RNA cargo in AML+ and AML- sEVs revealed novel insights into potential mechanistic consequences caused by sEV RNA cargo delivery

Knowing that both AML+ and AML- cells secrete sEVs of endosomal origin, my next investigations focused on profiling the RNA cargo of these sEV groups. In **Chapter 4**, AML+ and AML- sEV RNA cargoes were profiled for mTORC1 signalling components using qPCR, and a broader screen of AML+ sEV and AML- sEV RNA cargoes was examined using RNA-Seq, embodying the most comprehensive profiling of AML RNA cargo to date. The largest classes of RNA biotypes represented in the dataset were mRNAs, lncRNA, and miRNAs, which have also been previously associated in EVs in various diseases. It is important to state that the RNA-Seq kit used in this work was not optimal for miRNA detection and the procedure had purification methods that removes small RNA fragments, so miRNAs detected are likely to be an underrepresentation. However, this is not to say that other RNA biotypes, beyond mRNAs, lncRNAs and miRNAs, are of lesser importance in disease due to their low abundance, and exploration of their significant RNAs should be conducted to establish any functional role in TSC.

AML+ and AML- sEV cargoes were compared based on differential expression of RNAs between AML- compared to AML+ sEVs. There were 11,584 differentially expressed genes (DEGs) in AML- sEVs compared to AML+ sEVs, found by RNA-Seq. It is noteworthy here that some biases could obscure differential expression and downstream functional enrichment analysis in this study. Firstly, RNA-Seq differential expression relies on the application of thresholds (e.g. two- or five-fold changes as the *cut-off*) that, while commonly used, are arbitrarily selected. It also emphasises a bias that more differentially expressed components signify greater relevance to a particular disease, which is not necessarily dependable. Length, GC content, and chromosome biases are also important to consider when interpreting this data, as these biases can affect reads and sequencing of particular genes, thereby influencing a DEGs list.

The majority of RNAs in both AML+ and AML- sEVs were found to be mRNAs (**Fig. 4.4**), which functionally could have important protein translation capacities, depending on ribosome and transfer RNA (tRNA) availability in their recipient cells. Before determining their functionality in target cells, differential expression of specific mRNAs can be validated using qPCR, though with advancements and improved reliability of RNA-Seq technologies, this is becoming less of a necessity. However, sEVs can be putative sources of stable disease biomarkers, and qPCR could be useful as a cost-effective means to validate and detect specific RNA candidates as biomarkers. Functional enrichment analysis revealed that there were significantly enriched networks of genes involved in extracellular matrix (ECM) processes (**Figs. 4.6-4.7**), which suggests that AML- sEVs are enriched for mRNAs that could promote a tumour-supporting ECM around the kidneys. Furthermore,

various molecular functions associated with ion channels were also flagged as highly significant in AML- sEV mRNAs (**Fig. 4.5**), which could have particular significance in altering kidney function in TSC. This also links with similar findings of downregulated biological processes associated with normal kidney function, (including transmembrane transport; ion transport; excretion) in AML tumours (Martin *et al.*, 2017). Other significantly enriched biological pathways pointed towards growth factor binding and signalling, which suggests growth factor-associated mechanisms by which AML- sEVs could promote cell proliferation. Additionally, analysis also revealed the potential of a more multi-organ influence of AML- sEVs. Regulation of fat cell differentiation, and pathways associated with angiogenesis, have contextual relevance to AML, while those associated with bone and neural biological pathways may have relevance to other TSC manifestations besides AML (**Fig. 4.7**). Examining if delivery of AML- sEVs alters adipose cell differentiation or promotes angiogenesis, using *in vitro* assays such as an imaging-based fast adipose tracking system (FATS) or endothelial vessel formation assays, respectively; would be useful in the first instance to establish if these sEVs affect these particular phenotypes in recipient cells. This could be followed up by identifying key drivers behind these phenotypes, with the aim of determining potential anti-tumour strategies. This could be in part achieved by sequencing mRNA from cells treated with AML+ sEVs and AML- sEVs, compared to untreated cells, to establish transcriptomic changes induced following receipt of these sEVs, followed by various experiments using knock-down models of driver candidates.

The current EV-RNA literature focuses largely on EV-miRNAs. EV-miRNAs can regulate protein levels by targeting their mRNAs in recipient cells (Terlecki-

Zaniewicz *et al*., 2018), shown to play important roles in cell-cell communication between the tumour and its microenvironment. Given that this RNA-Seq experiment was not designed for optimal miRNA detection, and all except one miRNA with significant differential expression in AML- sEVs were downregulated, it is difficult to predict the role of miRNAs in AML- sEVs currently. More targeted analysis of the miRNA cargo in AML- sEVs could integrate technologies including miRNA sequencing, the high sensitivity of which would also permit use of low input starting volumes (Benesova *et al*., 2021) which could be particularly advantageous for EV experiments and liquid biopsy applications. There has also been some recent debate about how functional EV-miRNAs could be in actuality. One study reported that less than 5% of miRNAs were actually associated with purified EVs upon purification, with the vast majority remaining largely in the supernatant (Albanese *et al*., 2021). Similar results have been observed in other studies (Arroyo *et al*., 2011; as reviewed by Turchinovich *et al*., 2019), further calling into question how much miRNA can genuinely be delivered by sEVs. Coupling this with small amounts of sEVs from tumour cells amidst the abundance of sEVs secreted from all cell types in the body, it is difficult to know definitively the functional consequences of EV-miRNA.

Even less is known about the functional role played by EV-lncRNAs in cancer, as their roles in EVs have largely focused on their use in prognostic biomarker panels. As previously mentioned, validating expression of both miRNA and lncRNA before investigating their function in TSC or as biomarkers is important. This can be done using real time qPCR methods (Ferero *et al.*, 2019; Dhamija and Menon, 2021). Protocols for sequencing RNA at a single EV level may aid in gaining a better

understanding of RNA mechanistic function in disease more precisely and are currently in development. Sequencing EV-RNA at the single EV level has thus far used digital PCR platforms, such as Droplet Digital PCR System (Biorad) or QuantStudio™ 3D Digital PCR System (ThermoFisher). One study showed that microfluidic micropillars that were immuno-enriched with anti-CD8 monoclonal antibodies captured CD8-positive EVs of acute ischemic stroke patients, allowing RNA analysis of the EVs to correlate with the CD8 EV surface marker (Wijerathne *et al*., 2020). Additionally, further work in developing methods to detect coinciding surface proteins on single EVs using multiplex (Ko *et al*., 2020) and DNA-barcoded beads (Ko *et al*., 2021) has been published, which could reveal genuine EV-associated RNAs with greater specificity.

7.2.3. AML- sEVs are enriched for mTORC1-signalling components at both the mRNA and protein level

I report that AML- sEVs appear to be enriched for various mTORC1-signalling components at both the mRNA (**Fig. 4.3**) and protein (**Fig. 5.7**) level, using qPCR and western blot techniques. The findings that four mTORC1-signalling components - TSC2, Rheb, 4E-BP1, and Akt - had the same relative directional expression in AML- sEVs compared to AML+ sEVs at both the mRNA and protein levels were fascinating discoveries, as it supports with suggestion that intraluminal cargo of sEVs reflects the cytosolic composition of the parental cell. Seeing that *TSC2* mRNA and *TSC2* protein are carried by AML+ sEVs, and not AML- sEVs, could signify downstream consequences to mTOR in recipient cells, though it is difficult to interpret given its unknown association with other key elements of the TSC1/TSC2/TBC1D7 tumour suppressor complex within sEVs. As AML- sEVs

carry Rheb and Akt mRNA and proteins (with both proteins being relatively small in size), could suggest a mechanism of activating mTORC1 signalling in recipient cells, more efficiently than transporting bigger proteins such as mTOR itself. mTOR is required to translocate successfully to the lysosomal surface to function typically in the cell. This poses the question as to how sEV-mTOR would escape lysosomal degradation to elicit function. Furthermore, delivery of proteins that can activate receptors at the cell surface level are more likely to be effective at modulating signalling. Activation of Akt, for example, takes place at the plasma membrane (Barkdale and Bijur, 2009). From there, activated Akt can translocate to various subcellular structures, including the cytosol, the nucleus (Andjelković *et al*., 2003), and the mitochondria (Bijur and Jope, 2003); where it activates these compartment-specific substrates (Barkdale and Bijur, 2009). Therefore, sEVs could bring Akt to the plasma membrane to facilitate this signalling process. Furthermore, Rheb is a cytosolic protein, so sEVs could transport Rheb to the recipient cell cytosol via effective plasma membrane fusion. Enriched 4E-BP1 mRNA and protein in AML- sEVs could highlight differential protein translation capacities compared to that of AML+ sEVs, though it is important to reiterate that sEV delivery does not guarantee protein translation as other factors, such as successful transport towards the ribosomal sites for protein synthesis, are also critical to elicit a functional effect. With regard to EV protein effectors, bioavailability of compatible cell surface receptors and intracellular phosphate groups, for example, may also be vital for protein integration into the cell and effective functionality.

7.2.4. AML- sEVs carry distinct protein cargo with tumour-promoting potential

Twenty-nine tumour-associated proteins were differentially expressed in AML- sEVs compared to their AML+ sEV counterparts (**Fig. 5.2**). Validation of a number of these proteins was successful using ELISA (**Fig. 5.5**), and provided three candidates that would eventually be detected in TSC patient plasma-derived sEVs (**Fig. 6.3**). It is worth noting that this proteome profiler antibody array was based on a relatively small number of proteins (*n*=84), well known in oncology protein networks, and is not exhaustive. More comprehensive screens of the proteomes in these sEVs could be attained using mass spectrometry (MS)-based proteomics (as reviewed by Mallia *et al*., 2020), and subsequently downstream gene ontology analysis for enriched biological pathways, for example, could illustrate more clearly how these sEV protein networks could contribute to disease. Many EV proteomics studies use *bottom-up* MS approaches (i.e. extraction/separation of proteins pre-MS) (Li *et al.,* 2019; as reviewed by Mallia *et al*., 2020). Developments into a *top-down* (i.e. sequencing of intact proteins) MS approach have been made, though there are some obstacles including costly instrumentation, in-efficient dissociation techniques, and difficulty in interpreting mass spectra (Geis-Asteggiante *et al*., 2015; Barrachina *et al*., 2019). Other methods such as SOMAscan, an aptamer-based method of proteomics measures in the range of thousands of proteins, with reported greater sensitivity than specificity compared to MS (Billing *et al*., 2017).

7.2.5. AML- sEVs stimulate growth factor secretion from recipient fibroblasts

Determining the functional impact of sEVs delivered to recipient cells is an insightful avenue of exploration to gauge alterations in cell phenotypes or disease processes promoted, or indeed inhibited, by these sEVs. Given the differential RNA and

protein cargoes observed in AML+ sEVs and AML- sEVs (**Chapter 4** and **Chapter 5**), differential function of AML+ versus AML- sEVs, and therefore differences in their impact on recipient cells, was expected. The elevated secretion of the growth factors VEGF and HGF following treatment with AML- sEVs compared to treatment of recipient cells with AML+ sEVs (**Fig. 5.11**) was an interesting observation. Known roles of VEGF largely revolve around angiogenic processes, and HGF is known to be involved in promoting proliferation or cell migration, so secretion of these short-range growth factors could have impact in modifying the surrounding tumour microenvironment to support optimal tumour growth and development. Given that elevated soluble VEGF-D is used clinically as a biomarker for TSC-LAM and spontaneous LAM (Hirose *et al*., 2019), it is interesting that this experimental model of AML- sEV treatment of non-transformed lung fibroblasts could stimulate VEGF secretion from these recipient fibroblasts. Uncovering if these AML- sEVs stimulate non-transformed lung fibroblasts to become more LAM-like, through immunofluorescence imaging and molecular marker analysis post-sEV treatment, could be interesting to determine sEV mediated AML-LAM crosstalk. In the GO analysis conducted on the AML- sEV protein cargo, other mechanisms that could support tumour growth and development would be interesting to investigate further, such as activation of specified recipient cell-receptors of enriched sEVs proteins as outlined in **Table 5.4**. Furthermore, knowing that AML is characterised by a dense angiogenic network, it could also be interesting to understand if sEVs contribute to promoting angiogenesis in the microenvironment. This could be explored experimentally using endothelial vessel-formation assays, which utilise a co-culture of fibroblasts and endothelial cells to recapitulate the tumour microenvironment

(Sheldon *et al.*, 2010; Webber *et al*., 2015), perhaps more accurately than similar assays, such as the tube formation assay, which utilises endothelial cells alone.

7.2.6. Rapamycin can modulate EV-mediated signalling in recipient fibroblasts

mTORC1 inhibition by rapamycin and its rapalogs has some treatment limitations as anti-tumour therapy. In this study, I explored the existing knowledge gap and sought to understand if rapalog treatment affects AML- EVs characteristics and cargo, and if these treated cells have a different intercellular signalling capacity via sEVs compared to untreated AML- cells. To make findings as clinically relevant as possible, cells were treated with a concentration of rapamycin to match trough levels of patients in the three leading clinical trials investigating rapamycin's anti-tumour effect on AMLs (Bissler et al., 2008; Davies et al., 2011; Bissler et al., 2013). Rapamycin treatment appeared to reduce sEV secretion (**Fig. 5.8**) and expression of five selected cargo proteins, compared to the AML+ sEVs controls (**Fig. 5.10**). There have been some studies on EVs secreted from chemotherapy-treated tumour cells, and many report an increase in EV secretion from these chemotherapy-treated cells *in vitro* (Bandari *et al*., 2018) and *in vivo* (Emam *et al*., 2018). It is also plausible that EV secretion may be altered as an immediate response to cellular stress induced by chemotherapeutic agents (as reviewed by Ab Razak *et al*., 2019), but overall the transient secretion of sEVs across these treatment regimens remains unclear. Improved technologies that can quantify EVs more accurately and reproducibly will aid analysis of EV secretion in response to treatment.

In this study, I identified five sEV cargo proteins that showed reduced expression in sEVs from rapaAML- cells compared to sEVs from non-treated AML- cells *in vitro*. This change in EV cargo suggests that rapamycin treatment is able to impact EV biogenesis and loading of specific cargo into the sEV, which may in turn affect EV function. These findings are also reflective of the reduced mTORC1 activity of the parental cells as rapaAML- sEV cargo more closely resembles that of AML+ sEV cargo, from cells with lower mTORC1 activity, than untreated AML- sEV cargo from cells with high mTORC1 activity. Importantly, for this study, this data highlights the utility of EVs as a surrogate for reporting changes occurring within the tumour in response to therapeutic interventions, such as rapamycin treatment. One previous study has reported that rapamycin treatment (1.0×10^{-7} M, for a 24-hour period) altered only eleven miRNAs and two proteins significantly in the EV cargo secreted from HeLa cells grown in monolayer culture (Zou *et al*., 2019). Results presented in this Thesis, however, focused on the analysis of sEVs derived from long-term rapamycin treatment of AML- cells, which is likely to provide better representation of the long-term treatment regimens that TSC patients are administered to control their tumours. Further profiling, using transcriptomics and proteomics, is necessary to unveil the cargo of rapaAML- sEVs comprehensively.

Profiling rapaAML- sEV cargo seems even more important when considering the varying roles uncovered in this project that these sEVs play in modulating recipient cells. Regarding their intercellular functionality, rapaAML- sEVs acted as mediators of: **i**. a mechanism of treatment resistance with the increased stimulation of growth factor secretion from recipient cells, equal to that of AML- sEVs (**Fig. 5.11**); and **ii.** a potential intercellular therapeutic effect, by eliciting reduced mTORC1-related

signalling capacities in recipient cells (**Fig. 5.12**). More specifically, rapaAML- sEV treatment induced lower levels of phosphorylated MAPK and S6, suggesting reduced mTORC1 signalling, compared to that observed in AML- sEV-treated fibroblasts (**Fig. 5.12**). This is a previously unknown therapeutic intercellular effect of rapamycin. However, delineating a broader network of how these sEVs mediate phosphorylation of proteins associated with mTORC1 signalling in cells of the tumour microenvironment would shed further light on regulation of mTORC1 signalling by specific EV subtypes. Also, it is important to mention that this current study did not examine the presence of phospho-proteins within EVs, which may also affect this signalling activation capacity. The presence of phosphorylated proteins in EVs has been reported previously in oncology studies. For example, 144 phosphorylated proteins had elevated expression in EVs from breast cancer patient plasma compared to equivalent EVs from healthy donor plasma samples, with potential as disease biomarkers (Zhang *et al*., 2018). RapaAML- sEVs also induced similar elevated secretion of the tested growth factors to that induced by AML- sEVs. As rapamycin treatment did not attenuate growth factor secretion, this could suggest an intercellular treatment resistance mechanism induced by sEVs from rapamycin-treated cells. Further understanding of this mechanism could be sought by profiling of phenotypic alterations to vessel formation or migration, for example, post sEV treatment. Nonetheless, there is a need to further dissect the intercellular effects on signalling induced by rapamycin, as there is evidence of potential treatment resistance and therapeutic effects via sEVs following treatment.

However, a caveat to this experimental design was that I could not determine if rapamycin treatment of the parental cells has affected cargo loading and then

subsequent function, or if rapamycin has impacted EV characteristics that affect interactions with or internalisation into the recipient cell. Though sEV characteristics were not significantly different in rapaAML- and AML- sEVs, high resolution sEV characterisation and more extensive *omics* profiling of rapamycin sEV cargo would illuminate their true nature more clearly. This brings in another potential use of sEVs as biocompatible drug delivery vectors. Could rapamycin be packaged into sEVs for extracellular export, and could this have a favourable therapeutic effect in targeting the tumour microenvironment?

A potential limitation of these rapamycin-associated investigations was that one dose of rapamycin (10 ng/mL) was selected for use in this study. This dose was chosen to mimic trough levels seen in patients in various clinical trials. However, the trough level range is variable within these studies. One study testing sirolimus (*N*=25) reported serum trough levels of between 10-15 ng/mL, for all but one patient who achieved tumour shrinkage with the initial dose of 1-5 ng/mL (Bissler *et al*., 2008). Another study testing sirolimus (*N*=16) had most patients with tumour shrinkage with trough levels between 3-6 ng/mL, while four patients had escalated doses of 6-10 ng/mL to achieve tumour shrinkage (Davies et al., 2011). The EXIST-II trial (*N*=118) testing everolimus reported trough levels of between 7.63-9.37 ng/mL with significant interpatient variability after 24 weeks on trial (Bissler et al., 2013). Perhaps different doses of rapamycin should be included to determine if dose-dependent effects could affect EV secretion, cargo loading, and functionality in recipient cells. Furthermore, in the broader context of mTORC1 signalling, this could reveal important developments in understanding of how mTORC1 mediates EV biogenesis.

7.2.7. Three novel sEV cargo proteins as plasma-based biomarkers for TSC

Discovery of three sEV cargo proteins with potential as plasma-derived biomarkers for TSC brought the translational impact of this research to the fore, as set out in **Chapter 6**. Endoglin, enolase γ, and VEGF protein were detected at significantly elevated quantities in TSC patient plasma sEVs compared to healthy donor plasma sEVs (**Fig. 6.3**). A noted unmet clinical need within the TSC research and medical communities is the lack of a biofluid-derived biomarker for TSC. While this work completed a small pilot study (*N*=9/treatment group) to address this unmet clinical need, further testing and validation of these sEV proteins in larger patient cohorts is required to unravel if these findings have true translational impact. If any of these biomarkers were found to associate with a particular aspect of TSC e.g. TSC status, or presence of AMLs, they could be used to confirm diagnosis or aid in monitoring AML growth. Additionally, if any of the biomarkers were found to correlate with tumour shrinkage, they could be used in a therapeutic surveillance strategy.

There are some aspects of experimental design to consider in future validation of this work. In this study, I utilised healthy donor plasma as the control group. There may be additional benefit in examining expression of these sEV proteins in a control group of unaffected relatives of the TSC patients (e.g. parent or sibling), to determine thresholds of elevated expression in affected patients. In this case, these biomarkers could also be used to monitor family members having a genetic diagnosis of TSC with no clinical signs. This could be useful when contextualising the specificity of these cargoes to TSC specifically. A frequently arising challenge

in development of EV-based biomarkers is identifying the origin of the EVs, and therefore the overall disease specificity of the biomarker. One suggestion is to link investigation of sEV proteins with proteins co-expressed within the tumour tissue. Other mTORC1-active tumours also exist, including hepatocellular carcinomas (HCCs) or pancreatic neuroendocrine tumours (PNETs), and so determining if these sEV biomarkers were detectable in these tumour settings could help elucidate how TSC-specific or mTORC1-driven tumour-specific these biomarkers could be. Similarly, to determine if endoglin, enolase γ, and VEGF sEV proteins could be biomarkers for TSC specifically, sEVs from other similar inherited tumour conditions such as neurofibromatosis type 1 (NF1) and polycystic kidney disease (PKD) should be trialled as a control. Developing more sophisticated means of ensuring this specificity, such as using multiple-panel markers within EVs, capture methods, or mapping expression profiles of EV markers with disease progression or treatment regimens, could improve this. In the broader context of TSC, it could be worth exploring sEVs secreted from *TSC1*-deficient cells, or models of different manifestations of TSC, which could determine a more holistic insight into the TSC sEV secretome and its role in TSC. It would also be interesting to determine if there are mutation specific changes in EV cargo and functioning, given that *TSC2* mutant functionality is different (Dunlop *et al.*, 2011), as mutation specific signatures in EVs could be used in a personalised medicine approach. For example, Pasini *et al*. recently demonstrated that EGFR mutations L858R and T790M could be detected in vesicle RNA of non-small cell lung cancer patients (Pasini *et al*., 2021). Furthermore, knowing now that *TSC2* deficiency causes distinct alterations to RNA and protein cargo of secreted sEVs, it would be

interesting to establish if these *TSC2* mutation-associated findings broaden to relevance in other *TSC2*-mutant cancers.

Furthermore, normalisation of the protein biomarker candidates to CD9 is important to consider. Normalisation to multiple EV biomarkers may be necessary to include all sEVs in this discovery stage of biomarker development, so as to ensure that I are not biasing towards a subpopulation of CD9+ sEVs. Furthermore, mTORC1-signalling components (**Fig. 5.7**) with differential expression in AML- sEVs compared to AML+ sEVs *in vitro* could also be investigated as potential biomarkers for TSC.

Evidence of the diagnostic success of EVs came with the development of the ExoDx™ Prostate (IntelliScore) (EPI) test, developed by Dr Johan Skog (bio-techne, Martinsried, Germany). This test assesses urine-derived EVs for expression of a three-gene panel, to inform the need for further biopsy in suspected cases of high-grade prostate cancer (Tutrone *et al*., 2020; McKernan *et al*., 2020), and was granted FDA approval in 2020. Other companies include MetaguideX (Oxford, United Kingdom), focused on developing an EV-based *in vitro* diagnostic test for assessing metastatic risk in breast cancer. Furthermore, other studies have published evidence of EVs improving sensitivity and specificity of currently used clinical tests, such as a panel of five EV mRNAs used in combination, with or without prostate-specific antigen (PSA), in a multimodal liquid biopsy approach for prostate cancer patients (Shephard *et al.,* 2021).

7.3. CONCLUDING REMARKS

This research has examined TSC tumour growth and development in an intercellular context, and provides evidence for AML sEVs as important mediators in priming the tumour microenvironment to facilitate optimal TSC tumour growth.

Thus, the key findings of this work are:

I. TSC cells secrete sEVs of endosomal origin
II. AML- sEVs are enriched in RNAs predicted to mediate tumour-supporting functions, including extracellular matrix and growth factor binding; pathways associated with kidney function, including ion channel functioning, fat differentiation, and angiogenic processes; and processes affecting other TSC-relevant organs, including as bone and brain
III. AML- sEV protein cargo is distinct from healthy cell EV cargo, and has tumour-promoting potential, with rapamycin treatment altering this protein cargo and downstream signalling activation capacity in recipient fibroblasts
IV. Three sEV-associated proteins have elevated expression in TSC patient plasma compared to healthy donor controls, highlighting their potential as biomarkers for TSC

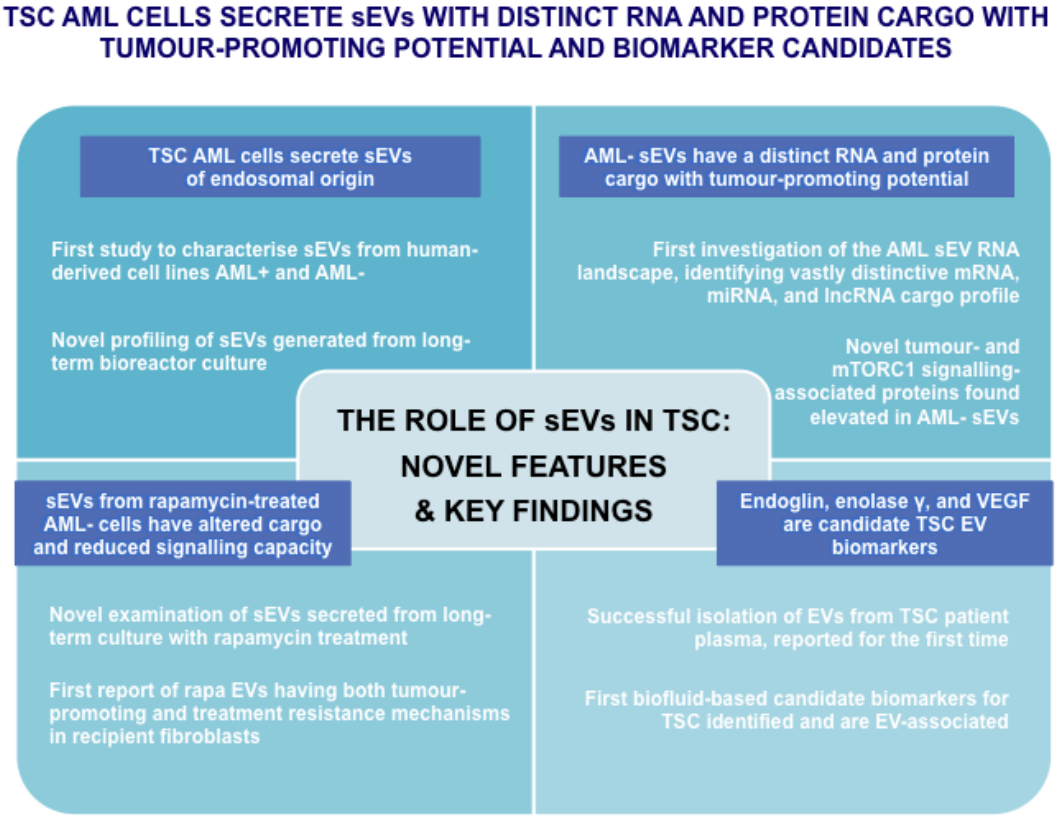

Figure 7.1: Graphical summary of novel features and key findings presented in this Thesis.

CHAPTER 8

BIBLIOGRAPHY

Ab Elmageed, Z. Y., Yang, Y., Thomas R., Ranjan, M., Mondal, D., Moroz, K., Fang, Z., Rezk, B. M., Moparty, K., Sikka, S. C., Sartor, O., Abdel-Mageed, A. B. (2014). Neoplastic reprogramming of patient-derived adipose stem cells by prostate cancer cell-associated exosomes. *Stem Cells*, 32, 4, pp. 983-97. DOI: 10.1002/stem.1619

Ab Razak, N. S., Ab Mutalib, N. S., Mohtar, M. A., Abu, N. (2019). Impact of chemotherapy on extracellular vesicles: understanding the chemo-EVs. *Front Oncol*, 9, 2019, pp. 1-6. DOI: 10.3389/fonc.2019.01113

Abels, E. R., Breakefield, X. O. (2016). Introduction to extracellular vesicles: biogenesis, RNA cargo selection, release and uptake. *Cell Mol Neurobiol*, 36, pp. 301-12. DOI: 10.1007/s10571-016-0366-z

Agormayor, M., Martin-Serrano, J. (2006). Interaction of AMSH with ESCRT-III and deubiquitination of endosomal cargo. *J Biol Chem*, 281, 32, pp. 23083-91. DOI: 10.1074/jbc.M513803200

Akers, J. C., Gonda, D., Kim, R., Carter, B. S., Chen, C. C. (2013). Biogenesis of extracellular vesicles (EV): exosomes, Microvesicles, retrovirus-like vesicles, and apoptotic bodies. *J Neurooncol*, 113, 1, pp. 1-11. DOI: 10.1007/s11060-013-1084-8

Al-Nedawi, K., Meehan, B., Micallef, J., Lhotak, V., May, L., Guha, A., Rak, J. (2008). Intercellular transfer of the oncogenic receptor EGFRvIII by Microvesicles derived from tumour cells. *Nat Cell Biol*, 10, 5, pp. 619-24. DOI: 10.1038/ncb1725

Albanese, M., Chen, Y.-F. A., Hüls, C., Gärtner, K., Tagawa, T., Mejias-Perez, E., Keppler, O. T., Göbel, C., Zeidler, R., Shein, M., Schütz, A. K., Hammerschmidt, W. (2021). MicroRNAs are minor constituents of extracellular vesicles that are rarely delivered to target cells. *PLoS Genet*, 17, 12, pp. e1009951. DOI: 10.1371/journal.pgen.1009951

Ambros, V. (2004). The functions of animal microRNAs. *Nature*, 431, pp. 350-6. DOI: 10.1038/nature02871

Andjelković, M., Alessi, D. R., Meier, R., Fernandez, A., Lamb, N. J., Frech, M., Cron, P., Cohen, P., Lococq, J. M., Hemmings, B. A. (1997). Role of translocation in the activation and function of protein kinase B. *J Biol Chem*, 272, pp. 31515-24. DOI: 10.1074/jbc.272.50.31515

Arezi, B., Xing, W., Sorge, J. A., Hogrefe, H. H. (2003). Amplification efficiency of thermostable DNA polymerases. *Anal Biochem*, 321, 2, pp. 226-35. DOI: 10.1016/s0003-2697(03)00465-2

Arraud, N., Linares, R., Tan, S., Gounou, C., Pasquet, J.-M., Mornet, S., Brisson, A. R. (2014). Extracellular vesicles from blood plasma: determination of their

morphology, size, phenotype and concentration. *J Thromb Haemost*, 12, 5, pp. 614-27. DOI: 10.1111/jth.12554

Arroyo, J. D., Chevillet, J. R., Kroh, E. M., Tewari, M. (2011). Argonaute2 complexes carry a population of circulating microRNAs independent of vesicles in human plasma. *Prot Natl Acad Sci*, 108, 12, pp. 5003-8. DOI: 10.1073/pnas.1019055108

Astrinidis, A., Senapedis, W., Coleman, T. R., Henske, E. P. (2003). Cell cycle-regulated phosphorylation of hamartin, the product of tuberous sclerosis complex 1 gene, by cyclin-dependent kinase 1/cyclin B. *J Biol Chem*, 278, 51, pp. 51372-79. DOI: 10.1074/jbc.M303956200

Au, K. S., Williams, A. T., Gambello, M. J., Northrup, H. (2004). Molecular genetic basis of tuberous sclerosis complex: from bench to bedside. *J Child Neurol*, 19, 9, pp. 699-709. DOI: 10.1177/08830738040190091101

Au, K. S., Williams, A. T., Roach, E. S., Batchelor, L., Sparagana, S. P., Delgado, M. R., Wheless, J. W., Baumgartner, J. E., Roa, B. B., Wilson, C. M., Smith-Knuppel, T. K., Cheung, M. Y., Whittemore, V. H., King, T. M., Northrup, H. (2007). Genotype/phenotype correlation in 325 individuals referred for a diagnosis of tuberous sclerosis complex in the United States. *Genet Med*, 9, 2, pp. 88-100. DOI: 10.1097/gim.0b013e31803068c7

Avila, N. A., Dwyer, A. J., Rabel, A., Darling, T., Hong, C.-H., Moss, J. (2010). CT of sclerotic bone lesions: imaging features differentiating tuberous sclerosis complex with lymphangioleiomyomatosis from sporadic lymphangioleiomyomatosis. *Radiology*, 254, 3, pp. 851-7. DOI: 10.1148/radiol.09090227

Aylett, C. H. S., Sauer, E., Imseng, S., Boehringer, D., Hall, M. N., Ban, N., Maier. (2016). Architecture of human mTOR complex 1. *Science*, 351, 6268, pp. 48-52. DOI: 10.1126/science.aaa3870

Azmi, A. S., Bao, B., Sarkar, F. H. (2013). Exosomes in cancer development, metastasis, and drug resistance: a comprehensive review. *Cancer Metastasis Rev*, 32, 3-4, pp. 623-42. DOI: 10.1007/s10555-013-9441-9

Baietti, M. F., Zhang, Z., Mortier, E., Melchoir, A., Degeest, G., Geeraerts, A., Ivarsson, Y., Depoortere, F., Coomans, C., Vermeiren, E., Zimmermann, P., David, G. (2012). Syndecan-syntenin-ALIX regulates the biogenesis of exosomes. *Nat Cell Biol*, 14, 7, pp. 677-85. DOI: 10.1038/ncb2502

Balkwill, F. R., Capasso, M., Hagemann, T. (2012). The tumor microenvironment at a glance. *J Cell Sci*, 125, pt. 23, pp. 5591-6. DOI: 10.1242/jcs.116392

Bandari, S. K., Purushothaman, A., Ramani, V. C., Brinkley, G. J., Chandrashekar, D. S., Varambally, S., Mobley, J. A., Zhang, Y., Brown, E. E., Vlodavsky, I., Sanderson, R. D. (2018). Chemotherapy induces secretion of exosomes loaded

with heparanase that degrades extracellular matrix and impacts tumor and host cell behaviour. *Matrix Biol*, 65, 2018, pp. 104-18. DOI: 10.1016/j.matbio.2017.09.001

Bao, Z., Zeng, W., Zhang, D., Wang, L., Deng, X. Lai, J., Li, J., Gong, J., Xiang, G. (2022). SNAIL induces EMT and lung metastasis of tumours secreting CXCL2 to promote the invasion of M2-type immunosuppressed macrophages in colorectal cancer. *Int J Biol Sci*, 18, 7, pp. 2867-81. DOI: 10.7150/ijbs.66854

Baranyai, T., Herczeg, K., Onódi, Z., Voszka, I., Módos, K., Marton, N., Nagy, G., Mäger, I., Wood, M. J., El Andaloussi, S., Pálinkás, Z., Kumar, V., Nagy, P., Kittel, Á., Buzás, E. I., Ferdinandy, P., Giricz, Z. (2015). Isolation of exosomes from blood plasma: qualitative and quantitative comparison of ultracentrifugation and size exclusion chromatography methods. *PLoS One*, 10, 12, pp. e0145686. DOI: 10.1371/journal.pone.0145686

Barksdale, K. A., Bijur, G. N. (2009). The basal flux of Akt in the mitochondria is mediated by heat shock protein 90. *J Neurochem*, 108, 5, pp. 1289-99. DOI: 10.1111/j.1471-4159.2009.05878.x

Barnie, P. A., Afrifa, J., Gyamerah, E. O., Amoani, B. (2022). 'Extracellular Vesicles as Biomarkers and Therapeutic Targets in Cancers', in M. K. Paul (ed.), Extracellular Vesicles - Role in Diseases, Pathogenesis and Therapy, IntechOpen, London. DOI: 10.5772/intechopen.101783

Barrachina, M. N., Sueiro, A. M., Casas, V., Izquierdo, I., Hermida-Noguiera, L., Guitián, E., Casanueva, F. F., Abián, J., Carrascal, M., Pardo, M., García, Á. (2018). A combination of proteomic approaches identifies a panel of circulating extracellular vesicle proteins related to the risk of suffering cardiovascular disease in obese patients. *Proteomics*, 19, 1-2, pp. e1800248. DOI: 10.1002/pmic.201800248

Bebelman, M. P., Smit, M. J., Pegtel, D. M., Baglio, S. R. (2018). Biogenesis and function of extracellular vesicles in cancer. *Pharmacol Ther*, 188, pp. 1-11. DOI: 10.1016/j.pharmthera.2018.02.013

Benesova, S., Kubista, M., Valihrach, L. (2021). Small RNA-sequencing: approaches and considerations for miRNA analysis. *Diagnostics (Basel),* 11, 6, pp. 964. DOI: 10.3390/diagnostics11060964

Bertolini, F., Casarotti, G., Righi, L., Bollito, E., Albera, C., Racca, S. A., Colangelo, D., Mognetti, B. (2018). Human renal angiomyolipoma cells of male and female origin can migrate and are influenced by microenvironmental factors. *PloS ONE*, 13, 6, pp. 1-16. DOI: 10.1371/journal.pone.0199371

Beruman Sánchez, G., Bunn, K .E., Pua, H. H., Rafat, M. (2021). Extracellular vesicles: mediators of intercellular communication in tissue injury and disease. *Cell Commun Signal,* 19, 104, pp. 1-19. DOI: 10.1186/s12964-021-00787-y

Bijur, G. N., Jope, R. S. (2003). Rapid accumulation of Akt in mitochondria following phosphatidylinositol 3-kinase activation. *J Neurochem*, 87, pp. 1427-35. DOI: 10.1046/j.1471-4159.2003.02113

Billing, A. M., Hamidane, H. B., Bhagwat, A. M., Cotton, R. J., Dib, S. S., Kumar, P., Hayat, S., Goswami, N., Suhre, K., Rafii, A., Graumann, J. (2017). Complementarity of SOMAscan to LC-MS/MS and RNA-seq for quantitative profiling of human embryonic and mesenchymal stem cells. *J Proteomics*, 150, 2017, pp. 86-97. DOI: 10.1016/j.jprot.2016.08.023

Biomarkers Definitions Working Group (2001). Biomarkers and surrogate endpoints: preferred definitions and conceptual framework. *Clin Pharmacol Ther*, 69, 3, pp. 89-95. DOI: 10.1067/mcp.2001.113989

Birchenall-Roberts, M. C., Fu, T., Bang, O.-S., Dambach, M., Resau, J. H., Sadowski, C. L., Bertolette, D. C., Lee, H.-J., Kim, S.-J., Ruscetti, F. W. (2004). Tuberous sclerosis complex 2 gene product interacts with human SMAD proteins. A molecular link of two tumor suppressor pathways. *J Biol Chem*, 279, 24, pp. 25605-13. DOI: 10.1074/jbc.M402790200

Bissler, J. J., Kingswood, J. C. (2004). Renal angiomyolipomata. *Kidney Int*, 66, 3, pp. 924-34. DOI: 10.1111/j.1523-1755.2004.00838.x

Bissler, J. J., Kingswoord, J. C., Radzikowska, E., Zonnenberg, B. A., Belousova, E., Frost, M. D., Sauter, M., Brakemeier, S., de Vries, P. J., Berkowitz, N., Voi, M.,

Peyrard, S., Budde, K. (2017). Everolimus long-term use in patients with tuberous sclerosis complex: four-year update of the EXIST-2 study. *PLoS One*, 12, 8, pp. e0180939. DOI: 10.1371/journal.pone.0180939

Bissler, J. J., McCormack, F. X., Young, L. R., Elwing, J. M., Chuck, G., Leonard, J. M., Schmithorst, V. J., Laor, T., Brody, A. S., Bean, J., Salisbury, S., Franz, D. N. (2008). Sirolimus for angiomyolipoma in Tuberous Sclerosis Complex or lymphangioleiomyomatosis. *New Eng J Med*, 358, 2, pp. 12-51. DOI: 10.1056/NEJMoa063564

Bissler, J. J., Zadjali, F., Bridges, D., Astrinidis, A., Barone, S., Yao, Y., Redd, J. R., Siroky, B. J., Wang, Y., Finley, J. T., Rusiniak, M. E., Baumann, H., Zahedi, K., Gross, K. W., Soleimani, M. (2019). Tuberous sclerosis complex exhibits a new renal cytogenic mechanism. *Physiol Rep*, 7, 2, pp. e13983, 1-21. DOI: 10.14814/phy2.13983

Bloomfield, G., Kay, R. R. (2016). Uses and abuses of macropinocytosis. *J Cell Sci*, 129, pp. 2697-705. DOI: 10.1242/jcs.176149

Bolukbasi, M. F., Mizrak, A., Ozdener, G. B., Madlener, S., Ströbel, T., Erkan, E., P., Fan, J. B., Breakefield, X. O., Saydam, O. (2012). miR-1289 and “Zipcode”-like sequence enrich mRNAs in Microvesicles. *Mol Ther Nucleic Acids*, 1, 2, pp. 1-10. DOI: 10.1038/mtna/2011.2

Borkowska, J., Schwartz, R. A., Kotulska, K., Jozwiak, S. (2011). Tuberous sclerosis complex: tumors and tumorigenesis. *Int J Dermatol*, 50, 1, pp. 13-20. DOI: 10.1111/j.1365-4632.2010.04727.x

Brugarolas, J., Lei, K., Hurley, R. L., Manning, B. D., Reiling, J. H., Hafen, E., Witters, L. A., Ellisen, L. W., Kaelin, W. G. Jr. (2004). Regulation of mTOR function in response to hypoxia by REDD1 and the TSC1/TSC2 tumor suppressor complex. *Genes Dev*, 18, 23, pp. 2893-904. DOI: 10.1101/gad.1256804

Caban, C., Khan, N., Hasbani D. M., Crino, P. (2016). Genetics of tuberous sclerosis complex: implcations for clinical practice. *Appl Clin Genet*, 10, pp. 1-8. DOI: 10.2147/TACG.S90262

Cai, X., Pacheco-Rodriguez, G., Fan, Q.-Y., Haughey, M., Samsel, L., El-Chemaly, S., Wu, H.-P., McCoy, J. P., Steagall, W. K., Lin, J.-P., Darling, T. N., Moss, J. (2010). Phenotypic characterisation of disseminated cells with TSC2 loss of heterozygosity in patients with lymphangioleiomyomatosis. *Am J Crit Care Med*, 182, 11, pp. 1410-18. DOI: 10.1164/rrcm.201003-0489OC

Cai, Y., Wang, W., Guo, H., Li, H., Xiao, Y., Zhang, Y. (2018). miR-9-5p, miR-124-3p, and miR-132-3p regulate BCL2L11 in tuberous sclerosis complex angiomyolipoma. *Lab Invest*, 98, 7, pp. 856-70. DOI: 10.1038/s41374-018-0051-6

Caliò, A., Brunelli, M., Gobbo, S., Pedron, S., Segala, D., Argani, P., Martignoni, G. (2021). Stimulator of interferon genes (STING) immunohistochemical expression in

the spectrum of perivascular epithelioid cell (PEC) lesions of the kidney. *Pathology*, 53, 5, pp. 579-85. DOI: 10.1016/j.pathol.2020.09.025

Cao, F.-Y., Zheng, Y.-B., Yang, C., Huang, S.-Y., He, X.-B., Tong, S.-L. (2020). miR-635 targets KIFC1 to inhibit the progression of gastric cancer. *J Invest Med*, 68, 8, pp. 1-11. DOI: 10.1136/jim-2020-001438

Carnino, J. M., Ni, K., Jin, Y. (2020). Post-translational modification regulates formation and cargo-loading of extracellular vesicles. *Front Immunol*, 11, 948, pp. 1-8. DOI: 10.3389/fimmu.2020.00948

Cerezo-Magaña, M., Bång-Rudenstam, A., Belting, M. (2020). The pleiotropic role of proteoglycans in extracellular vesicle mediated communication in the tumor microenvironment. *Semin Cancer Biol*, 62, 2020, pp. 99-107. DOI: 10.1016/j.semcancer.2019.07.001

Cha, D. J., Mengel, D., Mustapic, M., Liu, W., Selkoe, D. J., Kapogiannis, D., Galasko, D., Rissman, R. A., Bennett, D. A., Walsh, D. M. (2019). miR-212 and miR-132 are downregulated in neutrally derived plasma exosomes of Alzheimer's patients. *Front Neurosci*, 13, pp. e1208. DOI: 10.3389/fnins.2019.01208

Chen, C.-Y., Sheu, M.-J. (2018). Endoglin targeting inhibits tumor angiogenesis in non-small cell lung cancer. *FASEB*, 32, S1, pp. 695.16-695.16. DOI: 10.1096/fasebj.2018.32.1_supplement.695.16

Chen, I. H., Xue, L., Hsu, C.-C., Paez Paez, J. S., Pan, L., Andaluz, H., Wendt, M. K., Iliuk, A. B., Zhu, J.-K., Tao, W. A. (2017). Phosphoproteins in extracellular vesicles as candidate markers for breast cancer. *Proc Natl Acad Sci U S A*, 114, 12, pp. 3175-80. DOI: 10.1073/pnas.1618088114

Chen, W., Qin, Y., Liu, S. (2020). CCL20 signaling in the tumor microenvironment. *Adv Exp Med Biol*, 1231, pp. 53-65. DOI: 10.1007/978-3-030-36667-4_6

Chen, Y.-C., Liu, T., Yu, C.-H., Chiang, T.-Y., Hwang, C.-C. (2013). Effects of GC bias in next-generation sequencing data on de novo genome assembly. *PLoS One*, 8, 4, pp. e62856. DOI: 10.1371/journal.pone.0062856

Cheng, C., Wang, Q., Zhu, M., Liu, K., Zhang, Z. (2019). Integrated analysis reveals potential long non-coding RNA biomarkers and their potential biological functions for disease free survival in gastric cancer patients. *Cancer Cell Int,* 19, 123, pp. 1-17. DOI: 10.1186/s12935-019-0846-6

Cheng, L., Hill, A. F. (2022). Therapeutically harnessing extracellular vesicles. *Nat Rev Drug Discov*, 21, 5, pp. 379-99. DOI: 10.1038/s41573-022-00410-w

Chong-Kopera, H., Inoki, K., Li, Y., Zhu, T., Garcia-Gonzalo, F. R., Rosa, J. L., Guan, K.-L. (2006). TSC1 stabilises TSC2 by inhibiting the interaction between TSC2 and the HERC1 ubiquitin ligase. *J Biol Chem*, 281, 13, pp. 8313-6. DOI: 10.1074/jbc.C500451200

Chowdhury, R., Webber, J. P., Gurney, M., Mason, M. D., Tabi, Z., Clayton, A. (2015). Cancer exosomes trigger mesenchymal stem cell differentiation into pro-angiogenic and pro-invasive myofibroblasts. *Oncotarget*, 6, 2, pp. 715-31. DOI: 10.18632/oncotarget.2711

Ciferri, M. C., Quarto, R., Tasso, R. (2021). Extracellular vesicles as biomarkers and therapeutic tools: from pre-clinical to clinical applications. *Biology*, 10, 359, pp. 1-14. DOI: 10.3390/biology10050359

Clayton, A., Mitchell, J. P., Court, J., Mason, M. D., Tabi, Z. (2007). Human tumor-derived exosomes selectively impair lymphocytes responses to interleukin-2. *Cancer Res*, 67, 15, pp. 7458-66. DOI: 10.1158/0008-5472.CAN-06-3456

Clayton, A., Mitchell, J. P., Court, J., Linnane, S., Mason, M. D., Tabi, Z. (2008). Human tumor-derived exosomes down-modulate NKG2D expression. *J Immunol*, 180, 11, 7249-58. DOI: 10.4049/jimmunol.180.11.7249

Clayton, A., Al-Taei, S., Webber, J., Mason, M. D., Tabi, Z. (2011). Cancer exosomes express CD39 and CD73, which suppress T cells through adenosine production. *J Immunol*, 187, 2, pp. 676-83. DOI: 10.4049/jimmunol.1003884

Clayton, A., Bollard, E., Buzas, E. I., Cheng, L., Falcón-Perez, J. M., Gardiner, C., Gustafson, D., Gualerzi, A., Hendrix, A., Hoffman, A., Jones, J., Lässer, C., Lawson, C., Lenassi, M., Nazarenko, I., O'Driscoll, L., Pink, R., Siljander, P. R.-M., Soekmadji, C., Wauben, M., Welsh, J. A., Witwer, K., Zheng, L., Nieuwland, R.

(2019). Considerations towards a roadmap for collection, handling and storage of blood extracellular vesicles. *J Extracell Vesicles*, 8, 1, pp. 2-6. DOI: 10.1080/20013078.2019.1647027

Clément, T., Salone, V., Rederstorff, M. (2015). Dual luciferase gene reporter assays to study miRNA function. *Small non-coding RNAs: methods and protocols.* pp. 187-98.

Clements, D., Miller, S., Babaei-Jadidi, R., Adam, M., Potter, S., Johnson, S. R. (2022). Cross talk between LAM cells and fibroblasts may influence alveolar epithelial cell behaviour in lymphangioleiomyomatosis. *Am J Physiol Lung Cell Mol Physio*l, 322, 2, pp. 283-93. DOI: 10.1152/ajplung.00351.2021

Conde-Vancells, J., Rodriguez-Suarez, E., Embade, N., Gil, D., Matthiesen, R., Valle, M., Elortza, F., Lu, S. C., Mato, J. M., Falcon-Perez, J. M. (2008). Characterization and comprehensive proteome profiling of exosomes secreted by hepatocytes. *J Proteome Res*, 7, 12, pp. 5157-66. DOI: 10.1021/pr8004887

Corrado, C., Barreca, M. M., Zichittella, C., Alessandro, R., Conigliaro, A. (2021). Molecular mediators of RNA loading into extracellular vesicles. *Cells*, 10, 3355, pp. 1-14. DOI: 10.3390/cells10123355

Costa Verdera, H., Gitz-Francois, J., Schiffelers, R. M., Vader, P. (2017). Cellular uptake of extracellular vesicles is mediated by clathrin-independent endocytosis

and macropinocytosis. *J Control Release*, 266, pp. 100-108. DOI: 10.1016/j.jconrel.2017.09.019

Costa-Silva, B., Aiello, N. M., Ocean, A. J., Singh, S., Zhang, H., Thakur, B., K., Becker, A., Hoshino, A., Mark, M .T., Molina, H., Xiang, J., Zhang, T., Theilen, T.-M., García-Santos, G., Williams, C., Ararso, Y., Huang, Y., Rodriguez, G., Shen, T.-L., Labori, K. J., Lothe, I., M., B., Kure, E. H., Hernandez, J., Doussot, A., Ebbesen, S. H., Grandgenett, P. M., Hollingsworth, M. A., Jain, M., Mallya, K., Batra, S. K., Jarnagin, W. R., Schwartz, R. E., Matei, I., Peinado, H., Stanger, B. Z., Bromberg, J., Lyden, D. (2015). Pancreatic cancer exosomes initiate pre-metastatic niche formation in the liver. *Nat Cell Biol*, 17, 6, pp. 816-26. DOI: 10.1038/ncb3169

Crino, P. B., Nathanson, K., L., Henske, E. P. (2006). The tuberous sclerosis complex. *New Eng J Med*, 355(13), pp. 1345-56. DOI: 10.1056/NEJMra055323

Csibi, A., Fendt, S.-M., Li, C., Poulogiannis, G., Choo, A. Y., Chapski, D. J., Jeong, S. M., Dempsey, J. M., Parkhitko, A., Morrison, T., Henske, E. P., Haigis, M. C., Cantley, L. C., Stephanopoulos G., Yu, J., Blenis, J. (2013). The mTORC1 pathway stimulates glutamine metabolism and cell proliferation by repressing SIRT4. *Cell*, 153, 4, pp. 840-54. DOI: 10.1016/j.cell.2013.04.023

Chang, C.-H., Pauklin, S. (2021). Extracellular vesicles in pancreatic cancer progression and therapies. *Cell Death Dis*, 12, 973, pp. 1-12. DOI: 10.1038/s41419-021-04258-7

Chiriacò, M. S., Bianco, M., Nigro, A., Primiceri, E., Ferrera, F., Romano, A., Quattrini, A., Furlan, R., Arima, V., Maruccio, G. (2018). Lab-on-chip for exosomes and Microvesicles detection and characterisation. *Sensors*, 18, 3175, pp. 1-41. DOI: 10.3390/s18103175

Chong, W. P. K., Sim, L. C., Wong, K. T. K., Yap, M. G. S. (2009). Enhanced IFNγ production in adenosine-treated CHOCells: a mechanistic study. *Biotech Progress*, 25, 3, pp. 866-73. DOI: 10.1002/btpr.118

Chonov, D. C., Ignatova, M. M. K., Ananiev, J. R., Gulubova, M. V. (2019). IL-6 activitives in the tumour microenvironment: part I. *Open Access Maced J Med Sci*, 7, 14, pp. 2391-8. DOI: 10.3889/oamjms.2019.589

Cukovic, D., Bagla, S., Ukasik, D., Stemmer, P. M., Jena, B. P., Naik, A. R., Sood, S., Asano, E., Luat, A., Chugani, D. C., Dombkowski, A. A. (2021). Exosomes in epilepsy of tuberous sclerosis complex: carriers of pro-inflammatory microRNAs. *Non-coding RNA*, 7, 40, pp. 1-16. DOI: 10.3390/ncrna7030040

Curatolo, P., Bombardier R., Jozwiak, S. (2008). Tuberous sclerosis. *Lancet*, 372, 9639, pp. 657-68. DOI: 10.1016/S0140-6736(08)61279-9

Curatolo, P., Moavero, R., de Vries, P. J. (2015). Neurological and neuropsychiatric aspects of tuberous sclerosis complex. *Lancet Neurol*, 14, 7, pp. 733-45. DOI: 10.1016/S1474-4422(15)00069-1

D'Adamo, M. C., Catacuzzeno, L., Di Giovanni, G., Franciolini, F., Pessia, M. (2013). K+ channelepsy: progress in the neurobiology of potassium channels and epilepsy. *Front Cell Neurosci*, 7, 134, pp. 1-21. DOI: 10.3389/fncel.2013.00134

Dabora, S. L., Jozwiak, S., Franz, D. N., Roberts, P.S., Nieto, A., Chung, J., Choy, Y.S., Reeve, M.P., Thiele, E, Egelhoff, J.C., Kasprzyk-Obara, J., Domanska-Pakiela, D., Kwiatkowski, D. J. (2001). Mutational analysis in a cohort of 224 tuberous sclerosis patients indicates increased severity of TSC2, compared with TSC1, disease in multiple organs. *Am J Hum Genet*, 68, pp. 64–80. PubMed PMID: 11112665

Dan, H. C., Ebbs, A., Pasparakis, M., van Dyke, T., Basseres, D. S., Baldwin, A. S. (2014). Akt-dependent activation of mTORC1 complex involves phosphorylation of mTOR (mammalian target of rapamycin) by IκB kinase α (IKKα). *J Biol Chem*, 289, 36, pp. 25227-40. DOI: 10.1074/jbc.M114.554881

Davies, D. M., de Vries, P. J., Johnson, S.R., McCartney, D. L., Cox, J. A., Serra, A. L., Watson, P.C., Howe, C. J., Doyle, T., Pointon, K., Cross, J. J., Tattersfield, A. E., Kingswood, C., Sampson, J. R. (2011). Sirolimus therapy for angiomyolipoma in tuberous sclerosis and sporadic lymphangioleiomyomatosis: a phase 2 trial. *Clin Cancer Res*, 17, 12, pp. 4071-81. DOI: 10.1158/1078-0432.CCR-11-0445

de Andrade, A. V. G., Bertolino, G., Riewaldt, J., Bieback, K., Karbanová, J., Odendahl, M., Bornhäuser, M., Schmidt, M., Corbeil, D., Tonn, T. (2015). Extracellular vesicles secreted by bone marrow- and adipose tissue-derived

mesenchymal stromal cells fail to suppress lymphocyte proliferation. *Stem Cells Dev*, 24, 11, pp. 1-3. DOI: 10.1089/scd.2014.0563

Dhamija, S., Menon, M. B. (2021). Measuring lncRNA expression by real-time PCR. *Methods Mol Biol*, 2348, pp. 93-111. DOI: 10.1007/978-1-0716-1581-2_6

Dibble, C. C., Elis, W., Menon, S., Qin, W., Klekota, J., Asara, J. M., Finan, P. M., Kwiatkowski, D. J., Murphy, L. O., Manning, B. D. (2012). TBC1D7 is a third subunit of the TSC1-TSC2 complex upstream of mTORC1. *Mol Cell*, 47, 4, pp. 535-46. DOI: 10.1016/j.molcel.2012.06.009

Dobin, A., Davis, C. A., Schlesinger, F., Drenkow, J., Zaleski, C., Jha, S., Batut, P., Chaisson, M., Gingeras, T. R. (2013). STAR: ultrafast universal RNA-seq aligner. *Bioinformatics*, 29, 1, pp. 15-21. DOI: 10.1093/bioinformatics/bts635

Dodd, K. M., Yang, J., Shen, M. H., Sampson, J. R., Tee, A. R. (2015). mTORC1 drives HIF-1α and VEGF-A signalling via multiple mechanisms involving 4E-BP1, S6K1, and STAT3. *Oncogene*, 34(17), pp. 2239-50. DOI: 10.1038/onc.2014.164

Dolhman, T. H., Ding, J., Dana, R., Chauhan, S. K. (2017). T cell-derived granulocyte-macrophage colony-stimulating factor contributes to dry eye disease pathogenesis by promoting CD11b+ myeloid cell maturation and migration. *IOVS*, 58, 2, pp. 1330-6. DOI: 10.1167/iovs.16-20789

Dombkowski, A. A., Batista, C. E., Cukovic, D., Carruthers, N. J., Ranganathan, R., Shukla, U., Stemmer, P. M., Chugani, H. T., Chugani, D. C. (2016). Cortical tubers: windows into dysregulation of epilepsy risk and synaptic signaling genes by microRNAs. *Cerebral Cortex*, 26, 3, pp. 1059-71. DOI: 10.1093/cercor/bhu276

Dubochet, J. (2012). Cryo-EM – the first thirty years. *J Microscopy*, 245, 3, pp. 221-4. DOI: 10.1111/j.1365-2818.2011.03569.x

Dunlop, E. A., Dodd, K. M., Land, S. C., Davies, P. A., Martins, N., Stuart, H., McKee, S., Kingswood, C., Saggar, A., Corderio, I., Duarte Medeira, A. M., Kingston, H., Sampson, J. R., Davies, D. M., Tee, A. R. (2011). Determining the pathogenicity of patient-derived TSC2 mutations by functional characterisation and clinical evidence. *Eur J Hum Genet*, 19, 7, pp. 789-95. DOI: 10.1038/ejhg.2011.38

Dunlop, E. A., Tee, A. R. (2013). mTOR and autophagy: a dynamic relationship governed by nutrients and energy. *Semin Cell Dev Biol*, 36, pp. 121-9. DOI: 10.1016/j.semcdb.2014.08.006

Dunlop, E. A., Seifan, S., Claessens, T., Behrends, C., Kamps, M. A. F., Rozycka, E., Kemp, A. J., Nookala, R. K., Blenis, J., Coull, B. J., Murray, J. T., van Steensel, A. M., Wilkinson, S., Tee, A. R. (2014). FLCN, a novel autophagy component, interacts with GABARAP and is regulated by ULK1 phosphorylation. *Autophagy*, 10, 10, pp. 1749-60. DOI: 10.4161/auto.29640

Dunlop, E. A., Johnson, C. E., Wiltshire, M., Errington, R. J., Tee, A. R. (2017). Targeting protein homeostasis with nelfinavir/salinomycin dual therapy effectively induced death of mTORC1 hyperactive cells. *Oncotarget*, 8, 30, pp. 48711-24. DOI: 10.18632/oncotarget.16232

Eaves, L. A., Gardner, A. J., Fry, R. C. Chapter 2: tools for the assessment of epigenetic regulation. *Trans Epigenet*, 22, pp. 33-64. DOI: 10.1016/B978-0-12-819968-8.00002-0

Efeyan, A., Zoncu, R., Chang, S., Gumper, I., Snitkin, H., Wolfson, R. L., Kirak, O., Sabatini, D. D., Sabatini, D. M. (2013). Regulation of mTORC1 by the Rag GTPases is necessary for neonatal autophagy and survival. *Nature*, 493, 7434, pp. 679-83. DOI: 10.1038/nature11745

Eijkemans, M. J. C., van der Wal, W., Reijnders, L. J., Roes, K. C. B., Barjesteh can Waalwijk van Doorn-Khosrovani, S., Pelletier, C., Magestro, M., Zonnenberg, B. (2015). Long-term follow-up assessing renal angiomyolipoma treatment patterns, morbidity, and mortality: an observational study in tuberous sclerosis complex patients in The Netherlands. *Am J Kidney Disease*, 66, 4, pp. 638-45. DOI: 10.1053/j.ajkd.2015.05.016

Ekong, R., Nellist, M., Hoogeveen-Westerveld, M., Wentink, M., Panzer, J., Sparagana, S., Emmett, W., Dawson, N. L., Malinge, M. C., Nabbout, R., Carbonara, C., Barberis, M., Padovan, S., Futema, M., Plagnol, V., Humphries, S. E., Migone, N., Povey, S. (2015). Variants within TSC2 exons 25 and 31 are very

unlikely to cause clinically diagnosable tuberous sclerosis. *Hum Mutat*, 37, 4, pp. 364-70. DOI: 10.1002/humu.22951

Ekshyyan, O. Y., Rong, X., Moore-Medlin, T., Ma, X., Alexander, J. S., Nathan, C. O. (2016). Rapamycin targets interleukin 6 (IL-6) expression and suppresses endothelial cell invasion stimulated by tumor cells. *Cancer Res*, 76, 14_supplement, pp. 4044. DOI: 10.1158/1538-7445.AM2016-4044

El-Chemaly, S., Taveira-Dasilva, A., Goldberg, H. J., Peters, E., Haughey, M., Bienfang, D., Jones, A. M., Julien-Williams, P., Cui, Y., Villalba, J. A., Bagwe, S., Maurer, R., Rosas, I. O., Moss, J., Henske, E. P. (2017). Sirolimus and autophagy inhibition in lymphangioleiomyomatosis: results of a phase I clinical trial. *CHEST*, 151, 6, pp. 1302-10. DOI: 10.1016/j.chest.2017.01.033

El-Hashemite, N., Zhang, H., Henske, E. P., Kwiatkowski, D. J. (2003). Mutation in TSC2 and activation of mammalian target of rapamycin signaling pathway in renal angiomyolipoma. *Lancet*, 361, 9366, pp. 1348-9. DOI: 10.1016/S0140-6736(03)13044-9

Emam, S. E., Ando, H., Abu Lila, A. S., Shimizu, T., Okuhira, K., Ishima, Y., Mahdy, M. A., Ghazy, F. S., Sagawa, I., Ishida, T. (2018). Liposome co-incubation with cancer cells secreted exosomes (extracellular vesicles) with different proteins expressions and different uptake pathways. *Sci Rep*, 8, 14493. DOI: 10.1038/s41598-018-32861-w

Escola, J. M., Kleijmeer, M. J., Stoorvogel, W., Griffith, J. M., Yoshie, O., Geuze, H. J. (1998). Selective enrichment of tetraspan proteins on the internal vesicles of multivesicular endosomes and on exosomes secreted by human B-lymphocytes. *J Biol Chem*, 273, pp. 20121-7. DOI: 10.1074/jbc.273.32.20121

European Chromosome 16 Tuberous Sclerosis Consortium (1993). Identification and characterization of the tuberous sclerosis gene on chromosome 16. *Cell*, 75, 7, pp. 1305-15. DOI: 10.1016/0092-8674(93)90618-z

Fabbiano, F., Corsi, J., Gurrieri, E., Trevisan, C., Notarangelo, M., D'Agostino, V. G. (2020). RNA packaging into extracellular vesicles: an orchestra of RNA-binding proteins? *J Extracell Vesicles*, 10, pp. 1-29. DOI: 10.1002/jev2.12043

Fang, Y., Fullwood, M. J. (2016). Roles, functions, and mechanisms of long non-coding RNAs in cancer. *Genomics Proteomics Bioinformatics*, 14, 1, pp. 42-54. DOI: 10.1016/j.gpb.2015.09.006

Fang, T., Lv, H., Lv, G., Li, T., Wang, C., Han, Q., Yu, L., Su, B., Guo, L., Huang, S., Cao, D., Tang, L., Tang, S., Wu, M., Yang, W., Wang, H. (2018). Tumor-derived exosomal miR-1247-3p induces cancer-associated fibroblast activation to foster lung metastasis of liver cancer. *Nat Commun*, 9, 1, pp. 191. DOI: 10.1038/s41467-017-02583-0

Feng, Z., Hu, W., de Stanchina, E., Teresky, A. K., Jin, S., Lowe, S., Levine, A. J. (2007). The regulation of AMPK β1, TSC2, and PTEN expression by p53: stress,

cell and tissue specificity, and the role of these gene products in modulating the IGF-1-AKT-mTOR pathways. *Cancer Res*, 67, 7, pp. 3043-53. DOI: 10.1158/0008-5472.CAN-06-4149

Feng, Z., Levine, A. J. (2010). The regulation of energy metabolism and the IGF-1/mTOR pathways by the p53 protein. *Trends Cell Biol*, 20, 7, pp. 427-34. DOI: 10.1016/j.tcb.2010.03.004

Feng, Q., Zhang, C., Lum, D., Druso, J. E., Blank, B., Wilson, K. F., Welm, A., Antonyak, M. A., Cerione, R., A. (2017). A class of extracellular vesicles from breast cancer cells activates VEGF receptors and tumour angiogenesis. *Nat Commun*, 16(8), pp. 144-50. DOI: 10.1038/ncomms14450

Ferero, D. A., González-Giraldo, Y., Castro-Vega, L. J., Barreto, G. E. (2019). qPCR-based methods for expression analysis of miRNAs. *Biotechniques*, 67, pp. 192-99. DOI: 10.2144/btn-2019-0065

Filippakis, H.,Alesi, N., Ogorek, B., Nijmeh, J., Khabibullin, D., Gutierrez, C., Valvezan, A. J., Cunningham, J., Priolo, C., Henske, E. P. (2017). Lysosomal regulation of cholesterol homeostasis in tuberous sclerosis complex is mediated via NPC1 and LDL-R. *Oncotarget*, 8, 24, pp. 38099-112. DOI: 10.18632/oncotarget.17485

Finnson, K. M., Parker, W. L., Chi, Y., Hoemann, C. D., Goldring, M. B., Antoniou, J., Philip, A. (2010). Endoglin differentially regulates TGF-β-induced Smad2/3 and Smad 1/5 signaling and its expression correlates with extracellular matrix

production and cellular differentiation state in human chondrocytes. *Osteo Cart*, 18, 11, pp. 1518-27. DOI: 10.1016/j.joca.2010.09.002

Fonseka, P., Chitti, S. V., Sanwlani, R., Mathivanan, S. (2021). Sulfisoxazole does not inhibit the secretion of small extracellular vesicles. *Nat Commun*, 977, 12, pp.1127. DOI: 10.1038/s41467-021-21074-x

Franke, W., W., Schmid, E., Osborn, M., Weber, K. (1978). Different intermediate-sized filaments distinguished by immunofluorescence microscopy. *Proc Natl Acad Sci U S A*. 75, 10, pp. 5034-8. DOI: 10.1073/pnas.75.10.5034

Frankel, E. B., Audhya, A. (2018). ESCRT-dependent cargo sorting at multivesicular endosomes. *Semin Cell Dev Biol*, 74, pp. 4-10. DOI: 10.1016/j.semcdb.2017.08.020

Franz, D. N. (2013). Everolimus in the treatment of subependymal giant cell astrocytomas, angiomyolipomas, and pulmonary and skin lesions associated with tuberous sclerosis complex. *Biologics*, 7, pp. 211-21. DOI: 10.2147/BTT.S25095

Frick, M., Bright, N. A., Riento, K., Bray, A., Merrified, C., Nichols, B. J. (2007). Coassembly of flotillins induces formation of membrane microdomains, membrane curvature, and vesicle budding. *Curr Biol*, 17, 13, pp. 1151-6. DOI: 10.1016/j.cub.2007.05.078

Fujita, Y., Yoshioka, Y., Ochiya, T. (2016). Extracellular vesicle transfer of cancer pathogenic components. *Cancer Sci*, 107, 4, pp. 385-90. DOI: 10.1111/cas.12896

Gabbiani, G., Ryan, G. B., Majne, G. (1971). Presence of modified fibroblasts in granulation tissue and their possible role in wound contraction. *Experientia*, 27, 5, pp. 549-50. DOI: 10.1007/BF02147594

Gardiner, C., Di Visio, D., Sahoo, S., Théry, C., Witwer, K., Wauben, M., Hill, A. F. (2016). Techniques used for the isolation and characterization of extracellular vesicles: results of a worldwide survey. *J Extracell Vesicles*, 5, pp. 1-7. DOI: 10.3402/jev.v5.32945

Geis-Asteggiante, L., Dhabaria, A., Edwards, N., Ostrand-Rosenberg, S., Fenselau, C. (2015). Top-down analysis of low mass proteins in exosomes shed by murine myeloid-derived suppressor cells. *Int J Mass Spectrom*, 378, pp. 264-9. DOI: 10.1016/j.ijms.2014.08.035

Geissman, C., Grohmann, F., Deher, A., Häsler, R., Rosenstiel, P., Legler, K., Hauser, C., Egberts, J. H., Sipos, B., Schreiber, S., Linkermann, A., Hassan, Z., Schneider, G., Schäfer, H., Arlt, A. (2017). Role of CCL20 mediated immune cell recruitment in NF-κB mediated TRAIL resistance in pancreatic cancer. *Biochim Biophys Acta*, 1864, 5, pp. 782-96. DOI: 10.1016/j.bbamcr.2017.02.005

Ghossoub, R., Lembo, F., Rubio, A., Gaillaird, C. B., Bouchet, J., Vitale, N., Slavík, J., Machala, M., Zimmerman, P. (2014). Syntenin-ALIX exosome biogenesis and

budding intro multivesicular bodies are controlled by ARF6 and PLD2. *Nat Commun*, 5, pp. e3477. DOI: 10.1038/ncomms4477

Gibbings, D. J., Ciaudo, C., Erhardt, M., Voinnet, O. (2009). Multivesicular bodies associated with components of miRNA effector complexes and modulate miRNA activity. *Nat Cell Biol*, 11, 9, pp. 1143-9. DOI: 10.1038/ncb1929

Giusti, I., Di Francesco, M. D., Poppa, G., Esposito, L., D'Ascenzo, S., Dolo, V. (2022). Tumor-derived extracellular vesicles activate normal human fibroblasts to a cancer-associated fibroblast-like phenotype, sustaining a pro-tumorigenic microenvironment. *Front Oncol*, 12, pp. e839880. DOI: 10.3389/fonc.2022.839880

Glasgow, C. G., Steagall, W. K., Taveira-DaSilva, A., Pacheco-Rodriguez, G., Cai, X., El-Chemaly, S., Moses, M., Darling, T., Moss, J. (2010). Lymphangioleiomyomatosis (LAM): molecular insights lead to targeted therapies. *Respir Med*, 104, 1, pp. 45-58. DOI: 10.1016/j.rmed.2010.03.017

Goldberg, H. J., Harari, S., Cottin, V., Rosas, I. O., Peters, E., Biswal, S., Cheng, Y., Khindri, S., Kovarik, J. M., Ma, S., McCormack, F. X., Henske, E. P. (2015). Everolimus for the treatment of lymphangioleiomyomatosis: a phase II study. *Eur Respir J*, 46, 3, pp. 783-94. DOI: 10.1183/09031936.00210714

Goncharova, E. A., Goncharov, D. A., Li, H., Pimtong, W., Lu, S., Khavin, I., Krymskaya, V. P. (2011). mTORC2 is required for proliferation and survival of TSC2-null cells. *Mol Cell Biol*, 31, 12, pp. 2484-98. DOI: 10.1128/MCB.01061-10

Gong, W., Yang, L., Wang, Y., Xian, J., Qiu, F., Liu, L., Lin, M., Feng, Y., Zhou, Y., Lu, J. (2019). Analysis of survival-related lncRNA landscape identified a role for LINC01537 in energy metabolism and lung cancer progression. *Int J Mol Sci*, 20, 15, pp. e3713. DOI: 10.3390/ijms20153713

Gong, X., Ning, B. (2020). Five lncRNAs associated with prostate cancer prognosis identified by coexpression network analysis. *Technol Cancer Res Treat*, 19, 1533033820963578, pp. 1-10. DOI: 10.1177/1533033820963578

Gordon, S. (2016). Phagocytosis: an immunobiologic process. *Immunity*, 44, 3, pp. 463-75. DOI: 10.1016/j.immuni.2016.02.026

Gould, S. R. (1991). Hamartomatous rectal polyps are common in tuberous sclerosis. *Ann N Y Acad Sci*, 615, pp. 71-80. DOI: 10.1111/j.1749-6632.1991.tb37749.x

Gould, S. J., Raposo, G. (2016). As we wait: coping with the imperfect nomenclature for extracellular vesicles. *J Extracell Vesicles*, 2, 1, pp. 2-4. 10.3402/jev.v2i0.20389

Grange, C., Tapparo, M., Collino, F., Vitillo, L., Damasco, C., Deregibus, M. C., Tetta, C., Bussolati, B., Camussi, G. (2011). Microvesicles released from human

renal cancer stem cells stimulate angiogenesis and formation of lung premetastatic niche. *Cancer Res*, 71, 15, pp. 5346-56. DOI: 10.1158/0008-5472.CAN-11-0241

Grimmer, S., van Deurs, B., Sandvig, K. (2002). Membrane ruffling and macropinocytosis in A431 cells require cholesterol. *J Cell Sci*, 115, 14, pp. 2953-62. DOI: 10.1242/jcs.115.14.2953

Grzegorek, I., Drozdz, K., Podhorska-Okolow, M., Szuba, A., Dziegiel, P. (2013). LAM cells biology and lymphangioleiomyomatosis. *Folia Histochem Cytobiol*, 51, 1, pp. 1-10. DOI: 10.5603/FHC.2013.001

Guduric-Fuchs, J., O'Connor, A., Camp, B., O'Neill, C. L., Medina, R. J., Simpson, D. A. (2012). Selective extracellular vesicles-mediated export of an overlapping set of microRNAs from multiple cell types. *BMC Genomics*, 13, pp. 357. DOI: 10.1186/1471-2164-13-357

Guerreiro, E. M., Vestad, B., Steffensen, L. A., Aass, H. C. D., Saeed, M., Øvstebø, R., Costea, D. E., Galtung, H. K., Søland, T. M. (2018). Efficient extracellular vesicle isolation by combining cell media modifications, ultrafiltration, and size-exclusion chromatography. *PLoS One*, 13, 9, pp. e0204276. DOI: 10.1371/journal.pone.0204276

Guo, D., Chen, Y., Wang, S., Yu, L., Shen, Y., Zhong, H., Yang, Y. (2018). Exosomes from heat-stressed tumour cells inhibit tumour growth by converting

regulatory T cells to Th17 cells via IL-6. *Immunology*, 154, 1, pp. 132-43. DOI: 10.1111/imm.12874

Guo, J., Jayaprakash, P., Dan, J., Wise, P., Jang, G.-B., Liang, C., Chen, M., Woodley, D. T., Fabbri, M., Li, W. (2017). PRAS40 connects microenvironmental stress signaling to exosome mediated secretion. *Mol Cell Biol*, 37, 19, pp. 1-20. DOI: 10.1128/MCB.00171-17

Guo, S., Li, B., Xu, X., Wang, W., Wang, S., Lv, T., Wang, H. (2020). Construction of a 14-lncRNA risk score system predicting survival of children with acute myelocytic leukemia. *Exp Ther Med*, 20, 2, pp. 1521-31. DOI: 10.3892/etm.2020.8846

Gupta, N., Lee, H.-S., Young, L. R., Strange, C., Moss, J., Singer, L. G., Nakata, K., Barker, A. F., Chapman, J. T., Brantly, M. L., Stocks, J. M., Brown, K. K., Lynch, J. P., Goldberg, H. J., Downey, G. P., Taveira-DaSilva, A. M., Krischer, J. P., Setchell, K., Trapnell, B. C., Inoue, Y., McCormack, F. X., NIH Rare Lung Disease Consortium. (2019). Analysis of the MILES cohort reveals determinants of disease progression and treatment response in lymphangioleiomyomatosis. *Eur Respir J*, 53, 4, pp. 31802066. DOI: 10.1183/13993003.02066-2018

Gwinn, D. M., Shackelford, D. B., Egan, D. F., Mihaylova, M. M., Mery, A., Vasquez, D. S., Turk, B. E., Shaw, R. J. (2008). AMPK phosphorylation of raptor mediates a metabolic checkpoint. *Mol Cell*, 30, 2, pp. 214-26. DOI: 10.1016/j.molcel.2008.03.003

Han, J. M., Sahin, M. (2011). TSC1/TSC2 signaling in the CNS. *FEBS Lett*, 585, 7, pp. 973-80. DOI: 10.1016/j.febslet.2011.02.001

Han, L., Lam, E. W. F., Sun, Y. (2019). Extracellular vesicles in the tumor microenvironment: old stories, but new tales. *Mol Cancer*, 18, 1, pp. 59. DOI: 10.1186/s12943-019-0980-8

Hanahan, D., Weinberg, R. A. (2011). Hallmarks of cancer: the next generation. *Cell*, 144, 5, pp. 646-74. DOI: 10.1016/j.cell.2011.02.013

Harding, C., Heuser, J., Stahl, P. (1984). Endocytosis and intracellular processing of transferrin and colloidal gold-transferrin in rat reticulocytes: demonstration of a pathway for receptor shedding. *Eur J Cell Biol*, 35, 2, pp. 256-63.

Harris, T. E., Lawrence, J. C. Jr. (2003). TOR signaling. *Sci STKE*, 2003, 212, pp. 1-15. DOI: 10.1126/stke.2122003re15

Hartjes, T. A., Slotman, J. A., Vredenbregt, M. S., Dits, N., van der Meel, R., Duijvesv, D., Kulkarni, J. A., French, P. J., van Capellen, W. A., Schiffelers, R. M., Houtsmuller, A. B., Jenster, G. W., van Royen, M. E. (2020). EVQuant; high-throughput quantification and characterisation of extracellular vesicle (sub)populations. BioRxiv. DOI: 10.1101/2020.10.21.348375

Henske, E. P. (2003). Metastasis of benign tumor cells in tuberous sclerosis complex. *Genes Chromosomes Cancer*, 38, pp. 376-81. DOI: 10.1002/gcc.10252

Henske, E. P., Jóźwiak, S., Kingswood, J. C., Sampson, J. R., Thiele, E. A. (2016). Tuberous sclerosis complex. *Nat Rev Dis Primers*, 2, pp. e16035. DOI: 10.1038/nrdp.2016.35

Hill, A. F., Pegtel, D. M., Lambertz, U., Leonardi, T., O'Driscoll, L., Pluchino, S., Ter-Ovanesyan, D., Nolte-'t Hoen, E. N. M. (2013). ISEV position paper: extracellular vesicle RNA analysis and bioinformatics. *J Extracell Vesicles*, 2, 22859, pp. 1-8. DOI: 10.3402/jev.v2i0.22859

Hirose, M., Matsumuro, A., Arai, T., Sugimoto, C., Akira, M., Kitaichi, M., Young, L. R., McCormack, F. X., Inoue, Y. (2019). Serum vascular endothelial growth factor-D as a diagnostic and therapeutic biomarker for lymphangioleiomyomatosis. *PLoS One*, 14, 2, pp. e0212776. DOI: 10.1371/journal.pone.0212776

Hizawa, K., Iida, M., Matsumoto, T., Hirota, C., Yao, T., Fujishima, M. (1994). Gastrointestinal involvement in tuberous sclerosis. Two case reports. *J Clin Gastroenterol*, 19, 1, pp. 46-9. DOI: 10.1097/00004836-199407000-00012

Hogan, M. C., Manganelli, L., Woollard, J. R., Masyuk, A. I., Masyuk, T. V., Tammechote, R., Huang, B. Q., Leontovich, A. A., Beito, T. G., Madden, B. J., Charlesworth, M. C., Torres, V. E., LaRusso, N. F., Harris, P. C., Ward, C. J. (2009).

Characterization of PKD protein-positive exosome-like vesicles. *J Am Soc Nephrol*, 20, 2, pp. 278-88. DOI: 10.1681/ASN.2008060564

Holcar, M., Ferdin, J., Sitar, S., Tušek-Žnidarič, M., Dolžan, V., Plemenita, A., Žagar, E., Lenassi, M. (2020). Enrichment of plasma extracellular vesicles for reliable quantification of their size and concentration for biomarker discovery. *Sci Rep*, 10, 1, pp. e21346. DOI: 10.1038/s41598-020-78422-y

Hood J. L., San R. S., Wickline S. A. (2011). Exosomes released by melanoma cells prepare sentinel lymph nodes for tumor metastasis. *Cancer Res,* 71, pp. 3792–3801. DOI: 10.1158/0008-5472.CAN-10-4455

Hoogeveen-Westerveld, M., Ekong, R., Povey, S., Karbassi, I., Batish, S. D., den Dunnen, J. T., van Eeghen, A., Thiele, E., Mayer, K., Dies, K., Wen, L., Thompson, C., Sparagana, S. P., Davies, P., Aalfs, C., van den Ouweland, A., Halley, D., Nellist, M. (2012). Functional assessment of TSC1 missense variants identified in individuals with tuberous sclerosis complex. *Hum Mutat*, 33, 3, pp. 476-9. DOI: 10.1002/humu.22007

Hoogeveen-Westerveld, M., Ekong, R., Povey, S., Mayer, K., Lannoy, N., Elmslie, F., Bebin, M., Dies, K., Thompson, C., Sparagana, S. P., Davies, P., van Eeghen, A. M., Thiele, E. A., van den Ouweland, A., Halley, D., Nellist, M. (2013). Functional assessment of TSC2 variants identified in individuals with tuberous sclerosis complex. *Hum Mutat*, 34, 1, pp. 167-75. DOI: 10.1002/humu.22202

Hoshino, A., Costa-Silva, B., Shen, T.-L., Rodriguez, G., Hashimoto, A., Mark, M. T., Molina, H., Kohsaka, S., Di Giannatale, A., Ceder, S., Singh, S., Williams, C., Soplop, N., Uryu, K., Pharmer, L., King, T., Bojmar, L., Davies, A. E., Ararso, Y., Zhang, T., Zhang, H., Hernandez, J., Weiss, J. M., Dumont-Cole, V. D., Kramer, K., Wexler, L. H., Narendran, A., Schwartz, G. K., Healey, J. H., Sandstorm, P., Labori, K. J., Kure, E. H., Grandgenett, P. M., Hollingsworth, M. A., de Sousa, M., Kaur, S., Jain, M., Mallya, K., Batra, S. K., Jarnagin, W. R., Brady, M. S., Fodstad, O., Muller, V., Pantel, K., Minn, A. J., Bissell, M. J., Garcia, B. A., Kang, Y., Rajasekhar, V. K., Ghajar, C. M., Matei, I., Peinado, H., Bromberg, J., Lyden, D. (2016). Tumour exosome integrins determine organotropic metastasis. *Nature*, 527, 7578, pp. 329-35. DOI: 10.1038/nature15756

Hu, H., Wu, J., Yu, X., Zhou, J., Yu, H., Ma, L. (2019). Long non-coding RNA MALAT1 enhances the apoptosis of cardiomyocytes through autophagy inhibition by regulating TSC2-mTOR signaling. *Biol Res*, 29, 52, 1, pp. 58. DOI: 10.1186/s40659-019-0265-0

Hu, J., Zacharek, S., He, Y. J., Lee, H., Shumway, S., Duronio, R. J., Xiong, Y. (2008). WD40 protein FBW5 promotes ubiquitination of tumor suppressor TSC2 by DDB1-CUL4-ROC1 ligase. *Genes & Dev*, 22, pp. 866-71. DOI: 10.1101/gad.1624008

Huntzinger, E., Izaurralde, E. (2011). Gene silencing by microRNAs: contributions of translational repression and mRNA decay. *Nat Rev Genet*, 12, 2, pp. 99-110. DOI: 10.1038/nrg2936

Hurley, J. H. (2008). ESCRT complexes and the biogenesis of multivesicular bodies. *Curr Opin Cell Biol*, 20, 1, pp. 4-11. DOI: 10.1016/j.ceb.2007.12.002

Hurwitz, S. N., Olcese, J. M., Meckes, D. G. Jr (2019). Extraction of extracellular vesicles from whole tissue. *J Vis Exp*, 7, 144, pp. e59143. DOI: 10.3791/59143

Huynh, N. P. T., Gloss, C. C., Lorentz, J., Tang, R., Brunger, J. M., McAlinden, A., Zhang, B., Guilak, F. (2020). Long non-coding RNA GRASLND enhances chondrogenesis via suppressor of the interferon type II signaling pathway. *Elife*, 9, pp. e49558. DOI: 10.7554/eLife.49558

Hynes, R. O. (2009). Extracellular matrix: not just pretty fibrils. *Science*, 326, 5957, pp. 1216-9. DOI: 10.1126/science.1176009

Im, E., Lee, C., Moon, P., Rangaswamy, G. G., Lee, B., Lee, J. M., Lee, J., Jee, J., Bae, J., Kwon, T., Kang, K., Jeong, M., Lee, J., Jung, H., Ro, H., Jun, S., Kang, W., Seo, S., Cho, Y., Song, B., Baek, M. (2019). Sulfisoxazole inhibits the secretion of small extracellular vesicles by targeting the endothelin receptor A. *Nat Commun*, 10, 1387, pp. 9759. DOI: 10.1038/s41467-019-09387-4

Inoki, K., Ouyang, H., Zhu, T., Lindvall, C., Wang, Y., Zhang, X., Yang, Q., Bennett, C., Harada, Y., Stankunas, K., Wang, C., He, X., MacDougald, O. A., You, M., Williams, B. O., Guan, K.-L. (2006). TSC2 integrates Wnt and energy signals via a

coordinated phosphorylation by AMPK and GSK3 to regulate cell growth. *Cell*, 126, 5, pp. 955-68. DOI: 10.1016/j.cell.2006.06.055

Inoki, K., Zhu, T., Guan, K.-L. (2003). TSC2 mediates cellular energy response to control cell growth and survival. *Cell*, 115, 5, pp. 577-90. DOI: 10.1016/S0092-8674(03)00929-2

Islam, M. P., Roach, E. S. (2015). Tuberous sclerosis complex. *Handb Clin Neurol*, 132, pp. 97-109. DOI: 10.1016/B978-0-444-62702-5.00006-8

Iwai, K., Minamisawa, T., Suga, K., Yajima, Y., Shiba, K. (2016). Isolation of human salivary extracellular vesicles by iodixanol density gradient ultracentrifugation and their characterizations. *J Extracell Vesicles*, 5, pp. 2-17. DOI: 10.3402/jev.v5.30829

Jahn, R., Lang, T., Südhof, T. (2003). Membrane fusion. *Cell*, 112, 4, pp. 519-33. DOI: 10.1016/s0092-8674(03)00112-0

Jahn, R., Scheller, R. H. (2006). SNAREs – engines for membrane fusion. *Nat Rev Mol Cell Biol*, 7, 9, pp. 631-43. DOI: 10.1038/nrm2002

Jansen, L. A., Uhlmann, E. J., Crino, P. B., Gutmann, D. H., Wong, M. (2005). Epileptogenesis and reduced inward rectifier potassium current in tuberous sclerosis complex-1-deficient astrocytes. *Epilepsia*, 46, 12, pp. 1871-80. DOI: 10.1111/j.1528-1167.2005.00289.x

Jiang, Y.-L., Wang, Z.-X., Liu, X.-X., Wan, M.-D., Liu, Y.-W., Jiao, B., Liao, X.-X., Luo, Z.-W., Wang, Y.-Y., Hong, C.-H., Tan, Y.-J., Weng, L., Zhou, Y-.F., Rao, S.-S., Cao, J., Liu, Z.-Z., Wan, T.-F., Zhu, Y., Xie, H., Shen, S. (2022). The protective effects of osteocyte-derived extracellular vesicles against Alzheimer's Disease diminished with aging. *Adv Sci*, 9, 17, pp. e2105316. DOI: 10.1002/advs.202105316

Jing, X., Han, J., Zhang, J., Chen, Y., Yuan, J., Wang, J., Neo, S., Li, S., Yu, X., Wu, J. (2021). Long non-coding RNA MEG3 promotes cisplatin-induced nephrotoxicity through regulating AKT/TSC/mTOR-mediated autophagy. *Int J Biol Sci*, 17, 14, pp. 3968-80. DOI: 10.7150/ijbs.58910

Jinzaki, M., Silverman, S. G., Akita, H., Nagashima, Y., Mikami, S., Oya, M. (2014). Renal angiomyolipoma: a radiological classification and update on recent developments in diagnosis and management. *Abdom Imaging*, 39, 3, pp. 588-604. DOI: 10.1007/s00261-014-0083-3

Johnsen, K. B., Mar Gudbergsson, J., Skov, M. N., Pilgaard, L., Moos, T., Duroux, M. (2014). A comprehensive overview of exosomes as drug delivery vehicles – endogenous nanocarriers for targeted cancer therapy. *Biochim Biophys Acta*, 1846, 1, pp. 75-87. DOI: 10.1016/j.bbcan.2014.04.005

Johnson, C. E., Dunlop, E. A., Seifan, S., McCann, H. D., Hay, T., Parfitt, G. J., Jones, A. T., Giles, P. J., Shen, M. H., Sampson, J. R., Errington, R. J., Davies, D. M., Tee, A. R. (2018). Loss of tuberous sclerosis complex 2 sensitizes tumors to

nelfinavir− bortezomib therapy to intensify endoplasmic reticulum stress-induced cell death. *Oncogene*, *37*, 45, pp.5913-25. DOI: 10.1038/s41388-018-0381-2

Johnstone, R. M., Adam, M., Hammond, J. R., Orr, L., Turbide, C. (1987). Vesicle formation during reticulocyte maturation. Association of plasma membrane activities with released vesicles (exosomes). *J Biol Chem*, 262, 19, pp. 9412-20. PMID: 3597417

Joinson, C., O'Callaghan, F. J., Osborne, J. P., Martyn, C., Harris, T., Bolton, P. F. (2003). Learning disability and epilepsy in an epidemiological sample of individuals with tuberous sclerosis complex. *Psychol Med*, 33, 2, pp. 335-44. DOI: 10.1017/s0033291702007092

Jones, A. C., Shyamsundar, M. M., Thomas, M. W., Maynard, J., Idziaszczyk, S., Tomkins, S., Sampson, J. R., Cheadle, J.P. (1999), Comprehensive mutation analysis of TSC1 and TSC2-and phenotypic correlations in 150 families with tuberous sclerosis. *Am J Hum Genet*, 64, pp. 1305–15. PubMed PMID: 10205261.

Joyce, J. J., Pollard, J. W. (2009). Microenvironmental regulation of metastasis. *Nat Rev Cancer*, 9, 4, pp. 239-252. DOI: 10.1038/nrc2618

Kadakkuzha, B. M., Liu, X.-A., McCrate, J., Shankar, G., Rizzo, V., Afinogenova, A., Young, B., Fallahi, M., Carvalloza, A. C., Raveendra, B., Puthanveettil, S. (2015). Transcriptome analyses of adult mouse brain reveal enrichment of lncRNAs in

specific brain regions and neuronal populations. *Front Cell Neurosci*, 9, 63, pp. 1-14. DOI: 10.3389/fncel.2015.00063

Kaksonen, M., Roux., A. (2018). Mechanisms of clathrin-mediated endocytosis. *Nat Rev Mol Cell Biol*, 19, 5, pp. 313-26. DOI: 10.1038/nrm.2017.132

Kalluri, R. (2016). The biology and function of fibroblasts in cancer. *Nat Rev Cancer*, 16, pp. 582-98. DOI: 10.1038/nrc.2016.73

Kalra, H., Simpson, R. J., Ji, H., Akiama, E., Altevogt, P., Askenase, P., Bond, V. C., Borràs, F. E., Breakefield, X., Budnik, V., Buzas, E.,Camussi, G., Clayton, A., Cocucci, E., Falcon-Perez, J. M., Gabrielsson, S., Gho, Y. S., Gupta, D., Harsha, H. C., Hendrix, A., Hill, A. F., Inal, J. M., Jenster, G., Krämer-Albers, E., Lim, S. K., Llorente, A., Lötvall, J., Marcilla, A., Mincheva-Nilsson, L., Nazarenko, I., Nieuwland, R., Nolte-'t Hoen, E. N. M., Pandel, A., Patel., T., Piper, M. G., Pluchino, S., Keshava Prasad, T. S., Rajendran, L., Raposo, G., Record, M., Reid, G. E., Sánchez-Madrid, F., Schiffelers, R. M., Siljander, P., Stensballe, A., Stoorvogel, W., Taylor, D., Théry, C., Valadi, H., van Balkom, B. W. M., Vázquez, J., Vidal, M., Wauben, M. H. M., Yáñez-Mó, M., Zoeller, M., Mathivanan, S. (2012). Vesiclepedia: a compendium for extracellular vesicles and continuous community annotation. *PLoS Biology*, 10(12), pp. 8-12. DOI: 10.1371/journal.pbio.1001450

Kan, A. A., van Erp, S., Derijck, A. A., de Wit, M., Hessel, E. V., O'Duibhir, E., de Jager, W., van Rijen, P. C., Gosselaar, P .H., de Graan, P. N. E., Pasterkemp, R. J. (2012). Genome-wide microRNA profiling of human temporal lobe epilepsy

identifies modulators of the immune response. *Cell Mol Life Sci*, 69, pp. 3127-45. DOI: 10.1007/s00018-012-0992-7

Kang, S. Y., Lee, E. J., Byun, J. W., Han, D., Choi, Y., Hwang, D. W., Lee, D. S. (2021). Extracellular vesicles induce an aggressive phenotype in luminal breast cancer cells via PKM2 phosphorylation. *Front Oncol*, 11, pp. e785450. DOI: 10.3389/fonc.2021.785450

Kao, C.-Y., Papoutsakis, E. T. (2019). Extracellular vesicles: exosomes, microparticles, their parts, and their targets to enable their biomanufacturing and clinical applications. *Curr Opin Biotechnol*, 60, pp. 89-98. DOI: 10.1016/j.copbio.2019.01.005

Kerr, M .C, Teasdale, R. D. (2009). Defining macropinocytosis. *Traffic*, 10, 4, pp. 364-71. DOI: 10.1111/j.1600-0854.2009.00878.x

Keshava Prasaad, T. S., Goel, R., Kandasamy, K., Keerhikumar, S., Kumar, S., Mathivanan, S., Telikicheria, S., Raju, R., Shafreen, B., Venugopal, A., Balakrishnan, L., Marimuthu, A., Banerjee, S., Somanathan, D. S., Sebastian, A., Rani, S., Ray, S., Harrys Kishore, C. J., Kanth, S., Ahmed, M., Kashyap, M. K., Mohmood, R., Ramachandra, Y. L., Krishna, V., Rahiman, B. A., Mohan, S., Ranganathan, P., Ramabadran, S., Chaerkady, R., Pandey, A. (2009). Human Protein Reference Database – 2009 update. *Nucleic Acids Res*, 37, pp. 767-72. DOI: 10.1093/nar/gkn892

Klover, P. J., Thangapazham, R. L., Kato, J., Wang, J. A., Anderson, S. A., Hoffmann, V., Steagall, W. K., Li, S., McCart, E., Nathan, N., Bernstock, J. D., Wilkerson, M. D., Dalgard, C. L., Moss, J., Darling, T. N. (2017). Tsc2 disruption in mesenchymal progenitors results in tumors with vascular anomalies overexpressing *Lgals3*. *Elife*, 11, 6, pp. e23202. DOI: 10.7554/eLife.23202

Knudson, A. G. (1971). Mutation and cancer: statistical study of retinoblastoma. *Proc Natl Acad Sci U S A*, 68, pp. 820-3. DOI: 10.1073/pnas.68.4.820

Ko, S. Y., Lee, W., Kenny, H. A., Dang, L. H., Ellis, L. M., Jonasch, E., Lengyel, E., Naora, H. (2019). Cancer-derived small extracellular vesicles promote angiogenesis by heparin-bound, bevacizumab-insensitive VEGF, independent of vesicle uptake. *Commun Biol*, 18, pp. e386. DOI: 10.1038/s42003-019-0609-x

Ko, J., Hemphill, M., Yang, Z., Beard, K., Sewell, E., Shallcross, J., Schweizer, M., Sandmark, D. K., Diaz-Arrastia, R., Kim, J., Meaney, D., Issadore, D. (2020). Multi-dimensional mapping of brain-derived extracellular vesicle microRNA biomarker for traumatic brain injury diagnostics. *J Neurotrauma*, 37, pp. 2424-34. DOI: 10.1089/neu.2018.6220

Ko, J., Wang, Y., Carlson, J. C. T., Marquard, A., Gungabeesoon, J. ,Charest, A., Weitz, D., Pittet, M. J., Weissleder, R. (2020). Single extracellular vesicle protein analysis using immuno-droplet digital polymerase chain reaction amplification. *Adv Biosyst*, 4, 12, pp. e1900307. DOI: 10.1002/adbi.201900307

Ko, J., Wang, Y., Sheng, K., Weitz, D. A., Weissleder, R. (2021). Sequencing-based protein analysis of single extracellular vesicles. *ACS Nano*, 15, 3, pp. 5631-8. DOI: 10.1021/acsnano.1c00782

Koene, L. M. C., Niggl, E., Wallaard, I., Proietti-Onori, M., Rotaru, D. C., Elgersma, Y. (2021). Identifying the temporal electrophysiological and molecular changes that contribute to TSC-associated epileptogenesis, *JCI Insight*, 6, 23, pp. e150120. DOI: 10.1172/jci.insight.150120

Kosaka, N., Iguchi, H., Ochiya, T. (2010). Circulating microRNA in body fluid: a new potential biomarker for cancer diagnosis and prognosis. *Cancer Sci*, 101, 10, pp. 2087-92. DOI: 10.1111/j.1349-7006.2010.01650.x

Kothare, S. V., Singh, K., Chalifoux, J. R., Staley, B. A., Weiner, H. L., Menzer, K., Devinsky, O. (2014). Severity of manifestations in tuberous sclerosis complex in relation to phenotype. *Epilepsia*, 55, 7, pp. 1025-29. DOI: 10.1111/epi.12680

Kowal, J., Arras, G., Colombo, M., Jouve, M., Morath, J. P., Primdal-Bengtson, B., Dingli, F., Loew, D., Tkach, M., Théry, C. (2016). Proteomic comparison defines novel markers to characterise heterogeneous populations of extracellular vesicle subtypes. *Proc Natl Acad Sci U S A*, 113, 8, pp. e968-77. DOI: 10.1073/pnas.1521230113

Kozma, S. C., Thomas, G. (2002). Regulation of cell size in growth, development and human disease: PI3K, PKB and S6K. *Bioessays*, 24, 1, pp. 65-71. DOI: 10.1002/bies.10031

Kroemer, G., Pouyssegur, J. (2008). Tumor cell metabolism: cancer's Achilles' heel. *Cancer Cell*, 13, 6, pp. 472-82. DOI: 10.1016/j.ccr.2008.05.005

Kucharzewska, P., Christianson, H. C., Welch, J. E., Svensson, K. J., Fredlund, E., Ringnér, M., Mörgelin, M., Bourseau-Guilmain, E., Bengzon, J., Belting, M. (2013). Exosomes reflect the hypoxic status of glioma cells and mediate hypoxia-dependent activation of vascular cells during tumor development. *Proc Natl Acad Sci U S A*, 110, 18, pp. 7312-7. DOI: 10.1073/pnas.1220998110

Kumar, P., Zadjali, F., Yao, Y., Siroky, B., Astrinidis, A., Gross, K. W., Bissler, J. J. (2021). Tsc gene locus disruption and differences in renal epithelial extracellular vesicles. *Front Physiol*, 12, 630933, pp. 1-10. DOI: 10.3389/fphys.2021.630933

Kwok, Z. H., Wang, C., Jin, Y. (2021). Extracellular vesicle transportation and uptake by recipient cells: a critical process to regulate human diseases. *Processes*, 9, 273, pp. 1-16. DOI: 10.3390/pr9020273

L'Hostis, H., Deminiere, C., Ferriere, J.-M., Coindre, J.-M. (1999). Renal angiomyolipoma: a clinicopathologic, immunohistochemical, and follow-up study of 46 cases. *Am J Surg Pathol*, 23, 9, pp. 1011. DOI: 10.1097/00000478-199909000-00003

Lajoie, P., Nabi, I. R. (2010). Lipid rafts, caveolae, and their endocytosis. *Int Rev Cell Mol Biol*, 282, pp. 135-63. DOI: 10.1016/S1937-6448(10)82003-9

Lam, H. C., Siroky, B. J., Henske, E. P. (2018). Renal disease in tuberous sclerosis complex: pathogenesis and therapy. *Nat Rev Nephrol*, 14, pp. 704-16. DOI: 10.1038/s41581-018-0059-6

Lamparski, H. G., Metha-Damani, A., Yao, J. Y., Patel, S., Hsu, D. H., Ruegg, C., Le Pecq, J. B. (2002). Production and characterization of clinical grade exosomes derived from dendritic cells. *J Immunol Methods*, 270, 2, pp. 211-26. DOI: 10.1016/s0022-1759(02)00330-7

Laplante, M., Sabatini, D. M. (2012). mTOR signaling in growth control and disease. *Cell*, 149, 2, pp. 274-93. DOI: 10.1016/j.cell.2012.03.017

Lässer, C., Eldh, M., Lötvall, J (2012). Isolation and characterisation of RNA-containing exosomes. *J Vis Exp*, 59, pp. e3037. DOI : 10.3791/3037

Lazar, I., Clement, E., Attane, C., Muller, C., Nieto, L. (2018). A new role for extracellular vesicles: how small vesicles can feed tumors' big appetite. *J Lipid Res*, 59, 10, pp. 1793-1804. DOI: 10.1194/jlr.R083725

Lee, D. F., Kuo, H.-P., Chen, C.-T., Hsu, J.-M., Chou, C.-K., Wei, Y., Sun, H.-L., Li, L.-Y., Ping, B., Huang, W.-C., He, X., Hung, J.-Y., Lai, C.-C., Ding, Q., Su, J.-L.,

Yang, J.-Y., Sahin, A. A., Hortobagyi, G. N., Tsai, F.-J., Tsai, C.-H., Hung, M.-C. (2007). IKKβ suppression of TSC1 links inflammation and tumor angiogenesis via the mTOR pathway. *Cell*, 130, 3, pp. 440-5. DOI: 10.1016/j.cell.2007.05.058

Lee, M. N., Ha, S. H., Kim, J., Koh, A., Lee, C. S., Kim, J. H., Jeon, H., Kim, D.-H., Suh, P.-G., Ryu, S. H. (2009). Glycolytic flux signals to mTOR through glyceraldehyde-3-phosphate dehydrogenase-mediated regulation of Rheb. *Mol Cell Biol*, 29, pp. 3991-4001. DOI: 10.1128/MCB.00165-09

Lee, C. H., Hong, C. H., Yu, H. S., Chen, G. S., Yang, K. C. (2010). Transforming growth factor-β enhances metalloproteinase-2 expression and activity through AKT in fibroblasts derived from angiofibromas in patients with tuberous sclerosis complex. *Br J Dermatol*, 163, 6, pp. 1238-44. DOI: 10.1111/j.1365-2133.2010.09971.x

Lee, Y., EL-Andaloussi, S., Wood, M. J. A. (2012). Exosomes and Microvesicles: extracellular vesicles for genetic information transfer and gene therapy. *Hum Molec Genet*, 21, 1, pp. 125-34. DOI: 10.1093/hmg/dds317

Leung, A. K. C., Robson, W. L. M. (2007). Tuberous sclerosis complex: a review. *J Pediat Health Care*, 21, 2, pp. 108-14. DOI: 10.1016/j.pedhc.2006.05.004

Li, S., Takeuchi, F., Wang, J., Fuller, C., Pacheco-Rodriguez, G., Moss, J., Darling, T. N. (2005). MCP-1 overexpressed in tuberous sclerosis lesions acts as a paracrine factor for tumor development. *J Exp Med*, 202, 5, pp. 617-24. DOI: 10.1084/jem.20042469

Li, L., Zhu, D., Huang, L., Zhang, J., Bian, Z., Chen, X., Liu, Y., Zhang, C.-Y., Zen, K. (2012). Argonaute 2 complexes selectively protect the circulating microRNAs in cell-secreted Microvesicles. *PLoS One*, 7, 10, pp. 46957. DOI: 10.1371/journal.pone.0046957

Li, Y., Zhang, L., Liu, F., Xiang, G., ,, D., Pu, X. (2015). Identification of endogenous controls for analysing serum exosomal miRNA in patients with hepatitis B or hepatocellular carcinoma. *Dis Markers*, 2015, pp. e893594. DOI: 10.1155/2015/893594

Li, H., Gong, M., Zhao, M., Wang, X., Cheng, W., Xia, Y. (2018). LncRNAs KB-1836B5, LINC00566 and FAM27L are associated with the survival time of patients with ovarian cancer. *Oncol Lett*, 16, 3, pp. 3735-45. DOI: 10.3892/ol.2018.9143

Li, S., Jiang, J., Yang, Z., Li, Z., Ma, X., Li, X. (2018). Cardiac progenitor cell-derived exosomes promote H9C2 cell growth via Akt/mTOR activation. *Intl J Mol Med*, 42, 3, pp. 1517-25. DOI: 10.3892/ijmm.2018.3699

Li, Y., Barkovich, M. J., Karch, C. M., Nillo, R. M., Fan, C.-C., Broce, I. J., Tan, C. H., Cuneo, D., Hess, C. P., Dillon, W. P., Glenn, O. A., Glastonbury, C. M., Olney, N., Yokoyama, J. S., Bonham, L. W., Miller, B., Kao, A., Schmansky, N., Fischl, B., Andreassen, O. A., Jernigan, T., Dale, A., Barkovich, A. J., Desikan, R. S., Sugrue, L. P. (2018). Regionally specific *TSC1* and *TSC2* gene expression in tuberous sclerosis complex. *Sci Rep*, 8, 13373, pp. 1-10. DOI: 10.1038/s41598-018-31075-4

Li, Z., He, B., Feng, W. (2019). Evaluation of bottom-up and top-down mass spectrum identifications with different customised protein sequences databases. *Bioinformatics*, 36, 4, pp. 1030-6. DOI: 10.1093/bioinformatics/btz733

Li, X., Zou, Z.-Z., Wen, M., Xie, Y.-Z., Peng, K.-J., Luo, T., Liu, S.-Y., Gu, Q., Li, J.-J., Luo, Z.-Y. (2020). ZLM-7 inhibits the occurrence and angiogenesis of breast cancer through miR-212-3p/Sp1/VEGFA signal axis. *Mol Med*, 26, 109, pp. 1-13. DOI: 10.1186/s10020-020-00239-2

Li, Y., He, X., Li, Q., Lai, H., Zhang, H., Hu, Z., Li, Y., Huang, S. (2020). EV-origin: enumerating the tissue-cellular origin of circulating extracellular vesicles using exLR profile. *Comp Struct Biotech J,* 18, 2020, pp. 2851-9. DOI: 10.1016/j.csbj.2020.10.002

Li, Z., Shi, L., Li, X., Wang, X., Wang, H., Liu, Y. (2021). RNF144A-AS1, a TGF-β1- and hypoxia-inducible gene that promotes tumor metastasis and proliferation via targeting the miR-30c-2-3p/LOX axis in gastric cancer. *Cell Biosci*, 11, 1, pp. e177. DOI: 10.1186/s13578-021-00689-z

Liao, Z., Zheng, Q., Wei, T., Zhang, Y. (2020). MicroRNA-561 affects proliferation and cell cycle transition through PTEM/AKT signaling pathway by targeting P-REX2a in NSCLC. *Oncol Res Feat Preclin Clin Can Therapeut*, 28, 2, pp. 147-59. DOI: 10.3727/096504019X15732109856009

Liu, L., Ruan, J. (2014). Network-based pathway enrichment analysis. *Proceedings IEEE Int Conf Bioinformatics Biomed*, pp. 218-21. DOI: 10.1109/BIBM.2013.6732493

Liu, J., Wang, Y., Chu, Y., Xu, R., Zhang, D., Wang, X. (2020). Identification of a TLR-induced four-lncRNA signature as a novel prognostic biomarker in esophageal carcinoma. *Front Cell Dev Biol*, 8, 649, pp. 1-11. DOI: 10.3389/fcell.2020.00649

Loghry, H. J., Yuan, W., Zamanian, M., Wheeler, N. J., Day, T. A., Kimber, M. J. (2020). Ivermectin inhibits extracellular vesicle secretion from parasitic nematodes. *J Extracell Vesicles*, 10, 2, pp. 1-15. DOI: 10.1002/jev2.12036

Logozzi, M., De Milito, A., Lugini, L., Borghi, M., Calabrò, L., Spada, M., Perdicchino, M., Marino, M. L., Federici, C., Iessi, E., Brambilla, D., Venturi, G., Lozupone, F., Santinami, M., Huber, V., Maio, M., Rivoltini, L., Fais, S. (2009). High levels of exosomes expressing CD63 and caveolin-1 in plasma of melanoma patients. *PLoS One*, 4, 4, pp. e5219. DOI: 10.1371/journal.pone.0005219

Long, X., Ortiz-Vega, S., Lin, Y., Avruch, J. (2005). Rheb binding to mammalian target of rapamycin (mTOR) is regulated by amino acid sufficiency. *J Biol Chem*, 280, 25, pp. 23433-6. DOI: 10.1074/jbc.C500169200

Long, Y., Wang, X., Youmans, D. T., Cech, T. R. (2017). How do lncRNAs regulate transcription? *Sci Adv*, 3, 9, pp. e2110. DOI: 10.1126/sciadv.aao2110

Lötvall, J., Hill, A. F., Hochberg, F., Buzás, E. I., Di Vizio, D., Gardiner, C., Gho, Y. S., Kurochkin, I. V., Mathivanan, S., Quesenberry, P., Sahoo, S., Tahara, H., Wauben, M. H., Witwer, K. W., Théry, C. (2014). Minimal experimental requirements for definition of extracellular vesicles and their functions: a position statement from the International Society for Extracellular Vesicles. *J Extracell Vesicles*, 3, pp. 26913. DOI: 10.3402/jev.v3.26913

Love, M. I., Huber, W., Anders, S. (2014). Moderated estimation of fold change and dispersion for RNA-seq data with DESeq2. *Genome Biol*, 15, 550, pp. 1-21. DOI: 10.1186/s13059-014-0550-8

Lu, L., Liu, L.-P., Zhao, Q.-Q., Gui, R., Zhao, Q.-Y. (2021). Identification of a ferroptosis-related lncRNA signature as a novel prognosis model for lung adenocarcinoma. *Front Oncol*, 11, pp. 675545. DOI: 10.3389/fonc.2021.675545

Lucchetti, D., Litta, F., Ratto, C., Sgambato, A. (2018). The role of extracellular vesicles as biomarkers in colorectal cancer. *Tech Coloproctol*, 22, 12, pp. 989-90. DOI: 10.1007/s10151-018-1880-4

Luga, V., Zhang, L., Viloria-Petit, A. M., Ogunjimi, A. A., Inanlou, M. R., Chiu, E., Buchanan, M., Hosein, A. N., Basik, M., Wrana, J. L. (2012). Exosomes mediate stromal mobilization of autocrine Wnt-PCP signaling in breast cancer cell migration. *Cell*, 151, pp. 1542-56. DOI: 10.1016/j.cell.2012.11.024

Lv, Y., Sun, D., Han, Q., Yan, H., Dai, G. (2021). MicroRNA-425 promoted the proliferation and migration of colorectal cancer cells by targeting KLF3 through the PI3K/AKT pathway. *Minerva Med*, 112, 4, pp. 537-8. DOI: 10.23736/S0026-4806.19.06378-X

Lv, Z. D., Yang, D. X., Liu, X. P., Jin, L. Y., Wang, X. G., Yang, Z. C., Liu, D., Zhao, J. J., Kong, B., Li, F. N., Wang, H. B. (2017). MiR-212-5p suppresses the epithelial-mesenchymal transition in triple-negative breast cancer by targeting Prrx2. *Cell Physiol Biochem*, 44, pp. 1785-95. DOI: 10.1159/000485785

Ma, L., Chen, Z., Erdjument-Bromage, H., Tempst, P., Pandolfi, P. P. (2005). Phosphorylation and functional inactivation of TSC2 by Erk: implications for tuberous sclerosis and cancer pathogenesis. *Cell*, 121, 2, pp. 179-93. DOI: 10.1016/j.cell.2005.02.031

Ma, X. M., Blenis, J. (2009). Molecular mechanisms of mTOR-mediated translational control. *Nat Rev Mol Cell Biol*, 10, 5, pp. 307-18. DOI: 10.1038/nrm2672

Maeurer, C., Holland, S., Pierre, S., Potstada, W., Scholich, K. (2009). Sphingosine-1-phosphate induced mTOR-activation is mediated by the E3-ubiquitin ligase PAM. *Cell Signal*, 21, 2, pp. 293-300. DOI: 10.1016/j.cellsig.2008.10.016

Maglott, D., Ostell, J., Pruitt, K. D., Tatusova, T. (2007). Entrez Gene: gene-centred information at NCBI. *Nucleic Acids Res*, 35, pp. 26-31. DOI: 10.1093/nar/gkq1237

Maia, J., Caja, S., Strano Moraes, M. C., Couto, N., Costa-Silva, B. (2018). Exosome-based cell-cell communication in the tumor microenvironment. *Front Cell Dev Biol*, 6,18, pp. 1-19. DOI: 10.3389/fcell.2018.00018

Mak, B. C., Kenerson, H. L., Aicher, L. D., Barnes, E. A., Yeung, R. S. (2005). Aberrant beta-catenin signaling in tuberous sclerosis. *Am J Pathol*, 167, 1, pp. 107-16. DOI: 10.1016/s0002-9440(10)62958-6

Mak, B. C., Yeung, R. S. (2004). The tuberous sclerosis complex genes in tumor development. *Cancer Invest*, 22, 4, pp. 588-603. DOI: 10.1081/CNV-200027144

Mallia, A., Gianazza, E., Zoanni, B., Brioschi, M., Barbieri, S. S., Banfi, C. (2020). Proteomics of extracellular vesicles: update on their composition, biological roles and potential use as diagnostic tools in atherosclerotic cardiovascular diseases. *Diagnostics*, 10, 10, pp. 1-34. DOI: 10.3390/diagnostics10100843

Mardpour, S., Hamidieh, A. A., Taleahmad, S., Sharifzad, F., Taghikhani, A., Baharvand, H. (2019). Interaction between mesenchymal stromal cell-derived extracellular vesicles and immune cells by distinct protein content. *J Cell Physiol*, 234, 6, pp. 8249-58. DOI: 10.1002/jcp.27669

Margolis, L., Sadovsky, Y. (2019). The biology of extracellular vesicles: the known unknowns. *PLoS Biol*, 17, 7, pp. 3000363. DOI: 10.1371/journal.pbio.3000363

Maring, J. A., Trojanowska, M., ten Dijke, P. (2012). Endoglin in fibrosis and scleroderma. *Int Rev Cell Mol Biol*, 2012, 297, pp. 1-12. DOI: 10.1016/B978-0-12-394308-8.00008-X

Marsigliante, S., Vetrugno, C., Muscella, A. (2013). CCL20 induces migration and proliferation on breast epithelial cells. *J Cell Physiol*, 228, 9, pp. 1873-83. DOI: 10.1002/jcp.24349

Marsigliante, S., Vetrugno, C., Muscella, A. (2016). Paracrine CCL20 loop induces epithelial-mesenchymal transition in breast epithelial cells. *Mol Carcinog*, 55, 7, pp. 1175-86. DOI: 10.1002/mc.22360

Martelli, A. M., Tabellini, G., Bressanin, D., Ognibene, A., Goto, K., Cocco, L., Evangelisti, C. (2012). The emerging multiple roles of nuclear Akt. *Biochim Biophys Acta*, 1838, 12, pp. 2168-78. DOI: 10.1016/j.bbamcr.2012.08.017

Martin, K. R., Zhou, W., Bowman, M. J., Shih, J., Au, K .S., Dittenhafer-Reed, K. E., Sisson, K. A., Koeman, J., Weisenberger, D. J., Cottingham, S. L., DeRoos, S. T., Devinsky, O., Winn, M. E., Cherniack, A. D., Shen, H., Northup, H., Krueger, D. A., MacKeigan, J. P. (2017). The genomic landscape of tuberous sclerosis complex. *Nat Commun*, 8, 15816, pp. 1-13. DOI: 10.1038/ncomms15816

Mateescu, B., Kowal, E. J. K., van Balkom, B. W. M., Bartel, S., Bhattachuryya, S. N., Buzáz, E. I., Buck, A. H., de Candia, P., Chow, F. W. N., Das, S., Driedonks, T.

A. P., Fernández-Messina, L., Haderk, F., Hill, A. F., Jones, J. C., van Keuren-Jensen, K. R., Lai, C. P., Lässer, C., di Liegro, I., Lunavat, T. R., Lorenowicz, M. J., Maas, S. L. N., Mäger, I., Mittelbrunn, M., Momma, S., Mukherjee, K., Nawaz, M., Pegtel, D. M., Pfaffl, M. W., Schiffelers, R. M., Tahara, H., Théry, C., Tosar, J. P., Wauben, M. H. M., Witwer, K. W., Nolte-'t Hoen, E. N. M. (2017). Obstacles and opportunities in the functional analysis of extracellular vesicle RNA – an ISEV position paper. *J Extracell Vesicles*, 6, 1, pp. 1286095. DOI: 10.1080/20013078.2017.1286095

Mathew, M., Zade, M., Mezghani, N., Patel, R., Wang, Y., Momen-Heravi, F. (2020). Extracellular vesicles as biomarkers in cancer immunotherapy. *Cancers (Basel)*, 12, 10, pp. 1-22. DOI: 10.3390/cancers12102825

Mathieu, M., Martin-Jaular, L., Lavieu, G., Théry, C. (2019). Specificities of secretion and uptake of exosomes and other extracellular vesicles for cell-to-cell communication. *Nat Cell Biol*, 21, 1, pp. 9-17. DOI: 10.1038/s41556-018-0250-9

Mathieu, M., Névo, N., Jouve, M., Valenzuela, J. I., Maurin, M., Verweij, F., Palmulli, R., Lankar, D., Dingli, F., Loew, D., Rubinstein, E., Boncompain, G., Perez, F., Théry, C. (2021). Specificities of exosome versus small ectosome secretion revealed by live intracellular tracking of CD63 and CD9. *Nat Commun*, 12, 1, pp. 4389. DOI: 10.1038/s41467-021-24384-2

Mathivanan, S., Simpson, R. J. (2009). ExoCarta: a compendium of exosomal proteins and RNA. *Proteomics*, 9, 21, pp. 4997-5000. DOI: 10.1002/pmic.200900351

Matsumoto, A., Pasut, A., Matsumoto, M., Yamashita, R., Fung, J., Monteleone, E., Saghatelian, A., Nakayama, K. I., Clohessy, J. G., Pandolfi, P. P. (2017). mTORC1 and muscle regeneration are regulated by the LINC00961-encoded SPAR polypeptide. *Nature*, 541, 7636, pp. 228-32. DOI: 10.1038/nature21034

Mayer, K., Goedbloed, M., van Zijl, K., Nellist, M., Rott, H.-D. (2004). Characterisation of a novel TSC2 missense mutation in the GAP related domain associated with minimal clinical manifestations of tuberous sclerosis. *J Med Genet*, 41, 5, pp. 1-6. DOI: 10.1136/jmg.2003.010835

McKernan, J., Noerholm, M., Tadigotla, V., Kumar, S., Torkler, P., Sant, G., Alter, J., Donovan, M. J., Skog, J. (2020). A urine-based exosomal gene expression test stratifies risk of high-grade prostate cancer in men with prior negative prostate undergoing repeat biopsy. *BMC Urology*, 20, 138, pp. 1-6. DOI: 10.1186/s12894-020-00712-4

Meehan, K., Vella, L. J. (2015). The contribution of tumour-derived exosomes to the hallmarks of cancer. *Crit Rev Clin Lab Sci*, 53, 2, pp. 121-31. DOI: 10.3109/10408363.2015.1092496

Meister, M., Tikkanen, R. (2014). Endocytic trafficking of membrane-bound cargo: a

flotillin point of view. *Membranes*, 4, 3, pp. 356-71. DOI: 10.3390/membranes4030356

Melo, S.A., Luecke, L.B., Kahlert, C., Fernandez, A.F., Gammon, S.T., Kaye, J., LeBleu, V.S., Mittendorf, E.A., Weitz, J., Rahbari, N. and Reissfelder, C. (2015). Glypican-1 identifies cancer exosomes and detects early pancreatic cancer. *Nature*, *523*, 7559, pp.177-82. DOI: 10.1038/nature14581

Millimaggi, D., Mari, M., D'Ascenzo, S., Carosa, E., Jannani, E. A., Zucker, S., Carta, G., Pavan, A., Dolo, V. (2007). Tumor vesicle-associated CD147 modulates the angiogenic capability of endothelial cells. *Neoplasia*, 9, 4, pp. 349-57. DOI: 10.1593/neo.07133

Mills, J. D., Iyer, A. M., van Scheppingen, J., Bongaarts, A., Anink, J. J., Janssen, B., Zimmer, T. S., Spliet, W. G., van Rijen, P. C., Jansen, F. E., Feucht, M., Hainfellner, J. A., Krsek, P., Zamecnik, J., Kotulska, K., Jozwiak, S., Jansen, A., Lagae, L., Curatolo, P., Kwiatkowski, D. J., Pasterkamp, R. J., Senthilkumar, K., von Oerthel, L., Hoekman, M. F., Gorter, J. A., Crino, P. B., Mühlebner, A., Scicluna, B. P., Aronica, E. (2017). Coding and small non-coding transcriptional landscape of tuberous sclerosis complex cortical tubers: implications for pathophysiology and treatment. *Sci Rep*, 7, 8089, pp. 1-11. DOI: 10.1038/s41598-017-06145-8

Mineo, M., Garfield, S. H., Taverna, S., Flugy, A., De Leo, G., Alessandro, R., Kohn, E. C. (2012). Exosomes released by K562 chronic myeloid leukemia cells

promote angiogenesis in a Src- dependent fashion. *Angiogenesis*. 15: 33–45. DOI: 10.1007/s10456-011-9241-1

Mir, D., Goettsch, C. (2020). Extracellular vesicles as delivery vehicles of specific cellular cargo. *Cells*, 9, 7, pp. 1601. DOI: 10.3390/cells9071601

Mitchell, J. P., Court, J., Mason, M. D., Tabi, Z., Clayton, A. (2008). Increased exosome production from tumour cell cultures using the Integra CELLine Culture System. *J Immunol Methods*, 335, pp.98-105. DOI: 10.1016/j.jim.2008.03.001

Mohankumar, S., Patel, T. (2016). Extracellular vesicles long noncoding RNA as potential biomarkers of liver cancer. *Brief Funct Genomics*, 15, 3, pp. 249-56. DOI: 10.1093/bfgp/elv058

Moir, L. M., Black, J. L., Krymskaya, V. P. (2012). TSC2 modulates cell adhesion and migration via integrin-α1β1. *Am J Physiol Lung Cell Mol Physiol*, 303, 8, pp. 703-10. DOI: 10.1152/ajplung.00414.2011

Monteran, L., Erez, N. (2019). The dark side of fibroblasts: cancer-associated fibroblasts as mediators of immunosuppression in the tumor microenvironment. *Front Immunol*, 10, 1835, pp. 1-15. DOI: 10.3389/fimmu.2019.01835

Mosbach, M.-L., Pfafenrot, C., von Strandmann, E. P., Bindereif, A., Preuber, C. (2021). Molecular determinants for RNA release into extracellular vesicles. *Cells*, 10, 10, pp. 2674. DOI: 10.3390/cells10102674

Moumen, A., Patané, S., Porras, A., Dono, R., Maina, F. (2007). Met acts on Mdm2 via mTOR to signal cell survival during development. *Developmen*t, 134, 7, pp. 1443-51. DOI: 10.1242/dev.02820

Muraoka, S., Hirano, M., Isoyama, J., Nagayama, S., Tomonaga, T., Adachi, J. (2022). Comprehensive proteomic profiling of plasma and serum phosphatidylserine-positive extracellular vesicles reveals tissue-specific proteins. *iScience*, 25, 4, pp. e104012. DOI: 10.1016/j.isci.2022.104012

Muto, Y., Sasaki, H., Sumitomo, M., Inagaki, H., Kato, M., Kato, T., Miyai, S., Kurahashi, H., Shiroki, R. (2022). Genotype-phenotype correlation of renal lesions in the tuberous sclerosis complex. *Hum Genome Var*, 9, 1, pp. 1-5. DOI: 10.1038/s41439-022-00181-1

Mutschelknaus, L., Azimzadeh, O., Heider, T., Winkler, K., Vetter, M., Kell, R., Tapio, S., Merl-Pham, J., Huber, S. M., Edalat, L., Radulović, V., Anastasov, N., Atkinson, M. J., Moertl, S. (2017). Radiation alters the cargo of exosomes released from squamous head and neck cancer cells to promote migration of recipient cells. *Sci Rep*, 7, pp. 12423. DOI: 10.1038/s41598-017-12403-6

Nagpa, N., Kulshreshtha, R. (2014). miR-191: an emerging player in disease biology. *Front Genet*, 23, 5, pp. 99. DOI: 10.3389/fgene.2014.00099

Natarajan, N., Thiruvenkatam, V. (2020). An insight of scientific developments in TSC for better therapeutic strategy. Curr Topics Med Chem, 20, 3, pp. 2080-93. DOI: 10.2174/1568026620666200825170355

Nelson, C. P., Sanda, M. G. (2002). Contemporary diagnosis and management of renal angiomyolipoma. *J Urol*, 168, 4.1, pp. 1315-25. DOI: 10.1097/01.ju.0000028200.86216.b2

Ní Bhaoighill, M., Dunlop, E. A. (2019). Mechanistic target of rapamycin inhibitors: successes and challenges as cancer therapeutics. *Cancer Drug Resist*, 2, pp. 1609-85. DOI: 10.20517/cdr.2019.87

Nogués, A., Gallardo-Vara, E., Paz Zafra, M., Mate, P., Marijuan, J. L., Alonso, A., Botella, L. M., Prieto, M. I. (2020). Endoglin (CD105) and VEGF as potential angiogenic and dissemination markers for colorectal cancer. *World J Surg Oncol*, 18, 99, pp. 1-12. DOI: 10.1186/s12957-020-01871-2

Northrup, H., Koenig, M. K., Pearson, D. A., Au, K. S. (2020). Tuberous Sclerosis Complex. 1999 Jul 13 [Updated 2021 Dec 9]. In: Adam MP, Everman DB, Mirzaa GM, et al., editors. GeneReviews® [Internet]. Seattle (WA): University of Washington, Seattle; 1993-2022. Available from: https://www.ncbi.nlm.nih.gov/books/NBK1220/

Northup, H., Aronow, M. E., Bebin, E. M., Bissler, J., Darling, T. N., de Vries, P. J., Frost, M. D., Fuchs, Z., Gosnell, E. S., Gupta, N., Jansen, A. C., Jóźwiak, S.,

Kingswood, J. C., Knilans, T. K., McCormack, F. X., Pounders, A., Roberds, S. L., Rodriguez-Buritica, D. F., Roth, J., Sampson, J. R., Sparagana, S., Thiele, E. A., Weiner, H. L., Wheless, J. W., Towbin, A. J., Krueger, D. A., International Tuberous Sclerosis Complex Consensus Group. (2021). Updated International Tuberous Sclerosis Complex Diagnostic Criteria and Surveillance and Management Recommendations. *Pediatr Neurol*, 123, pp. 50-66. DOI: 10.1016/j.pediatrneurol.2021.07.011

Northup, H., Koenig, M. K., Pearson, D. A., Au, K. S., Adam, M. P., Everman, D. B., Mirzaa, G. M., Pagon, R. A., Wallace, S. E., Bean, L. J. H., Gripp, K. W., Amemiya, A. (1993). Tuberous sclerosis complex. In: GeneReviews® [Internet]. Seattle (WA): University of Washington, Seattle; 1993.

Northup, H., Krueger, D. A. (2013). Tuberous sclerosis complex diagnostic criteria update: recommendations of the 2012 International Tuberous Sclerosis Complex Consensus Conference. *Pediatr Neurol*, 49, 4, pp. 243-54. DOI: 10.1016/pediatrneurol.2013.08.001

Numis, A. L., Major, P., Montenegro, M. A., Muzykewicz, D. A., Pulsifer, M. B., Thiele, E. A. (2011). Identification of risk factors for autism spectrum disorders in tuberous sclerosis complex. *Neurology*, 76, 11, pp. 981-7. DOI: 10.1212/WNL.0b013e3182104347

O'Brien, K., Breyne, K., Ughetto, S., Laurent, L. C., Breakefield, X. O. (2020). RNA delivery by extracellular vesicles in mammalian cells and its applications. *Nat Rev Mol Cell Biol*, 21, 10, pp. 585-606. DOI: 10.1038/s41580-020-0251-y

O'Callaghan, F. J., Noakes, M. J., Martyn, C., N., Osborne, J. P. (2004). An epidemiological study of renal pathology in tuberous sclerosis complex. *BJU Intl*, 94, 6, pp. 853-7. DOI: 10.1111/j.1464-410X.2004.05046.x

Oggero, S., Austin-Williams, S., Norling, L. V. (2019). The contrasting role of extracellular vesicles in vascular inflammation and tissue repair. *Front Pharmacol*, 10, pp. 1479. DOI: 10.3389/fphar.2019.01479

Orlova, K. A., Crino, P. B. (2010). The tuberous sclerosis complex. *Ann N Y Acad Sci*, 1184, pp. 87-105. DOI: 10.1111/j.1749-6632.2009.05117.x

Oshlack, A., Wakefield, M. J. (2009). Transcript length bias in RNA-seq data confounds systems biology. *Biology Direct*, 4,14, pp. 1-10. DOI: 10.1186/1745-6150-4-14

Osborne, J. P., Jones, A. C., Burley, M. W., Jeganthan, D., Young, J., O'Callaghan, F. J., Sampson, J. R., Povey, S. (2000). Non-penetrance in tuberous sclerosis. *Lancet*, 355, 9216, pp. 1698. DOI: 10.1016/S0140-6736(00)02247-9

Ostenfeld, M. S., Jensen, S. G., Jeppesen, D. K., Christensen, L.-L., Thorsen, S. B., Stenvang, J., Hvam, M. L., Thomsen, A., Mouritzen, P., Rasmussen, M. H., Nielsen,

H. J., Ørntoft, T. F., Andersen, C. L. (2016). miRNA profiling of circulating EpCAM+ extracellular vesicles: promising biomarkers of colorectal cancer. *J Extracell Vesicles*, 5, pp. 31488. DOI:10.3402/jev.v5.31488

Ostrowski, M., Carmo, N. B., Krumeich, S., Fanget, I., Raposo, G., Savina, A., Moita, C. F., Schauer, K., Hume, A. N., Freitas, R. P., Goud, B., Benaroch, P., Hacohen, N., Fukuda, M., Desnos, C., Seabra, M. C., Darchen, F., Amigorena, S., Moita, L. F., Théry, C. (2010). Rab27a and Rab27b control different steps of the exosome secretion pathway. *Nat Cell Biol*, 12, 1, pp. 19-30. DOI: 10.1038/ncb2000

Overwater, I.E., Swenker, R., Ende, E.L., Hanemaayer, K.B., Hoogeveen-Westerveld, M., Eeghen, A.M., Lequin, M.H., Ouweland, A.V., Moll, H.A., Nellist, M., & Wit, M. (2016). Genotype and brain pathology phenotype in children with tuberous sclerosis complex. *Eur J Hum Genet, 24*, 1688-1695. DOI: 10.1038/ejhg.2016.85

Paez-Colasante, X., Figueroa-Romero, C., Sakowski, S. A., Goutman, S. A., Feldman, E. L. (2015). Amyotrophic lateral sclerosis: mechanisms and therapeutics in the epigenomic era. *Nat Rev Neurol*, 11, 5, pp. 266-79. DOI: 10.1038/nrneurol.2015.57

Pakravan, K., Babashah, S., Sadeghizadeh, M., Mowla, S. J., Mossahebi-Mohammedi, M., Ataei, F., Dana, N., Javan, M. (2017). MicroRNA-100 shuttled through mesenchymal stem cell-derived exosomes suppresses in vitro angiogenesis through modulating the mTOR/HIF-1α/VEGF signaling axis in breast

cancer cells. *Cell Oncol (Dordr)*, 40, 5, pp. 457-70. DOI: 10.1007/s13402-017-0335-7

Palviainen, M., Saraswat, M., Varga, Z., Kitka, D., Neuvonen, M., Puhka, M., Joenväärä, S., Renkonen, R., Nieuwland, R., Takatalo, M., Silijander, P. R. M. (2020). Extracellular vesicles from human plasma and serum are carriers of extravesicular cargo – implications for biomarker discovery. *PLoS One*, 15, 8, pp. 0236439. DOI: 10.1371/journal.pone.0236439

Pang, B., Zhu, Y., Ni, J., Thompson, J., Malouf, D., Bucci, J., Graham, P., Li, Y. (2020). Extracellular vesicles: the next generation of biomarkers for liquid biopsy-based prostate cancer diagnosis. *Theranostics*, 10, 5, pp. 2309-26. DOI: 10.7150/thno.39486

Pape, J., Magdeldlin, T., Stamati, K., Nyga, A., Loizidou, M., Emberton, M., Cheema, U. (2020). Cancer-associated fibroblasts mediate cancer progression and remodel the tumouroid stroma. *Br J Cancer,* 123, 7, pp. 1178-90. DOI: 10.1038/s41416-020-0973-9

Pardi, N., Hogan, M. J., Porter, F. W., Weissman, D. (2018). mRNA vaccines – a new era in vaccinology. *Nat Rev Drug Discov*, 17, 4, pp. 261-79. DOI: 10.1038/nrd.2017.243

Pardini, B., Sabo, A. A., Birolo, G., Calin, G. A. (2019). Noncoding RNAs in extracellular fluids as cancer biomarkers: the new frontier of liquid biopsies. *Cancers*, 11, 1170, pp. 1-52. DOI: 10.3390/cancers11081170

Pasini, L., Notarangelo, M., Vagheggini, A., Burgio, M. A., Crinò, L., Chiadini, E., Prochowski, A. I., Delmonte, A., Ulivi, P., D'Agostino, V. G. (2021). Unveiling mutational dynamics in non-small cell lung cancer patients by quantitative EGFR profiling in vesicular RNA. *Mol Oncol*, 15, 9, pp. 2423-38. DOI: 10.1002/1878-0261.12976

Patel, B., Patel, J., Cho,J.-H., Manne, S., Bonala, S., Henske, E., Roegiers, F., Markiewski, M., Karbowniczek, M. (2016). Exosomes mediate the acquisition of the disease phenotype by cells with normal genome in tuberous sclerosis complex. *Oncogene*, 35, 23, pp. 1-10. DOI: 10.1038/onc.2015.358

Pathan, M., Keerthikumar, S., Ang, C.-S., Gangoda, L., Quek, C. Y. J., Williamson, N. A., Mouradov, D., Sieber, O. M., Simpson, R. J., Salim, A., Bacic, A., Hill, A. F., Stroud, D. A., Ryan, M. T., Agbinya, J. I., Mariadason, J. M., Burgess, A. W., Mathivanan, S. (2015). FunRich: an open access standalone functional enrichment and interaction network analysis tool. *Proteomics*, 15, 15, pp. 2597-601. DOI: 10.1002/pmic.201400515

Peinado, H., Alečković, M., Lavotshkin, S., Matei, I., Costa-Silva, B., Moreno-Bueno, G., Hergueta-Redondo, M., Williams, C., García-Santos, G., Nitadori-Hoshino, A., Hoffman, C., Badal, K., Garcia, B. A., Callahan, M. K., Yuan, J., Martins, V. R.,

Skog, J., Kaplan, R. N., Brady, M. S., Wolchok, J. D., Chapman, P. B., Kang, Y., Bromberg, J., Lyden, D. (2012). Melanoma exosomes educate bone marrow progenitor cells toward a pro-metastatic phenotype through MET. *Nature Medicine*, 18, 6, pp. 883-91. DOI: 10.1038/nm.2753

Pérez-Gómez, E., Del Castillo, G., Francisco, S. J., López-Novoa, J. M., Bernabéu, C., Quintanilla, M. (2010). The role of the TGF-β coreceptor endoglin in cancer. *Scientific World Journal*, 14, 10, pp. 2367-84. DOI: 10.1100/tsw.2010.230

Phipson, B., Zappia, L., Oshlack, A. (2017). Gene length and detection bias in single cell RNA sequencing protocols. *F1000Res*, 6, 595, pp. 1-20. DOI: 10.12688/f1000research.11290.1

Pinno, J., Bongartz, H., Klepsch, O., Wundrack, N., Poli, V., Schaper, F., Dittrich, A. (2016). Interleukin06 influences stress-signalling by reducing the expression of the mTOR-inhibitor REDD1 in a STAT3-dependent manner. *Cell Signal*, 28, 8, pp. 907-16. DOI: 10.1016/j.cellsig.2016.04.004

Pomyen, Y., Segura, M., Ebbels, T. M., and Keun, H. C. (2015). Over-representation of correlation analysis (ORCA): a method for identifying associations between variable sets. *Bioinformatics,* 31, pp. 102–8. DOI: 10.1093/bioinformatics/btu589

Porstmann, T., Santos, C. R., Griffiths, B., Cully, M., Wu, M., Leevers, S., Griffiths, J. R., Chung, Y.-L., Schulze, A. (2008). SREBP activity is regulated by mTORC1

and contributes to Akt-dependent cell growth. *Cell Metab*, 8, 3, pp. 224-36. DOI: 10.1016/j.cmet.2008.07.007

Pradilla, M. J. B., Ballesté, T. M., Torra, R., Aubá, F. V. (2017). Recommendations for imaging-based diagnosis and management of renal angiomyolipoma associated with tuberous sclerosis complex. *Clin Kidney J*, 10, 6, pp. 728-37. DOI: 10.1093/ckj/sfx094

Prieto-Vila, M., Yoshioka, Y., Ochiya, T. (2021). Biological functions driven by mRNAs carried by extracellular vesicles in cancer. *Front Cell Dev Biol*, 9, pp. 620498. DOI: 10.3389/fcell.2021.620498

Radzikowska, E., Jaguś,P., Sobiecka, M., Chorostowska-Wynimko, J., Wiatr, E., Kuś, J., Roszkowski-Śliź, K. (2015). Correlation of serum vascular endothelial growth factor-D concentration with clinical presentation and course of lymphangioleiomyomatosis. *Respir Med*, 109, 11, pp. 1469-75. DOI: 10.1016/j.rmed.2015.09.005

Raiboug, C., Stenmark, H. (2009). The ESCRT machinery in endosomal sorting of ubiquitylated membrane proteins. *Nature*, 458, 7237, pp. 445-52. DOI: 10.1038/nature07961

Raimondo, F., Morosi, L., Corbetta, S., Chinello, C., Brambilla, P., Della Mina, P., Villa, A., Albo, G., Battaglia, C., Bosari, S., Magni, F., (2013). Differential protein

profiling of renal cell carcinoma urinary exosomes. *Molecular BioSystems*, *9*, 6, pp.1220-33. DOI: 10.1039/c3mb25582d

Rakowski, S. K., Winterkorn, E. B., Paul, E., Steele, D. J. R., Halpern, E. F., Thiele, E. A. (2006). Renal manifestations of tuberous sclerosis complex: incidence, prognosis, and predictive factors. *Kidney Int*, 70, 10, pp. 1777-82. DOI: 10.1038/sj.ki.5001853

Raposo, G., Nijman, H. W., Stoorvogel, W., Liejendekker, R., Harding, C. V., Melief, C. J., Gueze, H. J. (1996). B lymphocytes secrete antigen-presenting vesicles. *J Exp Med*, 183, 3, pp. 1161-72. DOI: 10.1084/jem.183.3.1161

Raposo, G., Stoorvogel, W. (2013). Extracellular vesicles: exosomes, Microvesicles, and friends. *J Cell Biol*., 200(4), pp. 373-83. DOI: 10.1083/jcb.201211138

Ratajczak, J., Miekus, K., Kucia, M., Zhang, J., Reca, R., Dvorak, P., Ratajczak, M. Z. (2006). Embryonic stem cell-derived Microvesicles reprogram hematopoietic progenitors: evidence for horizontal transfer of mRNA and protein delivery. *Leukemia*, 20, 5, pp. 847-56. DOI: 10.1038/sj.leu.2404132

Reimand, J., Isser, R., Voisin, V., Kucera, M., Tannus-Lopes, C., Rostamianfar, A., Wadi, L., Meyer, M., Wong, J., Xi, C., Merico, D., Bader, G. D. (2019). Pathway enrichment analysis and visualisation of omics data using g:Profiler, GSEA, Cytoscape and EnrichmentMap. *Nat Protoc*, 14, 2, pp. 482-517. DOI: 10.1038/s41596-018-0103-9

Riches, A., Campbell, E., Borger, E., Powis, S. (2014). Regulation of exosome release from mammary epithelial and breast cancer cells – a new regulatory pathway. *Eur J Cancer*, 50, 5, pp. 1025-34. DOI: 10.1016/j.ejca.2013.12.019

Ritchie, W., Rasko, J. E. J., Flamant, S. (2013). MicroRNA target prediction and validation. *MicroRNA Cancer Regulation: Advanced Concepts, Bioinformatics and Systems Biology Tools*. pp. 39-53.

Rizzuti, M., Filosa, G., Melzi, V., Calandriello, L., Dioni, L., Bollati, V., Bresolin, N., Comi, G. P., Barabino, S., NIzzardo, M., Corti, S. (2018). MicroRNA expression analysis identifies a subset of downregulated miRNAs in ALS motor neuron progenitors. *Sci Rep*, 8, 1, pp. e10105. DOI: 10.1038/s41598-018-28366-1

Roach, E. S., Gomez, M. R., Northup, H. (1998). Tuberous sclerosis complex consensus conference: revised clinical diagnostic criteria. *J Child Neurol*, 13, 12, pp. 624-8. DOI: 10.1177/088307389801301206

Ronchetti, D., Lionetti, M., Mosca, L., Agnelli, L., Andronache, A., Fabris, S., Deliliers, G. L., Neri, A. (2008). An integrative genomic approach reveals coordinated expression of intronic miR-335, miR-342, and miR-561 with deregulated host genes in multiple myeloma. *BMC Med Genomics*, 1, 37, pp. 1-9. DOI: 10.1186/1755-8794-1-37

Rong, Y., Liu, W., Wang, J., Fan, J., Luo, Y., Li, L., Kong, F., Chen, J. Tang, P., Cai, W. (2016). Neural stem cell-derived small extracellular vesicles attenuate apoptosis and neuroinflammation after traumatic spinal cord injury by activating autophagy. *Cell Death Dis*, 10, 5, pp. 340. DOI: 10.1038/s41419-019-1571-8

Rosset, C., Netto, C. B. O., Ashton-Prolla, P. (2017). *TSC1* and *TSC2* gene mutations and their implications for treatment in tuberous sclerosis complex: a review. (2017). *Genet Mol Biol*, 10, 1, pp. 69-79. DOI: 10.1590/1678-4685-GMB-2015-0321

Rosset, C., Vairo, F., Bandeira, I. C., Correia, R. L., de Goes, F. V., da Silva, R. T., Bueno, L. S. M., de Miranda Gomes, M. C. S., de Campos Reis Galvão, H., Neri, J. I. C. F., Achatz, M. I., Netto, C. B. O., Ashton-Prolla, P. (2017). Molecular analysis of TSC1 and TSC2 genes and phenotypic correlations in Brazilian families with tuberous sclerosis. *PLoS One*, 12, 10, pp. 185713. DOI: 10.1371/journal.pone.0185713

Roux, P. P., Ballif, B. A., Anjum, R., Gygi, S. P., Blenis, J. (2004). Tumor-promoting phorbol esters and activated Ras inactivate the tuberous sclerosis tumor suppressor complex via p90 ribosomal S6 kinase. *Proc Natl Acad Sci USA,* 101, 37, pp. 13489-94. DOI: 10.1073/pnas.0405659101

Ruiz-Orera, J., Messeguer, X., Subirana, J. A., Mar Alba, M. (2014). Long non-coding RNAs as a source of new peptides. *Elife*, 3, pp. e03523. DOI: 10.7554/eLife.03523

Ryskalin, L., Biagioni, F., Lenzi, P., Frati, A., Fornai, F. (2020). mTOR modulates intercellular signals for enlargement and infiltration in glioblastoma multiforme. *Cancers (Basel),* 12, 9, pp. 1-21. DOI: 10.3390/cancers12092486

Šabanović, B., Piva, F., Cecati, M., Giulletti, M. (2021). Promising extracellular vesicle-based vaccines against viruses, including SARS-CoV-2. *Biology*, 10, 2, pp. 1-14. DOI: 10.3390/biology10020094

Sadovska, L., Eglïtis, J., Linë, A. (2015). Extracellular vesicles as biomarkers and therapeutic targets in breast cancer. *Anticancer Res*, 35, 12, pp. 6379-90. PMID: 26637847

Sahai, E., Astsaturov, I., Cukierman, E., DeNardo, D. G., Egeblad, M., Evans, R. M., Fearon, D., Greten, F. R., Hingorani, S. R., Hunter, T., O Hynes, R., Jain, R. K., Janowitz, T., Jorgensen, C., Kimmelman, A. C., Kolonin, M. G., Maki, R. G., Scott Powers, R., Puré, E., Ramirez, D. C., Scherz-Shouval, R., Sherman, M. H., Stewart, S., Tlsty, T. D., Tuveson, D. A., Watt, F. A., Weaver, V., Weeraratna, A. T., Werb, Z. (2020). A framework for advancing our understanding of cancer-associated fibroblasts. *Nat Rev Cancer*, 20, 3, pp. 174-86. DOI: 10.1038/s41568-019-0238-1

Sampson, J. R., Maheshwar, M. M., Aspinwall, R., Thompson, P., Cheadle, J. P., Ravine, D., Roy, S., Haan, E., Bernstein, J., Harris, P. C. (1997). Renal cystic disease in tuberous sclerosis: role of the polycystic kidney disease 1 gene. *Am J Hum Genet*, 61, 4, pp. 843-51. DOI: 10.1086/514888

Samueli, S., Abraham, K., Dressler, A., Groeppel, G., Jonak, C., Muehlebner, A., Prayer, D., Reitner, A., Feucht, M., Pädiatrisches TSC-Zentrum Wien. (2015). Tuberous sclerosis complex: new criteria for diagnostic work-up and management. *Wein Klin Wochenschr*, 127, 15-16, pp. 619-30. DOI: 10.1007/s00508-015-0758-y

Sancak, O., Nellist, M., Goedbloed, M., Elfferich, P., Wouters, C., Maat-Kievet, A., Zonnenberg, B., Verhoef, S., Halley, D., van den Ouweland, A. (2005). Mutational analysis of the TSC1 and TSC2 genes in a diagnostic setting: genetype-phenotype correlations and a comparison of diagnostic DNA techniques in Tuberous Sclerosis Complex. *Eur J Hum Genet*, 13, 6, pp. 731-41. DOI: 10.1038/sj.ejhg.5201402

Sánchez-Elsner, T., Botella, L. M., Velasco, B., Langa, C., Bernabéu, C. (2002). Endoglin expression is regulated by transcriptional cooperation between the hypoxia and transforming growth factor-beta pathways. *J Biol Chem*, 277, 46, pp. 43799-808. DOI: 10.1074/jbc.M207160200

Sangüesa, G., Roglans, N., Baena, M., Velázquez, A. M., Laguna, J. C., Alegret, M. (2019). mTOR is a key protein involved in the metabolic effects of simple sugars. *Int J Mol Sci*, 20, 5, pp. e1117. DOI: 10.3390/ijms20051117

Santangelo, L., Giurato, G., Cicchini, C., Montaldo, C., Mancone, C., Tarallo, R., Battistelli, C., Alonzi, T., Weisz, A., Tripodi, M. (2016). The RNA-binding protein SYNCRIP is a component of the hepatocyte exosomal machinery controlling microRNA sorting. *Cell Rep*, 17, 3, pp. 799-808. DOI: 10.1016/j.celrep.2016.09.031

Santiago Lima, A.J., Hoogeveen-Westerveld, M., Nakashima, A., Maat-Kievet, A., van den Ouweland, A., Halley, D., Kikkawa, U., Nellist, M. (2014). Identification of regions critical for the integrity of the TSC1-TSC2- TBC1D7 complex. *PLoS One*, 9, 4, pp. 1-13. DOI: 10.1371/journal.pone.0093940

Saxton, R. A., Sabatini, D. M. (2017). mTOR signaling in growth, metabolism, and disease. *Cell*, 168, 6, pp. 960-76. DOI: 10.1016/j.cell.2017.02.004

Schenone, S., Brullo, C., Musumeci, F., Radi, M., Botta, M. (2011). ATP-competitive inhibitors of mTOR: an update. *Curr Med Chem*, 18, 20, pp. 2995-3014. DOI: 10.2174/092986711796391651

Schrötter, S., Yuskaitis, C. J., MacArthur, M. R., Mitchell, S. J., Hosios, A. M., Osipovich, M., Torrence, M. E., Mitchell, J. R., Hoxhaj, G., Sahin, M., Manning, B. (2022). The non-essential TSC complex component TBC1D7 restricts tissue mTORC1 signaling and brain and neuron growth. *Cell Reports*, 39, 7, pp. 110824. DOI: 10.1016/j.celrep.2022.110824

Seront, E., Pinto, A., Bouzin, C., Bertrand, L., Machiels, J.-P., Feron, O. (2013). PTEN deficiency is associated with reduced sensitivity to mTOR inhibitor in human bladder cancer through unhampered feedback loop driving PI3K/Akt activation. *Br J Cancer*, 109, 6, pp. 1584-92. DOI: 10.1038/bjc.2013.505

Sezgin, E., Levental, I., Mayor, S., Eggeling, C. (2017). The mystery of membrane organisation: composition, regulation and physiological relevance of lipid rafts. *Nat Rev Mol Cell Biol*, 18, 6, pp. 361-74. DOI: 10.1038/nrm.2017.16

Shaw, R., Bardeesy, N., Manning, B. D., Lopez, L., Kosmatka, M., DePinho, R. A., Cantley, L. C. (2004). The LKB1 tumor suppressor negatively regulates mTOR signaling. *Cancer Cell*, 6, 1, pp. 91-99. DOI: 10.1016/j.ccr.2004.06.007

Sheldon, I. M., Roberts, M. H. (2010). Toll-like receptor 4 mediates the response of epithelial and stromal cells to lipopolysaccharide in the endometrium. *PLoS One*, 5, 9, pp. e12906. DOI: 10.1371/journal.pone.0012906

Shen, X., Ye, Y., Qi, J., Shi, W., Wu, X., Ni, H., Cong, H., Ju, S. (2016). Identification of a novel microRNA, miR-4449, as a potential blood based marker in multiple myeloma. *Clin Chem Lab Med*, 55, 5, pp. 1-12. DOI: 10.1515/cclm-2015-1108

Shephard, A. P., Giles, P., Mbengue, M., Alraies, A., Spary, L. K., Kynaston, H., Gurney, M. J., Falcón-Pérez, J. M., Royo, F., Tabi, Z., Parthimos, D., Errington, R. J., Clayton, A., Webber, J. P. (2021). Stromal-derived extracellular vesicle mRNA signatures inform histological nature of prostate cancer. *J Extracell Vesicles*, 10, 12, pp. e12150. DOI: 10.1002/jev2.12150

Shepherd, C. W., Gomez, M. R., Lie, J. T., Crowson, C. S. (1991). Causes of death in patients with tuberous sclerosis. *Mayo Clin Proc*, 66, 8, pp. 792-6. DOI: 10.1016/s0025-6196(12)61196-3

Shu, H. F., Zhang, C. Q., Yin, Q., An, N., Liu, S. Y., Yang, H. (2010). Expression of the interleukin 6 system in cortical lesions from patients with tuberous sclerosis complex and focal cortical dysplasia type IIb. *J Neuropathol Exp Neurol*, 69, 8, pp. 838-49. DOI: 10.1097/NEN.0b013e3181eaeae5

Shurtleff, M. J., Temoche-Diaz, M. M., Karfilis, K. V., Ri, S., Schekman, R. (2016). Y-box protein 1 is required to sort microRNAs into exosomes in cells and in a cell-free reaction. *Elife*, 5, pp. 19276. DOI: 10.7554/eLife.19276

Sinha, S., Hoshino, D., Hong, N. H., Kirkbride, K. C., Grega-Larson, N. E., Seiki, M., Tyska, M. J., Weaver, A. M. (2016). Cortactin promotes exosome secretion by controlling branched actin dynamics. *J Cell Biol*, 214, 2, pp. 197-213. DOI: 10.1083/jcb.201601025

Siroky, B. J., Yin, H., Babcock, J. T., Lu, L., Hellmann, A. R., Dixon, B. P., Quilliam, L. A., Bissler, J. J. (2012). Human TSC-associated renal angiomyolipoma cells are hypersensitive to ER stress. *Am J Physiol Renal Physiol*, 303, 6, pp. 831-44. DOI: 10.1152/ajprenal.00441.2011

Skog, J., Würdinger, T., van Rijn, S., Meijer, D. H., Gainche, L., Sena-Esteves, M., Curry, W. T., Carter, B. S., Krichevsky, A. M., Breakefield, X. O. (2008).

Glioblastoma Microvesicles transport RNA and proteins that promote tumour growth and provide diagnostic biomarkers. *Nat Cell Biol*, 10, pp. 1470-6. DOI: 10.1038/ncb1800

Schmidt, O., Teis, D. (2012). The ESCRT machinery. *Curr Biol*, 22, 4, pp. 116-20. DOI: 10.1016/j.cub.2012.01.028

Sokolova, V., Ludwig, A.-K., Hornung, S., Rotan, O., Horn, P. A., Epple, M., Giebel, B. (2011). Characterisation of exosomes derived from human cells by nanoparticle tracking analysis and scanning electron microscopy. *Colloids Surf B Biointerfaces*, 87, 1, pp. 146-50. DOI: 10.1016/j.colsurfb.2011.05.013

Sonenberg, N., Gingras, A.-C. (1998). The mRNA 5' cap-binding protein eIF4E and control of cell growth. *Curr Opin Cell Biol*, 10, 2, pp. 268-75. DOI: 10.1016/S0955-0674(98)80150-6

Statello, L., Guo, C.-J., Chen, L.-L., Huarte, M. (2021). Gene regulation by long non-coding RNAs and its biological functions. *Nat Rev Mol Cell Biol*, 22, 2, pp. 96-118. DOI: 10.1038/s41580-020-00315-9

Stone, C. H., Lee, M. W., Amin, M. B., Yaziji, H., Gown, A. M., Ro, J. Y., Têtu, B., Paraf, F., Zarbo, R. J. (2001). Renal angiomyolipoma: further immunophenotypic characterisation of an expanding morphologic spectrum. *Arch Pathol Lab Med*, 125, 6, pp. 751-8. DOI: 10.5858/2001-125-0751-RA

Stoorvogel, W., Strous, G. J., Geuze, H. J., Oorschot, V., Schwartzt, A. L. (1991). Late endosomes derive from early endosomes by maturation. *Cell*, 65, 3, pp. 417-27. DOI: 10.1016/0092-8674(91)90459-C

Südhof, T. C., Rothman, J. E. (2009). Membrane fusion: grappling with SNARE and SM proteins. *Science*, 323, 5912, pp. 474-77. DOI: 10.1126/science.1161748

Szczepanski, M. J., Szajnik, M., Welsh, A., Whiteside, T. L., Boyiadzis, M. (2011). Blast-derived Microvesicles in sera from patients with acude myeloid leukemia suppress natural killer cell function via membrane-associated transforming growth factor-β1. *Haematologica*, 96, 9, pp. 1-8. DOI: 10.3324/haematol.2010.039743

Tee, A. R., Manning, B. D., Roux, P. P., Cantley, L. C., Blenis, J. (2003). Tuberous sclerosis complex gene products, tuberin and hamartin, control mTOR signaling by acting as a GTPase-activating protein complex toward Rheb. *Curr Biol*, 13, 15, pp. 1259-68. DOI: 10.1016/S0960-9822(03)00506-2

Teng, F., Fussenegger, M. (2021). Shedding light on extracellular vesicle biogenesis and bioengineering. *Adv Sci*, 8, 1, pp. 2003505. DOI: 10.1002/advs.202003505

Terlecki-Zaniewicz, L., Lümmermann, I., Latreille, J., Bobbili, M. R., Pils, V., Schosserer, M., Weinmüllner, R., Dellago, H., Skalicky, S., Pum, D., Carlos, J., Almaraz, H., Scheideler, M., Morizot, F., Hackl, M., Gruber, F., Grillari, J. (2018). Small extracellular vesicles and their miRNA cargo are anti-apoptotic members of

the senescence-associated secretory phenotype. *Aging (Albany NY),* 10, 5, pp. 1103-32. DOI: 10.18632/aging.101452

The AACR Project GENIE Consortium. (2017). AACR Project GENIE: powering precision medicine through an international consortium. *Cancer Discov*, 7, 8, pp. 818-31. DOI: 10.1158/2159-8290.CD-17-0151

Théry, C., Amigorena, S., Raposo, G., Clayton, A. (2006). Isolation and characterization of exosomes from cell culture supernatants and biological fluids. *Curr Prot Cell Biol*, 30, 3.22.1-3.22.29. DOI: 10.1002/0471143030.cb0322s30

Théry, C., Witwer, K. *et al.* (2018). Minimal information for studies of extracellular vesicles 2018 (MISEV2018): a position statement of the International Society for Extracellular Vesicles and update of the MISEV2014 guidelines. *J Extracell Vesicles*, 8, 1, pp. e1535750. DOI: 10.1080/20013078.2018.1535750

Tian, L., Guo, Z., Wang, H., Liu, X. (2017). MicroRNA-635 inhibits the malignancy of osteosarcoma by inducing apoptosis. *Mol Med Rep,* 16, 4, pp. 4829-34. DOI: 10.3892/mmr.2017.7127

Tian, H., Huang, J. J., Golzio, C., Gao, X., Hector-Greene, M., Katsanis, N., Blobe, G. C. (2018). Endoglin interactis with VEGFR2 to promote angiogenesis. *FASEB J*, 32(6), pp. 2934-49. DOI: 10.1096/fj.201700867RR

Tomasetti, M., Lee, W., Santarelli, L., Neuzil, J. (2018). Exosome-derived microRNAs in cancer metabolism: possible implications in cancer diagnostics and therapy. *Exp Mol Med*, 49, 1, pp. 285. DOI: 10.1038/emm.2016.153

Tomczak, A., Mortensen, J.M., Winnenburg, R., Liu, C., Alessi, D.T., Swamy, V., Vallania, F., Lofgren, S., Haynes, W., Shah, N.H. and Musen, M.A., 2018. Interpretation of biological experiments changes with evolution of the Gene Ontology and its annotations. *Scientific reports*, *8*, 1, pp.1-10. DOI: 10.1038/s41598-018-23395-2

Tong, X., Yang, Z., Wang, Q., Zhang, D. (2021). RNF144A-AS1 promotes the development of glioma cells by targeting miR-665/HMGA1 axis. *Neurosci Lett*, 765, e136259. DOI: 10.1016/j.neulet.2021.136259

Trajkovic, K., Hsu, C., Chiantia, S., Rajendran, L., Wenzel, D., Wieland, F., Schwille, P., Brügger, B., Simons, M. (2008). Ceramide triggers budding of exosome vesicles into multivesicular endosomes. *Science*, 319, 5867, pp. 1244-7. DOI: 10.1126/science.1153124

Trams, E. G., Lauter, C. J., Salem, N. Jr., Heine, U. (1981). Exfoliation of membrane ecto-enzymes in the form of micro-vesicles. *Biochim Biophys Acta*, 645, 1, 63-70. DOI: 10.1016/0005-2736(81)90512-5

Treichel, A. M., Hamieh, L., Nathan, N. R., Tyburczy, M. E., Wang, J.-A., Oyerinde, O., Raiciulescu, S., Julien-Williams, P., Jones, A. M., Gopalakrishnan, V., Moss, J.,

Kwiatkowski, D. J., Darling, T. N. (2019). Phenotypic distinctions between mosaic forms of tuberous sclerosis complex. *Genet Med*, 21, 11, pp. 2594-604. DOI: 10.1038/s41436-019-0520-3

Trelinska, J., Fendler, W., Dachowska, I., Kotulska, K., Kozwiak, S., Antosik, K., Gnys, P., Borowiec, M., Mlynarski, W. (2016). Abnormal serum microRNA profiles in tuberous sclerosis are normalised during treatment with everolimus: possible clinical implications. *Orphanet J Rare Dis*, 11, 1, pp. e129. DOI: 10.1186/s13023-016-0512-1

Trinh, X. B., Tjalma, W. A. A., Vermeulen, P. B., van den Eynden, G., van der Auwera, I., van Laere, S. J., Helleman, J., Berns, E. M. J. J., Dirix, L. Y., van Dam, P. A. (2009). The VEGF pathway and the AKT/mTOR/p70S6K1 signalling pathway in human epithelial ovarian cancer. *Br J Cancer*, 100, 6, pp. 971-8. DOI: 10.1038/sj.bjc.6604921

Truffi, M., Mazzucchelli, S., Bonizzi, A., Sorrentino, L., Raffaele, A., Vanna, R., Morasso, C., Corsi, F. (2019). Nano-strategies to target breast cancer-associated fibroblasts: rearranging the tumour microenvironment to achieve antitumor efficacy. *Int J Mol Sci*, 20, 6, pp. 1263. DOI: 10.3390/ijms20061263

Turchinovich, A., Drapkina, O., Tonevitsky, A. (2019). Transcriptome of extracellular vesicles: state-of-the-art. *Front Immunol*, 10, 202, pp. 1-13. DOI: 10.3389/fimmu.2019.00202

Tutrone, R., Donovan, M. J., Torkler, P., Tadigotla, V., McLain, T., Noerholm, M., Skog, J., McKiernan, J. (2020). Clinical utility of the exosome based ExoDx Prostate(IntelliScore) EPI test in men presenting for initial biopsy with a PSA 2-10 ng/mL. *Prostate Cancer Prostatic Dis*, 23, 4, pp. 607-14. DOI: 10.1038/s41391-020-0237-z

Tyburczy, M. E., Dies, K. A., Glass, J., Camposano, S., Chekaluk, Y., Thorner, A. R., Lin, L., Krueger, D., Franz, D. N., Thiele, E. A. Sahin, M., Kwiatkowski, D. J. (2015). Mosaic and intronic mutations in TSC1/TSC2 explain the majority of TSC patients with no mutation identified by conventional testing. *PLoS Genet*, 11, 11, pp. 1-17. DOI: 10.1371/journal.pgen.1005637

UniProt Consortium (2010). Ongoing and future developments at the Universal Protein Resource. *Nucleic Acids Res*, 39, pp. 214-9. DOI: 10.1093/nar/gkq1020

Usman, W. M., Pham, T. C., Kwok, Y. Y., Vu, L. T., Ma, V., Peng, B., Chan, Y. S., Wi, L., Chin, S. M., Azad, A., He, A. B.-L., Leung, A. Y. H., Yang, M., Shyh-Chang, N., Cho, W. C., Shi, J., Le, M. T. N. (2018). Efficient RNA drug delivery using red blood cell extracellular vesicles. *Nat Commun*, 9, 1, pp. e2359. DOI: 10.1038/s41467-018-04791-8

Valadi., H., Ekström, K., Bossios, A., Sjöstrand, M., Lee, J. J., Lötvall, J. O. (2007). Exosome-mediated transfer of mRNAs and microRNAs is a novel mechanism of genetic exchange between cells. *Nat Cell Biol*, 9, pp. 654-9. DOI: 10.1038/ncb1596

van Deun, J., Mestdagh, P., Agostinis, P., Akay, Ö, Anand, S., Anckaert, J., Martinez, Z. A., Baetens, T., Beghein, E., Bertier, L., Berx, G., Boere, J., Boukouris, S., Bremer, M., Buschmann, D., Byrd, J. B., Casert, C., Cheng, L., Cmoch, A., Daveloose, D., de Smedt, E., Demirsoy, S., Depoorter, V., Dhondt, B., Driedonks, T., Dudek, A., Elsharawy, A., Floris, I., D'Foers, A., Gärtner, K., Garg, A. D., Geeurickx, E., Gettemans, J., Ghazavi, F., Giebel, B., Kormelink, T. G., Hancock, G., Helsmoortel, H., Hill, A. F., Hyenne, V., Kalra, H., Kim, D., Kowal, J., Kraemer, S., Leidinger, P., Leonelli, C., Liang, Y., Lippens, L., Liu, S., Cicero, A. L., Martin, S., Mathivanan, S., Pathiyalagan, P., Matusek, T., Milani, G., Monguio-Tortajada, M., Mus, L. M., Muth, D. C., Németh, A., Nolte-'t Hoen, E. N. M., O'Driscoll, L., Palmulli, R., Pfaffl, M. W., Primdal-Bengtson, B., Romano, E., Rousseau, Q. Sahoo, S., Sampaio, N., Samuel, M., Scicluna, B., Soen, B., Steels, A., Swinnen, J. V., Takatalo, M., Thaminy, S., Théry, C., Tulkens, J., van Audenhove, I., van der Grein, S., van Goethem, A., van Herwijnen, M., van Niel, G., van Roy, N., van Vilet, A. R., Vandamme, N., Vanhauwaert, S., Vergauwen, G., Verweij, F., Wallaert, A., Wauben, M., Witwer, K. W., Zonneveld, M. I., de Wever, O., Vandesompele, J., Hendrix, A., EV-TRACK Consortium (2017). EV-TRACK: transparent reporting and centralising knowledge in extracellular vesicle research. *Nat Methods*, 14, 3, pp. 228-32. DOI: 10.1038/nmeth.4185

van Niel, G., D'Angelo, G., Raposo, G. (2018). Shedding light on the cell biology of extracellular vesicles. *Nat Rev Mol Cell Biol*, 19, 4, pp. 213-28. DOI: 10.1038/nrm.2017.125

van Scheppingen, J., Mills, J. D., Zimmer, T. S., Broekaart, D. W. M., Iori, V., Bongaarts, A., Anink, J. J., Iyer, A. M., Korotkov, A., Jansen, F. E., van Hecke, W., Spliet, W. G., van Rijen, P. C., Baayen, J. C., Vezzani, A., van Vliet, E. A., Aronica, E. (2018). miR147b: a novel key regulatory of interleukin 1 beta-mediated inflammation in human astrocytes. *Glia*, 66, 5, pp. 1082-97. DOI: 10.1002/glia.23302

van Slegtenhorst, M., deHoogt R., Hermans, C., Nellist, M., Janssen, B., Verhoef, S., Lindhout, D., van den Ouweland, A., Halley, D., Young, J., Burley, M., Jeremiah, S., Woodward, K., Nahmias, J., Fox, M., Ekong, R., Osborne, J., Wolfe, J., Povey, S., Snell, R. G., Cheadle, J. P., Jones, A. C., Tachataki, M., Ravine, D., Sampson, J. R., Reeve, M. P., Richardson, P., Wilmer, F., Munro, C., Hawkins, T. L., Sepp, T., Ali, J. B., Ward, S., Green, A. J., Yates, J. R., Kwiatkowska, J. K., Henske, E. P., Short, M. P., Haines, J. H., Jozwiak, S., Kwiatkowski, D. J. (1997). Identification of the tuberous sclerosis gene TSC1 on chromosome 9q34. *Science*, 277, 5327, pp. 805-8. DOI: 10.1126/science.277.5327.805

Vaughan, R. M., Kordich, J. J., Chan, C.-Y., Sasi, N. K., Celano, S. L., Sisson, K. A., van Baren, M., Kortus, M. G., Aguiar, D. J., Martin, K. R., MacKeigan, J. P. (2022). Chemical biology screening identifies a vulnerability to checkpoint kinase inhibitors in TSC2-deficient renal angiomyolipomas. *Front Oncol*, 12, pp. e85859. DOI: 10.3389/fonc.2022.852859

Verkoef, S., Vrtel, R., van Essen, T., Bakker, L., Sikkens, E., Halley, D., Lindhout, D., van den Ouweland, A. (1995). Somatic Mosaicism and clinical variation in

tuberous sclerosis complex. *Lancet*, 345, 8943, pp. 202. DOI: 10.1016/s0140-6736(95)90213-9

Verweij, F. J., Bebelman, M. P., Jimenez, C. R., Garcia-Vallejo, J. J., Janssen, H., Neefjes, J., Knol, J. C., de Goeij-Haas, R., Piersma, S. R., Baglio, S. R., Verhage, M., Middeldorp, J. M., Zomer, A., van Rheenen, J., Coppolino, M. G., Hurbain, I., Raposo, G., Smit, M. J., Toonen, R. F. G., van Niel, G., Pegtel, D. M. (2018). Quantifying exosome secretion from single cells reveals a modulatory role for GPCR signaling. *J Cell Biol*, 217, 3, pp. 1129-42. DOI: 10.1083/jcb.201703206

Verwer, E. E., Kavanagh, T. R., Mischler, W. J., Feng, Y., Takahashi, K., Wang, S., Shoup, T. M., Neelamegam, R., Yang, J., Gueli, N. J., Ran, C., Massefski, W., Cui, Y., El-Chemaly, S., Sadow, P. M., Oldham, W. M., Kijewski, M., El Fakhri, G., Normandin, M. D., Priolo, C. (2018). [^{18}F]Fluorocholine and [^{18}F]Fluoroacetate PET as imaging biomarkers to assess phosphatidylcholine and mitochondrial metabolism in preclinical models of TSC and LAM. *Clin Cancer Res*, 24, 23, pp. 5925-38. DOI: 10.1158/1078-0432.CCR-17-3693

Veziroglu, E. M., Mias, G. I. (2020). Characterising extracellular vesicles and their diverse RNA contents. *Front Genet*, 11, pp. 700. DOI: 10.3389/fgene.2020.00700

Vickers, K. C., Palmisano, B. T., Shoucri, B. M., Shamburek, R. D., Remaley, A. T. (2011). MicroRNAs are transported in plasma and delivered to recipient cells by high-density lipoproteins. *Nat Cell Biol*, 13, 4, pp. 423-33. DOI: 10.1038/ncb2210

Vickers, K. C., Remaley, A. T. (2012). Lipid-based carriers of microRNAs and intercellular communication. *Curr Opin Lipidol*, 23, 2, pp. 91-7. DOI: 10.1097/MOL.0b013e328350a425

Villorroya-Beltri, C., Gutiérrez-Vázquez, C., Sánchez-Cabo, F., Pérez-Hernández, D., Vázquez, J., Martin-Cofreces, N., Martinez-Herrera, D., Pascual-Montano, A., Mittelbrunn, M., Sánchez-Madrid, F. (2013). Sumoylated hnRNPA2B1 controls the sorting of miRNAs into exosomes through binding of specific motifs. *Nat Commun*, 4, pp. 2980. DOI: 10.1038/ncomms3980

Vizin, T., Kos, J. (2015). Gamma-enolase: a well-known tumour marker, with a less-known role in cancer. *Radiol Oncol*, 49, 3, pp. 217-26. DOI: 10.1515/raon-2015-0035

Vos, N., Oyen, R. (2019). Renal angiomyolipoma: the good, the bad, and the ugly. *J Belgian Soc Radiol*, 102, 1, pp. e41. DOI: 10.5334/jbsr.1536

Walkup, L. L., Roach, D. J., Hail, C. S., Gupta, N., Thomen, R. P., Cleveland, Z. I., McCormack, F. X., Woods, J. C. (2019). Cyst ventilation heterogeneity and alveolar airspace dilation as early disease markers in lymphangioleiomyomatosis. *Ann Am Thoras Soc*, 16, 8, pp. 1008-16. DOI: 10.1513/AnnalsATS.201812-880OC

Wang, Z., Gerstein, M., Snyder, M. (2009). RNA-Seq: A revolutionary tool for transcriptomics. *Nat Reviews Genetics*. 10, 1, pp. 57-63. DOI: 10.1038/nrg2484

Wang, B., Shi, L., Sun, X., Wang, L., Wang, X., Chen, C. (2016). Production of CCL20 from lung cancer cells induces the cell migration and proliferation through PI3K pathway. *J Cell Mol Med*, 20, 5, pp. 920-9. DOI: 10.1111/jcmm.12781

Wang, Y., Yang, X., Li, J., Li, P., Zhao, Y., Duan, W., Chen, Y., Wang, Y., Mao, H., Wang, C. (2020). A nomogram combining long non-coding RNA expression profiles and clinical factors predicts survival in patients with bladder cancer. *Aging*, 12, 3, pp. 2857-79. DOI: 10.18632/aging.102782

Wang, J., Filippakis, H., Hougard, T., Du, H., Ye, C., Liu, H.-J., Zhang, L., Hindi, K., Bagwe, S., Nijmeh, J., Asara, J. M., Shi, W., El-Chemaly, S., Henske, E. P., Lam, H. C. (2021). Interleukin06 mediates PSAT1 expression and serine metabolism in TSC2-deficient cells. *Proc Natl Acad Sci U S A*, 118, 39, pp. e2101268118. DOI: 10.1073/pnas.2101268118

Wang, Q.-G., Cheng, B. C.-Y., He, Y.-Z., Li, L.-J., Ling, Y., Luo, G., Wang, L., Liang, S., Zhang, Y. (2021). miR-320a in serum exosomes promotes myocardial fibroblast proliferation via regulating the PIK3CA/Akt/mTOR signaling pathway in HEH2 cells. *Exp Ther Med*, 22, 2, pp. 873. DOI: 10.3892/etm.2021.10305

Wang, W., Li, J., Lin, F., Guo, J., Zhao, J. (2021). Identification of N^6-methyladenosine-related lncRNAs for patients with primary glioblastoma. *Neurosurg Rev*, 44, pp. 463-70. DOI: 10.1007/s10143-020-01238-x

Wataya-Kaneda, M., Tanaka, M., Hamasaki, T., Katayama, I. (2013). Trends in the prevalence of tuberous sclerosis complex manifestations: an epidemiological study of 166 Japanese patients. *PLoS One*, 8, 5, pp. 63910. DOI: 10.1371/journal.pone.0063910

Webb, D. W., Osborne, J. P. (1991). Non-penetrance in tuberous sclerosis. *J Med Genet*, 28, 6, pp. 417-9. DOI: 10.1136/jmg.28.6.417

Webber, J., Steadman, R., Mason, M. D., Tabi, Z., Clayton, A. (2010). Cancer exosomes trigger fibroblast to myofibroblast differentiation. *Cancer Res*, 70(23), pp. 9621-30.

Webber, J., Clayton, A. (2013). How pure are your vesicles? J Extracell Vesicles, 10, 2, pp. e19861. DOI: 10.3402/jev.v2i0.19861

Webber, J. P., Spary, L. K., Sanders, A. J., Chowdhury, R., Jiang, W. G., Steaman, R., Wymant, J., Jones, A. T., Kynaston, H., Mason, M. D., Tabi, Z., Clayton, A. (2015). Differentiation of tumour-promoting stromal myofibroblasts by cancer exosomes. *Oncogene*, 24, 3, pp. 290-302. DOI: 10.1038/onc.2013.560

Weber, C. E., Luo, C., Hotz-Wagenblatt, A., Gardyan, A., Kordaß, Holland-Letz, T., Osen, W., Eichmüller, S. B. (2016). miR-339-3p is a tumor suppressor in melanoma. *Cancer Res,* 76, 12, pp. 3562-71. DOI: 10.1158/0008-5472.CAN-15-2932

Wei, Z., Batagov, A. Schinello, S., Wang, J., Wang, Y., El fatimy, R., Rabinovsky, R., Balaj, L., Chen, C., Hockberg, F., Carter, B. S., Breakefield, X. O., Krichevsky, A. (2017). Coding and noncoding landscape of extracellular RNA released by human glioma stem cells. *Nature Commun*, 8, 1, pp. 1-11. DOI: 10.1038/s41467-017-01196-x

Welton, J. L., Webber, J. P., Botos, L.-A., Jones, M., Clayton, A. (2015). Ready-made chromatography columns for extracellular vesicle isolation from plasma. *J Extracell Vesicles*, 4, 1, pp. 27269. DOI: 10.3402/jev.v4.27269

Wijerathne, H., Witek, M. A., Jackson, J. M., Brown, V., Hupert, M. L., Herrera, K., Kramer, C., Davidow, A. E., Li, Y., Baird, A. E., Murphy, M. C., Soper, S. A. (2020). Affinity enrichment of extracellular vesicles from plasma reveals mRNA changes associated with acute ischemic stroke. *Commun Biol*, 3, 1, pp. e613. DOI: 10.1038/s42003-020-01336-y

Willis, C. M., Nicaise, A. M., Bongarzone, E. R., Givogri, M., Reiter, C. R., Heintz, O., Jellison, E. R., Sutter, P. A., TeHennepe, G., Ananda, G., Vella, A. T., Crocker, S. J. (2020). Astrocyte support for oligodendrocyte differentiation can be conveyed via extracellular vesicles but diminishes with age. *Sci Rep*, 10, 1, pp. e828. DOI: 10.1038/s41598-020-57663-x

Willms, E., Cabańas, C., Mäger, I., Wood, M. J. A., Vader, P. (2018). Extracellular vesicle heterogeneity: subpopulations, isolation techniques, and diverse functions

in cancer progression. *Front Immunol*, 8, pp. e738. DOI: 10.3389/fimmu.2018.00738

Witsch, E., Sela, M., Yarden, Y. (2010). Roles for growth factors in cancer progression. *Physiol Bethesda*, 25, 2, pp. 85-101. DOI: 10.1152/physiol.00045.2009

Woodcock, H. V., Eley, J. D., Guillotin, D., Platé, M., Nanthakumar, C. B., Martufi, M., Peace, S., Joberty, G., Poeckel, D., Good, R. B., Taylor, A. R., Zinn, N., Redding, M., Forty, E. J., Hynds, R. E., Swanton, C., Karsdal, M., Maher, T. M., Bergamini, G., Marshall, R. P., Bianchard, A. D., Mercer, P. F., Chambers, R. C. (2019). The mTORC1/4E-BP1 axis represents a critical signalling node during fibrogenesis. *Nat Commun,* 10, 1, pp. 6-20. DOI: 10.1038/s41467-018-07858-8

Wu, T., Dai, Y. (2017). Tumor microenvironment and therapeutic response. *Cancer Lett*, 387, pp. 61-8. DOI: 10.1016/j.canlet.2016.01.043

Xiang, C., Chen, J., Fu, P. (2017). HGF/Met signaling in cancer invasion: the impact on cytoskeleton remodeling. *Cancers*, 9, 44, pp. 1-12. DOI: 10.3390/cancers9050044

Xie, X., Guo, L.-W., Kent, K. C. (2021). miR548ai antagonism attenuates exosome-induced endothelial cell dysfunction. *Cell Death Discov*, 7, 1, pp. e318. DOI: 10.1038/s41420-021-00720-9

Xu, Q., Liu, X., Liu, Z., Zhou, Z., Wang, Y., Tu, J., Li, L., Bao, H., Yang, L., Tu, K. (2017). MicroRNA-1296 inhibits metastasis and epithelial-mesenchymal transition of hepatocellular carcinoma by targeting SRPK1-mediated PI3K/AKT pathway. *Mol Cancer*, 16, 2017, pp. e103. DOI: 10.1186/s12943-017-0675-y

Yalamanchili, H. K., Wan, Y.-W., Liu, Z. (2017). Data analysis pipeline for RNA-seq experiments: from differential expression to cryptic splicing. *Curr Protoc Bioinformatics*, 59, 11.15, pp. 1-21. DOI: 10.1002/cpbi.33

Yáñes-Mó, M., Siljander, P. R.-M., Andreu, Z., Zavec, A. B., Borràs, F. E., Buzas, E. I., Buzas, K., Casal, E., Cappello, F., Carvalho, J., Colàs, E., Cordeira-da Silva, A., Fais, S., Falcon-Perez, J. M., Ghobrial, I. M., Giebel, B., Gimona, M., Graner, M., Gursel, I., Gursel, M., Heegaard, N. H. H., Hendrix, A., Kierulf, P., Kokubun, K., Kosanovic, M., Kralj-Iglic, V., Krämer-Albers, E.-M., Laitinen, S., Lässer, C., Lener, T., Ligeti, E., Linē, A., Lipps, G., Llorente, A., Lötvall, J., Manček-Keber, M., Marcilla, A., Mittelbrunn, M., Nazarenko, I., Nolte-'t Hoen, E. N. M., Nyman, T. A., O'Driscoll, L., Olivan, M., Oliveira, C., Pállinger, É., del Portillo, H. A., Stoorvogel, W., Stukelj, R., van der Grein, S., Vasconcelos, M. H., Wauben, M. H. M., De Wever, O. (2015). Biological properties of extracellular vesicles and their physiological functions. *J Extracell Vesicles*, 14, 4, pp. e27066. DOI: 10.3402/jev.v4.27066

Yang, J.-M., Gould, S. J. (2013). The cis-acting signals that target proteins to exosomes and Microvesicles. *Biochem Soc Trans*, 41, 1, pp. 277-82. DOI: 10.1042/BST20120275

Yang, P., Cornejo, K. M., Sadow, P. M., Cheng, L., Wang, M., Xiao, Y., Jiang, Z., Oliva, E., Jozwiak, S., Nussbaum, R. L., Feldman, A. S., Paul, E., Thiele, E. A., Yu, J. J., Henske, E. P., Kwiatkowski, D. J., Young, R. H., Wu, C.-L. (2014). Renal cell carcinoma in tuberous sclerosis complex. *Am J Surg Pathol*, 38, 7, pp. 895-909. DOI: 10.1097/PAS.0000000000000237

Yang, H., Lin, H.-C., Liu, H., Gan, D., Jin, W., Ciu, C., Yan, Y., Qian, Y., Han, C., Wang, Z. (2020). A 6 lncRNA-Based Risk Score System for Predicting the Recurrence of Colon Adenocarcinoma Patients. Front Oncol, 10, 81, pp. 1-11. DOI: 10.3389/fonc.2020.00081/full

Yang, T., Guo, J.P., Li, F., Xiu, C., Wang, H., Duan, X.L. (2021). Long non-coding RNA-DUXAP8 regulates TOP2A in the growth and metastasis of osteosarcoma via microRNA-635. *Mol Med Rep*, 24, 115, pp. 1-9. DOI: 10.3892/mmr.2021.12150

Yang, H., Yu, Z., Chen, X., Li, J., Li, N., Cheng, J., Gao, N., Yuan, H.-X., Ye, D., Guan, K.-L., Xu, Y. (2021). Structural insights into TSC complex assembly and GAP activity on Rheb. Nature Comms, 12, 339, pp. 1-10. DOI: 10.1038/s41467-020-20522-4

Yang-chun, F., Sen-Yu, W., Yuan, Z., Yan-Chun, H. (2020). Genome-wide profiling of human papillomavirus DNA integration into human genome and its influence on PD-L1 expression in Chinese Uygur cervical cancer women. *J Immunol Res*, 2020, 6284960, pp. 1-12. DOI: 10.1155/2020/6284960

Yekula, A., Yekula, A., Muralidharan, K., Kang, K., Carter, B. S., Balaj, L. (2020). Extracellular vesicles in glioblastoma tumour microenvironment. *Front Immunol*, 10, pp. 3137. DOI: 10.3389/fimmu.2019.03137

Yellon, D. M., Davidson, S. M. (2014). Nanoparticles involved in cardioprotection? *Circ Res*, 114, 2, pp. 325-32. DOI: 10.1161/CIRCRESAHA.113.300636

Yeung, R. S. (2003). Multiple roles of the tuberous sclerosis complex genes. *Genes Chromo Cancer*, 38, 4, pp. pp. 368-75. DOI: 10.1002/gcc.10256

Yeung, V., Webber, J. P., Dunlop, E. A., Morgan, H., Hutton, J., Gurney, M., Jones, E., Falcon-Perez, J., Tabi, Z., Errington, R., Clayton, A. (2018). Rab35-dependent extracellular nanovesicles are required for induction of tumour supporting stroma. *Nanoscale*, 10, 18, pp. 8547-59. DOI: 10.1039/c8nr02417k

Yin, Y., Shelke, G. V., Lässer, C., Brismar, H., Lötvall, J. (2020). Extracellular vesicles from mast cells induce mesenchymal transition in airway epithelial cells. *Respir Res*, 21, 101, pp. 1-13. DOI: 10.1186/s12931-020-01346-8

Young, L. R., Inoue, Y., McCormack, F. X. (2008). Diagnostic potential of serum VEGF-D for lymphangioleiomyomatosis. *New Eng J Med*, 358, 2, pp.199-200. DOI: 10.1056/NEJMc0707517

Young, L. R., van Dyke, R., Gulleman, P. M., Inoue, Y., Brown, K. K., Schmidt, L. S., Linehan, W. M., Hajjar, F., Kinder, B. W., Trapnell, B. C., Bissler, J. J., Franz, D.

N., McCormack, F. X. (2010). Serum vascular endothelial growth factor-D prospectively distinguishes lymphangioleiomyomatosis from other diseases. *Chest*, 138, 3, pp. 674-81. DOI: 10.1378/chest.10-0573

Young, L., Lee, H. S., Inoue, Y., Moss, J., Singer, L. G., Strange, C., Nakata, K., Barker, A. F., Chapman, J. T., Brantly, M. L., Stocks, J. M., Brown, K. K., Lynch, J. P. 3rd, Goldberg, H. J., Downey, G. P., Swigris, J. J., Taveira-DaSilva, A. M., Krischer, J. P., Trapnell, B. C., McCormack, F. X., MILES Trial Group. (2013). Serum VEGF-D a concentration as a biomarker of lymphangioleiomyomatosis severity and treatment response: a prospective analysis of the Multicenter International Lymphangioleiomyomatosis Efficacy of Sirolimus (MILES) trial. *Lancet Respir Med*, 1, 6, pp. 445-52. DOI: 10.1016/S2213-2600(13)70090-0

Young, M.D., Wakefield, M.J., Smyth, G.K. and Oshlack, A. (2010). Gene ontology analysis for RNA-seq: accounting for selection bias. *Genome biology*, *11*, 2, pp.1-12. DOI: 10.1186/gb-2010-11-2-r14

Yu, J., Astrinidis, A., Howard, S., Henske, E. P. (2004). Estradiol and tamoxifen stimulate LAM-associated angiomyolipoma cell growth and activate both genomic and non-genomics signaling pathways. *Am J Physiol Lung Cell Mol Physiol*, 286, 4, pp. 694-700. DOI: 10.1152/ajplung.00204.2003

Yu, X., Cao, Y., Tang, L., Yang, Y., Chen, F., Xia, J. (2018). Baicalein inhibits breast cancer growth via activating a novel isoform of the long noncoding RNA PAX8-AS1-N. *J Cell Biochem*, 119, 8, pp. 6842-56. DOI: 10.1002/jcb.26881

Yuan, H., Guan, K. (2016). Structural insights of mTOR complex 1. *Cell Res*, 26, 3, pp. 267-68. DOI: 10.1038/cr.2016.10

Yuan, X., Smith, R. J. Jr, Guan, H., Ionita, C. N., Khobragade, P., Dziak, R., Liu, Z., Pang, M., Wang, C., Guan, G., Andreadis, S., Yang, S. (2016). Hybrid biomaterial with conjugated growth factors and mesenchymal stem cells for ectopic bone formation. *Tissue Engin*, 22, 13-14, pp. 928-39. DOI: 10.1089/ten.tea.2016.0052

Yue, M., Pacheco, G., Cheng, T., Li, J., Wang, Y., Henske, E. P., Schuger, L. (2016). Evidence supporting a lymphatic endothelium origin for angiomyolipoma, a TSC2(-) tumor regulated to lymphangioleiomyomatosis. *Am J Pathol*, 186, 7, pp. 1825-36. DOI: 10.1016/j.ajpath.2016.03.009

Zaborowski, M. P., Balaj, L., Breakefield, X. O., Lai, C. P. (2015). Extracellular vesicles: composition, biological relevance, and methods of study. *Bioscience*, 65, 8, pp. 783-97. DOI: 10.1093/biosci/biv084

Zadjali F., Kumar, F., Yao, Y., Johnson, D., Astrinidis, A., Vogel, P., Gross, K. W., Bissler, J. J. (2020). Tuberous sclerosis complex axis controls renal extracellular vesicle production and protein content. *Intl J Mol Sci*, 21, 1729, pp. 1-15. DOI: 10.3390/ijms21051729

Zeng, H., Lu, B., Zamponi, R., Yang, Z., Wetzel, K., Loureiro, J., Mohammadi, S., Beibel, M., Bergling, S., Reece-Hoyes, J., Russ, C., Roma, G., Tchorz, J. S.,

Capodieci, P., Cong, F. (2018). mTORC1 signaling suppresses Wnt/β-catenin signaling through DVL-dependent regulation of Wnt receptor FZD level. *Proc Natl Acad Sci U S A*, 115, 44, pp. e10362-9. DOI: 10.1073/pnas.1808575115

Zhan, P., Zhao, S., Yan, H., Yin, C., Xiao, Y., Wang, Y., Ni, R., Chen, W., Wei, G., Zhang, P. (2017). Alpha-enolase promotes tumorigenesis and metastasis via regulating AMPK/mTOR pathway in colorectal cancer. *Mol Carcinog*, 56, 5, pp. 1427-37. DOI: 10.1002/mc.22603

Zhang, H., Cicchetti, G., Onda, H., Koon, H. B., Asrican, K., Bajraszewski, N., Vazquez, F., Carpenter, C. L., Kwiatkowski, D. J. (2003). Loss of Tsc1/Tsc2 activates mTOR and disrupts PI3K-Akt signalling through downregulation of PDGFR. *J Clin Invest*, 112, 8, pp. 1223-33. DOI: 10.1172/JCI17222

Zhang, Y., Ueno, Y., Liu, X., S., Buller, B., Wang, X., Chopp, M., Zhang, Z. G. (2013). The microRNA-17-92 cluster enhances axonal outgrowth in embryonic cortical neurons. *J Neurosci*, 33, 16, pp. 6885-94. DOI: 10.1523/JNEUROSCI.5180-12.2013

Zhang, Q., Si, S., Schoen, S., Chen, J., Jin, X.-B., Wu, G. (2013). Suppression of autophagy enhances preferential toxicity of paclitaxel to folliculin-deficient renal cancer cells. *J Exp Clin Cancer Res*, 32, 1, pp. e99. DOI: 10.1186/1756-9966-32-99

Zhang, Y., Sun, Z., Zhang, Y., Fu, T., Liu, C., Liu, Y., Lin, Y. (2016). The microRNA-635 suppresses tumorigenesis in non-small cell lung cancer. *Biomed Pharmacother*, 84, pp. 1274-81. DOI: 10.1016/j.biopha.2016.10.040

Zhang, P., Samuel, G., Crow, J., Godkin, A. K., Zeng, Y. (2018). Molecular assessment of circulating exosomes towards liquid biopsy diagnosis of Ewing sarcoma family of tumors. *Translational Res*, 201, pp. 2-43. DOI: 10.1016/j.trsl.2018.05.007

Zhang, H., Zhu, M., Du, Y., Zhang, H., Zhang, Q., Liu, Q., Huang, Q., Zhang, L., Li, H., Xu, L., Zhou, X., Zhu, W., Shu, Y., Liu, P. (2019). A panel of 12-lncRNA signature predicts survival of pancreatic adenocarcinoma. *J Cancer*, 10, 6, pp. 1550-9. DOI: 10.7150/jca.27823

Zhang, X., Wang, S., Wang, H., Cao, J., Huang, X., Chen, Z., Xu, P., Sun, G., Xu, J., Lv, J., Xu, Z. (2019). Circular RNA circNRIP1 acts as a microRNA-149-5p sponge to promote gastric cancer progression via the AKT1/mTOR pathway. *Mol Cancer*, 18, 1, pp.1-20. DOI: 10.1186/s12943-018-0935-5

Zhang, Y., Li, F., Chen, J. (2019). MYC promotes the development of papillary thyroid carcinoma by inhibiting the expression of lncRNA PAX8AS1:28. *Oncol Rep*, 41, 4, pp. 2511-7. DOI: 10.3892/or.2019.6996

Zhang, D. X., Vu, L, T., Ismail, N. N., Le, M. T. N., Grimson, A. (2021). Landscape of extracellular vesicles in the tumour microenvironment: interactions with stromal

cells and with non-cell components, and impacts on metabolic reprogramming, horizontal transfer of neoplastic traits, and the emergence of therapeutic resistance. *Semin Cancer Biol*, 74, 2021, pp. 24-44. DOI: 10.1016/j.semcancer.2021.01.007

Zhang, X., Takeuchi, T., Takeda, A., Mochizuki, H., Nagai, Y. (2022). Comparison of serum and plasma as a source of blood extracellular vesicles: increased levels of platelet-derived particles in serum extracellular vesicle fractions alter content profiles from plasma extracellular vesicle fractions. *PLoS One*, 17, 6, pp. e0270634. DOI: 10.1371/journal.pone.0270634

Zheng, G., Wang, H., Zhang, X., Yang, Y., Wang, L., Du, L., Li, W., Li, J., Qu, A., Liu, Y., Wang, C. (2019). Identification and validation of reference genes for qPCR detection in serum microRNAs in colorectal adenocarcinoma patients. *PLoS One*, 8, 12, pp. e83025. DOI: 10.1371/journal.pone.0083025

Zhou, J., Yang, Z., Cheng, S., Yu, J., Huang, C., Feng, Q. (2020). miRNA-425-5p enhances lung cancer growth via the PTEN/PI3K/AKT signaling axis. *BMC Pulmon Med*, 223, 2020, pp. 1-7. DOI: 10.1186/s12890-020-01261-0

Zhou, B., Xu, K., Zheng, X., Chen, T., Wang, J., Song, Y., Shao, Y., Zheng, S., (2020). Application of exosomes as liquid biopsy in clinical diagnosis. *Signal Transduct Targ Ther*, *5,* 1, pp.1-14. DOI: 10.1038/s41392-020-00258-9

Zordan, P., Cominelli, M., Cascino, F., Tratta, E., Poliani, P. L., Galli, R. (2018). Tuberous sclerosis complex-associated CNS abnormalities depend on

hyperactivation of mTORC1 and Akt. *J Clin Invest*, 128, 4, pp. 1688-1706. DOI: 10.1172/JCI96342

Zou, W., Lai, M., Zhang, L., Zheng, L., Xing, Z., Li, T., Zou, Z., Song, Q., Zhao, X., Xia, L., Yang, J., Liu, A., Zhang, H., Cui, Z.-K., Jiang, Y., Bai, X. (2019). Exosome release is regulated by mTORC1. *Adv Sci*, 6, 1801313, pp. 1-12. DOI: 10.1002/advs.201801313

CHAPTER 9

APPENDICES

Amino acid	Three letter code	One letter symbol
Alanine	Ala	A
Arginine	Arg	R
Asparagine	Asn	N
Aspartic acid	Asp	D
Cysteine	Cys	C
Glutamic acid	Glu	E
Glutamine	Gln	Q
Glycine	Gly	G
Histidine	His	H
Isoleucine	Ile	I
Leucine	Leu	L
Lysine	Lys	K
Methionine	Met	M
Phenylalanine	Phe	F
Proline	Pro	P
Serine	Ser	S
Theonine	Thr	T
Tryptophan	Trp	W
Tyrosine	Tyr	Y
Valine	Val	V

Appendix A: Amino acids and corresponding three-letter codes and one-letter symbols.

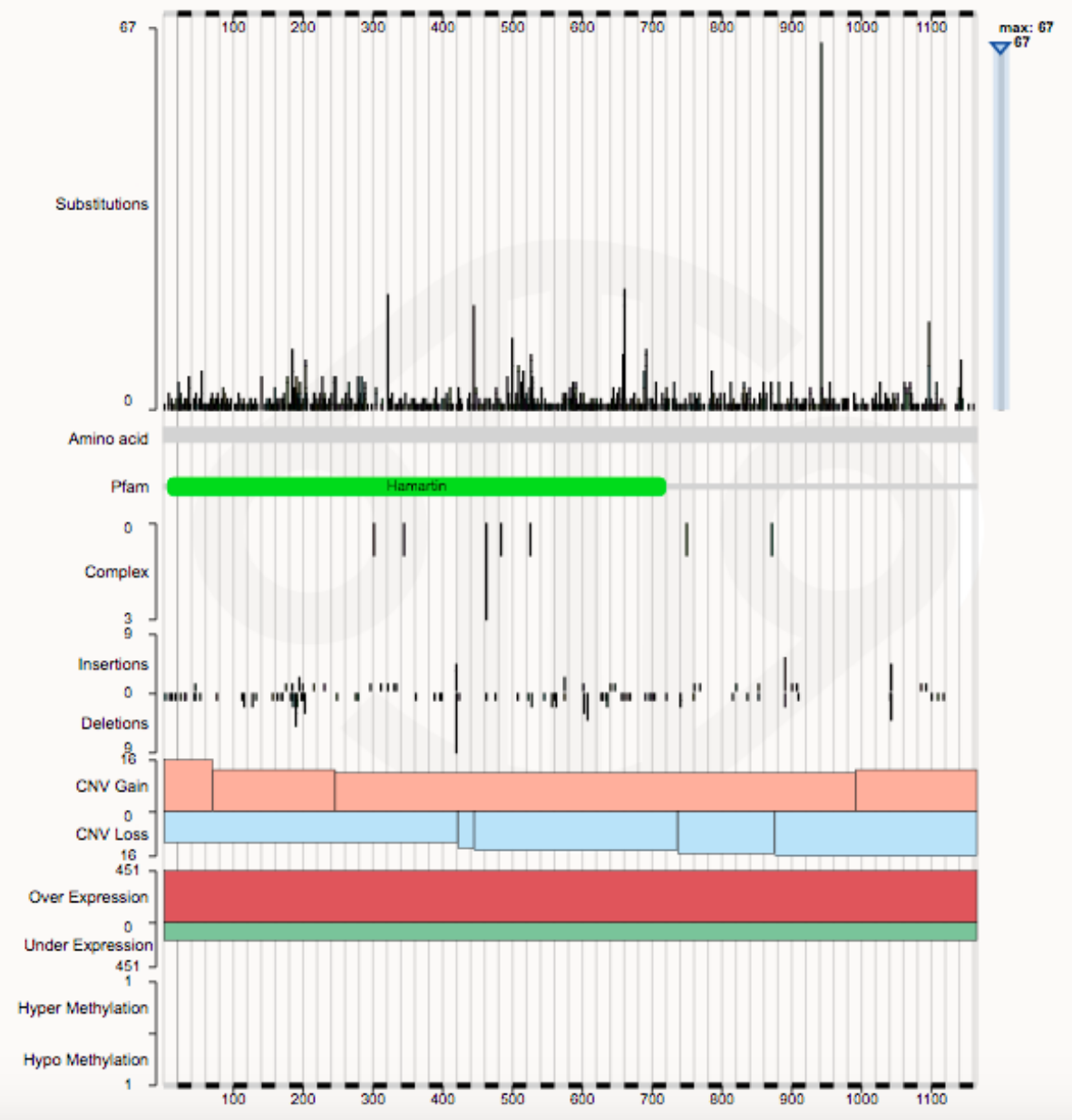

Appendix B: Mutations across *TSC1* gene. Data from COSMIC (www.cancer.sanger.ac.uk/cosmic).

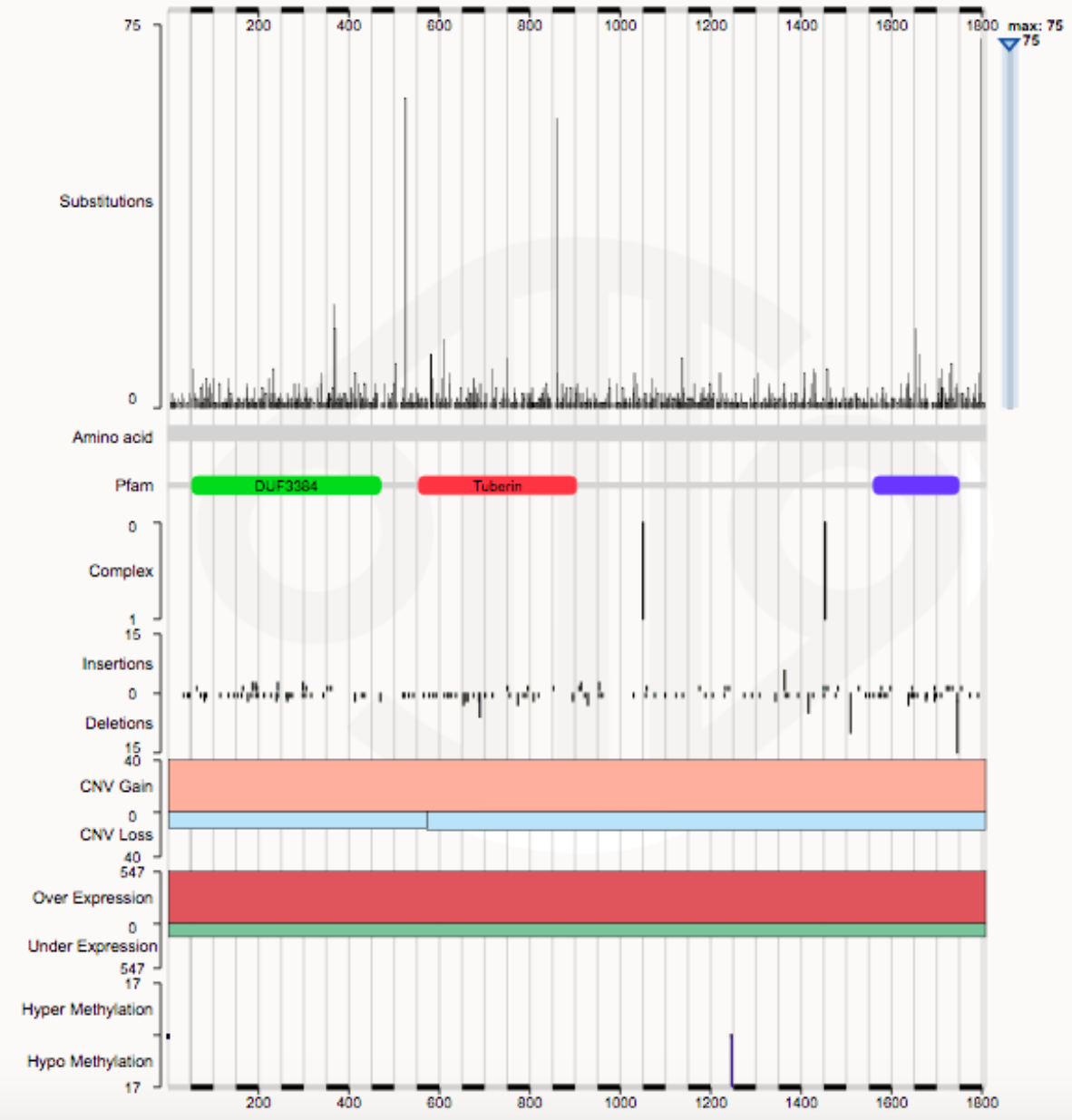

Appendix C: Mutations across *TSC2* gene. Data from COSMIC (www.cancer.sanger.ac.uk/cosmic).

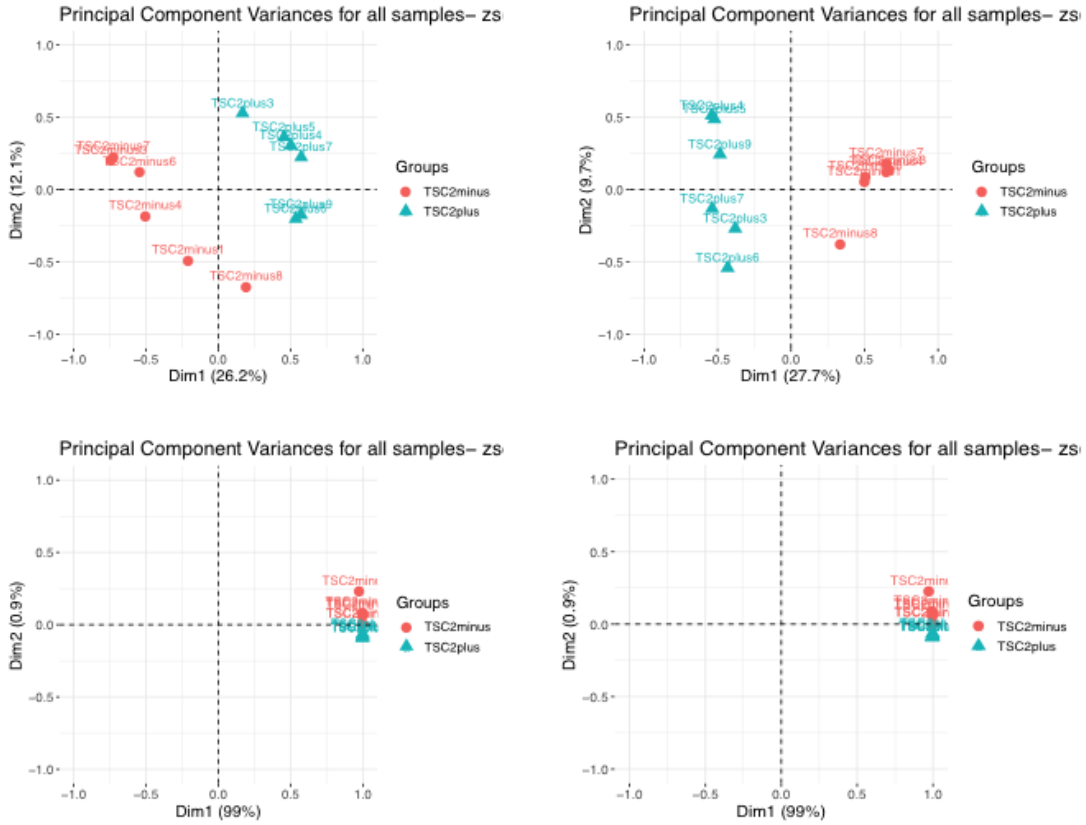

Appendix D: Principal Component Analysis (PCA) plots for RNA-Sequencing.

TSC2plus denotes AML+; TSC2minus denotes AML-.